Department of Chemistry and Materials Science

Multilayer carbon hybrid based electrodes for direct electrochemical detection of analgesics and biomolecules

Development of an electrochemical sensor for determination of analgesics in blood samples

Niklas Wester

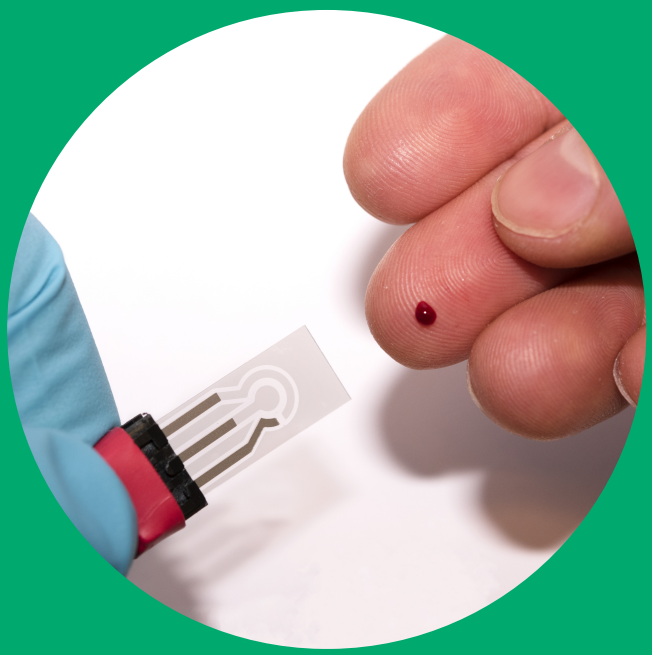

Aalto University

DOCTORAL DISSERTATIONS

Aalto University publication series
DOCTORAL DISSERTATIONS 14/2021

Multilayer carbon hybrid based electrodes for direct electrochemical detection of analgesics and biomolecules

Development of an electrochemical sensor for determination of analgesics in blood samples

Niklas Wester

A doctoral dissertation completed for the degree of Doctor of Science (Technology) to be defended, with the permission of the Aalto University School of Chemical Engineering, at a public examination held at the lecture hall KE2 (Komppa Auditorium) of the school on the 5th of March 2021 at 12:00.

Aalto University
School of Chemical Engineering
Department of Chemistry and Materials Science
Physical Characteristics of Surfaces and Interfaces

Supervising professor
Professor Jari Koskinen, Aalto University, Finland

Thesis advisor
Professor Tomi Laurila, Aalto University, Finland

Preliminary examiners
Associate professor Stéphane Marinesco, Lyon Neuroscience Research Center, France
Professor Yutaka Ohno, Nagoya University, Japan

Opponent
Professor, Andrew Ewing, University of Gothenburg, Sweden

Aalto University publication series
DOCTORAL DISSERTATIONS 14/2021

ISBN 978-952-64-0257-4 (printed)
ISBN 978-952-64-0258-1 (pdf)
ISSN 1799-4934 (printed)
ISSN 1799-4942 (pdf)
http://urn.fi/URN:ISBN:978-952-64-0258-1

Unigrafia Oy
Helsinki 2021

Finland

Printed matter
4041-0619

Aalto University

Abstract

Aalto University, P.O. Box 11000, FI-00076 Aalto www.aalto.fi

Author
Niklas Wester

Name of the doctoral dissertation
Multilayer carbon hybrid based electrodes for direct electrochemical detection of analgesics and biomolecules

Publisher School of Chemical Engineering

Unit Department of Chemistry and Materials Science

Series Aalto University publication series DOCTORAL DISSERTATIONS 14/2021

Field of research Materials Science

Manuscript submitted 9 October 2020 **Date of the defence** 5 March 2021

Permission for public defence granted (date) 27 January 2021 **Language** English

☐ **Monograph** ☒ **Article dissertation** ☐ **Essay dissertation**

Abstract

There is increasing interest in point-of-care (POC) determination of drugs and biomolecules, as well as real-time monitoring of these analytes, with wearable and in vivo sensors. Rapid response POC tests can improve patient safety in situations like poisoning and enable personalized treatments whereas real time detection of physiological processes such as neurotransmission events can improve our understanding of neurophysiology and enable novel treatments for neurological disorders. Electrochemical detection is an attractive technology for both POC in vitro diagnostics and wearable sensors alike, due to its low price, simple instrumentation and small required sample volume.

Many analgesic drugs show highly individual dose response and thus a dose that causes dangerous side effects in one patient may lack analgesic effect in another. Analgesics are also some of the most abused prescription drugs. Opioid overdoses kill tens of thousands of people annually in the United states alone. Both intentional and unintentional poisoning of over-the-counter analgesics, such as paracetamol, also regularly occur. Therefore, a quantitative POC test for determination of analgesics in capillary blood samples, could be a powerful diagnostic tool for poisoning. However, the POC determination of small drug and biomolecules in unprocessed blood samples has proven to be difficult.

In this thesis, we have investigated the use of tetrahedral amorphous carbon (ta-C) and single-walled carbon nanotube (SWCNT) thin films in electrochemical sensing. We have carried out extensive physicochemical characterization of these electrode materials. We combine synchrotron based x-ray spectroscopy with electron microscopy, diffraction and conventional spectroscopic techniques. Both the studied materials were found to support facile electron transfer and show low background currents enabling highly sensitive detection of dopamine and morphine. They, however, lack the fouling resistance and selectivity required for detection of dopamine and analgesics in complex biological samples. Modification with carbon nanomaterials or polymer membranes significantly improved the selectivity as well as reduced the electrode fouling, allowing for detection of dopamine and analgesics in blood samples without precipitation of proteins. We show that such multilayer electrodes can be tailored for the requirements of detection of neurotransmitters and analgesic drugs.

Finally, we demonstrate a process for mass production of electrochemical test strips. These sensor strips were shown to be capable of detecting clinically meaningful concentrations of paracetamol from a 20 µL blood sample in less than 5 min. Based on these results we propose an electrochemical assay for quantitative detection of paracetamol.

Keywords Amorphous carbon, ta-C, carbon nanotubes, SWCNT, electroanalytical chemistry, dopamine, paracetamol, morphine, opioids

ISBN (printed) 978-952-64-0257-4 **ISBN (pdf)** 978-952-64-0258-1

ISSN (printed) 1799-4934 **ISSN (pdf)** 1799-4942

Location of publisher Helsinki **Location of printing** Helsinki **Year** 2021

Pages 210 **urn** http://urn.fi/URN:ISBN:978-952-64-0258-1

Tekijä
Niklas Wester

Väitöskirjan nimi
Monikerroksiset hiilipohjaiset hybridielektrodit sähkökemiallisessa analgeettien ja biomolekyylien havaitsemisessa

Julkaisija Kemian tekniikan korkeakoulu

Yksikkö Kemian ja materiaalitieteen laitos

Sarja Aalto University publication series DOCTORAL DISSERTATIONS 14/2021

Tutkimusala Materiaalitiede

Käsikirjoituksen pvm 09.10.2020 **Väitöspäivä** 05.03.2021

Väittelyluvan myöntämispäivä 27.01.2021 **Kieli** Englanti

☐ **Monografia** ☒ **Artikkeliväitöskirja** ☐ **Esseeväitöskirja**

Tiivistelmä

Kiinnostus vierimittauksiin sekä lääkkeiden ja biomolekyylien reaaliaikaiseen mittaamiseen kasvaa jatkuvasti. Lisäksi näiden analyyttien monitorointi puettavilla- sekä in vivo -antureilla on kiivaan tutkimuksen kohde. Nopeat vierimittaukset voivat parantaa potilaan hoitoa myrkytystapauksissa sekä mahdollistaa yksilöidyn terveydenhoidon. Neurotransmissioiden reaaliaikainen havaitseminen tutkimuksessa voi myös parantaa neurofysiologian ymmärrystä ja edelleen kehittää neurodegeneratiivisten sairauksien hoitoa. Sähkökemiallisten mittausten matalan hinnan, yksinkertaisen laitteiston ja pienen näytevolyymin vuoksi se on kilpailukykyinen menetelmä vierimittauksissa sekä puettavissa antureissa.

Potilaiden vasteet analgeettisiin lääkkeisiin ovat usein yksilöllisiä. Tämän vuoksi annos, jolla ei ole analgeettista vaikutusta yhdellä potilaalla, voi aiheuttaa vaarallisia sivuvaikutuksia toisella. Lisäksi analgeettien väärinkäyttö on yleistä ja erityisesti opioidien aiheuttamiin yliannostuksiin kuolee pelkästään Yhdysvalloissa kymmeniä tuhansia ihmisiä vuosittain. Myös tahalliset ja tahattomat yliannostukset reseptivapailla lääkkeillä kuten parasetamolilla, ovat yleisiä. Näistä syistä kvantitatiivinen vierimittausmenetelmä analgeettien määrittämiseen kapillaariverinäytteestä voisi olla tehokas työkalu yliannostusten diagnoosissa. Vierimittausmenetelmän kehittäminen pienmolekyylien määrittämiseen käsittelemättömästä verinäytteestä on kuitenkin osoittautunut haastavaksi.

Tässä työssä tutkimme tetraedrisestä amorfisesta hiilestä ja yksiseinämäisistä hiilinanoputkista valmistettujen ohutkalvojen käyttöä sähkökemiallisissa antureissa. Lisäksi tutkimme näiden materiaalien fysikaaliskemiallisia ominaisuuksia yhdistämällä synkrotronisäteilyyn perustuvan röntgenspektroskopian elektronimikroskopiaan, elektronidiffraktioon sekä perinteisiin spektroskooppisiin menetelmiin. Tutkittujen materiaalien hyvät elektroninsiirto-ominaisuudet ja matala taustavirta mahdollistavat dopamiinin ja analgeettien herkän mittaamisen. Materiaalien rajallinen selektiivisyys ja biolikaantuminen kuitenkin rajoittavat niiden käyttöä biologisissa näytteissä. Näitä ominaisuuksia sekä herkkyyttä voitiin kuitenkin parantaa hiilinanomateriaali- ja polymeeripinnoitteilla. Osoitamme, että nämä monikerroksiset elektrodit voidaan räätälöidä dopamiinin ja analgeettien havaitsemiseen. Lisäksi näillä elektrodeilla voidaan havaita analgeetteja ihmisen veriplasmassa ja kokoveressä ilman proteiinien saostusta. Tämän työn tulosten perusteella kyseisiä elektrodeja voidaan käyttää lääkeaineiden vapaan pitoisuuden määrittämiseen lähes reaaliajassa. Lopuksi, kehitimme massatuotantoon soveltuvan prosessin sähkökemiallisten mittaliuskojen valmistamiseen. Näiden anturien avulla voitiin mitata kliinisesti relevantteja konsentraatioita parasetamolia 20 µL verinäytteestä alle viidessä minuutissa.

Avainsanat Amorfinen hiili, ta-C, hiilinanoputket, SWCNT, sähkökemia, voltammetria, dopamiini, parasetamoli, morfiini, opioidit

ISBN (painettu) 978-952-64-0257-4 **ISBN (pdf)** 978-952-64-0258-1

ISSN (painettu) 1799-4934 **ISSN (pdf)** 1799-4942

Julkaisupaikka Helsinki **Painopaikka** Helsinki **Vuosi** 2021

Sivumäärä 210 **urn** http://urn.fi/URN:ISBN:978-952-64-0258-1

Acknowledgements

The experimental work for this thesis was carried out between December 2015 and September 2020 at Aalto University. The funding by Business Finland (FEDOC211637 and FEPOD 2117731 projects), Orion Research Foundation sr, Emil Aaltonen Foundation, Foundation for Aalto University Science and Technology, and by the School of Chemical Engineering are gratefully acknowledged. Use of the Stanford Synchrotron Radiation Lightsource, SLAC National Accelerator Laboratory, is supported by the U.S. Department of Energy, Office of Science, Office of Basic Energy Sciences under contract no. DE-AC02-76SF00515.

It is no exaggeration to state that this work has literally required blood, sweat and tears. During this work, I have enjoyed numerous joyous moments of discovery as well as a fair share of failures. Siddhartha Mukherjee describes failure in science as “a moment that a scientist often encounters alone.”. However, with the supportive atmosphere cultivated in Professor Jari Koskinen’s and Professor Tomi Laurila’s groups, I never felt alone in these moments. I would like to express my deepest gratitude to my supervising Professor Jari Koskinen for his support, guidance and belief in my abilities. I am also grateful to my thesis Advisor Professor Tomi Laurila for his invaluable guidance and expertise without which this work would not have been possible.

I am deeply honoured to have Professor Stéphane Marinesco and Professor Yutaka Ohno as pre-examiners. I would also like to express my gratitude to Professor Andrew Ewing for acting as the opponent at the public defense of this thesis. Dr. Jessica Koehne and Dr. Dennis Nordlund also deserve my thanks for hosting my visits at NASA Ames Research Center and Stanford Synchrotron Radiation Lightsource during this work.

I feel privileged to have carried out this work in a highly interdisciplinary research consortium. The expert medical opinions and insight of Professor Eija Kalso and Dr. Tuomas Lilius are highly appreciated. I would also like to thank Professor Esko Kauppinen for contributing with his vast knowledge about carbon nanotubes. I am also extremely grateful for the collaboration with Ilkka Varjos and Bjørn Mikladal whose input made industrial manufacturing of the developed test strips possible. The expertise of Juuso Juhila on the subject of in vitro diagnostics and point-of-care testing is also acknowledged. With the presence of such highly regarded experts in their respective fields, I can scarcely remember finishing a project meeting without learning something.

In addition, I would like to express my gratitude to all the co-authors for their valuable contributions and the fruitful collaboration. In particular, I would like to thank Elsi Verrinder, Jarkko Etula, Sami Sainio and Tommi Palomäki for their help and support. Tommi Palomäki deserves special thanks for teaching me much of what I know about electroanalytical

chemistry. In addition, the opportunity for close collaboration with Dr. Noora Isoaho and Dr. Emilia Peltonen is greatly appreciated and has been highly educational. I am especially grateful to Dr. Sami Sainio for the opportunity to be a part of his postdoctoral research at the Stanford Synchrotron Radiation Lightsource. Dr. Leena-sisko Johansson and Dr. Dennis Nordlund also deserve my thanks for help with XPS and XAS analysis.

The peer support of my co-workers Elli Leppänen, Dr. Ville Rontu, Dr. Ajai Iyer and Vasuki Durairaj is also greatly appreciated. Vasuki Durairaj deserves a special thanks for the proofreading of this thesis and the language corrections. I would especially like to thank Dr. Ajai Iyer for the exhilarating discussions on the widest range of topics imaginable. Those moments often provided me with much needed energy to get through dull data analysis or just a bad morning. The "powerspots" both at the crag and at the workplace by Elli Leppänen, the undisputed "betamaster" of our groups, is also highly appreciated.

I also want to thank my family and loved ones for their unconditional love and support. Firstly, I am deeply grateful to my parents for showing confidence in my abilities and nurturing my early interest in science and technology. Finally, I would like to express my deepest appreciation to Lotta Vuolamo, for her love and support.

Helsinki 12th of January 2021

Niklas Wester

Contents

List of Publications

This thesis consists of an overview and includes the following publications which are referred to in the thesis text by their roman numerals.

I. **Niklas Wester**, Sami Sainio, Tommi Palomäki, Dennis Nordlund, Vivek Kumar Singh, Leena-Sisko Johansson, Jari Koskinen and Tomi Laurila. Partially Reduced Graphene Oxide Modified Tetrahedral Amorphous Carbon Thin-Film Electrodes as a Platform for Nanomolar Detection of Dopamine. *The Journal of Physical Chemistry C*, 121, 14, 8153-8164, March 2017;
https://doi.org/10.1021/acs.jpcc.6b13019

II. Sami Sainio, **Niklas Wester**, Charles J. Titus, Yongping Liao, Qiang Zhang, Dennis Nordlund, Dimosthenis Sokaras, Sang-jun Lee, Kent D. Irwin, William B. Doriese, Galen C. O'Neil, Daniel S. Swetz, Joel N. Ullom, Esko I. Kauppinen, Tomi Laurila and Jari Koskinen. Hybrid X-ray Spectroscopy-Based Approach To Acquire Chemical and Structural Information of Single-Walled Carbon Nanotubes with Superior Sensitivity. *The Journal of Physical Chemistry C*, 123, 10, 6114-6120, February 2019;
https://doi.org/10.1021/acs.jpcc.9b00714

III. **Niklas Wester**, Elsi Mynttinen, Jarkko Etula, Tuomas Lilius, Eija Kalso, Bjørn F. Mikladal, Qiang Zhang, Sami Sainio, Dennis Nordlund, Esko I. Kauppinen, Tomi Laurila and Jari Koskinen. Single-Walled Carbon Nanotube Network Electrodes for the Detection of Fentanyl Citrate. *ACS Applied Nano Materials*, 3, 2, 1203-1212, January 2020;
https://doi.org/10.1021/acsanm.9b01951

IV. **Niklas Wester**, Jarkko Etula, Tuomas Lilius, Sami Sainio, Tomi Laurila and Jari Koskinen. Selective detection of morphine in the presence of paracetamol with anodically pretreated dual layer Ti/tetrahedral amorphous carbon electrodes. *Electrochemistry Communications*, 86, 166-170, January 2018;
https://doi.org/10.1016/j.elecom.2017.12.014

V. **Niklas Wester**, Elsi Mynttinen, Jarkko Etula, Tuomas Lilius, Eija Kalso, Esko I. Kauppinen, Tomi Laurila, and Jari Koskinen. Simultaneous Detection of Morphine and Codeine in the Presence of Ascorbic Acid and Uric Acid and in Human Plasma at Nafion Single-Walled Carbon Nanotube Thin-Film Electrode. *ACS omega*, 4, 18, 17726-17734, October 2019;
https://doi.org/10.1021/acsomega.9b02147

VI. Niklas Wester, Bjørn F. Mikladal, Ilkka Varjos, Antti Peltonen, Eija Kalso, Tuomas Lilius, Tomi Laurila, and Jari Koskinen. Disposable Nafion-coated single-walled carbon nanotube test strip for electrochemical quantitative determination of acetaminophen in finger-prick whole blood sample. *Analytical Chemistry*, 2020, 92, 19, 13017–13024, August 2020;
https://doi.org/10.1021/acs.analchem.0c01857

Author Contribution

Publication I: Partially Reduced Graphene Oxide Modified Tetrahedral Amorphous Carbon Thin-Film Electrodes as a Platform for Nanomolar Detection of Dopamine

The author defined the research plan, deposited the used ta-C electrodes, fabricated the PRGO modified electrodes, interpreted the results and wrote the publication under the guidance of Prof. Jari Koskinen and Prof. Tomi Laurila. The author also carried out Raman spectroscopy and SEM analysis of the fabricated electrodes and interpreted the results. V. K. Singh was responsible for synthesizing the PRGO. Anne Tanskanen performed the FT-IR analysis. Tommi Palomäki helped with the electrochemical measurements. Leena-Sisko Johansson was responsible for XPS analysis, data processing and guidance for the data interpretation. D.Sc. (Tech.) Sami Sainio and Dr. Dennis Nordlund performed and processed the results of the XAS analysis.

Publication II: Hybrid X-ray Spectroscopy-Based Approach To Acquire Chemical and Structural Information of Single-Walled Carbon Nanotubes with Superior Sensitivity

The author contributed to defining the research plan and assisted D.Sc. (Tech.) Sami Sainio in performing X-ray based spectroscopy at the Stanford Synchrotron Radiation Lightsource facilities. The author also contributed in preparing the samples and in plasma and nitric acid treatments of the specimens for analysis. The author also helped with performing the measurements and interpreting the data, as well as writing the publication, under the guidance of Dennis Nordlund, Dimosthenis Sokaras, Prof. Jari Koskinen and Prof. Tomi Laurila. Prof. Esko I. Kauppinen provided the SWCNT used in this publication, synthesized by Yongping Liao and Qiang Zhang. Sang-jun Lee and Charles J. Titus performed the XES measurements and helped interpret the data. The others were responsible for producing and commissioning of the XES detector.

Publication III: Single-Walled Carbon Nanotube Network Electrodes for the Detection of Fentanyl Citrate

The author defined the research plan, fabricated the used electrodes, performed most of the electrochemical measurements, interpreted the results and wrote the publication under the supervision of Prof. Jari Koskinen and advice of Prof. Tomi Laurila. Elsi Mynttinen helped with electrode fabrication, performing the electrochemical measurements and interpreting the

results of the electrochemical measurements. Esko I Kauppinen and Bjørn F. Mikladal were responsible for providing the SWCNT samples used in this publication. Dr. Qiang Zhang performed the UV-Vis measurement and data analysis. Jarkko Etula was responsible for SEM, Raman and TEM analysis of the samples and analysis of the TEM results. The XPS and XAS measurements were performed by D.Sc. (Tech.) Sami Sainio. He also processed the measurement data together with Dr. Dennis Nordlund.

Publication IV: Selective detection of morphine in the presence of paracetamol with anodically pretreated dual layer Ti/tetrahedral amorphous carbon electrodes

The author defined the research plan, deposited the used Ti/ta-C electrodes, carried out the anodic treatments, performed the electrochemical measurements, interpreted the results and wrote the publication under the guidance of Prof. Jari Koskinen and Prof. Tomi Laurila. D.Sc. (Tech.) Sami Sainio performed the XPS measurements and provided guidance for XPS data interpretation. Jarkko Etula performed Raman spectroscopy and AFM measurements. Ph.D. (M.D.) Tuomas Lilius contributed with expert medical opinions during the writing of the publications.

Publication V: Simultaneous Detection of Morphine and Codeine in the Presence of Ascorbic Acid and Uric Acid and in Human Plasma at Nafion Single-Walled Carbon Nanotube Thin-Film Electrode

The author defined the research plan and performed the electrochemical measurements together with Elsi Mynttinen. The author was responsible for interpreting the results and writing the publication under the supervision of Prof. Jari Koskinen and advice of Prof. Tomi Laurila. Elsi Mynttinen also helped with interpreting the results of the electrochemical measurements and writing of the manuscript. Prof. Esko I. Kauppinen provided the SWCNT used in this publication. Jarkko Etula was responsible for SEM, Raman and TEM analysis of the samples. Ph.D. (M.D.) Tuomas Lilius and Prof. Eija Kalso contributed with expert medical opinions during the writing of the publications.

Publications VI: Disposable Nafion-coated single-walled carbon nanotube test strip for electrochemical quantitative determination of acetaminophen in finger-prick whole blood sample

The author defined the research plan, carried out all the electrochemical measurements, interpreted the results and wrote the publication under the supervision of Prof. Jari Koskinen and advice of Prof. Tomi Laurila. The electrochemical test strips were fabricated together with Ilkka Varjos and Bjørn F. Mikladal. Antti Peltonen prepared the cross-section samples and carried out the SEM imaging of the SWCNT/Nafion electrodes. Ph.D. (M.D.) Tuomas Lilius and Prof. Eija Kalso contributed with expert medical opinions during the writing of the publications.

List of Abbreviations

AA	ascorbic acid
AAG	a1-acid glycoprotein
aC	amorphous carbons
BDD	boron doped diamond
BSA	bovine serum albumin
CNF	carbon nanofibers
CO	Codeine
CSF	cerebrospinal fluid
CV	cyclic voltammetry
CVD	chemical vapor deposition
CYP	cytochrome P450
DA	dopamine
DAC	dopaminechrome
DAQ	dopamine quinone
DBS	deep brain stimulation
DHA	dehydroascorbic acid
DKG	2,3-diketogluonic acid

DLC	diamond-like carbon
DOPAC	3,4-dihydroxyphenylacetic acid
DOS	density of states
DPV	differential pulse voltammetry
EDS	energy dispersive X-ray spectroscopy
EDTA	ethylenediaminetetraacetic acid
EIS	electrochemical impedance spectroscopy
EW	equivalent weight
FBS	foetal bovine serum
$FcMeOH^{0/1+}$	ferrocenemethanol redox couple
$FcTMA^{+/2+}$	ferrocenylmethyl-(trimethylammonium) redox probe
FCVA	filtered cathodic vacuum arc
$Fe(CN)_6^{4-/3-}$	ferrocyanide redox couple
fMRI	functional magnetic resonance imaging
FTIR	Fourier transform infrared spectroscopy
FY	fluorescence yield
GC	glassy carbon
GO	graphene oxide
HiPCO	high-pressure carbon monoxide
HOPG	highly oriented graphitic carbon
ICH	International Council for Harmonisation of Technical Requirements for Pharmaceuticals for Human Use
$IrCl_6^{3-/2-}$	hexachloroiridate(IV) redox couple
ISR	inner sphere redox
IUPAC	International Union of Pure and Applied Chemistry
LC–MS–MS	liquid chromatography with tandem mass spectrometry
LDAC	leucodopaminechrome
L-DOPA	l-3,4-dihydroxyphenylalanine
LOD	limit of detection
LOQ	limit of quantitation

MO	Morphine
MWCNT	multi-walled carbon nanotubes
NAD	nicotinamide adenine dinucleotide
NADH	nicotinamide adenine dinucleotide (NAD) + hydrogen
NAPQI	N-acetyl-p-benzoquinone imine
NEXAFS	near edge X-ray absorption fine structure
NSAID	non-steroidal anti-inflammatory drugs
OSR	outer sphere redox
PA	Paracetamol
PEN	polyethylene naphthalene
PET	polyethylene terephthalate
PET	positron emission tomography
PLD	pulsed laser deposition
POC	point-of-care
PRGO	partially reduced graphene oxide
PTFE	polytetrafluoroethylene
QRE	quasi-reference electrodes
RBM	radial breathing modes
$Ru(bpy)^{2+}$	tris(bipyridine)ruthenium(II) redox probe
$Ru(NH_3)_6^{2+/3+}$	hexaammineruthenium(III) redox couple
SCE	saturated calomel electrode
SECCM	scanning electrochemical cell microscopy
SEM	scanning electron microscopy
SPCE	screen-printed carbon electrode
SSRL	Stanford Synchrotron Radiation Lightsource
STEM	scanning transmission electron microscopy
SWCNT	single-walled carbon nanotube
ta-C	tetrahedral amorphous carbon
TEM	transmission electron microscopy
TES	transition-edge sensor

TEY	total electron yield
TFE	tetrafluoroethylene
UA	uric acid
UV-Vis-NIR	ultraviolet-visible-near infrared spectroscopy
vHS	van Hove singularities
XES	X-ray emission spectroscopy
XRR	X-ray reflectivity

List of Symbols

ν	scan rate [mV/s]
ΔE_p	peak potential separation
I_{pa}/I_{pc}	peak current ratio
k^o	heterogeneous electron transfer coefficient (at formal potential)
σ	standard deviation
R_s	solution resistance [Ω]
m_T	mass transfer coefficient
Λ	kinetic parameter (dimensionless)
F	Faraday constant
D	diffusion constant
R	gas constant
T	temperature (K)
ψ	kinetic parameter (dimensionless)
C_{dl}	double-layer capacitance [μF/cm²]
A	electrode area [cm²]
R_{ct}	charge transfer resistance [Ω]
n	number of electrons
α	transfer coefficient (dimensionless)
c_O^b	bulk concentrations of the oxidized species
c_R^b	bulk concentrations of the reduces species
ω	angular velocity [rad/s]
C_s	spherical aberration
E^0	electrode standard potential

E	electrode potential
pI	isoelectric point
pK_a	logarithm of the acid dissociation constant

1 . Introduction

1.1 Background

Most healthcare systems are reactive, and the treatments are not individualized. This is despite the well-established knowledge that the human metabolome and the metabolism of drugs are affected by our personal attributes, such as genetics, age, diseases, sex, other concurrent drugs, and what we eat and drink. Realizing personalized healthcare requires more cost-effective analytical methods and new technologies that allow for decentralized analysis of biological samples. Such technologies can mitigate the increasing healthcare burden due to an aging population, as well as improve the safety and efficacy of a wide range of treatments. Moreover, point-of-care (POC) testing has the potential to expedite decision making and treatment in the clinical setting and has thus become increasingly popular[1].

Analgesics are widely used to treat post-operative, acute and chronic pain, and cancer pain[2,3]. It has been estimated that up to 19 % of Europeans suffer from chronic pain and it is a major source of disability. Moreover, chronic pain is also a significant cause of lost productive working time.[4] Clinicians who care for patients with chronic pain often struggle to provide effective pain management, while avoiding the support of addiction behaviors and substance abuse[5]. The efficacy of a certain dose of analgesic can be highly individual. Extreme case examples are prodrugs, such as codeine and tramadol, that require biotransformation into their active metabolites[6]. Misuse of prescription painkillers is also a growing problem and overdoses can cause significant side-effects and even death[7,8]. In the United States alone, in 2017 more than 70 000 people died from drug overdose, out of which 67.8 % were related to opioids[8]. In addition, paracetamol poisoning is currently the leading cause of liver failure in the United States and Europe[9,10]. In fact, it is so common that the National Academy of Clinical Biochemistry has endorsed screening for acetaminophen in all patients who present with intentional drug overdose[11].

The quantitative POC determination of analgesics from less invasive capillary blood samples could be highly beneficial, both in differential diagnosis of intoxication, and as an enabler of individualized pain treatments. At present, small molecule analysis is commonly carried out using gas chromatography or liquid chromatography, coupled with mass spectrometry. These methods are considered to provide the ultimate performance in selectivity and sensitivity, but require time-consuming sample treatments and highly skilled personnel. Semi-rapid tests based on spectrophotometric immunoassays are also increasingly available for emergency care of suspected poisoning[12,13]. This method is, however, also confined to specialized laboratories and is poorly suited for point-of-care (POC) testing. In addition, various lateral flow immunoassays are also available for various drug molecules, such as acetaminophen and opioids[14,15]. While immunoassays enables the measurements of dozens of proteins and other

analytes in biological samples to help in establishing the diagnosis and prognosis of disease, the detection of small molecules remains challenging, since they are too small to bind to the two different binding agents required for a sandwich-type assay. Currently there is no technology available for near real time detection of analgesics from small blood samples.

Many drug and biomolecules are electrochemically active and can be readily electrochemically detected by monitoring the current due to their redox reactions. Therefore, electroanalytical methods can be used for highly sensitive detection of small molecules in blood samples[16,17]. In addition, they show great potential for continuous monitoring of drug and biomolecules using wearable or implantable sensors[18–21]. The rapid technological advancements and increasing availability of miniaturized and more affordable wireless potentiostats, have made electroanalytical methods more attractive in point-of-care testing. Further, miniaturized potentiostats on chip have also been fabricated and used for detection dopamine (DA)[22]. The detection of dopamine is of special interest, for research into neurochemistry and neurodegenerative diseases[19,23]. Advances in printing and microfabrication technologies have enabled low cost mass production of fully integrated electrochemical platforms, with working, reference and auxiliary electrodes. Direct electrochemical determination of uric acid (UA)[17] and chlotazepine[24] have been demonstrated from small volumes of whole blood. Wearable electrochemical sensors for direct detection of trace metal[25], glucose[26], uric acid[20] and tyrosine[20] have also been reported.

Miniaturized electrochemical sensors can provide a combination of sensitivity, selectivity, and spatial and temporal resolution, unmatched by competing techniques and thereby allow for real time monitoring of metabolic processes[23]. The simple instrumentation, combined with other advantages summarized in Table 1, has resulted in electroanalytical techniques being increasingly used for detection of a wide range of bio and drug molecules, including neurotransmitters, neuro drugs, antibiotics, antiallergic drugs, antihypertensive drugs, pesticides and insecticides, and anticancer drugs[27].

Table 1. Advantages and disadvantages of electrochemical detection.

Advantages	Disadvantages
Low price	Limited selectivity
Low specialization required	Rapid Passivation in biological fluids
Small sample volume (few to tens of μL)	Life time of electrodes
Small analyte loss	
Minimal/no sample processing	
Simple instrumentation	

Conventional carbon electrodes, such as glassy carbon (GC), highly ordered pyrolytic graphite (HOPG) and boron doped diamond (BDD), are widely used in electroanalytical applications due to their large water window, low background current and potential for wide range of surface chemistry modifications[28]. Microfabrication compatible electrode materials, such as pyrolyzed photoresist, amorphous carbon and diamond thin films, as well as screen-printed carbon electrodes, are also increasingly used. All these electrodes typically suffer from limited

selectivity and rapid inactivation due to fouling in complex biological matrices. The selectivity and fouling resistance of these electrodes can, however, be significantly improved by chemical treatments and modifications with carbon nanomaterials and polymer coatings[29–31].

Carbon nanomaterials have additional attractive properties including large surface area, tailorable surface chemistry and electrocatalytic properties. Advances in carbon nanotechnology are making the novel chemical and physical properties of carbon nanomaterials more easily available. For example, industrial quantities of CNTs[32] and graphene oxides and reduced graphene oxide can now be produced. Most drug and biomolecules are so called "inner sphere analytes", whose voltammetric response is highly dependent on the electrode surface chemistry. Due to the ease of functionalization with a wide range of functional groups, carbon nanomaterials show significant potential for improving selectivity of electroanalytical chemistry. Simultaneously, the variations in surface chemistry and morphology, upon modification with carbon nanomaterials, can also reduce the fouling of the electrode[29]. Advancements in incorporating highly electrocatalytic, and functionalized nanomaterials with large surface area, has resulted in renewed interest in screen printed electrodes.

An overwhelming majority of publications still study the electrochemical detection of the neurotransmitter dopamine, but the detection of other drugs is also increasing[33]. Recovery tests in complex biological matrices are also increasingly reported. Despite the significant progress of using modified electrodes for multianalyte detection in complex biological matrices, especially in the selective detection of dopamine, most studies measuring blood samples still rely on considerable dilution and further processing of the samples[30]. We hypothesize that all the requirements of electrochemical POC detection can be simultaneously achieved by combining the advantageous properties of carbon nanomaterials with permselective membranes, into multilayer electrodes. In this approach, a permselective membrane filters out the bulk of the endogenous and some xenobiotic interferents. Additional selectivity is achieved by tailoring the morphology and surface chemistry of the carbon nanomaterials.

The overall objective is to realize a concept of a multilayered electrode structure based on carbonaceous nanomaterials for point-of-care diagnostics that is feasible for mass production. In order to achieve this overall aim one needs to address the following targets: (i) In-depth characterization of the chosen carbon allotropes, (ii) assessment of their electrochemical properties and linking them with the physicochemical ones, (iii) evaluate the sensing performance of the electrodes in biological matrices for the chosen analytes, (iv) carry out initial tests for manufacturability and integration of the carbon nanomaterials with polymer membranes to realize multilayered structures, and (v) provide a proof-of-concept electrochemical assay for detection of drugs in whole blood samples.

1.2 Objectives and scope

There is an apparent need for more selective, sensitive and fouling resistant electrode materials for electroanalytical applications. In some applications, these requirements need to be met without compromising the response time of the sensor. Moreover, implantable and wearable sensors must also show biocompatibility and long-term stability in harsh environments. This further highlights the fact that, each application has its own unique set of requirements on

sensitivity, selectivity, fouling resistance and biocompatibility, and this must be addressed individually for each application. To achieve this, both increased understanding of the interactions between the analytes and the electrode, as well as improved control of electrode properties such as surface chemistry and nanostructure, are needed.

With the aim of developing highly selective and sensitive carbon electrode materials for implantable sensors and *in vitro* diagnostics, the main objectives of this thesis are as follows:

(i) Identify carbon thin film materials suitable for mass scale microfabrication of electrochemical sensors

(ii) Deepen the understanding of the link between the surface chemistry of the used materials and their electrochemical properties

(iii) Fabricate sensitive and selective sensors based on carbon nanostructures

(iv) Combine the favorable properties of carbon electrodes with polymer membranes to improve the performances in complex biological matrices

(v) Fabricate a mass production compatible prototype electrode capable of in vitro detection of small molecules in blood samples.

Based on these objectives, we have investigated the use of tetrahedral amorphous carbon (ta-C), modified ta-C and SWCNT thin films as electrochemical electrodes for detection of analgesic drugs and dopamine. In depth characterization of both these materials are carried out in Publications I-IV. In publication I, we study the feasibility of replacement of conventional carbon electrodes with Ti/ta-C thin films electrodes, and their further modification with partially reduced graphene oxide (PRGO) to confer improved selectivity and sensitivity towards dopamine.

The other area of focus in this work is on the in vitro diagnostics of analgesics, with the aim of developing electrodes capable of selective and sensitive nanomolar point-of-care detection in untreated blood samples. To this end, in publication IV, we study the effect of surface chemistry modification of Ti/ta-C thin films electrodes, to induce selectivity towards morphine in the presence of paracetamol. In Publications II and III, we characterize the surface and bulk chemical properties of SWCNT thin film electrodes, and present their applicability for electrochemical detection of the synthetic opioid fentanyl, respectively. In Publication V, we further combine the advantageous properties of SWCNT network electrodes with Nafion membranes, to realize a selective detection of morphine and codeine in human plasma. Finally, in Publication VI we demonstrate mass production of the multilayer electrode, for quantitative point-of-care detection of paracetamol. Table 2 summarizes the work carried out in publications I-VI, their main aim, and the used characterization methods.

To deepen the understanding of the electrochemical and physicochemical properties of the Ti/ta-C electrode, the author has also contributed to further research in[34–36]. In addition, further modifications of the Ti/ta-C electrodes were carried out in [37,38], to improve upon the properties of the ta-C electrodes. Because commercial potential was found, two patent applications have been drafted and filed alongside of this work.

Table 2. Summary of the electrode materials, aim and used characterization methods in Publications I-IV

Publication	Electrode	Aim	Characterization
I	PRGO modified Ti/ta-C electrode	Fabricate a highly sensitive and selective sensor, usable with fast response-time methods	SEM, Raman, FTIR, XPS, XAS, CV, DPV, EIS
II	SWCNT	Characterize detailed surface and bulk chemistry of aerosol CVD SWCNT thin films	SEM, TEM, Synchrotron based XPS, XAS and XES
III	SWCNT	Demonstrate the advantageous electrochemical properties of SWCNT thin films on insulating substrates. Show significant improvement in the sensitivity towards the lipophilic synthetic opioid fentanyl	Raman, UV-Vis, XPS, TEM, EDS, XPS, XAS
IV	Anodically pretreated Ti/ta-C	Apply surface modification for selective detection of morphine in the presence of paracetamol	Raman, AFM, XPS, CV, EIS
V	SWCNT/Nafion	Combine the advantageous properties of SWCNT thin film electrodes with Nafion, to reduce the matrix effect in human plasma samples as well as enable simultaneous selective detection of morphine and codeine	SEM, Raman, TEM, EDS, CV, DPV
VI	SWCNT/Nafion	Demonstrate sensitive and selective detection of paracetamol in finger-prick whole blood	SEM, CV, DPV

2 . Characterization methods

In this chapter, the used characterization methods will be briefly presented. Focus is based on their applicability and limitations in characterization of carbon nanomaterial thin film electrodes used in this work. Special emphasis will be placed on the electrochemical characterization and synchrotron based X-ray spectroscopy techniques utilized in this thesis.

2.1 Electrochemistry

Electrochemistry is a powerful tool to probe electron transfer reactions. In electrochemical reactions, redox reactions occur via heterogeneous electron transfer from a molecule to the working electrode (oxidation), and from the electrode to a molecule (reduction). By the use of an external power source, such as a potentiostat, the voltage of the electrode can be controlled and swept over a potential window in a controlled fashion. In this thesis, we use the IUPAC convention, where oxidation occurs at a positive (anodic) potential and is associated with a positive current. Whereas, reduction occurs at the negative (cathodic) potential and is associated with a negative current.[39] Different molecules oxidize at different potentials and therefore limited selectivity can be achieved with voltammetric techniques.

2.1.1 Cyclic voltammetry

Cyclic voltammetry (CV) is a simple and fast technique to study electrochemical reactions. It is a powerful and popular transient technique, employed to study electron transfer-initiated chemical reactions. It is also commonly used to assess the performance of electrochemical sensors. In publications I, III, IV and VI, CV is used to study the electron transfer properties of the electrode materials with outer sphere redox probes. In Publication I, CV is also used to detect dopamine in the presence of ascorbic acid (AA).

In CV experiments, a potential is applied between the working and counter electrodes, and is scanned with a predetermined scan rate (ν). The scan is started at the lower end and performed until the upper limit, also called the switching potential. When the upper limit is reached, the scan direction is reversed so that the scan rate becomes $-\nu$. During one or many such scans, the current is recorded and usually plotted as function of the potential, yielding the cyclic voltammogram. The voltammogram can be regarded as the electrochemical map of the system under study. The potential window where measurements can be carried out is, however, limited by the oxidation and reduction potentials of the supporting electrolyte. For aqueous electrolytes this is called the water window, and is limited by oxygen and hydrogen evolution at the anodic and cathodic ends, respectively. The thermodynamic water window is always 1.23 V, but in practice, due to kinetic limitations of carbon electrodes, the kinetic water window can

exceed 3.5 V[39–42]. Figure 1A shows an example of a cyclic voltammogram of a reversible redox reaction, involving the transfer of 1 electron.

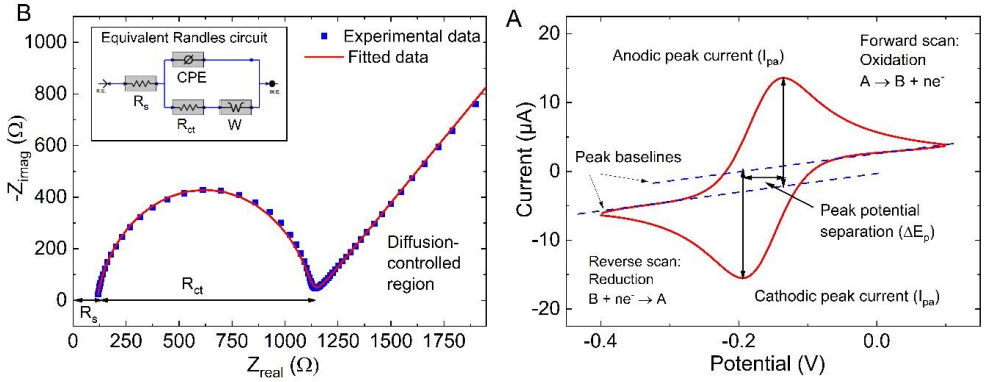

Figure 1. A) a typical cyclic voltammogram and B) a Nyquist plot of a 30 nm ta-C electrode. The inset in B shows the common Randles equivalent circuit used to fit the experimental data.

The most important parameter of the cyclic voltammogram is the peak potential separation (ΔE_p), which gives information about the electron transfer kinetics of the reaction, and the reversibility of the reaction with the used scan rate. When a reaction is completely reversible, the ΔE_p will be equal to 59/n mV, where n is the number of electrons transferred in the reaction. For a completely reversible reaction, all the oxidized species should also be reduced on the reverse scan. From this, it follows that the peak current ratio (I_{pa}/I_{pc}) must be equal to 1. A value deviating from 1 indicates complications in the oxidation process, or coupled homogeneous chemical reactions of the reaction products. Chemical reaction with water can render some analytes, such as ascorbic acid and fentanyl, completely irreversible at most scan rates.

The heterogeneous electron transfer coefficient (k^0) at formal potential is used as an intrinsic measure of the kinetics of a redox reaction. A large k^0 value indicates fast reaction kinetics. The k^0 is specific to a system, that is - a certain redox probe under specific conditions with a specified electrode material, and is therefore an important parameter for comparing electrode materials. The reversibility of an electrochemical reaction is determined by the relative rates of k^o and the rate of mass transfer, expressed as the mass transfer coefficient (m_T). Matsuda and Ayabe[43] proposed the parameter Λ that is related to k^o and and m_T as:

$$\Lambda = \frac{k^0}{m_T} = \frac{k^0}{\left(\frac{FDv}{RT}\right)^{\frac{1}{2}}} \qquad (1)$$

where F is the Faraday constant, D the diffusion constant of the oxidizing species, v the scan rate, k^0 is the standard reaction rate constant, R is the gas constant and T is the temperature.

They further suggested limits for reversible, quasi-reversible and irreversible cases as follows:

Reversible:	$\Lambda \geq 15$	$k^0 \geq 0.3\,(v)^{\frac{1}{2}}\,cm\,s^{-1}$
Quasi-reversible:	$15 > \Lambda > 10^{-3}$	$0.3 \times v^{\frac{1}{2}} > k^0 > 2 \times 10^{-5}\,(v)^{\frac{1}{2}}\,cm\,s^{-1}$

Irreversible: $\Lambda \leq 10^{-3}$ $k^0 \leq 2 \times 10^{-5} (v)^{\frac{1}{2}} cm\, s^{-1}$

These limits apply when T = 298 K, n = 1 and α ~0.5, and are dependent on the used scan rate. At higher scan rates, the diffusion layer becomes thinner and therefore mass transport becomes faster. Therefore, any reaction can be made irreversible when sufficiently fast scan rates are used. Nicholson[44] further proposed the kinetic parameter ψ that can be used to relate the ΔE_p to k^o with the following equation:

$$\psi = \Lambda \pi^{-1/2} = \frac{k^0}{\left(\frac{\pi F D \nu}{RT}\right)^{1/2}} \quad (2).$$

ψ can be determined by the measured ΔE_p assuming that T=298 K and α = 0.5, and when the uncompensated resistance is small enough that its effect on the ΔE_p is negligible. In addition, absence of adsorption, or chemical reactions, is assumed, and one of the electron transfer steps should be the rate determining step.

The current in the CV is a combination of faradic and non-faradic processes. The faradic currents are due to electron transfer across the electrode-solution interface that take place when the analyte undergoes redox reactions, while non-faradic processes do not involve electron transfer across the electrode-solution interface. The electrical double layer acts like a capacitor in CV experiments and the capacitive charging current can be described with the equation:

$$i = AC_{dl}\nu, \quad (3)$$

where A is the geometrical electrode area, C_{dl} the double layer capacitance and ν the scan rate. For this reason, the double layer capacitance may be measured with CV measurements. Most electrodes materials always have functional groups or metals on the surface, that may be electrochemically active and cause currents due to redox reactions. As the capacitive current also contains this faradic component, the capacitive current measured with cyclic voltammetry is often referred to as the apparent pseudocapacitance.

While Farady's law states that the oxidation and reduction peak currents arise due to the amount of species undergoing redox reactions, the background currents make the accurate measurement of the peak currents difficult. Due to these background currents, the measurements of the peak currents in the cyclic voltammograms is not precise enough for quantitative analysis, and is better suited for qualitative analysis. The background current can also cause deterioration in sensor performance, and has typically limited the CV measurements to relatively narrow concertation ranges of approximately 10 μM to 10 mM[45].

Because all drug and biomolecules give a different sensitivity (current/concentration) with different electrodes, the sensors have to be calibrated with known standard solutions. The background current and its stability are important parameters for electrochemical sensors, as they affect the limit of detection (LOD) and limit of quantitation (LOQ) obtained as

$$LOD = \frac{3.3\sigma}{S} \quad (4)$$
$$LOQ = \frac{10\sigma}{S} \quad (5)$$

where σ is the standard deviation of the background current or a current measured with a low concentration of analyte and S is the sensitivity, usually given as μA/μM for electrochemical sensors.[46] Ideally, a high signal must be achieved in combination with a stable background current. In some cases, modified electrodes with much improved sensitivity may also increase the background noise to the same extent, leading to no improvement in detection limits[47].

2.1.2 Outer vs inner sphere probes

In this thesis, both inner sphere and outer sphere redox probes are used. Outer sphere redox (OSR) probes are insensitive to the surface chemistry of the electrode, and are generally considered to lack adsorption and electrocatalytic steps and often have low reorganization energies[28]. Therefore, OSR probes can be used to probe the electronic properties of the electrode material. Commonly used OSR redox probes include hexaammineruthenium(III) ($Ru(NH_3)_6^{2+/3+}$), hexachloroiridate(IV) ($IrCl_6^{3-/2-}$) and ferrocenemethanol ($FcMeOH^{0/1+}$)[28,48]. It should be noted that most OSR redox systems have been experimentally established, mostly by the absence of effect on their peak separation, after modification of test electrodes with physiosorbed or chemisorbed monolayers. While such experiments imply that significant changes in surface chemistry have no observable effects on electron transfer kinetics, they do not rigorously establish a redox system as outer sphere[28]. For example, weak adsorption of ferrocene derivatives on highly oriented pyrolytic graphite electrodes has been reported[49]. This suggests that $FcMeOH^{0/1+}$ may not behave as a true OSR probe under all conditions, despite the fact that it is widely regarded as an OSR probe.

In contrast to OSR probes, inner sphere redox (ISR) probes depend on the surface chemistry of the electrode. Their oxidation generally requires interactions with the electrode surface and formation of a common ligand[42]. The electrochemical activity of an ISR probe may depend on adsorption or surface functional groups on the electrode[28]. Therefore, some ISR probes may also be used to probe the electrode surface chemistry. For example, the oxidation of the $Fe^{2+/3+}$, $Eu^{3+/2+}$ and $V^{3+/2+}$ have been reported to be surface oxide sensitive, and specifically carbonyl groups can catalyze the oxidation of $Fe^{2+/3+}$.[28] On the other hand, Chen and McCreery suggested that the commonly used redox probe Ferrocyanide ($Fe(CN)_6^{4-/3-}$) is surface sensitive, but that, oxides have only minor effect in its electrochemistry[48]. Its electrochemical oxidation has also been shown to depend on the cation concentrations of the supporting electrolyte, and involves changes in the solvation shell[50–52]. Thus, we will not consider $Fe(CN)_6^{4-/3-}$ as an outer OSR probe in this work. Most drugs and biomolecules are considered to be ISR systems, and their electrochemistry may therefore be influenced by altering the surface chemistry of the electrode. Nevertheless, studies should be carried out with both ISR and OSR probes, as reversible electron transfer with an outer sphere redox probe does not guarantee fast electron transfer kinetics with ISR probes.

2.1.3 Electrochemical impedance spectroscopy

In electrochemical impedance spectroscopy (EIS), the impedance of the electrochemical system is measured as a function of the applied frequency. A constant potential is applied to the working electrode of the cell, on top of which a sinusoidal input voltage with amplitudes in

the range of 5-20 mV is applied. The current output is recorded over a desired frequency range. The results are often plotted as Bode plots (impedance and phase as function of frequency) or as a Nyquist plot (imaginary component of impedance as a function of the real component in the Randles circuit).

The Nyquist plot, shown in Figure 1B, is commonly reported, as it provides important information about the electrochemical properties of both the working electrode and the electrochemical cell. From the Nyquist plot, the solution resistance (R_s) and charge transfer resistance (R_{ct}) can be obtained visually. More accurate results can be obtained by modelling the circuit and fitting the theoretical equivalent circuit to the experimental data, as shown in Figure 1B. The commonly used equivalent circuit is the Randles circuit, that contains a solution resistance in series with a double layer capacitance, arranged in parallel with a charge transfer resistance and a Warburg element. The Warburg element is used to model the impedance due to diffusion in an electrochemical cell. In the diffusion-controlled region, the lower frequencies used allow for time for diffusion. This shows as a line with a 45 ° slope in the Nyquist plot. With many modified electrodes, the roughness and porosity will cause unideal behavior, leading the experimental data to a deviation from the theoretical model below the fitted line. Therefore, the Warburg element should only be used in case of semi-infinite diffusion. More complicated porous modified electrode and / or study and use of surface sensitive redox probes, however, usually require more complicated equivalent circuit models.

When EIS is used to study the electron transfer resistance, R_{ct} is the most important parameter, as it is a measure of the rate of electron transfer and defines the kinetically controlled region of the Nyquist plot. In the kinetically controlled region, the R_{ct} can be described as

$$R_{ct} = \frac{RT}{nFi_0}, \quad (6)$$

where R is the gas constant, T is the temperature, n is the number of electrons transferred in the reaction and $i_0 = Fk^0c$, where c is the analyte concentration and k^0 the standard reaction rate constant at formal potential. By combining, we obtain

$$k^0 = \frac{RT}{n^2F^2AR_{ct}(c_O^b)^{\alpha}(c_R^b)^{1-\alpha}} \quad (7)$$

where, A is the geometrical area of the electrode α is the transfer coefficient (usually = 0.5, with OSR probes), c_O^b and c_R^b are the bulk concentrations of the oxidized and reduced species, respectively. Equation 7 shows that we can obtain the k^o with EIS. In Publication I and IV, we use EIS to determine the k^o of ta-C, PRGO modified ta-C and anodically treated ta-C electrodes. As we show in Publication I, EIS is better suited for determining the k^o than CV experiments with Nicholson's method, which produces relatively large errors when electrodes show quasi-reversible behavior, but with ΔE_p that are close to reversible.

In the high frequency region, faradic reactions contribute only very little to the measured current. Therefore, the capacitance arising from the rearrangement of the electrical double layer can be more accurately measured with EIS (provided that a good fit is achieved). Due to inhomogeneities of the electrode surface, the double layer capacitance does not, however, behave like an ideal capacitor. For this reason, a constant phase element is often used to

account for these inhomogeneities. Hsu and Mansfeld[53] proposed the following equation for determining the C_{dl} based on EIS measurements

$$C_{dl} = A_{dl}(\omega)^{a-1}, \qquad (8)$$

where A_{dl} and a are parameters of the constant phase element and ω is the angular frequency defined as $\omega = 2\pi f$. The frequency f, is obtained by fitting the Nyquist plot, and corresponds to the highest value on the semicircle in the kinetically controlled region. The constant a can have values between 1 and 0, and describes the deviation from an ideal capacitor, with a value 1 describing an ideal capacitor.

In Publication I, we use EIS to study the electron transfer at Ti/ta-C and partially reduced graphene oxide (PRGO) modified Ti/ta-C electrodes. In Publication IV, we study the effect of anodic treatment on the electron transfer. Both works utilize the outer sphere redox probe $Ru(NH_3)_6^{2+/3+}$ and the applied DC potential is the formal potential, where the oxidized and reduced forms are in thermodynamic balance.

2.1.4 Differential pulse voltammetry

Differential pulse voltammetry (DPV) is a potential step technique widely used in electrochemistry due to its better selectivity and better signal-to-noise ratio, compared to linear sweep techniques, such as cyclic voltammetry. The applied wave form is a combination of pulses with staircase wave form. The wave form, together with common parameters, is shown in Figure 2A.

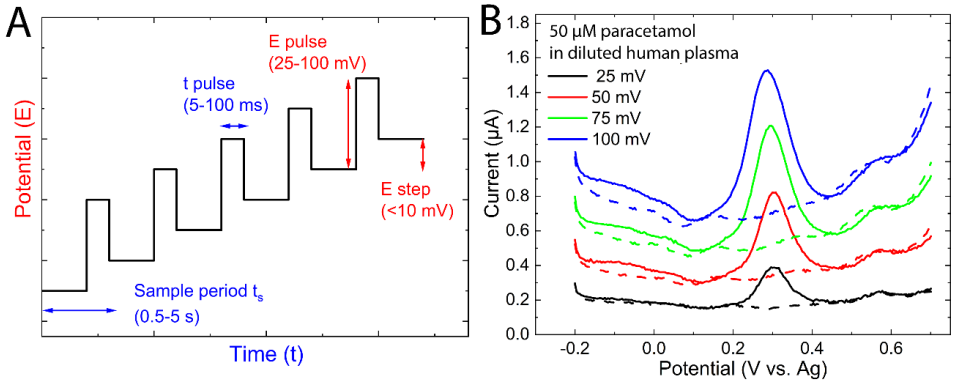

Figure 2. A) The waveform applied in differential pulse voltammetry measurements as well as the typical used measurement parameters. B) The effects of different pulse amplitude on the faradic paracetamol peak (solid line) as well as the blank background (dashed line) in human plasma. Figure 2B adapted from Publication VI.

The current is measured just before and at the end of the pulse, and the differential of these currents is plotted against the staircase potential. The measured current is a combination of Faradic and capacitive contributions. Because the capacitive contribution dies away much faster (often within 1-2 ms) than the Faradic contributions, the differential current contains mostly Faradic contributions. With carefully chosen parameters, the signal-to-noise ratio may be greatly improved as shown in Figure 2A. Usually, the pulse time is chosen so that no time is

allowed for natural convection, and thereby perturbation of the expected diffusional response, thus improving the selectivity. For these reasons, DPV is often used for trace analysis. Generally, a longer pulse time will decrease contribution of the capacitive current, but too long pulse time will reduce the signal, due to depletion of analyte[54]. Another factor increasing the sensitivity of DPV is the pulse step, and as seen from Figure 2B an increase in pulse amplitude leads to higher sensitivity, but also an increase in capacitive background current. The main drawback of DPV is the limited temporal resolution, as scans usually take around 1 min. In Publication I, we show the improved sensitivity and selectivity that can be achieved with DPV, as compared to the faster cyclic voltammetry.

2.2 Synchrotron based soft X-ray spectroscopy

2.2.1 Introduction to soft X-ray based spectroscopy

Soft X-ray spectroscopy is particularly powerful for probing of the local electronic structure of a material and is thus particularly well suited for studying carbon nanomaterials. It is also well suited for studying light elements and 3d transition metals, that are often used as catalysts for synthesis of carbon nanomaterials. In addition, most elements can be excited with soft X-rays, making it a powerful method for chemical analysis.

In X-ray spectroscopy, a sample is irradiated with monochromatic X-rays and the emitted electrons and photons are analyzed by energy. The excitation process and decay processes are shown in Figure 3. In the photoelectric effect, the incident beam causes emission of electrons leaving vacancies. With X-ray radiation, the electrons in the lowest atomic orbitals can also be emitted, leaving core-holes. The emitted electron is called a photoelectron, and when scattered elastically, has a kinetic energy that is specific to the atom and orbital from which it was emitted.[55]

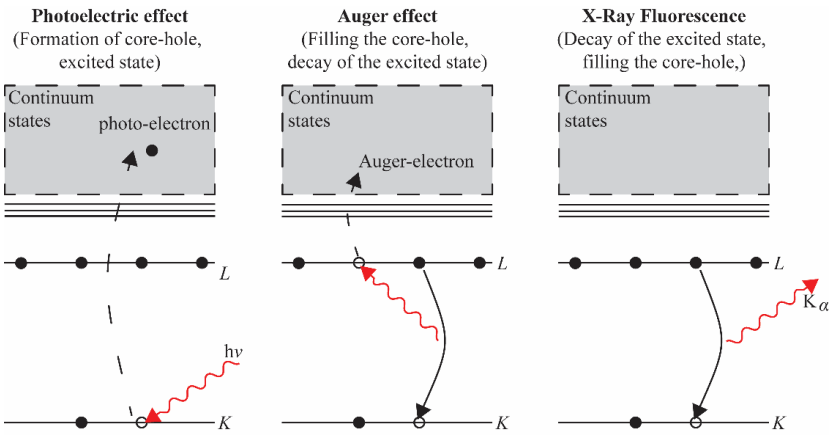

Figure 3. Schematic representation of the photoelectric effect, Auger effect and X-ray fluorescence.

When the excited state is relaxed, via filling of the core hole with an electron of lower binding energy, either fluorescence photons or Auger electrons are emitted as a result[55]. In the soft X-ray regime, the core-hole decay is dominated by nonradiative processes, in particular Auger transitions and only ~1% of the decays are radiative[56]. In the radiative X-ray decay, the

difference in energy will be emitted as X-rays that are characteristic to each element. This process is called X-ray fluorescence, and is used for chemical analysis. In the Auger process, an outer electron falls into the inner orbital vacancy, emitting a second electron called an Auger electron. The Auger electron has a kinetic energy equal to the difference in energies of the initial ion and the doubly charged final ion.[55]

The probabilities of electrons interacting with matter far exceed those of the photons. While soft X-rays can excite samples to a few micrometers, only the electrons that originate few nm from the surface can be emitted without energy loss[55]. In soft X-ray spectroscopy, photoelectrons escape the sample from 5-10 nm from the surface. Whereas Auger electrons have very short mean free paths, making Auger spectroscopy able to probe only the very surface (< 2 nm) of the sample[57]. Fluorescent photons on the other hand can be used to probe to depths of at least 50-100 nm[56]. Due to the small mean free path of photoelectrons, X-ray spectroscopy requires ultrahigh vacuum conditions, which places limitations on the samples that can be measured. For porous carbon nanomaterials, for example, outgassing can be a problem. Therefore, removal of volatiles is usually achieved by long-term pumping in a separate vacuum system.

Synchrotron beamlines are often equipped with several detectors enabling the simultaneous analysis of Auger electrons, photoelectrons, total electron yield (TEY) and fluorescence yield (FY)[56]. In this way information from different depths can be obtained.

2.2.2 X-ray photoelectron spectroscopy

X-ray photoelectron spectroscopy is one of the most common methods for chemical analysis of nanomaterials. The incident radiation is usually generated with an Al K_α or Mg K_α source, as they provide sufficiently powerful beams with well-known stable energies[58]. The produced X-rays are reflected to a monochromator with Si mirrors, where a single wavelength is selected. The monochromatic beam then hits the sample with a fixed instrument dependent angle, exciting the sample through the photoelectric effect. This causes the emission of photoelectrons, which are collected with hemispherical or circular mirror analyzers. In this way, the energy allowed to reach the detector is scanned, leading to the collection of a spectrum, where the binding energy is plotted on the x-axis and the counts for each energy on the y-axis (see Figure 4).

The energy resolution is equipment dependent, but is also affected by the scan time. Similarly, the sensitivity is dependent on the collection time. Because each element has a unique set of binding energies, faster wide spectra are usually first acquired for quantitative elemental detection. An example of a wide spectrum from Publication II is shown in Figure 4. XPS detection limits are generally described as being in the 1 at% to 0.1 at% range, and depend on many factors, such as the measurement matrix[59]. To study the bonding of the samples, longer high-resolution scans are collected over the edges of interest. Figure 4 shows the C 1s spectrum of a SWCNT sample. A sharp peak is observed due to sp^2 carbon.

Variations in elemental binding cause chemical shifts that can be used to identify the chemical state of the electrode materials. Generally, binding to a more electronegative element causes shifts to higher binding energies and vice versa. Despite the chemical shifts, especially in the C1s spectra, the peaks are highly convoluted, and data must be extracted through deconvoluting by peak fitting, as shown in Figure 5. Prior to peak fitting, the energy shifts due

to charging have to be corrected. Therefore, known reference samples, usually Au, are used. In this thesis, we use cellulose filter paper (Whatman) as an in-situ reference for XPS. The binding energies were charge corrected using the 286.7 eV peak for carbon which is singly bonded to one oxygen atom, and 285.0 eV peak for aliphatic carbon[60].

As photoelectrons are readily absorbed by the sample, they can escape only from depths of approximately 0-10 nm below the surface. Because the electrons originating from below the very surface of the sample (> 1 nm depth) will experience energy losses, the peak intensity and the shape of the background can be used to provide limited depth information[61]. The highly surface sensitive nature of XPS, however, presents a problem for analyzing many nanomaterial-based electrodes, as they are often porous. Therefore, complementary measurements with bulk methods may be required.

In publication I, II, III and IV, we use XPS to study the difference in elemental composition. Furthermore, in Publications I and IV, XPS is also used to study the effect of chemical treatments of Ti/ta-C electrodes, as well as graphene oxide modified Ti/ta-C.

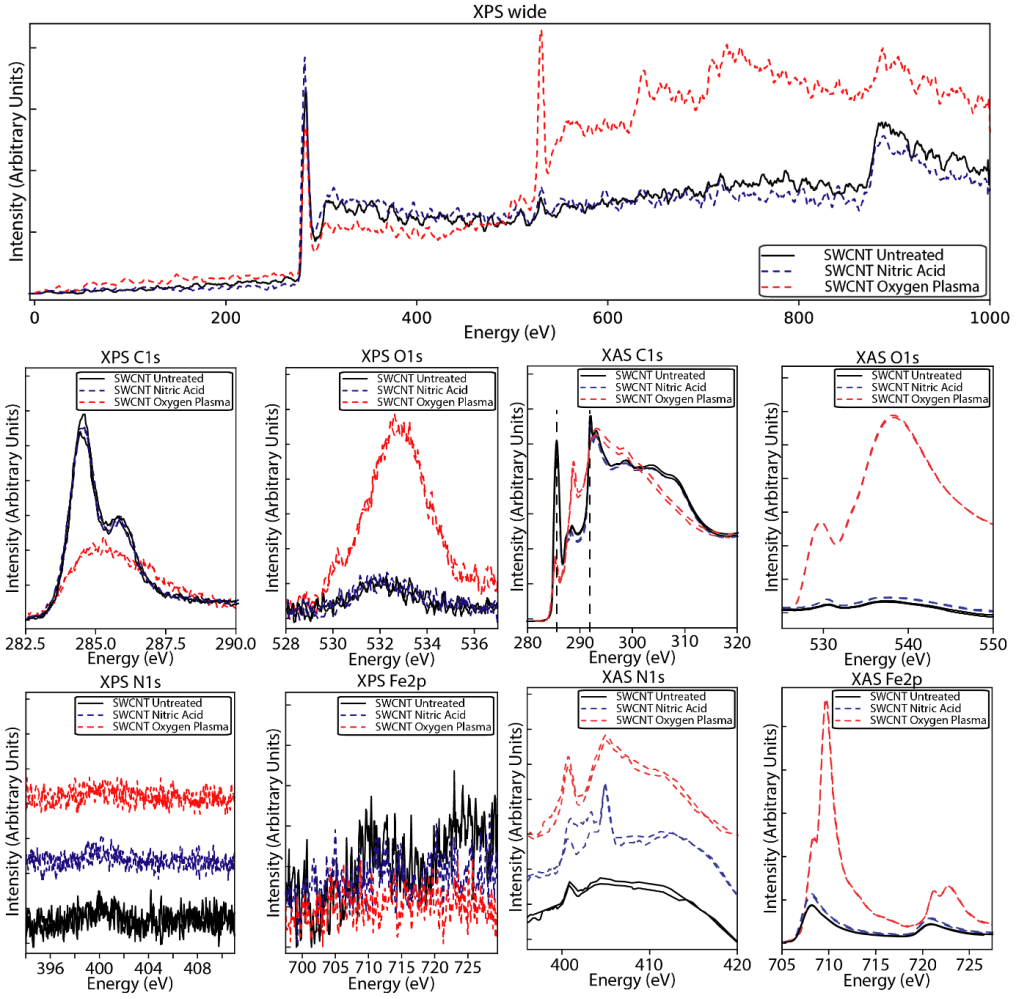

Figure 4. Comparison of synchrotron based XPS and XAS spectroscopies. Adapted from Publication II.

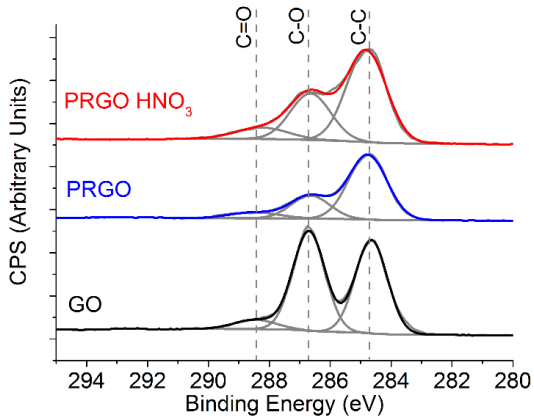

Figure 5. High-resolution C1s XPS spectra with peak fitting of GO, PRGO and nitric acid treated PRGO modified Ti/ta-C electrodes from Publication I.

2.2.3 X-ray absorption spectroscopy

Like in XPS, in X-ray absorption measurements (XAS), an incident X-ray beam is used to excite the studied sample. In XAS, the energy of the incident beam is scanned over an edge of interest. For this reason, XAS measurements require a synchrotron lightsource that produces continuous X-rays. X-ray absorption spectroscopy can provide element, site, symmetry, and spin selective information on the electronic structure of samples[56]. The high yield of Auger and secondary electrons in the decay of the excited state, combined with the ability to attain high energy resolution and large solid angles in electron detection, have driven total-electron-yield (TEY) XAS, and other electron-detected spectroscopies, to dominate in the soft X-ray regime[56]. In TEY mode, the sample-mounting rod is electrically isolated from the chamber, allowing for sample drain current to be measured. Many soft X-ray beamlines are also equipped with additional detectors, allowing for analysis of photoelectron, Auger electrons and fluorescent photons. By combining the data from these detectors, XAS spectra can be obtained from different depths of the samples. This is particularly powerful when porous nanomaterials or core-shell nanostructures are studied. In this thesis, XAS measurements were carried out at the beamlines 8-2 and 10-1 of Stanford Synchrotron Radiation Lightsource (SSRL) in TEY mode.

Because the energy is scanned over the edge, the excitation efficiency is much increased, leading to much improved sensitivity compared to XPS. Figure 4 shows the large differences in the high-resolution XPS and XAS spectra of the same SWCNT sample. The difference is especially pronounced in the N1s and Fe2p spectra, that are present at low concentrations.

Figure 6 shows a diatomic molecule along with the valence and continuum states. The transition of an electron from the 1s-shell to the continuum is the same process that occurs in XPS measurements. In addition to the excitation to continuum (shown in Figure 6), several excitations to valence states are also allowed, providing additional information. The combination of these transitions can be observed in the XAS spectrum, shown to the right in Figure 6. The near edge region called the near edge X-ray absorption fine structure (NEXAFS) for carbon is shown in Figure 6, and carries important information about the bonding of the sample. The ability to probe these unfilled states is a major advantage of the XAS method.[62]

This allows for the study of pre-edge features of carbon, including the π* transition that provides information about the sp^2 bonding in carbon samples. In addition, the carbon core exciton peak provides information about the long-range order of crystalline samples.[63–66] These features also proved information about defects on graphene and SWCNT samples. In Publication I, we show that this peak is absent in partially reduced graphene oxide that is highly defective and contains a relatively large amount of oxygen containing functionalities. In contrast, in publication III we show a clear long-range order peak for the SWCNT film with low defect density and amorphous carbon content.

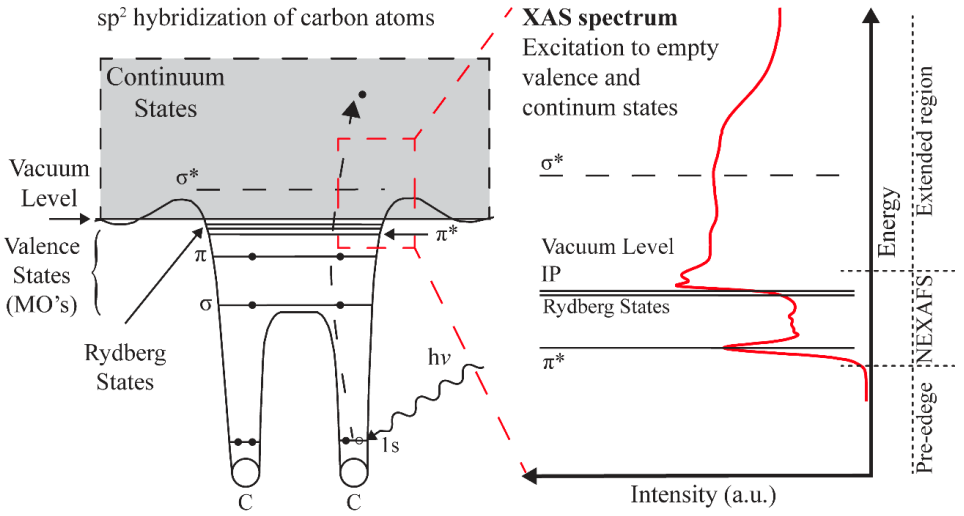

Figure 6. Schematic representation of a diatomic molecule with valence and continuum states on the left. On the right, the connection between the electronic structure of the samples and the XAS spectrum for a graphitic sample is shown.

Like in XPS, the bonding with neighboring atoms causes chemical shifts that can be used to identify chemical states. The C1s spectrum is particularly interesting for the study the surface chemistry of carbon nanomaterials, since oxygen and nitrogen containing functional groups have been proposed to significantly affect the voltammetry of inner sphere analytes, as will be discussed in Chapter 3. Nitrogen and oxygen can, however, cause similar chemical shifts in the C1s spectrum and therefore produce peaks at similar energies[67–71]. For this reason, the O1s and N1s spectra should be individually acquired to corroborate the assignments made in the C1s spectrum. Similar chemical shifts in the metal edges also reveal information about the oxidation state of metals, but with much improved sensitivity compared to XPS.

Despite the improved chemical selectivity compared to XPS, particularly complicated carbon materials, such as graphene oxides and amorphous carbon, still give highly convoluted spectra. Therefore, chemical information has to be extracted by peak fitting as shown in Figure 7 (from Publication I). In XPS, all the peaks in the C1s spectra are highly convoluted and the sp^2 and sp^3 peaks are separated by less than 1 eV[72]. In contrast, even highly convoluted XAS C1s spectra show well separated π* peak, providing information about the carbon bonding. Despite this benefit, the sp^3 peak is severely convoluted with peaks of oxygen and nitrogen containing functional groups, as well as the ionization potential and core exciton, if present. Nevertheless,

information about the oxygen containing functional groups and sp^2/sp^3 ratio may be extracted by peak fitting even for highly complex Ti/ta-C thin films, as shown by Sainio et al[73].

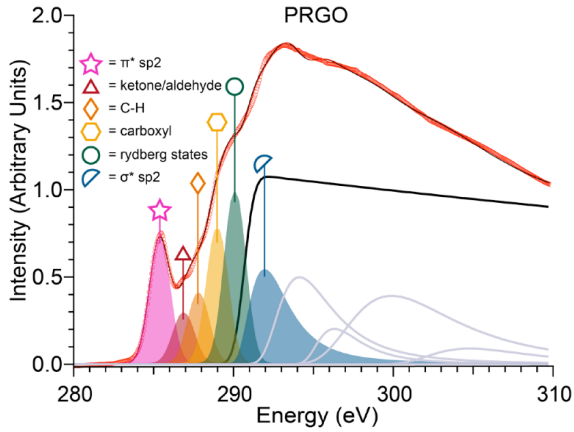

Figure 7. XAS spectrum of partially reduced graphene oxide modified Ti/ta-C electrode from Publication I.

Due to possible shifts in the beamline energy, known references should also be measured for energy calibration. For studying carbon, highly oriented pyrolytic carbon (HOPG) is widely regarded as the 'gold standard' reference for energy calibration and background correction[63–66]. Likewise, well known metal samples should be included for each metal that is studied. The energy correction, background subtraction and peak fitting protocols used are described in greater detail in [Sainio 2020].

2.2.4 X-ray emission spectroscopy with transition edge detector

X-ray fluorescence is a bulk technique capable of sample interrogation to depths of around 1 µm. As will be discussed in detail in chapter 3, the presence of trace metal impurities, below the detection limit of EDS or XPS, can affect the electrochemical properties of carbon materials. Moreover, the presence of such metal impurities cannot always be reliably detected with XPS due to the porous nature of carbon nanomaterial-based electrodes, where it is conceivable that the surface chemistry inside the pores of the material might differ from that of the very surface. In contrast, X-ray fluorescence is a powerful tool for chemical bulk analysis of porous nanomaterials. Similar information can be obtained with EDS measurements in STEM, but this method provides only very local information. In contrast, beam spots of around 1 mm^2 in X-ray emission spectroscopy provide chemical information from a much larger area in synchrotron-based X-ray spectroscopy, in a non-destructive manner.

Hard X-ray beamlines and even laboratory-based X-ray fluorescence spectroscopy can also be used to detect ppm levels of most elements. Those beamlines can, however, not be used to study the bonding of light elements such as carbon, nitrogen and oxygen. The use of X-ray emission spectroscopy (XES) has, however, previously been limited by the low sensitivity of soft X-ray emission spectroscopy[56]. Recently, an energy dispersive soft X-ray spectrometer based on a transition-edge sensor (TES), composed of Mo/Cu bilayer spectrometer, with superior sensitivity has been developed and successfully commissioned at the Stanford Synchrotron Radiation Lightsource beamline 10-1. This setup is described in detail in[56]. The

workable range of this particular detector is limited due to the vacuum window, as well as by the Al IR filters at the low energy end and the grating at the high energy end (~1200 eV). Despite this limitation, the detector is particularly well suited to study carbon nanomaterials and 3D transition metals, such as Fe, Ni, Co, that are often used as catalysts in their synthesis. The TES detector can be used with much improved sensitivity to study the fluorescence of XAS scans. In this way, information may be obtained about both the chemical composition and bonding of the samples. In addition, the high sensitivity allows for the detection of N and M lines, in addition to L lines, greatly increasing the number of elements that can be detected[74].

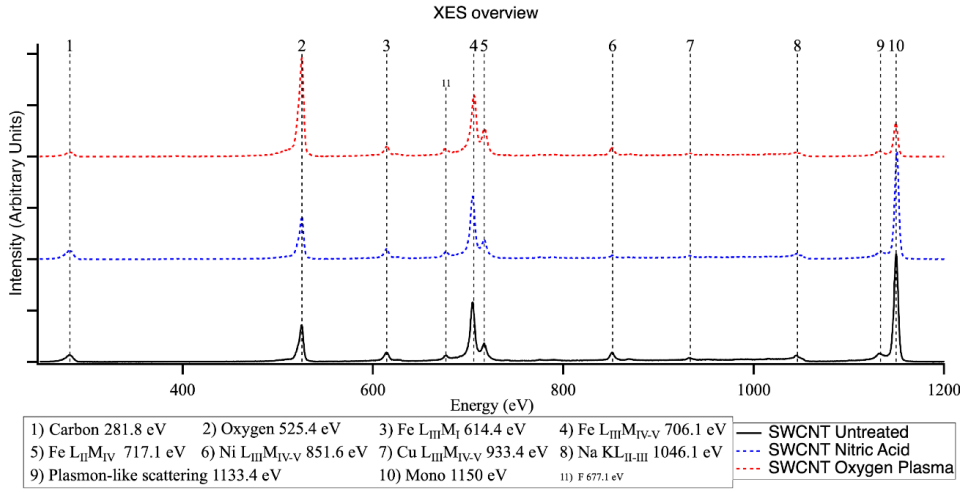

Figure 8. XES spectra collected with 1150 eV mono energy of pristine, nitric acid and oxygen plasma treated SWCNT films from Publication II from Publication II.

In publication II, we used the TES detector to study the chemical composition of a SWCNT sample transferred onto a Si wafer. Figure 8 shows the XES overview scans. In addition to the expected C, O and Fe, small peaks for F, Ni, Cu and Na were also detected. F is a known beamline contaminant and therefore likely does not originate from the sample. Moreover, Ni, Cu and Na were not found in the TEY XAS spectra, indicating that these are not surface contaminants. At present, this method only provides qualitative data, because it has not been calibrated with large number of studies. Work is in progress to calibrate the method so that quantitative or semiquantitative data may be obtained. Thus, this new detector can provide information about the bulk composition of porous samples in an analogous way to XPS wide spectra, but with far superior sensitivity.

2.3 Other characterization methods

2.3.1 Fourier transform infrared spectroscopy

Fourier transform infrared spectroscopy (FTIR) has excellent chemical selectivity and can specifically identify many functional groups, interesting for electrochemistry. In this method, the absorbance or transparency of a sample is measured in the IR region. FTIR can be particularly powerful in combination with XPS and XAS studies. The main disadvantage of

FTIR is the relatively low sensitivity. For example, a 7 nm film of ta-C prepared on an intrinsic Si wafer was almost completely transparent throughout the spectra, despite the fact that it is expected to possess several functionalities known to absorb IR. Thus, the method required a relatively large amount of sample to obtain meaningful data. Nevertheless, due to its simplicity, relatively low cost and excellent chemical selectivity, it is commonly used to provide qualitative information about the presence of functional groups on carbon nanomaterials. FTIR has been previously used to study the bonding and presence of functional groups in both amorphous carbon films[75] and SWCNTs[76].

FTIR can be a non-destructive method, particularly in transmission mode. Due to the requirement of IR transparent substrates, such as quartz, KBr pellets or crystals or undoped silicon wafers, separate samples usually need to be prepared, different from the samples used in electrochemistry. Similarly, the use of the ATR mode requires powder or a flexible substrate, so that the sample can be pressed against the ATR crystal, which makes it tricky to measure thin film samples. For many standard systems, it can also be challenging to make good contact with the ATR crystal when thin films are deposited on solid substrates. The physical contact may also damage porous carbon nanomaterial layers. On the other hand, the ATR mode allows for easy measurement of powders and liquids without any sample preparation.

In publication I, FTIR is used as a complementary method to XPS and XAS, to study the changes in the oxygen containing functional groups of as synthesized graphene oxide (GO), partially reduced graphene oxide (PRGO) and nitric acid treated PRGO.

2.3.2 Raman spectroscopy

Raman spectroscopy is commonly used to study the bonding of carbon, due to its ease of use and non-destructive nature. Both amorphous carbons and SWCNTs have their own distinct Raman features that will be briefly summarized in this section. Raman spectroscopy is often used for qualitative evaluation of the sp^2/sp^3 ratio in amorphous carbon films, and the defect density and presence of amorphous carbon in SWCNT samples.

SWCNT

Raman spectra show several characteristic features for SWCNTs, including the first-order single-resonance radial breathing modes (RBM) and the multipeak feature G mode around 1580 cm^{-1}. In addition, several harmonics and combination modes, including iTOLA, M, and G′ bands, as well as a disorder-induced D band around 1315 cm^{-1}, are also.[77,78]

The electron and phonon density of states (DOS) in SWCNT are in the form of sharp peaks called van Hove singularities (vHS), due to 1-D confinement. The distribution of DOS is dependent upon the chirality (which is also correlated to the tube diameter). Therefore, Raman signal from a carbon nanotube can be observed when the laser excitation energy is equal to the energy separation between vHS in the valence and conduction bands.[77] These modes are called radial breathing modes (RBM) and are specific to carbon nanotubes. The tube diameter can be obtained with Equation 9[77],

$$\omega_{RBM} = \left(\frac{A}{d_t}\right) + B, \qquad (9)$$

where A = 234 nm/cm and B = 10 cm^{-1}. As the tube diameter is related to the chirality, the RBM region can be used to study the electrical properties of the SWCNT. The RBM intensity of a SWCNT is, however, a function of the laser energy and achieves a sharp maxima when the optical transition energy E_{ii} matches the laser energy. Therefore, Raman studies with several laser excitations have become a widely used tool for quantifying the fraction of either metallic or semiconducting nanotubes[79].

The I_D/I_G ratio is also often reported, as the D peak intensity has been proposed to depend upon defects and presence of amorphous carbon. Low I_D/I_G ratio is often taken as an indication of low defect density and low presence of amorphous carbon, although it can't be used to quantitatively study the presence of defects nor the defect types. Nevertheless, large D-band intensities in comparison to G band intensity indicate the presence of amorphous carbon.[79]

Symmetry breaking of the tangential G mode around 1580 cm^{-1}, when the graphene sheet is rolled to make a cylindrically shaped tube, gives rise to a characteristic multi-peak G mode. In this multi-peak feature, up to six Raman peaks can be observed in a first-order Raman process. The main observable peaks are the G^+ (atomic displacements along the tube axis) and G^- (atomic displacement along the circumferential direction) modes. Spectra in this frequency range can also be used for SWCNT characterization. Difference in the line-shape gives information about the metallic character of the SWCNT in resonance with a given wavelength.[80] Because SWCNT thin films contain both semiconducting and metallic tubes and are bundled, such studies are most informative with individual SWCNTs. The peak shape and G position can, however, be used to study the doping of bundled SWCNT films. It has been shown that the G band peak position is shifted to higher frequencies (blue shift) when doped with electron-accepting dopants[81]. This p-type doping decreases the resistance of the SWCNT network by enhancing the conduction of semiconducting tubes. Similar blue shift can be observed also in the G' band[82]. This dominant feature of the second-order Raman spectra of SWCNT has a two-peak structure, and their intensities have been used to assign chirality and study the electrical properties. Because the G' peak has a larger dispersion and lower dependence on defects, at individual carbon nanotubes, this peak may be particularly useful for corroborating specific (n, m) assignments made in the RBM region[77]. In Publication III, Raman spectroscopy was used to study the SWCNT properties. The effect of Nafion coating was further studied with Raman spectroscopy in Publication V.

Tetrahedral amorphous carbon

The Raman spectra of amorphous carbons (aC) have two prominent features, namely the D and G bands, which lie around 1355 and 1500-1630 cm^{-1}, respectively. The G band arises due to in-plane bond stretching of pairs of sp^2 C atoms. The mode does not require six-fold symmetry and occurs at all sp^2 sites. The D peak is a breathing mode, forbidden in perfect graphite and only becomes active in the presence of disorder.[83] Ferrari and Robertson proposed a phenomenological three-stage model describing the amorphization of graphite[83]. According to this model, the Raman spectrum is considered to depend on:

(i) clustering of the sp^2 phase
(ii) bond disorder
(iii) presence of rings or chains
(iv) the sp^2/sp^3 ratio

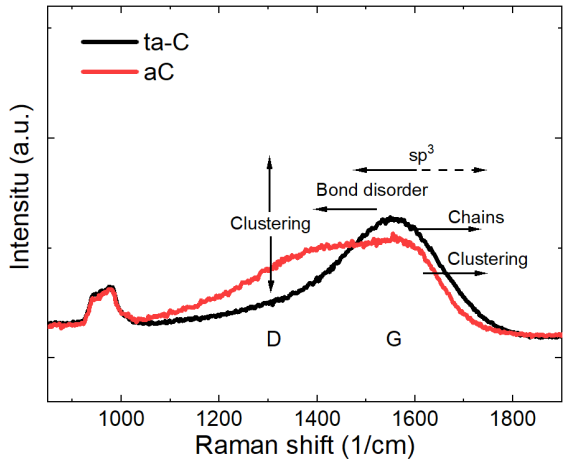

Figure 9. Diagram of the factors affecting the Raman spectra. The dotted arrow indicates the indirect effect of increasing sp^3 content for amorphous carbon films.

The effect of these changes on the Raman spectra are summarized in Figure 9. Based on this model, the G position combined with the I_D/I_G ratio, can be used to approximate the sp^2/sp^3 ratio of amorphous carbon films with sp^3 ratio higher than approximately 20%. Therefore, the I_D/I_G ratio is the most commonly studied parameter for ta-C films. As discussed in Section 4.1, ta-C films deposited with energetic carbon ions are layered and consist of an sp^2 rich surface layer and an sp^3 rich bulk. Because the probing depth of Raman spectroscopy is considerably larger than the thickness of the ultrathin Ti/ta-C films used in this work, the Raman spectrum arises from a combination of the aC-like surface and sp^3 rich bulk. As seen from Figure 9, the contribution of the sp^2 rich surface will increase the I_D/I_G ratio. Because the thickness of the surface layer depends upon the deposition system and its ion energy, it is independent of film thickness[84,85]. Therefore, the I_D/I_G will decrease as the thickness of the film increases, saturating at around 50 nm[34,35,86]. Raman spectroscopy is still a powerful method for qualitatively probing changes in the carbon bonding in ultrathin ta-C films. Due to the thickness dependence, additional methods, such as X-ray reflectivity (XRR) or transmission electron microscopy (TEM) should be used to characterize the thickness, before changes in the Raman spectra are attributed to changes in carbon bonding. XRR has the added benefit of giving the density of the bulk, which is closely related to the sp^3 content of the film[85,87].

The Raman spectra of amorphous carbon films are usually fitted with two Gaussians or two Lorentzian peaks, to determine the I_D/I_G ratio. In Publication IV, we use Raman spectroscopy to study the changes in carbon bonding after anodic treatment of a Ti/ta-C electrode.

2.3.3 Optical absorption

While Raman scattering is used for qualitative evaluation of SWCNTs, absorption spectroscopy can be used for quantitative measurements. Unlike Raman studies with confocal Raman systems, where individual SWCNT can be studied, optical absorption spectroscopy provides a way to study large amounts of SWCNTs. Other advantages include stronger signals and the

ability to probe lower energy bands such as S_{11}, that are not accessible with standard Raman equipment[80].

In ultraviolet-visible-near infrared (UV-Vis-NIR) spectroscopy, van Hove transitions may be directly observed, thus providing information about the electronic structure. The spectra consist of the M_{11} transition for metallic nanotubes (645 to 440 nm), the S_{11} and S_{22} of semiconducting nanotubes (1600-830 nm and 800-600 nm, respectively) as well as the absorption due to plasmon resonances in the free electron cloud of the nanotubes (310-155 nm)[88]. The position of these peaks is dependent on the tube chirality and tube diameter, and thus the tube diameter can be calculated based on the absorption spectra and Kataura plot[88]. Because the S_{11} and S_{22} transitions of semiconducting SWCNTs and M_{11} transition of metallic SWCNTs are clearly visible, the ratio of metallic-to-semiconducting SWCNTs in a thin film can be quantitatively evaluated[89].

This also makes optical absorption spectroscopy particularly useful for studying the doping of SWCNTs, carried out to improve the conductivity of SWCNT films. Chemical doping suppresses the peaks due to a shift of the Fermi level[82,90]. Optical absorption spectroscopy has also been proposed as a method for evaluating the purity of SWCNTs in terms of carbonaceous impurities[91,92] Finally, the optical transparency of SWCNT films is usually evaluated with optical absorption spectroscopy. Moreover, the thickness of SWCNT films has also been evaluated based on the optical absorbance[82].

In publication III, SWCNT networks were press transferred onto quartz substrates and the intrinsic electrical properties, the optical transparency and the average SWCNT diameter were evaluated based on optical absorption spectroscopy. In publication VI, the optical transparency was also used to control the thickness of the SWCNT films.

2.3.4 Scanning electron microscopy

In scanning electron microscopy (SEM), a focused beam of electrons is scanned over the sample in high vacuum. This produces, secondary and backscattered electrons that carry different information. Secondary electrons are ejected from the surface as a result of inelastic collisions with the incident electrons. They are used to study the topography and morphology of the specimen. Back scattered electrons on the other hand, provide Z contrast and therefore carry local chemical information. In this work, mainly secondary electron are used, to study the morphology of the electrode materials. SEM is also used to measure the thickness of Nafion membranes from cross-sections prepared either by cryo-cleaving or focused ion beam milling. In cases where samples are not conductive, such as Nafion coatings, the samples are coated with gold prior to imaging.

2.3.5 Transmission electron microscopy

In transmission electron microscopy (TEM), a thin specimen (< 100 nm thick) is subjected to an electron beam in which the intensity is uniform over the illuminated area. The electrons in the electron beam can be either transmitted or deflected by elastic and inelastic scattering. This scattering of electrons makes TEM imaging feasible, as it creates differences in electron intensity. The TEM micrograph is made up of the intensity of electrons for each pixel of the detector. With instrumentation including spherical and chromatic aberration correction, TEM

image resolution of well below 0.1 nm can be achieved. Therefore, high-resolution TEM (HRTEM) allows for imaging of single atoms. Elastically scattered electrons also make up most of the intensity of diffraction patterns. These diffraction patterns contain information about the crystal structure, lattice repeat distance and specimen shape.[93] In Publication III and V, we use TEM and HRTEM to study the morphology of SWCNT films, in particular the bundling, tube diameter and size and distribution of the catalyst particles. In addition, electron diffraction is used to study the crystallinity of the catalyst particles in the SWCNT networks.

The main challenge with TEM analysis is usually the specimen preparation. Care should also be taken to avoid changes in structure and chemistry of the sample during the thinning process or as a result of beam damage. In addition, only a small part of the sample can be examined with TEM. Therefore, this high resolution technique should be combined with other analysis methods that offer poor resolution, but better sampling, such as SEM.[93]

2.3.6 Energy dispersive X-ray spectroscopy

The electron beam is a form of ionizing radiation. Therefore, like in soft X-ray spectroscopy, the electron beam can also be used to excite the specimen, resulting in emission of characteristic X-rays. Moreover, SEM and TEM systems are often equipped with energy dispersive X-ray detectors for elemental analysis.

In the SEM, energy dispersive X-ray spectroscopy (EDS) is a bulk technique (excited volume ~1 μm^3) with interaction volumes in the μm range.[93] The large probing depth and relatively high detection limits significantly limits the applicability of EDS in SEM for study of thin films. In combination, with scanning transmission electron microscopy (STEM), lower detection limits can be achieved due to the focusing of the beam in the desired location. In modern TEM equipment with C_s correction, single-atom detection is possible with EDS. The sensitivity is affected by the atomic number, absorption of X-ray within the specimen and the fluorescence. TEM samples are usually thin enough that the absorption and fluorescence can be ignored. Sensitivity factors, also called k-factors, can be determined and used for quantitative X-ray analysis. The values of k-factor are not constants and accurate determination of the k-factor requires the use of well characterized reference samples.

Due to its ability to provide chemical information with high spatial resolution, TEM-EDS is especially powerful in combination with selected area electron diffraction. With this combination, both crystallinity and chemistry of catalyst particles in carbon nanomaterials can be studied. In Publication III and V, EDS was used to study the elemental composition of the SWCNT network electrodes.

3 . Electrocatalytic properties of carbon electrodes

Many bio and drug molecules are so called inner sphere redox systems, whose oxidation/reduction behaviors are sensitive to the surface chemistry of the electrode material[94]. Several factors that affect the electrochemical properties of carbon nanomaterial electrodes have been identified, including at least:

i) Bonding of carbon to carbon
ii) Bonding of carbon to oxygen and nitrogen
iii) Presence of surface and bulk metal
iv) Oxidation state of metal
v) Surface morphology

It is well known that the sp^2/sp^3 ratio affects the physicochemical properties of carbon materials. Thus, the carbon to carbon bonding is known to affect the performance of electrochemical sensors[34,40,73,95]. This is evident with amorphous carbon thin film electrodes, whose electrochemical properties resemble those of glassy carbon, when sp^2 rich[95,96]. Whereas, properties closely resembling those of boron doped diamond are observed for sp^3 rich amorphous carbon thin film electrodes[97]. Generally, high sp^2 ratios are associated with faster oxidation kinetics, with many inner sphere probes. Whereas, high sp^3 ratio is attributed to wider potential windows, high chemical stability and low background currents. Improved rates of electron transfer have also been attributed to clustering or ordering of the sp^2 carbon in amorphous carbon coatings[95]. In addition, the density of basal plane and edge plane sites in graphitic materials seems to affect the electron transfer kinetics of OSR probes. It has been suggested that electron transfer may occur only at the edge plane or defect sites of graphitic materials, and that pristine basal planes are electrochemically inert or support extremely slow electron transfer kinetics[98,99]. It has also been suggested that when heterogenous electron transfer occurs at basal planes, it is only due to the presence of defects. Furthermore, it has been proposed that nanographite impurities, rich in edge plane sites, dominate the electrochemistry of carbon nanotubes[100].

The oxidation kinetics at basal and edge planes of HOPG electrodes have been intensively studied by various groups. Kneten et al.[101] for example, showed 1-5 orders of magnitude slower oxidation kinetics at HOPG basal plane electrodes compared to GC electrode, with 13 different redox probes, including both outer and inner sphere probes. Their study showed large ΔE_p values of 285 mV and 1200 mV for $Ru(NH_3)_6^{+2/+3}$ and dopamine, respectively. Poor oxidation kinetics for $Fe(CN)_6^{3-/4-}$ and dopamine were observed also by Bowling et al[102] at basal plane

HOPG electrodes. More recently, similar results have been obtained by Velicky et al.[103], showing the same phenomenon with the outer sphere redox probes $Ir(Cl_6)^{3-/2-}$ and $Ru(NH_3)_6^{2+/3+}$, with localized measurements using a microdroplet electrochemical cell. They concluded that the basal planes have small, but non-zero, electron transfer rates compared to edge plane sites. Yuan et al.[104] also observed higher activity at the edge plane for ascorbic acid, nicotinamide adenine dinucleotide (NAD) + hydrogen (NADH) and oxygen reduction reaction (ORR). Nevertheless, it should be noted, that while the oxidation peaks were anodically shifted, the basal plane also produced well defined waves for AA and NAD in their study. Copper was, however, also used in the fabrication of their electrodes and no studies of potential metal contamination were provided.

These results seem to confirm the widely held conclusion that defect and edge plane sites are the active sites of graphitic electrodes. As a consequence, there has been consensus that electrodes should be designed to optimize surface step edge or defect density. Contradicting results have, however, been reported by Patel and coworkers[105–107], leading them to conclude that the pristine basal plane of HOPG electrodes is much more active for many classes of electrode reactions than previously believed. These works reported fast oxidation kinetics of the catecholamines dopamine and epinephrine, at the basal plane of HOPG electrodes in macroscopic voltammetric studies. Facile oxidation kinetics was also confirmed at defect free sites with scanning electrochemical cell microscopy (SECCM)[105,108]. Rapid inactivation of the electrode by fouling was, however, observed, indicating that some of the above results may be due to fouling. To date, however, such contradicting results seem to be limited to catecholamines, possessing a benzene ring. The electrocatalytic properties of novel sp^2 carbon materials, such as CNT and graphene, have been previously attributed to π-electron interactions between the conjugated aromatic systems in the analyte molecule and the electrode. It has been suggested that the π-π stacking can facilitate the adsorption on the electrodes' surface[109–112]. This phenomenon is of significant importance in biology, and several commonly studied analytes, including dopamine, paracetamol and opioids have conjugated π-electrons. It should, however, be pointed out that the modified electrodes used in these studies are also rich in edge plane and defect sites, and none of these works show any direct experimental evidence to support these claims.

Oxygen containing functional groups are inevitably present at carbon electrodes, and it is widely acknowledged that the presence of oxygen and nitrogen containing functionalities have profound effects on the electrochemical properties of carbon electrodes. Ji et al.[113] showed that the oxidation of both basal and edge planes influences the oxidation kinetics of inner sphere redox couples, while that of outer sphere redox systems remains relatively unaffected. They also observed contrasting behavior between HOPG and MWCNT, where the latter showed fast oxidation kinetics also in its oxidized sate. Similarly, Chou et al[114] reported favorable electrochemical properties that they attributed to oxygenated carbon in general, and carboxylic moieties in particular, at the ends of SWCNT. Importantly for electroanalytical chemistry, oxygen-containing functional groups have a strong influence on the electrochemistry of many biological compounds and drug molecules, such as dopamine[73,115,116], NADH[117], ascorbic acid[73,116], paracetamol[118] and morphine[119].

It has been proposed that nitrogen doping of graphene and amorphous carbon affects their electrocatalytic properties. Nitrogen doping has long been used in amorphous carbon electrodes, mainly to improved conductivity by doping and promoting clustering of sp^2

carbon[40]. Different levels of nitrogen doping of such electrodes have been reported to influence the electrochemical properties to different extents[120]. Cao et al.[121] also reported a significant increase in the activity of ORR with nitrogen doped amorphous carbon. Further, they found that both the total nitrogen content and pyridinic/graphitic nitrogen percentage, influence the ORR activity.

More recently, nitrogen doped graphene and CNT have attracted attention due to proposed electrocatalytic properties. Incorporation of nitrogen into the graphene structure changes the spin density and charge distribution of the surrounding carbon atoms[122,123]. There are three forms of nitrogen groups that can be incorporated into the carbon lattice, namely quaternary (graphitic), pyridinic, and pyrrolic nitrogen. In addition, amino nitrogen groups can decorate the edges and defects.[123] Nitrogen doping of CNT has been reported to improve the sensitivity in the detection of hydrogen peroxide[124]. Increased activity towards oxygen reduction reaction has also been reported[125]. Nitrogen doped graphene modified electrodes have also been used for selective and sensitive detection of dopamine[126–129]. Most of these works did not, however, systematically study the role of nitrogen doping. Li et al.[127] on the other hand, synthesized nitrogen-doped graphene with different distributions of nitrogen groups. They found that the relative distribution of the nitrogen functionalities affected both the activity and sensitivity toward AA, DA and UA. Further, they concluded that the pyrrolic-N structure showed better catalytic activity than pyridinic-N and graphitic-N structures. It should, however, be noted that differences in the amount of oxygen were also observed with XPS analysis and was not discussed. On the other hand, it has been proposed that the enhanced activity towards ORR can be correlated with the amount of pyridinic and/or quaternary nitrogen[130,131]. In a review of metal free graphene based catalysis, Haag et al.[123] pointed out that it is still under debate how to correctly characterize the different forms of nitrogen, which makes it difficult to correlate catalytic properties to specific nitrogen groups. Furthermore, to the best of our knowledge, no studies have been carried out systematically studying the effect of nitrogen doping of graphitic materials on electroanalytical chemistry.

Presence of metals and their oxidation states are known to affect the electrochemical properties of carbon nanomaterials. Most carbon nanomaterials are synthesized using metal catalysts, and the complete removal of these catalysts is difficult or impossible[76,132]. Many, works also claim observation of electrocatalysis with "metal-free" carbon electrodes[121–123,125,127,130,131,133,134]. Most of these studies advertise their materials as metal-free without sufficient characterization to verify that they are indeed metal free. In some studies, XPS is used to show that the material is metal-free[121,127,131,133]. As explained in section 2.2, however, XPS can probe only the very surface the electrode. Most electrodes made with nanomaterials are porous and have pores inaccessible for probing with XPS, but accessible to the electrolyte solutions and analytes. Moreover, levels of metal impurities much below the detection limits of XPS have been shown to affect the electrochemical properties of carbon electrodes[135–138]. In addition, these metal impurities may also influence the toxicological properties[139], which is of importance with implantable and wearable sensors.

Moreover, Wang et al.[140] found Fe, Co, Ni, and Mn impurities at ppm levels in both synthetic and natural graphite. These metal impurities are known to be present also in the final products when graphite is used as precursor for fabrication of carbon electrodes. Similarly, in some cases, other chemicals, such as potassium permanganate, may leave metal impurities in the final product. For example Mn has been found in graphene oxide produced by Hummer's

method[116,141] and graphene oxide nanoribbons obtained by oxidative opening of nanotubes[137]. Metal impurities affecting the electrochemical properties have also been found in CVD graphene even after purification[138]. We have also observed relatively high metal content in sputtered amorphous carbon coatings[115].

There is mounting evidence that the electrocatalytic properties of nanocarbon materials is at least in some cases due to metal catalysts that are used in their synthesis, or other metal impurities. For example, electrocatalytic properties in oxidation of hydrazine have been attributed to Fe impurities in carbon nanotubes[76,136] as well as Ni and Cu in graphene oxide nanoribbons[137]. Similarly, electrocatalytic properties toward oxidation of HS^- have been attributed to Ni content of less than 2 ppb[137]. Moreover, improved activity towards oxygen reduction reaction has been attributed to trace levels of metal impurities[141].

While the influence of minor and trace element impurities has been reported and extensively studied in energy conversion and storage applications, much less work has been devoted to understanding the effect of these impurities on the voltammetric sensing with carbon nanomaterial electrodes. Nevertheless, Dai et al.[142] have reported that copper nanoparticle impurities within the walls of multi-walled carbon nanotubes (MWCNT) are the active sites for reduction of the anesthetic halothane. Sainio et al.[143] have also recently shown that carbon nanofibers (CNF) grown with Ni and Fe show superior activity toward oxidation of AA compared to detonation nanodiamond grown CNF. In another study, a nitric acid treatment was used to activate the CNF electrodes[144]. Later it was shown, that the nitric acid treatment also heavily oxidized the Ni metal catalysts in the of the CNF electrode[145]. Based on these results, it is highly likely that both the residual metal catalysts as well as their oxidation state affect the performance in electroanalytical applications. Surprisingly, to the best knowledge of the author, the effect of these metal impurities on electroanalytical chemistry has not been more widely studied.

Finally, one must not overlook the possible changes in morphology after modification of conventional electrodes. Modification with carbon nanomaterials usually produces a porous layer in which pockets of solution are trapped. Streeter et al.[146] showed that the formation of such a porous layer can influence the electrochemical properties due to altered diffusion profile and trapped analyte. Furthermore, they found that the changes observed in voltammetry may often be obtained in simulations without changes the heterogeneous rate constant. Compton's group has demonstrated such thin layer effects with ferrocyanide[146], dopamine[147] and nicotine[148]. Thus, it is possible that many of the advantageous properties reported for modified electrodes, often attributed to electrocatalysis, are in some cases at least partially due to the formation of porous layer leading to thin layer diffusion. Furthermore, commonly used oxidative treatments, which are expected to increase the number of defects and oxygen containing functional groups, can also significantly alter the morphology of the materials[149–152] even in the absence of chemical modifications. Therefore, careful characterization of the morphology should also be carried out before any observed changes in voltammetry are attributed to electrocatalysis. Care should also be taken before labeling observed changes in voltammetric peak-to-peak potential separation, after modification of conventional electrodes or after chemical treatments, as electrocatalytic properties.

It is clear that much more work is required to fully understand the effects of the structure, morphology and the surface chemistry of carbon nanomaterials, on electroanalytical chemistry. Sainio et al.[143] recently concluded the key elements seemingly required for achieving

both high sensitivity and selectivity towards dopamine with carbon nanomaterial based electrodes as (i) the presence of active metal catalyst particles, (ii) crystalline areas available (basal plane with plenty of defects), and (iii) porous surface morphology possibly resulting in the formation of thin liquid layer near the surface. This, however, represents only one electroanalytical application, and these findings cannot directly be extended to cover detection of other analytes. Nevertheless, this example shows the complexity of such systems and the importance of thorough characterization. Unfortunately, a review by Pumera in 2012[153] found that many publications on the electrochemistry of CNT and graphene suffer from poor characterization or no characterization at all. A recent review by Laurila et al.[154] on carbon hybrid materials, found that this is still the case. They found that, there is a serious lack of (i) systematic characterization of carbon nanomaterials and (ii) standardized protocols for characterizing the surface functional groups of carbon nanomaterials. This shows that there is much more to the development of carbon based electrode materials, than simply optimizing the defect density of the electrode. We welcome a far more holistic approach to electrode material development, combining the thorough physical, chemical and structural characterization of electrode materials, combined with extensive electrochemical characterization and testing with analytes in settings closely mimicking the end application. With such an approach, electrode development relying solely on trial and error could be avoided.

4 . Physical and electrochemical properties of carbon thin film electrodes

In this chapter, a brief introduction of the two thin film electrode materials utilized in this thesis will be given. The physical and electrical properties have been studied and reviewed extensively elsewhere, and this will therefore not be attempted here. Instead, this chapter will focus on the electrochemical properties of tetrahedral amorphous carbon and single-walled carbon nanotubes. Select characterization results, that likely influence the electrochemical performance, are also presented.

4.1 Tetrahedral amorphous carbon

Hard amorphous carbon coatings, also referred to as diamond-like carbon (DLC), have been researched extensively and applied industrially as protective coatings[87]. The diamond-like properties arise due to the sp^3 bonded carbon fraction. Amorphous carbon films can be deposited by different methods, including ion beam, magnetron sputtering, cathodic arc, pulsed laser deposition (PLD) and plasma enhanced chemical vapor deposition. These deposition methods and different deposition parameters produce amorphous carbon coatings with varying sp^2/sp^3 fractions and hydrogen content, as described in detail in a comprehensive review by Robertson[87]. The bonding in amorphous carbon coatings is best described with the ternary phase diagram of bonding in amorphous carbon-hydrogen films. The physical, chemical and electrochemical properties of ta-C films depend on the ratio of sp^2/sp^3 and also the incorporation of hydrogen, nitrogen, as well as other dopants and impurities[40,85,87,120,155,156].

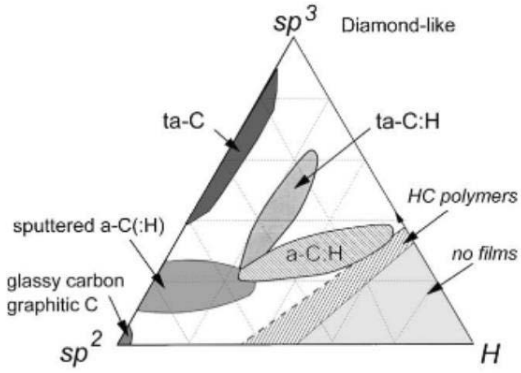

Figure 10. Ternary phase diagram of bonding in amorphous carbon-hydrogen alloys. Reprinted from[87] with permission from Elsevier.

Tetrahedral amorphous carbon is a form of amorphous carbon with high sp^3 fraction (40-88 %) and low hydrogen content, giving it properties such as high hardness, high wear resistance, low friction, low electrical conductivity, large band gap, optical transparency in the IR region, chemical inertness and biocompatibility[87,156,157]. Due to the high sp^3 fraction, the electrochemical properties resemble those of diamond, namely wide water window and low background current[40]. Like diamond films, ta-C electrodes are also usually regarded as biocompatible[47,158] and show antifouling properties[159]. Unlike BDD films, ta-C films can be deposited at room temperatures on a wide range of substrates, including silicon, glass and polymers. However, due to poor adhesion and large compressive stress, adhesion promoting layers, such as Ti, are often required. Unlike conventional carbon electrodes, such as glassy carbon and highly oriented pyrolytic graphite, ta-C is also patternable and fully compatible with standard silicon microprocessing.

Experimental and simulation works suggest that films with high sp^3 fraction are formed only under bombardment of energetic C^+ ions with energies around 20-100 eV[87,155–157,160]. In these works, the sp^3 fraction increases with increasing ion energy, reaching a maximum around 100 eV, after which the sp^3 fraction falls with further increase in ion energy. This led to the postulation of a growth mechanism based on a subplantation model, which is based on incident energetic ions penetrating the surface and providing subsurface growth[156]. Recently, Caro et al.[161] used molecular dynamics simulations based on machine-learning derived interatomic potential, trained from data at the density functional level of theory. Based on these results, which are in better agreement with experimental results than previous models, they suggested a "peeing" model as the dominant mechanism for formation of sp^3 carbon. Both these mechanisms predict the formation of an sp^2 rich surface layer. The layered nature of ta-C films deposited by filtered cathodic vacuum arc (FCVA) and PLD have been has also been confirmed experimentally by EELS[84] and X-ray reflectivity measurements[85]. Furthermore, Raman spectroscopy studies also support the existence of an sp^2 rich surface layer[34,35,86].

Due to the high sp^3 fraction, undoped ta-C films have relatively high resistivity[135]. For this reason, nitrogen doped ta-C films are often used for fabrication of electrochemical electrodes[40,120]. Nitrogen doping can increase the sp^2 content of ta-C films[120] and promote clustering of sp^2 carbon[40], thus improving the conductivity of the films. Undoped ultrathin ta-C electrodes can also support facile electron transfer[34,35,41]. Protopopova et al.[35,36] and later Palomäki et al.[34] researched the effect of the thickness on the electrochemical properties of ta-C thin film electrodes with CV and EIS. They found optimal reaction kinetics with a 7 nm thick ta-C film. A linear increase in electron transfer resistance was observed with increasing thickness. Palomäki et al. postulated that the electron transport through the sp^3 rich bulk slows down the overall reaction kinetics, as observed with CV and EIS experiments with outer sphere redox probes. The reaction kinetics of the inner sphere analytes AA, DA and UA have also been found to be affected by the thickness of the ta-C film[47]. With films thinner than 7 nm, the Ti adhesion layer was found to dominate the electrochemical properties, likely due to pinholes extending through the film. Palomäki et al.[34] also found that the use of a 20 nm Ti adhesion layer reduced the electron transfer resistance with a constant value for all studied ta-C thicknesses. This effect was attributed to a lowering of the contact resistance between the Si wafer and the ta-C film. Later, a much higher R_{ct} value of 841 ± 160 Ω was observed by Etula et al.[135] for a 36 nm ta-C electrode, suggesting that small differences in sp^2/sp^3 ratio,

macroparticle or metal contamination or some other unknown variation, may heavily influence the reaction kinetics at ta-C thin film electrodes.

In this thesis, we will focus on the properties of the dual layer Ti/ta-C thin film electrodes. This electrode uses a 20 nm Ti adhesion layer deposited by direct current magnetron sputtering. A 7 nm ta-C top layer is then deposited with FCVA, as described in Publication I. In this process, plasma is generated with an electric arc leading to the formation of highly ionized carbon plasma, but also neural particles[162–164]. The plasma is directed through an electromagnetic filter to filter out the neutrals. In this thesis, a 45 degree open knee-filter is used to filter out the macroparticles[162]. It should be noted that few FCVA systems can completely filter out all the macroparticles. Virtually macroparticle free ultrathin films, however, have been made in industrial quantities with systems utilizing double off-plane filters. Due to high plasma losses, such filters are usually used only in demanding applications, such as in protective coatings for magnetic media.[164]

The physicochemical properties of these Ti/ta-C electrodes have been thoroughly characterized in this thesis and other works, and are summarized in Table 3. In Publication I and Publication IV, we show that the Ti/ta-C electrodes support reversible electron transfer with the outer sphere redox probes $FcMeOH^{+/0}$ and $Ru(NH_3)_6^{3+/2+}$. Both studies report reversible electron transfer as measured with cyclic voltammetry, but small differences can be observed with the more accurate EIS measurements. The surface sensitive analyte $Fe(CN)_6^{4-/3-}$ shows quasi-reversible electron transfer, with a potential peak separation (ΔE_p) of 131 mV. The low double layer capacitance makes this electrode capable of reaching detection limits in the low nanomolar concentration range with cyclic voltammtey[143]. Palomäki et al.[47] also reached low detection limits of 84.3 ± 14 and 39.8 ± 5.9 nM for 15 and 50 nm thick ta-C films, respectively.

As we show in Publication I, and other work[47], the main limitation of this electrode is the limited selectivity in biological matrices. Especially, the poor reaction kinetics for AA that leads to a wide poorly defined oxidation peak, significantly limits its selectivity, particularly in the detection of dopamine. The Ti/ta-C electrode, however, presents an excellent candidate for modification with various carbon nanomaterials to improve its electrochemical performance as we show in Publication I and other works[37,38].

Due to the small thickness of the ta-C layer, the Ti adhesion layer likely also affects the electrochemical properties. Usually ta-C films are ultra-smooth with RMS roughness values of 0.16 nm[135]. With Ti adhesion layer, RMS roughness values of 0.81-1.6 nm are observed due to the crystallinity of the Ti adhesion layer[41,118]. Moreover, the Ti present at or close to the surface, likely also affects the water window. Etula et al.[135] reported a potential window of 5.2 V in 0.15 M H_2SO_4 and 4 V in 1 M KOH with a 36 nm ta-C electrode deposited directly on Si. Similarly, Mynttinen and coworkers[16] reported a water window of 5 V with a Nafion coated 15 nm ta-C electrode in PBS. In contrast, water windows of 3.5 V in 0.15 M H_2SO_4 and 3 V in PBS have been reported for the Ti/ta-C electrodes[35,41]. In Publication IV, we further show that an anodic pretreatment at 2.5 V, exposes the underlaying Ti layer, which alters the electrochemistry of paracetamol, enabling the selective detection of morphine (see Figure 26 in Section 8.1). The role of Ti in the electrochemical properties is also supported by surface sensitive XPS and XAS measurements that detect Ti at the surface of the Ti/ta-C electrodes[96,165,166]. In XPS studies, around 0.3-0.5 at% Ti is detected on the surface of the Ti/ta-C electrodes. More studies are

required to fully understand the role of Ti in the electrochemical properties, and its influence on the performance of electrodes in electroanalytical applications.

As discussed in Chapter 3, other aspects of the surface chemistry are also expected to influence the electrochemistry of inner sphere analytes. XPS studies have also found a relatively high amount of 7.5-12 at% oxygen, as well as 0.4-0.8 at% of nitrogen at the surface of Ti/ta-C electrodes[96,166]. Lower surface oxygen of 4.2 ± 0.2 at% was found also by Etula et al.[135] on a 36 nm ta-C film, deposited with the same FCVA system, without the Ti adhesion layer, indicating that the use of Ti adhesion layer may also influence the oxygen content of the surface. Nevertheless, further studies with high resolution XPS revealed the presence of C-O (7.5 ± 0.1 %), C=O (3.7 ± 0.2 %) and COO (2.1 ± 0.1 %) groups[166]. Similarly, XAS studies have confirmed the presence of ketone/aldehyde and carboxylic groups on the surface of the Ti/ta-C thins films[73,165]. These groups are expected to give the surface of the electrode a negative charge. Zeta potential measurements carried out for the Ti/ta-C electrode gave pH 2.6 as the isoelectric point, clearly supporting the presence of acidic functional groups on the surface[41].

Table 3. Summary of physical, chemical and electrochemical characterization of Ti/ta-C thin film electrodes.

Method	Observations	Reference
XRR	Bulk density (g/cm^3): 3.04[a]	135
AFM	Roughness: 0.81-1.6	41, IV
Raman	I_D/I_G: 0.62 ± 0.01, 0.56 ± 0.01	IV
XPS	**Wide:** 91.2 ± 0.3 % C, 7.5 ± 0.1 % O, 0.5 ± 0.03 Ti, 0.67-0.71 at% Si	IV
	C1s: CC Gr 28.7 ± 1.3 %, CC sp^3 57.9 ± 1.4 %, C-O 7.5 ± 0.1 %, C=O 3.7 ± 0.2 %, COO (2.1 ± 0.1 %)	166
XAS[b]	**C1s:** Presence of π* sp^2, and σ sp^2, sp^3, aldehyde/no long range order	165
	O1s: ketone/aldehyde, carboxyl,	
	Ti 2p: oxidized Ti detected	
CV	**Water window:** 3.5 V (0.15 M H_2SO_4) 3V (PBS)	35,41
	$FcMeOH^{+/0}$: ΔE_p (mV) 59.1 ± 0.9, k^o (cm^{s-1}): 0.402	I
	$Ru(NH_3)_6^{3+/2+}$: ΔE_p (mV) 57.1 ± 2.9, k^o (cm^{s-1}): 0.245	I
	$Fe(CN)_6^{4-/3-}$: ΔE_p (mV) 131, k^o (cm^{s-1}): 0.003	I
EIS	**$Ru(NH_3)_6^{3+/2+}$:** Rs (Ω): 17.78 ± 3.69, Rct (Ω): 10.06 ± 2.28, Cdl (μF/cm^2): 10.37 ± 7.04, k^o_{app} (cm s^{-1}): 0.420	I

[a] Bulk density of a 36 nm ta-C sample deposited on Si with the same FCVA process as the Ti/ta-C samples

[b] All spectra acquired in total electron yield mode

4.2 Single-walled carbon nanotubes

Carbon nanotubes have attracted wide attention since their discovery in 1991 by Ijima[167], due to their exceptional electrical[168], mechanical[169], thermal[170] and optical properties[32,82]. Single-walled carbon nanotubes (SWCNTs) are hollow cylindrical nanostructures, consisting of a single rolled up sheet of graphene. Whereas, carbon nanotubes with several hollow cylinders stacked inside one another are called multi-walled carbon nanotubes (MWCNTs). MWCNTs

have been more widely applied in electrochemical sensing, due to their higher number of defects, thought to support fast reaction kinetics, and ease of chemical functionalization without the loss of electrical conductivity. SWCNTs also have a number of interesting properties for electrochemical sensing, including high conductivity, chemical stability, relatively low capacitance, and optical transparency[32,82,171,172]. Like most carbon electrodes, they also show wider potential window compared to noble metal electrodes[173]. Their small size also results in high mass transfer coefficients and improved signal-to-noise ratio[45].

The chemical stability, however, also makes altering the surface chemistry with chemical treatments difficult. In Publication II, we show that the SWCNT networks are almost impervious to short immersion in concentrated nitric acid, used to activate other carbon-based nanomaterials[47]. Whereas in Publication I, the same treatment affected both the surface chemistry and the electrochemical response of the PRGO modified Ti/ta-C electrode. Oxygen plasma treatments and harsher chemistries lead to damage of SWCNTs causing a decrease in conductivity[152]. Atmospheric plasma and electrochemical treatments have, however, been shown to be effective ways for surface chemistry functionalization, while preserving the conductivity of the networks[171]. Moreover, chemistries have been developed for covalent modification of the sidewalls and adsorption of modifiers through hydrophobic interactions[174,175].

Due to the SWCNT dimensions, phonons are confined in 1-D. Therefore, the density of states (DOS) are in the form of sharp peaks called van Hove singularities (vHS), and thus a SWCNT with a certain chirality will have a discrete set of vHS in its valence and conduction bands[77]. The electrical properties are determined by the chirality of the SWCNT, i.e. how the graphene sheet is rolled up. SWCNT can be either metallic or semiconducting and most synthesis methods yield 1/3 metallic and 2/3 semiconducting tubes[170]. Theoretical modeling has been used to predict that SWCNTs with different chirality have different rates of electron transfer[172]. These results are supported by SECCM studies of individual SWCNTs with nanoscale electrochemical devices[176–178]. Guell et al.[176] found that, while both metallic and semiconducting SWCNTs exhibited high rate constants for ferrocenylmethyl-(trimethylammonium) ($FcTMA^{+/2+}$), the electrochemistry of the outer sphere redox probe $Ru(NH_3)_6^{2+/3+}$ is very sensitive to the electronic character of the SWCNT. At semiconducting SWCNT no reduction was observed for $Ru(NH_3)_6^{2+/3+}$, except at large overpotentials. In an earlier work, it was noted that the semiconducting SWCNTs are in the charge accumulation state in the potential range of $FcTMA^{+}$ and thus shows metal like behavior[178]. They further noted that the redox potential of $Ru(NH_3)_6^{2+/3+}$ lies in the depletion region of the semiconducting SWCNT. They suggested the simultaneous measurement of $Ru(NH_3)_6^{2+/3+}$ and $FcTMA^{+}$ as a way to distinguish between metallic and semiconducting SWCNTs in SECCM measurements.

There is a widely adopted view, that the carbon nanotubes are highly electrocatalytically inert unless modified, doped, or defected. Moreover, it has been proposed that the electrocatalytic properties are at least in some cases due to the presence of metal catalysts or nanographite impurities[100,153]. Scanning electrochemical cell microscopy, however indicates that pristine SWCNT sidewalls show high rates of electron transfer with OSR probes, as well as high activity towards oxygen reduction[179] and oxidation of serotonin[176]. In fact, Byers et al.[179] reported activity comparable to that of standard gold electrocatalysis, at pristine SWCNT sidewalls. Despite this, they reported significantly enhanced activity towards oxygen reduction at kinked sites and regions modified by oxidation. These studies, however, clearly show that pristine

sidewalls of SWCNTs are electrochemically active and can support fast reaction kinetics for both OSR and ISR probes.

In electrochemical sensors, SWCNTs are used both as conductive elements in electrode material composites, as well as in the form of porous thin films also called SWCNT networks. In this thesis, we focus on the latter. Such SWCNT network electrodes show interesting properties for electroanalytical applications. First, the porosity of the SWCNT films can trap pockets of solution between the SWCNTs leading to the formation of thin liquid layer[146]. Second, low density SWCNT networks on insulating substrates show very low background currents, but enhanced mass transfer, leading to increased signal-to-noise ratio[45]. Both these properties are very attractive in trace analysis.

The large aspect ratio of SWCNTs causes them to stick together, forming large bundles held together by van der Waals forces. Therefore, one major challenge in fabricating CNT films is to separate the tubes without using covalent chemistries or harsh conditions, which could lower their electrical conductivity. The weak forces holding together the bundles, allow for slippage, of the SWCNTs, making the network mechanically weak. This, however, also makes SWCNT networks able to retain their conductivity after large deformation, enabling their use in flexible electronics. SWCNT networks electrodes have been shown to retain their conductivity even after 30 000 bending cycles at extreme bending angles of 180°.[32] To make the electrodes mechanically more robust, SWCNT electrodes are often embedded in a polymer matrix[180].

The SWCNTs in the networks used in this thesis are randomly oriented. As the SWCNT bundles consist of a mixture of metallic and semiconducting SWCNTs, the electronic properties are dependent on the density of SWCNTs. Thus, a very low-density network may have no percolation paths to support conduction. With increased density, the network will exhibit semi-conducting properties due to the larger fraction of semiconducting tubes. Further increase in the density increases the amount of metallic tubes and confers metallic behavior to the network.[82] The electrical conductivity of such SWCNT films with thicknesses above a few monolayers can be described by bulk metal conductivity laws[82].

An overwhelming majority of CNT studies utilizes commercially sourced SWCNTs grown using mainly high-pressure carbon monoxide (HiPCO), arc discharge or laser ablation and purified to different grades of purity[181]. These SWCNT powders are usually made into porous conductive networks, mainly by drop casting onto inert substrates or conventional electrodes, but also increasingly by printing technologies. In contrast, SWCNT networks with controlled properties can be directly grown with aerosol chemical vapor deposition (CVD), collected and dry-transferred onto a wide range of substrates[82,182,183]. In this thesis, we focus on the SWCNT networks grown with aerosol CVD process and press-transferred onto insulating substrates, such as glass or polymers. The step-by-step fabrication process of the electrodes used in Publication III and V is shown in Figure 11.

SWCNTs may contain significant amounts of metallic impurities encapsulated within graphite sheets or located on the sidewalls of the tubes[181]. Presence of defects, amorphous carbon and functional groups may also influence the electrochemical properties[153]. Therefore, thorough characterization of the SWCNT thin film electrodes is required to understand the origins of their electrochemical properties. These electrodes have been characterized in detail in Publications II, III and IV and the results are summarized in Table 4. Raman and optical absorption analysis (shown in Figure 12 A and B) indicate the presence of SWCNTs with a

mean diameter of 2.1 nm and low defect density. TEM and HR TEM images, shown in Figure 12 C and D, respectively, show both SWCNT bundles and individual SWCNTs.

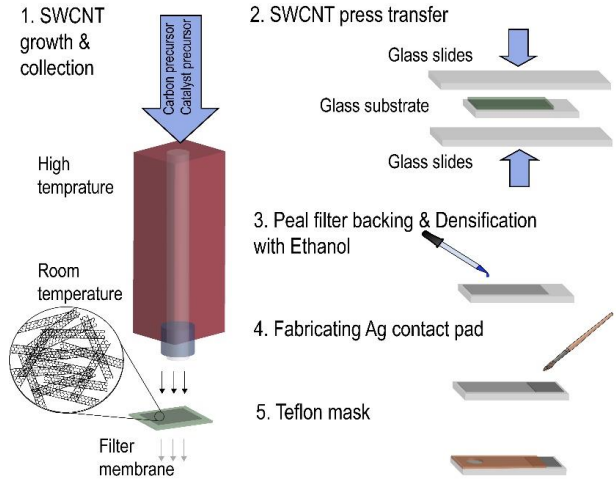

Figure 11. Fabrication process of SWCNT electrodes on glass substrates from Publication III.

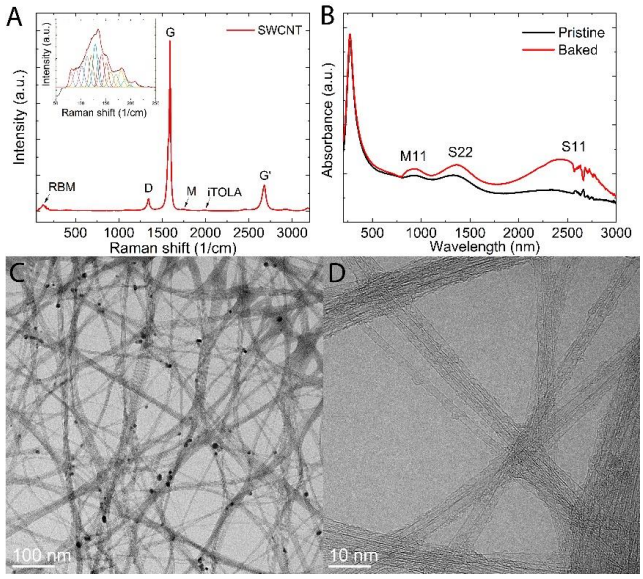

Figure 12. A) Raman spectrum and B) UV-Vis spectrum of SWCNT network electrodes. C) TEM and D) HRTEM images of the SWCNT electrodes press-transferred directly on TEM grids. From publication III.

HR TEM analysis reveals larger particles, with diameters in the range of 5-15 nm, on the sidewalls of the SWCNTs, that are encapsulated by few layers of carbon. This likely explains the resistance to oxidation of the Fe particles during short treatments in concentrated nitric acid, as observed in Publication II. In addition, smaller 2-5 nm particles are observed within the bundles. Furthermore, EDS analysis detected only C at the SWCNT sidewalls and C and Fe on catalyst particles. In Publication IV we indexed the diffraction spots as metallic α-Fe and

iron oxide. Further analysis in Publication III indicated the possible presence of metallic iron and the iron carbide Fe_3C. This TEM analysis indicates that the predominant crystalline phase seems to be Fe_3C for both the samples used in Publication III and Publication V. The XPS Fe 2p spectrum shown in Publication III, could indicate the presence of both metallic Fe, iron oxide and iron carbides. Similarly, the XAS Fe 2p spectrum indicates the presence of iron oxide or carbide as well as possible contributions from metallic Fe. Based on these results, it is highly likely that the SWCNT network contains some mixture of metallic iron, iron carbides and amorphous iron oxides. The XAS C1s spectrum further indicates, large number of π* orbitals and long-range order, indicating low defect density. The C1s spectrum also revealed the presence of ketone/aldehyde and carboxyl functional groups. The O1s spectrum further supports these findings.

In CV measurements, we show that the SWCNT electrodes support facile electron transfer with various outer sphere analytes. Furthermore, we show low apparent double layer pseudocapacitance and high signal-to-noise ratio in trace detection of analytes. The hydrophobic nature of the sidewalls has also been proposed to facilitate the adsorption of analytes with conjugated π-electron systems[109–112]. In Publication III, we also show the spontaneous accumulation of the lipophilic synthetic opioid fentanyl, leading to a much lower detection limit than previously reported. This same hydrophobicity, however, makes the SWCNT electrodes highly susceptible to irreversible fouling by proteins, as will be discussed in more detail in Section 6.1.1. In applications where high temporal resolution is not required, conductive polymer coatings and permselective membranes can be used to improve the selectivity and reduce protein fouling.

Table 4. Summary of physical, chemical and electrochemical characterization of SWCNT network electrodes.

Method	Observations	Reference
SR[a]	88 Ω/sq	III
Raman	0.102 ± 0.003, 0.021	III, VI
UV-Vis	Mean diameter: 2.1 nm, optical transparency: 86.6 %	III
TEM	Catalyst particle size: 2-15 nm, Diffraction patters: metallic Fe and iron carbide	III
EDS	Catalyst particles: C and Fe, SWCNT sidewall: C	III
XPS	C 71.7 ± 0.2, O 8.7 ± 0.2, Si* 19.5 ± 0.3, Fe 0.1 ± 0.01	III
XAS[a]	**C1s:** Highly sp^2 bound carbon with clear long-range order, Ketone/aldehyde and carboxyl peaks detected **O1s:** ketone/aldehyde, carboxyl, σ region convoluted by native oxide of Si wafer substrate **N1s:** Only very small signal detected for as deposited samples	III
CV	**Apparent double layer pseudocapacitance: (C_{dl}):** 10.3 ± 1.0 μF/cm²	III
	$Ru(NH_3)_6^{3+/2+}$: ΔE_p (mV): 73 ± 3.7 (100 mV/s) **$Fe(CN)_6^{4-/3-}$:** ΔE_p (mV): 95.4 ± 12.1 **$IrCl_6^{-3-/2-}$:** ΔE_p (mV): 51.0 ± 9.6	V

[a] Sheet resistance

5 . Miniaturized integrated electrochemical platforms

5.1 Printing technologies

In the last 20 years, printing technology has emerged as one of the most promising methods for serial production of reliable single-use devices, keeping both their affordability and analytical performance[184,185]. There is no doubt about the role of printed technologies as an enabling technology for the manufacturing of POC devices. Many comprehensive reviews on the topic have been published and will therefore not be attempted here[184–190]. Instead, the screen printing and dry printing processes are briefly introduced. The challenges in fabrication of miniaturized reference electrodes are also discussed in Section 5.2.

Whereas standard microfabrication techniques are still predominantly used for fabrication of integrated implantable sensors, wearable sensors and integrated electrochemical test strips are often produced by screen-printing or other printing technologies[184]. Ink-jet printing is also increasingly used for production of patterned electrodes[190] and modification of screen-printed electrodes[184]. The main advantage of ink-jet printing is the reduced lead-time for pattern design changes, as no masks are required. With a fixed design, screen-printing is often more efficient, requires less complicated equipment and is fully roll-to-roll compatible. Moreover, once design patterns have been fixed, screen-printing is a high throughput technology. The cost competitiveness and industrial maturity of the screen-printing process, coupled with the potential for mass utilization, easy customization, portability and ease of use, have made SPEs the most used printed sensors reported in literature[184]. Commercial glucose test strips have long been mass produced by screen-printing. These fully integrated sensor platforms are capable of reliable analysis from small samples with volumes from a few to tens of μL. Recently, such screen-printed integrated electrode strips have become commercially available from several reputable companies[184], and are therefore increasingly used as electrochemical platforms, as received or after further modification, by researchers.

In the screen-printing process, an ink or a paste is squeezed through a mesh-screen onto a substrate with a blade. The mesh contains a pattern that defines the dimensions of the electrode.[185] In contrast, ink-jet printing ejects small picoliter volume droplets from an ink-jet head. Both these technologies can produce linewidths with lower limits of 30-50 μm[32,191,192] , easily enough for most applications. Fabrication of nanoelectrodes, however, still requires standard lithography for patterning of electrodes. Despite the many advantages of screen-printing, design changes still produce lead-times due to the need to redesign the mesh-screens. In addition, carbon inks are usually resistive. Therefore, conductive base-patterns, usually Ag, have to be screen-printed in a separate step. In integrated sensor platforms, this step is usually

made in the same set as the base-pattern required for the Ag/AgCl reference electrode. In addition, the used ink/paste formulations are complex and include solvents, binders, plasticizers and modifiers.[188] Moreover, the compositions of these ink formulations are usually regarded by the manufacturers as proprietary information. Differences in the ink composition, such as type, size and particle loading, as well as the printing and curing conditions, may affect the electrode performance.[193]

Most screen-printed electrodes where the working electrode is graphite based, often referred to as screen-printed carbon electrode (SPCE), suffer from the same limitations as conventional carbon electrodes, namely limited sensitivity and selectivity. Their performance can, however, be modified with a wide range of nanomaterials, polymers, enzymes, nucleic acids, and electrochemical mediators, directly in the ink or subsequently by using drop-castable dispersions[184]. To this end, homemade ink formulations including modifiers, such as carbon nanoparticles, are also increasingly reported[188]. Screen-printed electrodes are also increasingly modified by drop casting, ink-jet printing, electrodeposition or dip-coating[184]. This customization of composite inks makes a large range of properties and hybrid materials possible. Moreover, screen-printed carbon electrodes functionalized with carbon nanomaterials have also recently become commercially available.

Recently, dry-printing technologies have emerged as industrially compatible ways to produce patterned nanomaterial-based electrodes. One such process is the dry printing of SWCNT networks[32,82], that can be used to make electrochemical electrodes. These can be prepatterned by collection through a mask, or by subsequent pattering using laser or standard lithography and dry-etching techniques. Direct patterning down to 10 μm line widths has been demonstrated[194]. Laser patterning is a roll-to-roll compatible, high throughput process with accuracy of 30 μm[32], making it capable of linewidths comparable to other printing technologies. Instead of developing new ink formulations functionalized with nanomaterials or subsequent modifications, SWCNT films can be synthesized with aerosol CVD, collected and dry-transferred onto a wide range of substrates, including polymers, silicon and glass. By varying the process parameters of the aerosol CVD process, SWCNT film properties such as the thickness, morphology amount of metal catalysts, chirality and defect density can be controlled[82,182]. In Publication VI, we show the fabrication of fully integrated, patterned SWCNT electrodes, by dry printing of SWCNT films onto polymer sheets followed by laser pattering. This process is discussed in detail in Chapter 8.

5.2 Miniaturized reference electrodes

In miniaturized electrochemical platforms, the reference electrode is a crucial component used to measure and control the solution side potential. Despite the recent increase in the availability of screen-printed electrodes, the challenge of fabricating inexpensive, durable and reliable miniaturized reference electrodes still remains challenging[195]. The poor performance of miniaturized reference electrodes has significantly limited the applicability of miniaturized electrochemical platforms, particularly in potentiometric sensing[195]. In this section, we will focus on the challenges of producing inexpensive pseudo-reference electrodes, also called quasi-reference electrodes (QRE), for disposable test strips. In implantable sensors, long term stability is also required, and more complicated designs and fabrication techniques including standard microprocessing techniques are used. The most commonly used reference electrode

in electrochemical sensing is the Ag/AgCl electrode. This reference electrode operates based on two simultaneous reversible reactions

$$Ag^{+}_{(aq)} + e^{-} \leftrightharpoons Ag_{(s)} \quad (10)$$
$$Ag^{+}_{(aq)} + Cl^{-} \leftrightharpoons AgCl_{(s)} \quad (11)$$

And the potential of the electrode is determined by the Nernst Equations as follows

$$E = E^{0} - 2.303\frac{RT}{nF}\log([Cl^{-}]), \quad (12)$$

where E^0 is the electrode standard potential, n is the number of electrons transferred in the reactions, R is the molar gas constant, T is the temperature in Kelvin and F is the Faraday constant and [Cl^-] denotes the free chloride ion concentration. From this, it follows that the Ag/AgCl electrode in theory exhibits a susceptibility of – 59.16 mV/pCl (at a temperature of 25 °C) toward the Cl^- ion concentration. In conventional Ag/AgCl electrodes the environment is controlled by incasing the Ag/AgCl wire in a glass capillary filled with electrolyte with known [Cl^-] concentration. The main difference between QRE and normal Ag/AgCl electrodes is that, in the QRE electrode the [Cl^-] is not maintained by a layer with constant Cl^- concentration. This makes the QRE susceptible to fluctuations in Cl^- and Ag^+ concentrations. For the same reason, the potential of screen-printed Ag/AgCl electrodes can also be susceptible to interference from other ions[196,197].

Pt, Ag or Ag/AgCl wires are examples of commonly used pseudo-reference electrodes[189]. Miniaturized reference electrodes are commonly fabricated both by screen-printing and other microfabrication techniques or a combination thereof. These fabrication methods have been thoroughly reviewed by Shinwari et al.[198] and Sophocleous et al[196]. A major problem with silver thin film pseudo-reference electrodes in miniaturized systems, is the rapid dissolution of small electrode volumes, leading to short life times[198]. Quasi-reference electrodes also suffer from drifting potentials during measurements, long run-in times before the potential stabilizes and relatively short shelf life[195,196]. Therefore, thick film technology, predominantly screen-printing, is the main method used to fabricate Ag/AgCl electrodes. Presently, both Ag and AgCl inks are commercially available. In a typical process, silver is first screen-printed as the conducting layer, after which an AgCl top layer is screen-printed. General requirements of miniaturized reference electrodes include:

i) Must have high exchange current and thus be non-polarizable
ii) Reproducible potentials
iii) Minimize potential drift, over the expected lifetime of the sensor
iv) Minimize susceptibility to chloride ion concentration
v) Minimize susceptibility to other anions

The performance of these QRE is generally described by its potential stability, drift rate, lifetime, hydration period, shelf-life, price and compatibility with mass production. To achieve satisfactory performance in applications requiring long-term stability, such as implantable sensors and environmental monitoring, all the components of conventional reference electrodes, including metal, salt filling solution and interfaces need to be miniaturized. Other

limitations on materials selection may also be imposed by the nature of the experiment. For example, in the case of an implantable sensor, the electrodes should not introduce foreign toxins into humans, which necessitates the use of highly polarizable electrodes.

Various multilayer designs incorporating coatings that aim to reduce the fluctuation of Cl^- concentration, as well decrease potential drift and increase shelf-life, have been reported. With these designs, susceptibilities much lower than the 59 mV, predicted by the Nernst equation, can be achieved. These designs have been thoroughly reviewed by Sophocleous et al.[196]. It should be noted, however, that such complex designs may significantly increase the cost of the electrodes and in some cases compromise the mass producibility of the sensor. Moreover, such designs often involve a trade-off between hydration time and drift rate of the electrode, which is not desirable in POC testing.

Many of the more complicated designs have been fabricated for potentiometric sensing applications requiring high stability and drift rates below 1 mV. Such strict requirements are, however not required in voltammetric and amperometric sensing, and therefore simpler designs may be used. Even with these techniques, however, fouling and other degradation mechanisms have to be considered in implantable sensors.

Polymer coatings have been widely used to stabilize the potential of Ag/AgCl reference electrodes. Nafion coatings in particular, have been found to be effective in stabilizing the potential of Ag/AgCl electrodes, as well as in improving the long term stability in vivo[199–201]. Nolan et al.[200] used Nafion coatings to stabilize the potential of screen-printed Ag/AgCl electrodes. Moussy et al.[199] have also shown that the potential of a Nafion-coated Ag/AgCl electrode remained constant for up to 2 weeks after implantation in a rat. Similarly, Hashemi et al.[141] also found that Nafion coated Ag/AgCl electrodes implanted in the brain of rats remained stable for up to 28 days. In contrast, the uncoated electrode showed a potential shift of +0.2V already after 4 days. They further observed that, while both the uncoated and coated electrode implantation sites showed extensive glial encapsulation, the lesion around the Nafion-coated electrode showed more intact cells, implying that they adsorb less strongly than on the uncoated electrode. In Publication VI, we propose a process for the fabrication of Ag pseudo-reference electrodes by screen-printing Ag and slot die coating with Nafion. To ensure adequate performance, both uncoated and Nafion coated electrodes were studied in supporting electrolytes with different Cl^- concentrations.

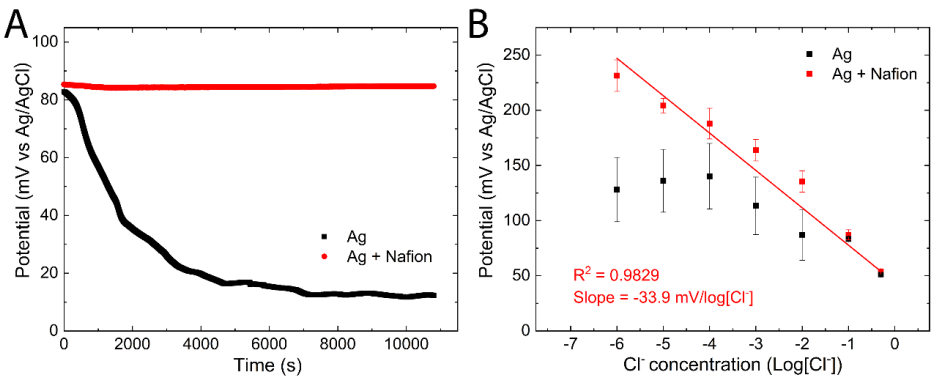

Figure 13. A) Potential of the uncoated and Nafion-coated Ag quasi-reference electrode vs. Ag/AgCl(sat.) in 0.01 M PBS solution. B) Potential as function of the Cl- concentration in KCl solutions and. Error bars show the standard deviations of measurements with 3 different electrodes. Adapted from Publication VI.

Figure 13 A shows the potential of uncoated and Nafion coated Ag reference electrodes in 0.01 M PBS solution, vs. a Ag/AgCl(sat KCl) electrode. Both the measured electrodes start at a potential of 84 ± 1mV. The potential of the uncoated electrode, however, drifts significantly during the measurement and stabilizes only after approximately 2h. In contrast, the Nafion-coated electrodes immediately shows a stable potential that remains stable for up to 7 days, with a potential drift of only 9.85 mV. In the study by Moussy et al.[199], 30-35 min was required for the potential to stabilize. During a 7.5 h measurement in Publication VI, a potential of 84.78 mV with a maximum deviation of less than ±1 mV was obtained. The potential stability and drift rate are comparable to screen printed Ag/AgCl electrodes with much more complicated design, with protective layers incorporating a salt matrix (KCl)[196]. Moreover, we also showed that the potential remains stable for approximately 1.5 years under ambient conditions, indicating excellent shelf-life.

The susceptibility to Cl^- concentration was further studied by measuring the potential in KCl solutions with different concentrations. Figure 13 B shows the average potential of three uncoated and Nafion coated reference electrodes as a function of the logarithm of the Cl^- concentration. The potential of the Nafion coated Ag reference electrode depends linearly on the logarithm of the Cl^- concentration of the electrolyte with a slope of -33.9 mV/log[Cl^-]. The potential of the uncoated electrode shows less dependence on the Cl^- concentration.

These results show that the Nafion-coated electrodes can be used for voltammetric measurements in POC applications without any preconditioning. The uncoated electrode also shows a sufficiently slow drift rate, that it can be used as a disposable electrode for single determinations. The potential drift, however, significantly limits its use in applications requiring long-term stability. Furthermore, while the susceptibility of the Nafion coated electrode is lower than that predicted by the Nernst equation[196], its use is still limited to applications where the sample Cl^- concentration is known. The ionic strength of blood is close to that of PBS and variations are relatively small[202]. The interference of other anions and further studies in biological matrices with varying pH and ionic strength still need to be carried out, to assess their applicability in implantable sensors and POC testing in other biological matrices.

6 . Electrochemical measurements in biological matrices

6.1 Challenges in electrochemical detection in biological matrices

Sensors developed for *in vivo* detection or *in vitro* determination of drugs and biomolecules from minimally processed biological samples have to be highly selective and resistant to biofouling. Biological matrices such as urine, blood and saliva are highly complex matrices with an abundance of chemicals that may cause interference and passivation of the electrode. Especially whole blood is a highly complex matrix with blood cells, proteins and a wide range of biomolecules at relatively high concentrations.

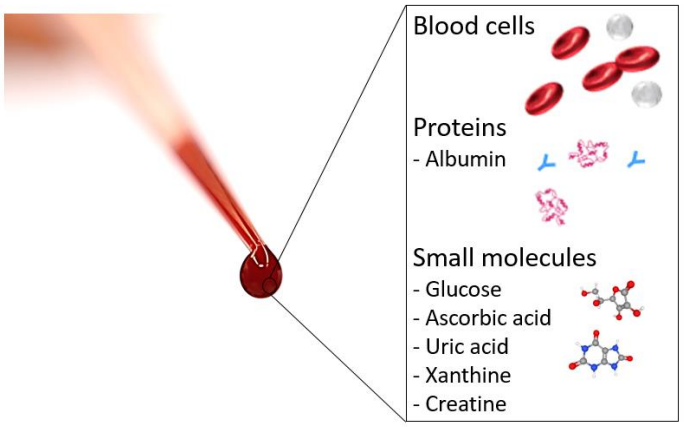

Figure 14. Composition of whole blood samples.

This complexity, shown in Figure 14, presents several challenges to any point-of-care testing. In conventional laboratory-based analysis, several pretreatment steps are usually required, including centrifugation to obtain serum or plasma and protein precipitation[203]. In contrast, only minimal processing can be carried out in the POC detection, and in vivo detection naturally allows for no altering of the measuring environment. Therefore, these challenges need to be considered when electrodes are designed.

6.1.1 Electrode fouling

Electrode fouling is a phenomenon that generally involves the passivation of an electrode surface by a fouling agent that forms an impermeable layer on the electrode. The increasing buildup of such a layer can hinder the direct contact of an analyte of interest with the electrode surface, making electron transfer impossible[29]. The fouling agent may be a component of the

matrix, the analyte itself, or a product of the electrochemical or subsequent chemical reactions. The fouling agent binds to the electrode surface through hydrophilic, hydrophobic and electrostatic interactions[29,204]. Covalent modification of carbon surfaces by electrogenerated radicals has also been reported[205]. Generally, carbon electrodes are considered to be less susceptible to electrode fouling compared to noble metal electrodes in complex matrices, but they also suffer from electrode fouling[29,105,159].

Many factors, including surface chemistry and surface roughness[29,105,204,206–208], affect the fouling of carbon electrodes. The electrode fouling and degradation mechanisms, as well as different antifouling strategies to maintain electrode performance in biological environment, have been discussed in great detail in the reviews by Hanssen et al.[29] and Wisniewski and Reichert[31]. They found that, common methods to reduce biofouling include surfactant modification, hydrogel coatings, polymer and cellulose membranes, naturally derived membranes, hydrogels, as well as surface chemistry and topography modifications.

In both POC testing of blood samples and *in vivo* monitoring of neurotransmitters, the electrode needs to be able to produce reliable results in the presence of proteins. Especially blood samples contain large amounts of proteins, mainly albumin, but also globulins, and fibrinogen[202], that may rapidly foul most electrodes. In aqueous solutions, the outer layers of soluble proteins are hydrophilic and they are hydrophobic on the inside, to maintain the protein folding. Due to this dual nature, proteins can foul both hydrophobic and hydrophilic electrodes[29]. This was further shown by Sweryda-Krawiec et al.[209] who observed that the water contact angles of hydrophobic and hydrophilic surfaces approach the same value of approximately 60° upon adsorption of bovine serum albumin (BSA), indicating direct functionalization of both surfaces by adsorption of BSA. The fouling of hydrophilic surfaces has been postulated to occur mainly through hydrogen bonding and electrostatic interactions between charged groups, making the fouling of hydrophilic surfaces reversible. In contrast, fouling of hydrophobic surfaces is irreversible, and usually involves unfolding of the protein to allow for hydrophobic inner parts to interact with the electrode surface.[29,210]

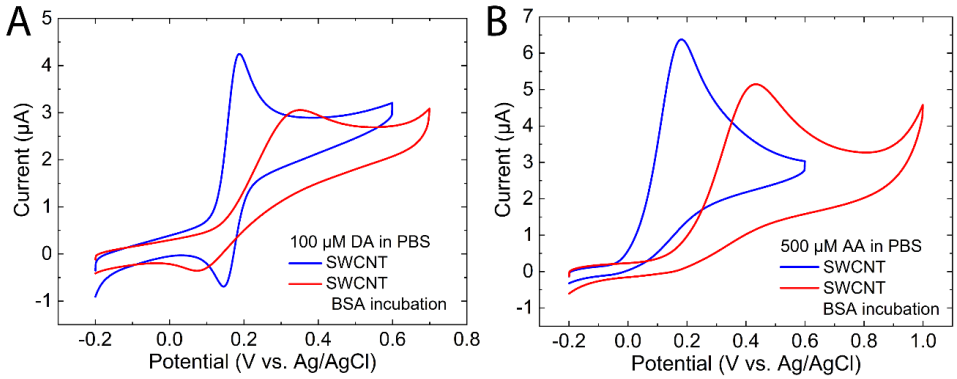

Figure 15. Effect of 1h incubation in 4 wt% BSA at room temperature. Cyclic voltammogram in A) 100 µM DA and B) 500 µM AA with pristine (blue) and BSA incubated electrodes after 15 min rinsing in PBS (red). Scan rate: 100 mV/s. Supporting electrolyte pH 7.4, 0.01 M PBS.

Due to the hydrophobic nature of the defect free SWCNT sidewall, SWCNT electrodes are highly susceptible to irreversible hydrophobic protein fouling[29]. To further investigate the effect of fouling, similar electrodes as the ones used in Publication III were measured in DA

and AA, after the 1h incubation in 4 wt% BSA and washing in PBS for 15 min. Figure 15 shows clear passivation of the electrodes after incubation in BSA, in the cyclic voltammograms of A) 100 µM DA and B) 500 µM AA. Thus, modification of the electrode surface chemistry or coating of the electrode is required to improve the fouling resistance. In Publication V and VI, we use Nafion membranes to enable measurements in mildly diluted human plasma and capillary whole blood, without protein precipitation.

In contrast, DLC films, including ta-C, are often-reported to be resistant to biofouling[29,206,207]. This fouling resistance has been attributed to the high sp^3 fraction of ta-C films. Similarly, the high sp^3 content of BDD films, together with the low presence of polar surface functional groups, is thought to make this electrode resistant to fouling by many fouling agents.[29] BDD electrodes have also been found to be more resistant to biofouling than GC electrodes[211] and more resistant to fouling by DA than a wide range of other carbon electrodes[105]. Moreover, Trouillon & O'Hare[211] found that the presence of oxygen containing functional groups on the surface reduced the fouling of GC electrodes. Similar results have been obtained also for DLC films[206]. In contrast to BDD films, our Ti/ta-C films have an sp^2 rich surface layer with presence of polar functional groups, such as carbonyl and carboxyl[37,165,212]. This is further supported by the low isoelectric point of 2.6, for the Ti/ta-C films[41]. Isoaho et al.[159] showed that Ti/ta-C electrodes preserve their activity toward the outer sphere redox probe FcMeOH after incubation in BSA.

In contrast, Peltola et al.[208] showed that, while the electron transfer of $Ru(NH_3)_6^{2+/3+}$ was not significantly affected by BSA fouling, incubation in fetal bovine serum (FBS) caused a small increase in electron transfer resistance of the Ti/ta-C electrode. The negatively charged OSR probe $IrCl_6^{2-}$, was significantly affected by both BSA and FBS incubation. Moreover, significant fouling by both BSA and FBS was found for the ISR probe DA, known to require adsorption prior to electrochemical oxidation[213,214]. These results suggest that Ti/ta-C films are not resistant to protein fouling, but are in some cases capable of preserving the electrochemical activity despite protein adsorption. For this reason, studies with only BSA may not accurately reflect the electrode fouling. Peltola et al. further noted that BSA fouling also had barely any effect on $Ru(NH_3)_6^{2+/3+}$ on a pyrolytic carbon electrode. It could be that the negative charge of BSA (pI = 4.9) adsorbed on the surface, does not cause any electrostatic hindrance for cations. Moreover, it has been proposed that complex multiprotein matrices, such as FBS, can form passivation layers with multiple proteins, which could explain the more complete fouling[210]. Therefore, fouling experiments should also be carried out in more complicated matrices and with several redox probes, preferably including also the target analytes.

In addition to proteins in the matrices, electrogenerated reaction products also have the potential for electrode fouling. Especially phenol, catechol and nitrogen containing functional groups are known for their ability to foul the electrode[29,205,215,216]. The fouling has been proposed to be due to high molecular weight reaction products or by covalent attachment to the electrode surface. This is of special concern for wearable and implantable sensors that need to preserve their activity for up to weeks. Patel et al.[105] showed that different carbon electrodes foul at different rates with consecutive scans in DA solutions. Electrodes with high surface roughness have also been found to be more resistant to fouling by electrogenerated reaction products[29].

The Ti/ta-C electrode is highly susceptible to electrode fouling by electrogenerated reaction products of dopamine[96]. In Publication I, we showed that the electrode fouling can be greatly

reduced by modifying the Ti/ta-C electrode with PRGO. Porous electrodes are generally considered to have higher fouling resistance to a wide range of fouling agents[29,208]. Figure 16 shows the passivation study for the SWCNT electrode, with consecutive scans in 15 µM fentanyl citrate, carried out in Publication III. Despite the passivation observed at high concentrations, no passivation was observed with over 10 consecutive scans at concentrations of 1 µM and 500 nM. In contrast, the Ti/ta-C electrode was severely passivated already on the 3rd scan in 1 µM fentanyl citrate, despite very low sensitivity to begin with. It is likely that the porous nature of SWCNT electrode protects it from passivation.

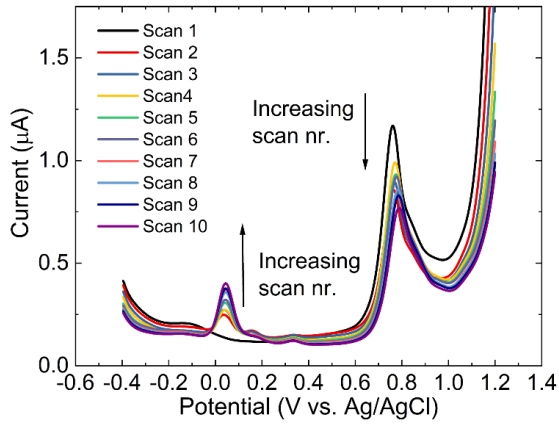

Figure 16. Passivation study with consecutive differential pulse voltammetry measurements with 15 µM fentanyl in PBS with SWCNT electrode from Publication III.

6.1.2 Selectivity

Analytical interference from a wide range of sources, is a well-known phenomenon in the clinical laboratory[217]. The capability of a method to deliver signals free of interferences, and true results is an important quality criterion of an analytical method. This capability is often referred to as the "selectivity" of the sensor for analytical method. The same meaning is often given to the term "specificity" and unfortunately, the two terms are often used interchangeably in literature[218]. The International Union of Pure and Applied Chemistry (IUPAC) defines selectivity as follows:

"Selectivity refers to the extent to which the method can be used to determine particular analytes in mixtures or matrices without interference from other components of similar behavior."

They also define the word "specific" (in analysis) as being considered the ultimate of selectivity. They also advocate the use of selectivity.[218] In addition, the International Council for Harmonisation of Technical Requirements for Pharmaceuticals for Human Use (ICH) defines specificity as "the ability to assess unequivocally the analyte in the presence of components which may be expected to be present"[219]. As it is generally recognized, that no assay is completely specific under all conditions, and it is not always possible to demonstrate that an analytical procedure is completely specific, the term selective will be used in this thesis, where

the interference of different chemicals is considered. While it is acknowledged that few methods are completely free from interference under all conditions, liquid chromatography with tandem mass spectrometry (LC–MS–MS) yields a selectivity which is rarely compromised. Therefore it is often required in legal situations when positive and nonbiased identification is needed.

For electrochemical POC assays, the limited selectivity in complex samples is almost always the limiting factor. The selectivity is also an important parameter studied in the validation of laboratory-based immunoassays for detecting small molecules. In the ICH validation guidelines, the procedure used to demonstrate selectivity will depend on the intended application, and therefore expertise is required to asses which interferents should be studied. In addition to proteins (discussed in the previous section), biological samples contain a wide range of small molecules that can cause interference in electroanalysis. In addition, variations in the ionic strength and pH may cause altered voltammetric response. Therefore, at least the following classes of chemicals should be considered for each application:

i. Endogenous chemicals
ii. Other drugs and xenobiotics expected to be present
iii. Metabolites of drugs and xenobiotics
iv. Changes in pH and ionic strength

The first group of interferents is the biomolecules present in biological samples. Table 5 presents a non-exhaustive list of the concentrations of mainly small molecules, found in blood and cerebrospinal fluid (CSF), that are known to be electroactive. It should be noted that Table 5 is not intended to be an exhaustive summary of the composition of blood and CSF. Rather, the aim is to show some of the approximate concentrations of some endogenous chemicals with the potential to cause interference. Urine is also commonly used in recovery tests of electrochemical sensors, because it contains many of the same interferents as blood and is easy to collect. Moreover, the low protein concentrations (albumin 7-70 mg/L[220]) makes direct analysis possible without protein precipitation. Despite its applicability for screening of drugs or other biomarkers, urine in most cases provides little information about the blood concentrations. It is also highly variable in composition and metabolite concentrations[221]. Therefore, an electrode developed for analysis of urine samples is not necessarily applicable in analysis of blood samples. For this reason, urine has been excluded from Table 5 and its composition is discussed in great detail elsewhere[221].

As seen from Table 5, the plasma protein concentration is also much higher compared to that of CSF, making protein fouling a real challenge in blood samples. Over 90 percent of plasma is water, with the remainder being mostly proteins, such as albumin, globulins, and fibrinogen—as well as other solutes such as lipids, glucose, electrolytes, and dissolved gases. In addition, biological matrices contain various inorganic constituents, such as salts, that can have variable concentrations.[202] Blood also contains a large number of small molecules with the potential of causing significant interference in electrochemical measurements. It has been shown that the blood concentrations of many of these interferents vary with diet and exercise, time of day, sex, age and diseases[202,243,280,281]. Therefore, any electrode platform has to be able to cope with not only these relatively large interferent concentrations, but also with relatively large variations in these concentrations.

Table 5. Non-exhaustive list of endogenous chemicals in blood and CSF samples known to be electrochemically active. The oxidation potentials have been reported for various carbon-based electrodes with a wide range of chemistries in various supporting electrolytes with pH close to physiological. If other reference electrodes were used, the potentials have been converted to Ag/AgCl reference electrode.

Molecule	Concentration		Oxidation potential (V vs. Ag/AgCl)
	plasma/serum	CSF	
Proteins			
Albumin	38.63-42.59 g/L[222]	170-269 mg/L[222]	0.745-0.845[223]
Total protein	67.2 g/L[202]	0.25-0.39 g/l[222]	NA
Purine derivatives			
Uric acid	160-470µM[224–226]	15.3-24 µM[226,227]	0.27-0.32[228,229]
Adenosine	0.2 ± 0.1 µM[226]	<0.1 µM[226]	Peak 1: 1.0-1.2 Peak 2: 1.5[23,230]
Adenine	0.3 ± 0.1 µM[226]	< 0.2 µM	0.94-1.2[231,232]
Xanthine	0.4 ± 0.1 µM[226]	1.69-2.3 µM[226,227]	0.64-0.71[228,229]
Hypoxanthine	0.6 ± 0.1 µM[226]	2.23-3.06 µM [226,227]	1.04-1.1[228,229]
Glutathione	941 ± 155 µM[233]	0.24 ± 0.07 µM[234]	0.35-0.67[235–237]
Amino acids			
Histidine	40 ± 17 µM[238]	7.7 ± 5.6 µM[238]	1.1[239]
Tyrosine	35.1-69 µM[226,238]	7.6 ± 4.9 µM[226,238]	0.67-0.78[239–242]
Methionine	25-36 µM[238,243]	2.8 ± 1.9 µM[238]	~1.2[239]
Tryptophan	35 ± 13 µM[226,238]	1.2 ± 0.8 µM[238]	0.79-0.96[239,240]
Cysteine	45 ± 23 µM[243]	traces[244]	0-0.75[235,245–248]
Cystine	29-49 µM[249]	0.2 ± 0.3 µM[244]	1.2-1.42[239,250]
Vitamins			
Ascorbic acid, vitamin C	43.48 ± 13.34 µM[251]	166 ± 45.08 µM[251252]	0-0.7[47,241,253]
Vitamin B	0.3-132 nM[243,254]	0.008-24 nM[255]	0.76-0.795[256,257]
Vitamin A	1.9 ± 0.5 µM[254]	0-927.57 nM[258]	0.8-0.9[259]
Vitamin D	17.5-89.9 nM[254,260 x]	5-61 nM[260 x]	1.1[261]
Vitamin E	10-40 µM[224,254,262]	23.9 ± 9.3 nM[262]	0.2-0.5[259,263]
Hormones			
Thyroxine	0.102-0.115 µM[264,265] (total)	2.41 ± 0.46 nM[265] (total)	0.3[266]
Estrogen	73-440 pM[267]	8.4 ± 0.7 pM[267]	0.6[268,269]
Neurotransmitters and metabolites			
Histamine	2.6-6.3 nM[270]	2.70 ± 0.36 nM[271]	1.245-1.445[272]
DOPA	6.24-8.37 nM[273]	0.51-2.54 nM[273]	0.4[23]
Dopamine	0.06-3.9 nM[273,274]	0.59-2.96 nM[273]	0.2[23,275]
Norepinephrine	0.07-4.31 nM[273,274]	0.65-3.26 nM[273]	0.2[23,275]

Table 6. Continued.

Epinephrine	0.11-0.33 nM[273]	0-0.11 nM[273]	0.2[23]
3-Methoxy-4-hydroxyphenylglycol	37.14 ± 9.77 nM[274]	49.2±11.4 pM[276]	0.2[275]
Homovanillic acid	38.48 ± 5.54 nM[274]	0.198 ± 0.052 nM[276]	0.5[23]
3-methoxytyramine	0.024-0.789 nM[277]	15-200 nM[278]	0.5[23]
DOPAC	8.39-11.89 nM[273]	1.31-2.91 nM[273]	0.2[23]
Serotonin	1.41-30.51 nM[273,274,279]	1.25-2.78 nM[273]	0.35[23]
5-Hydroxyindole-acetic acid	9.10 ± 1.36 nM[274]	0.107±0.028 nM[276]	0.35[23]

[x]25-hydroxyvitamin D

Despite the wide range of molecules that have been electrochemically detected, very little research has been carried out on the origin of the matrix effect observed in biological samples. Moreover, few studies actually show the results of recovery studies carried out in biological matrices. Nevertheless, interference due to anti-oxidants, such as ascorbic acid and uric acid are often reported. The interference of AA and UA is frequently studied as they have oxidation potentials close to that of dopamine, paracetamol and morphine that are some of the most studied analytes in electrochemical detection[33].

Ascorbic acid

Ascorbic acid (AA), or vitamin C, is an important anti-oxidant acting as a free radical scavenger in intracellular and extracellular fluid[282–284]. AA has also been linked to differentiation of stem cells into neurons, and neurotransmission of DA and glutamate[285,286]. Under physiological conditions (pK_a = 4.2), AA exists in its deprotonated anion ascorbate form[282]. AA functions as a one-electron donor, capable of reducing reactive oxygen and nitrogen species generated during cellular metabolism.[283] As can be seen from Table 5, AA is present at relatively high concentrations in bodily fluids. The blood concentration of AA has been shown to vary in a wide range depending on dietary and supplement intake[202]. AA is concentrated in the central nervous system and is therefore of special importance for DA sensors[287,288].

Ascorbic acid is electrochemically active and oxidized in the wide potential range of 0-0.6 V (vs. Ag/AgCl), depending on the electrode material[37,47,105,193]. AA has been reported to cause interference in the detection of many analytes, including DA, PA, MO and CO[37,47,289,290]. With many electrode materials, such as GC, ta-C and screen-printed carbon electrodes, AA shows slow reaction kinetics with a poorly defined broad peak in cyclic voltammetry, making it particularly problematic in detection of dopamine. The postulated oxidation pathway for AA at physiological pH is shown in Figure 17. In this mechanism, AA is first deprotonated to form an ascorbate anion, after which ascorbate undergoes a reversible $2e^- 1H^+$ transfer, resulting in dehydroascorbic acid (DHA). DHA further undergoes hydrolysis to from 2,3-diketogluonic acid (DKG)[291]. It should be noted that this chemical step involves intermediates, that have been omitted from Figure 17[292,293]. The first electrochemical step has been proposed to proceed with

an overall ECE mechanism[294,295]. In this mechanism, an e^- is first transferred, followed by proton transfer, and finally the transfer of the second electron. Ruitz et al.[292] suggested that the electron transfer steps are reversible and that the chemical reaction is the rate limiting step, whereas Pietro et al.[295] argued that the second proton transfer is rate limiting. Nevertheless, the reversible nature of the electron transfer was later confirmed by Perone et al.[296] who observed a reduction wave of DHA with a hanging mercury electrode at scan rates above 100 V/s. The peak potential separation of 30 mV, further indicated a reversible 2 e- transfer.

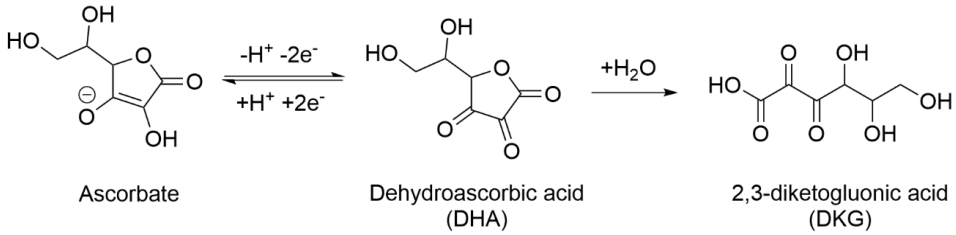

Figure 17. Proposed oxidation pathway for ascorbic acid at carbon electrodes.

Uric acid

Uric acid (UA) is a cellular waste product formed by oxidation of purine derivatives hypoxanthine and xanthine. Like AA, UA has important antioxidant activity, and has been reported to contribute over 50% of the antioxidant capacity in blood. Its concentration in blood is highly variable by factors such as diet, sex, age and metabolic syndrome.[297] Patients with hyperuricemia have high blood uric acid concentrations (≥ 7 mg/dl for men and ≥ 6 mg/dl for women), and it is a prerequisite for gout. The role of diet in hyperuricemia is not fully understood, but high intake of fructose-rich foods and high alcohol intake seems to influence hyperuricemia[225,297]. Due to its low solubility in blood, the risk of urate crystal formation and precipitation increases above concentrations of 6.8 mg/ml[298]. As can be seen from Table 5, the UA concentration in CSF is considerably lower than in blood. UA is a weak acid (pK_a = 5.8) and therefore is present predominantly (98%) as its monovalent anion urate, at physiological pH[297–299]. It circulates relatively free of protein binding (< 4%).

Interference from UA is often reported in the detection of PA, morphine and even other opioids that oxidize at much higher potentials than UA, such as codeine[290,300]. For this reason, the highly variable concentrations of UA in biological samples is likely a major source of matrix effect in electroanalytical chemistry. The proposed pathway for oxidation of UA is shown in Figure 18, and involves reversible transfer of $2e^-$ and $2H^+$ to produce a very unstable quinonoid diimine. This diimine radical further reacts with water to form imine alcohol.[301–303] The first electrochemical step has been shown to be reversible and a reduction peak can be observed at fast scan rates (>1-20 V/s). The further chemical reactions are not well understood, but the final products have been identified. The pathway of the last chemical steps is known to be dependent upon the pH and phosphate ions concentration. A low pH favors formation of alloxan and urea, whereas neutral pH leads to formation of allantoin and alloxan. Mechanisms for these reactions have been proposed and are discussed elsewhere.[301,303,304] To the best of our knowledge, no electroactivity of the final products allantoin and alloxan has been reported, whereas urea has been detected by nickel catalyst modified electrodes in alkaline media[305].

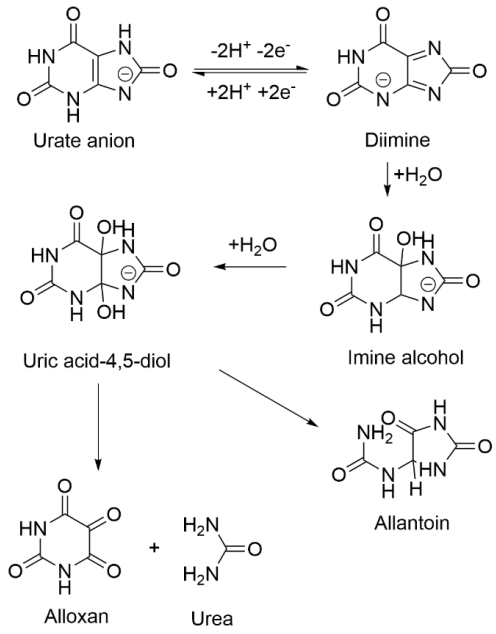

Figure 18. The pathway for electrochemical oxidation of uric acid at neutral pH.

Other endogenous interferents

To the knowledge of the author, the matrix effect in electrochemical analysis of blood samples has not been systematically studied. In addition, very few works actually show the voltammograms of the recovery studies in biological matrices. In publications V and VI, as well as other work[16], we observe significant matrix effects in plasma samples. As shown in Figure 35 and in[16], the matrix effect can be significantly reduced, but not completely removed, when electrodes are coated with Nafion. Several additional potential interferents that may cause the matrix effects are identified in Table 5.

The purine metabolites, xanthine and hypoxanthine, have been previously proposed to cause peaks in voltammetry of blood and urine samples. In addition to a peak attributed to UA, Raj et al.[228] reported peaks around 0.65 V and 0.97 V in both human blood serum and urine samples, with an electrochemically reduced graphene oxide modified GC electrode. They further spiked the samples with xanthine and hypoxanthine and found that the currents of both these peaks increased. The increased current in this experiment does not, however, prove that the peaks observed in bank plasma are due to xanthine and hypoxanthine. As seen from Table 5, relatively low concentrations of xanthine and hypoxanthine are found in plasma and CSF. Moreover, the samples were diluted 10 times, making it unlikely that the peaks are only due to xanthine and hypoxanthine.

In contrast, amino acids are present at relatively high concentrations up to few tens of μM. Moreover, daily rhythms and diets cause variations in the concentrations of these amino acids[280]. There are at least five electroactive amino acids, namely cysteine, histidine, methionine, tyrosine, and tryptophan, whose electrochemical oxidation at carbon electrodes has been reported[239,306]. In addition, electrochemical oxidation of cystine, a dimer of two

cysteine molecules, has also been reported[239,250]. Other amino acids have also been studied, but did not show any oxidation peaks in the pH range of 4-10[307]. Moreover, it has been shown that several proteins, including BSA, ribonuclease, lysozyme, histone fraction H1, insulin and poly-L-tyrosine produced voltammetric waves between 0.7 and 0.8 V (vs saturated calomel electrode (SCE)). These peaks have been attributed to the tyrosine and tryptophan residues in proteins[223,308]. Electrochemical analysis in combination with mass spectroscopy revealed a specific cleavage of the peptide bond at the C-terminal side of tryptophan and tyrosine residues[309,310]. More recently, oxidation of histidine residues in proteins and methionine residues in peptides have been reported at high potentials with carbon electrodes[206].

Tryptophan and tyrosine contain phenol functionalities and are usually oxidized around 0.6 V. Histidine has a side chain with an amine and oxidizes around 1 V depending on the electrode. Cysteine and methionine are sulfur containing amino acids. The oxidation potentials for thiols in these amino acids show highly variable values depending on the electrode. That of cysteine varies in the range of 0-1 V, whereas methionine is usually oxidized above 1V.[239–242] The relatively high plasma concentrations make it likely that amino acids contribute to the matrix effect observed in plasma samples in Publication V (for codeine) and tramadol in[16]. Amino acids could also explain the residual peaks observed in biological matrices with Nafion coated SWCNT electrodes (see Figure 34) as at least some amino acids have been reported to be able to permeate Nafion membranes[311].

In addition, biological samples contain hormones, vitamins and neurochemicals. These endogenous chemicals are present at low concentrations but could be enriched by Nafion. Despite their low concentrations, they also have the potential to cause interference, particularly with highly sensitive modified electrodes used in trace analysis. For example, the list of potential interferents is much longer for morphine compared to that of paracetamol, simply due to the extremely large difference in the concentrations of these two analgesics expected to be found in real patient samples.

It should be noted that biomolecules and drugs that are not electrochemically active may also cause interference in electroanalytical chemistry, through competitive adsorption or electrode fouling. For example, lipids and fatty acids can tightly adsorb to carbon electrode surfaces, fouling the electrode[29]. Similarly, various small molecules that are not electrochemically active can adsorb to the active sites of the electrode. Thus, this phenomenon can cause interference by reducing the sensitivity of the electrode, causing deviation from the linear calibration of the sensor. Finally, chemical reactions between analytes can also not be ruled out. For example, ascorbic acid has been reported to re-reduce dopamine providing more dopamine for oxidation[23]. This phenomenon has been proposed as an explanation to the higher current response observed in the presence of AA[47]. Careful validation of the assay is required to ensure absence of such effects.

Other drugs

In addition to the endogenous substances, other drugs can also cause significant interference in electrochemical detection. The voltammetric detection of a wide range of different drugs have been reviewed[30,312,313]. The redox potentials of a wide variety of compounds have also been obtained by modelling[314]. Because systems with non-aqueous supporting electrolytes are often used in modelling studies, the results are not always in agreement with experimental results obtained in aqueous electrolytes. Moreover, with the vast number of drugs of abuse and

accepted active pharmaceutical ingredients, these lists are clearly incomplete. In addition, various other xenobiotics can be present in the samples. For example, caffeine and nicotine, as well as their metabolites, should be expected to be present in many samples. In addition, several chemicals may also be present due to environmental and food exposure to pesticide, herbicides and plastic additives, to name a few[221,315].

As it is not always feasible to test for all drugs, particularly in research, the ICH states that expertise is required to assess which interferents need to be tested for[46]. The selectivity requirement of an analytical method always depends on the application, and potential interference from sources, such as other concomitant drugs and xenobiotics, should be carefully considered. Because molecules with similar functionalities and structure tend to oxidize at similar potentials, this information may be used to identify the compounds that are most likely to cause interference. Figure 19 shows a non-exhaustive summary of the approximate oxidation potentials, of certain functionalities based on literature[316–326]. It also shows these functionalities in a few selected molecules important for this thesis.

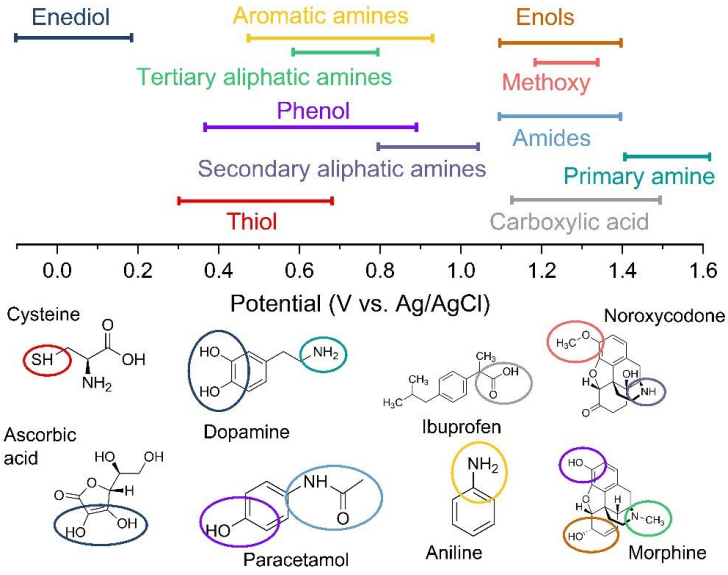

Figure 19. Approximate oxidation potentials based on literature[316–326] of different functional groups and examples of bio and drug molecules with these functionalities, with various carbon and Pt electrodes.

As seen from Figure 19, structurally non-related functionalities may also cause overlapping voltammetric signals. Furthermore, many biomolecules and xenobiotics contain more than one electrochemically active group, significantly limiting the selectivity in multianalyte detection. The oxidation potentials of these functionalities are also highly dependent upon the structure of the molecules. Both oxidation and reduction is energetically favored with unsaturated base or acid groups, likely because it is easier to remove or add electrons when rings contain π-bonding.[327] In addition, the π-resonance stabilizes the oxyl radical reaction products of enols, such as AA and catechols. Therefore, enediols and phenols have much lower oxidation potentials, compared to aliphatic alcohols. The oxidation potential of the functional group is also affected by substitution with electron withdrawing or donating substituents. Both the electron withdrawing nature and position of substituents affects the oxidation potential.

Generally, an electronegative substituent will increase the oxidation potential and vice versa.[327] While, this general trend can be used to assess the effect of substitution on the oxidation potential of a molecule, Peltzer et al.[327] noted that molecules containing two or more functional groups present a far more complicated problem, from which it is difficult to extract information about the effect of a particular functional group.

It should further be noted here that the changes in electrode surface chemistry can also significantly alter the voltammetry of drug molecules. Therefore, different molecules with the same electroactive functionality may oxidize at different potentials at different electrodes. As an example in Publication IV, we showed that the oxidation potential for PA was anodically shifted by 300 mV after anodic treatment of a Ti/ta-C electrode. In contrast, the oxidation potential of morphine was not significantly affected, despite the fact that the main peaks of both these analytes have been proposed to be due to oxidation of the phenol functionality[322,328,329]. It should be further noted, that even small changes in the molecule can significantly alter the interactions between electrode surface and the molecule, altering the voltammetry response[231]. This further highlights the importance of the electrode surface chemistry, and interference studies with the electrode used in the assay. With the vast amount of potential interferents in most applications, there is no substitute for validation studies with real patient samples.

Finally, chemicals introduced upon sampling of blood must also be taken into account. If tubes are used for collection of samples, an assay should study the potential matrix effects and specify a protocol for sample collection. A wide range of test tubes with different additives are available. Because, the additives are calibrated to provide the optimum blood/additive ratio, improper filling or mixing may also cause interference in assays.[203] Plasma and serum are commonly used for recovery tests in electrochemical analysis. Plasma sampling tubes usually contain anticoagulants, such as ethylenediaminetetraacetic acid (EDTA), heparin and sodium citrate. Therefore, if samples are collected in test tubes after venipuncture, the results need to be validated, to make sure that the tube additives (if present) do not cause interference in the analysis.

Metabolites

The metabolites of the target analyte or other co-administered dugs, are often overlooked in development of electrochemical sensors. Most drugs have complicated metabolic pathways leading to the formation of several metabolites, that are expected to co-exist in the sample at different concentrations. Because many drugs and other xenobiotics are detoxified in the liver and excreted in urine, the metabolites are expected to co-exist with the target analyte in biological samples. Particularly in urine samples, these metabolites can be present at higher concentrations than the analyte[221]. Due to their similar structure and closely related chemistry, the various metabolites have significant potential to cause interference in many analysis methods, including immunoassays and electrochemical analysis[325,330]. Therefore, when assessing the selectivity of a sensor, the presence of metabolites of the analyte of interest, and also those of other interferent drugs, should be considered. The metabolic pathways of paracetamol and morphine are discussed in detail in Chapter 7. For controlled substances, however, procuring all the metabolites of the analyte of interest alone may involve a lot of bureaucracy and incur high costs. This, in conjunction with the fact that the number of possible interferents quickly grows beyond what is practical to study, further highlights the importance

of real patient samples and clinical studies, with parallel determinations using established technology, to validate electrochemical assays.

Moreover, many of the same functional groups that are electrochemically active also undergo chemical reactions catalyzed by various endogenous enzymes. This is particularly the case for the oxidative metabolites catalyzed by CYP P450 enzymes. If sufficient selectivity is achieved, individual pharmacokinetic parameters can be obtained in close to real time measurements. This makes voltammetry an interesting technique for close to real time phenotyping. In Publication V, we show that we can selectively detect the active metabolite morphine, in presence of its parent drug codeine. Similarly, we showed selective detection of O-desmethyltramadol and tramadol in[16]. Recently, we also showed that we can selectively detect oxycodone in the presence of its main metabolites noroxycodone and oxymorphone[325].

7 . Electrochemical detection of drug and biomolecules

Each electroanalytical application presents its own unique set of requirements for sensitivity, selectivity, as well as other properties. Naturally, it is desirable to have as high sensitivity and selectivity as possible, but trade-offs between these properties are often required to achieve overall satisfactory performance. For example, in the in vivo detection of neurotransmitters, biocompatibility, long term sensor stability and fast temporal resolution are required. Due to the temporal resolution requirement, control of background currents and selectivity are not currently possible to the point where real-time quantitative detection can be achieved. In contrast, the quantitative point-of-care detection requires extreme selectivity and control of background current and matrix effects in biological samples. These two applications have very different requirements that are summarized in Figure 20. Both these applications however, usually require high sensitivity. Moreover, in both these applications the requirements need to be achieved by tailoring of the electrode properties, as extensive sample processing is not an option due to measuring environment or limited time for analysis. In this section, the challenges and progress in two applications of electroanalytical chemistry, namely *in vivo* detection of the neurotransmitter dopamine and point-of-care detection of analgesics, are discussed.

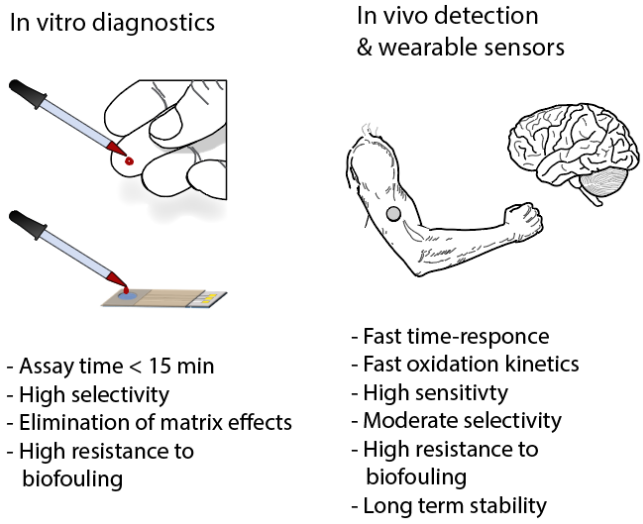

Figure 20. Summary of requirements for POC in vitro diagnostics and in vivo detection of neurotransmitters.

7.1 In-vivo detection of dopamine

Dopamine is known to be an important neurotransmitter, modulating many aspects of brain circuitry. It is an extrasynaptic messenger molecule functioning via volume transmission. Abnormal transmissions have been linked to many neurological disorders, including Parkinson's disease, schizophrenia, attention deficit disorder, Huntington's disease, obsessive compulsive disorder and Tourette's syndrome[331,332]. In addition, DA has important roles in neuronal plasticity, learning, memory, attention span and the brain reward system.[23,331,333] The precise mechanism by which DA mediates brain function is not fully understood. Its involvement in so many aspects of brain function makes its real-time detection highly interesting to many fields of research, and could contribute to increased understanding about neurodegenerative disorders and improve the efficacy of treatments[18]. Moreover, invasive treatments, mainly deep brain stimulation (DBS), are increasingly used to treat a variety of neurogenerative disorders despite the fact that their mechanism of action remains largely unknown. Real-time monitoring of the neurotransmission events secondary to DBS-targeted regions has the potential to advance functional neurosurgical procedures.[18]

During DA transients, dopamine escapes the synaptic cleft and binds to extrasynaptic receptors and transporters. The concentration of DA in the brain is determined by the rates of release, uptake and mass transport. DA is released by dopaminergic neurons in asynchronous low frequency tonic firing and periodic synchronous high frequency firing. The former is responsible for the low basal levels in the range of 10-100 nM[19]. The latter is of high interest in electrochemical detection, and has been corelated to reward seeking behavior[334,335]. After electrical stimulation, increases in DA concentrations can be observed for approximately 100 milliseconds and they return to basal levels within few seconds. Similarly, transients in the sub-second time scale (200-900 ms) have been reported after natural stimuli[334,335]. The peak concentrations are usually in the 200-750 nM range[334,335], but can reach concentrations up to 1350 nM[335]. Due to the low concentrations and sub-second duration of these transients, sensors with fast temporal resolution and high sensitivity are required.

Miniaturized electrodes with dimensions below 10 μm, providing spatial resolution of <1 mm in awake animals, can easily be fabricated and implanted. Such miniaturized electrodes have been fabricated with carbon fiber (CF), BDD and CNT/CNF, and in vivo detection of DA has been achieved[19,336–338]. Typically, temporal resolutions of 100 ms can be achieved with fast scan cyclic voltammetry (FSCV). Because different molecules oxidize at different potentials, selectivity can be achieved[23,339]. Fluctuations in the background current, however, significantly limits the applicability of FSCV in determining basal level concentrations, and it is therefore mainly used for the detection of fluctuations in DA concentrations during transients[23]. Amperometry can achieve faster response times, but has limited selectivity, as a constant potential is applied for oxidizing analytes of interest. Due to its ability to reduce the background current and improve selectivity, DPV has also been used for semi-quantitative detection of DA in-vivo. The limited temporal resolution of approximately 1 min, however, significantly limits the use of DPV in real-time detection of DA transients[23]. Because the same sensor can be used with all these techniques, different information can be obtained. Therefore, neurotransmission events may be correlated with behavior, such as reward seeking, in awake animals.

For these reasons, electrochemical detection offers a unique combination of high sensitivity, selectivity, temporal and spatial resolution, that competing technologies cannot achieve.

However, due to the highly invasive nature, and in some cases limited selectivity, other techniques, including positron emission tomography (PET), functional magnetic resonance imaging (fMRI) and micro dialysis combined with conventional chemical analysis, are also used. Other techniques are also required to analyze non-electrochemically active neurotransmitters, although enzymatic electrochemical sensors can be used for some, such as glutamate and acetyl choline[23].

The main advantage of the PET and fMRI techniques is their non-invasiveness. These techniques are, however, indirect and do not directly measure DA. PET detects gamma rays emitted from radio-labelled biomolecules of interest. These radiolabeled molecules are usually agonists or antagonists of receptors for the studied neurotransmitter. Their displacement through competitive displacement provides information about intrasynaptic dopamine concentrations[23,340]. In contrast, fMRI measures the changes in blood oxygen levels. Increasing neuronal activity in a specific area leads to increased cerebral blood flow. This leads to a change in oxygenated/deoxygenated hemoglobin, that can be measured and correlated with brain activity by measuring the blood flow in a certain brain region.[23,341] Both these methods have limited spatial and temporal resolution, and require expensive equipment and are not readily available everywhere. Most studies to date have been carried out with microdialysis[19]. In this method, a probe with a dialysis membrane is inserted into the area of interest in the brain. A perfusion fluid is pumped within the membranes and small molecules are able to diffuse through the membrane into the dialysate. The main advantage of this method is the high sensitivity and selectivity of both electrochemically active and inactive analytes. Upon removal, the dialysate can be further processed and analyzed with a wide range of methods, including LC-MS. On the other hand, microdialysis has limited temporal resolution of over 1 min, and the highly invasive nature also limits its use.[23] The used probes usually have diameters of 200-300 μm[23], giving the method a spatial resolution of < 1 mm. Studies have, however, shown that the insertion can cause tissue damage up to 1 mm away from the probe, potentially altering the DA concentrations at the implantation site[342,343].

Despite the recent advancements in the sensitivity and selectivity of both in vivo and in vitro electrochemical detection of dopamine, there are still challenges to overcome. While dopamine is one of the most studied analytes in electrochemical detection[33], most work is carried out with modified GC electrodes that are not compatible with microfabrication or miniaturization. Therefore, their miniaturization for in vivo experiments may not be straight forward. Moreover, large electrodes are problematic to calibrate in vitro, due to restricted diffusion when implanted[288]. Therefore, electrode materials should ideally be compatible with standard microfabrication techniques. It should be noted, however, that the CF electrodes can also be modified with carbon nanomaterials, and such electrodes have also been used for detection of DA[337]. Most in vivo measurements, however, still utilize unmodified carbon fiber microelectrodes. Although, DA sensors made with microfabrication compatible materials are also increasingly reported[338,344–346].

Most studies on electrode materials for the selective detection of DA, rarely discuss essential factors, such as response time, long term stability, resistance to biofouling and biocompatibility. In addition, most works use only DPV to achieve selectivity, severely limiting the response time[30,347]. Only few works have reported detection of low concentrations of DA in the presence of AA and UA, using relatively fast methods, such as CV, with high scan rates[38,47,116,348–350], fast scan cyclic voltammetry[338] or amperomtery[338]. In Publication I, we show

the large difference in selectivity between DPV and CV measurements, with a PRGO modified ta-C electrode.

Because the electrodes need to be implanted into the brain, resistance to fibrous encapsulation and proteins fouling is also required. The electrode also has to be resistant to other degradation mechanisms, such as corrosion, membrane delamination, and biodegradation and passivation of the electrode.[351] Dopamine is known to produce polymeric reaction products that readily foul the sensor leading to loss of activity[96,105,215]. Finally, all the used materials should be biocompatible and not introduce foreign toxins into the body. In addition, strategies used to improve the corrosion and passivation resistance should not form a diffusion barrier, limiting the temporal resolution. Failure of the device commonly occurs due to corrosion and passivation of the sensors. In the fabrication of implantable sensors, care has to be taken to reduce failure due to residual stress, pinholes, corrosion, swelling and diffusion processes.

It is clear that more research is required to produce microfabrication compatible electrode materials, simultaneously combining high sensitivity and selectivity with long term stability and high temporal resolution. DA sensors must be able to provide a specific signal in the presence of various interferents, most notably AA and UA, but also other tyrosine and tryptophan derivatives and their metabolites[23]. While significant progress in selective detection of DA has been made with modified electrodes, achieving sufficient selectivity in combination with high temporal resolution is still the main challenge in electrochemical detection of DA. The interferents and their approximate redox potential are discussed in detail by Robinson et al.[23]. They identified AA, adrenaline, noradrenaline and DOPAC as the main interferents, for in vivo detection of DA with carbon electrodes. The oxidation potentials as well as the expected concentrations of these interferents are shown in Table 5.

The selective detection in the presence of AA, in particular, is a major hurdle to selective detection of DA. While the sensitivity towards AA with fast scan methods (400 V/s) is low in comparison to that of DA[338], AA is enriched in the brain, and present at 10^4-10^6 times higher concentrations than catecholamines. Early studies assigned AA the role of a relatively passive redox buffer. But it has been long accepted that the compound plays a more direct neurochemical role[285]. It is known to affect the affinity of DA for its receptors and modulate the release of acetylcholine and norepinephrine from synaptic vesicles. Moreover, changes in the brain AA concentrations parallel changes in the biogenic amines, and corelease with catecholamines has been reported. Increase in signal in the *in vivo* experiments after amphetamine injection has been attributed to an increase in AA concentration[288]. It was further noted that AA increase could be sufficiently large, that it obscures the observation of DA.

AA shows sluggish reaction kinetics at most carbon electrodes and therefore has significant overlap with DA, despite its lower oxidation potential. The lower onset potential also significantly reduces the utility of amperometric detection. In fact, early amperometric measurements attributed most of the signal recorded in the brain to AA[23,352]. In contrast, in FSCV, selectivity can be achieved at untreated CF electrodes as the oxidation shifts to more positive potentials as a result of the slower kinetics[23]. Oxidative treatments have also been shown to improve the electron transfer kinetics with both conventional and carbon nanomaterial-based electrodes[47]. Highly selective detection of DA has also been achieved with modified ta-C electrodes[38,47].

The metabolites of dopamine may also cause interference in the detection of DA. In 3,4-dihydroxyphenylacetic acid (DOPAC), the primary amine of the dopamine side chain is replaced with a carboxylic group. Because, both molecules share the catechol functionality, they produce overlapping voltammetric peaks[23]. Moreover, DOPAC concentrations of 3-30 μM in the brain extracellular fluid have been reported[273,353,354]. The presence of relatively high concentration of anions, such as AA, UA and DOPAC may necessitate the use of permselective membranes such as Nafion. Nafion membranes have been shown to efficiently prevent these anions from reaching the electrode[355]. When Nafion membranes are used, however, the DA has to partition into the membrane and diffuse through the film, to the electrode surface.[356] This may significantly increase the response time of the sensor and therefore thin films need to be used. This strategy does not, however, work for adrenaline and noradrenaline as they are also cations under physiological conditions. Noradrenaline and adrenaline also have nearly identical structures to DA, and therefore oxidize at the same potential. The presence of epinephrine may, however, be confirmed due to the second oxidation peak attributed to oxidation of the secondary amine. Due to the overlapping main peaks, selectivity is achieved by implanting the electrodes in dopaminergic sites known to have low norepinephrine concentrations[19].

Other monoamine neurotransmitters, as well as their precursors and metabolites, may also cause interference. The monoamine metabolites 3-methoxytyramine, homovanillic acid and 3-methoxy-4-hydroxyphenylglycol, have methoxy substituted phenols that are expected to oxidize around 0.5 V. Other interferents that oxidize around 0.3 V, include uric acid and serotonin.[23] Additionally, L-3,4-dihydroxyphenylalanine (L-DOPA), the precursor of DA, has been reported to oxidize around 0.4 V. Likewise, tyrosine is electrochemically active and the phenol functionality of this L-DOPA precursor is electrochemically active, and has been reported to oxidize around 0.7 V[239–242].

Because the oxidation potentials of DA as well as the endogenous interferents may vary between different electrodes, the interference from these analytes should also be studied when DA sensors are developed. In addition, even with electrodes showing electrocatalytic properties, the rate of electron transfer can be overrun with fast scan methods. This may lead to anodic shifts of the peaks leading to limited selectivity. Especially with conventional CF microelectrodes, the anodic waves of these analytes usually overlap with that of DA in FSCV experminets[19].

Electrochemistry of dopamine

Like its derivatives epinephrine and norepinephrine, dopamine is a catecholamine that is electrochemically active and can be directly electrochemically oxidized. DA is known to be a surface sensitive analyte, requiring adsorption on the electrode prior to electrochemical oxidation. Early studies by Duvall et al.[213,214] showed that monolayers of nitrophenyl and (trifluoromethyl)phenyl on GC electrodes, almost completely inhibited electron transfer of DA, while having only small effect on the electron transfer of the outer sphere redox probe $Ru(NH_3)_6^{2+/3+}$. This indicates that adsorption of DA is required for fast oxidation kinetics of DA.

As seen from the proposed oxidation pathway shown in Figure 21, DA is oxidized in a $2e^- 2H^+$ transfer process, leading to the formation of dopamine quinone (DAQ). Like for other quinone/hydroquinone redox systems, the order of proton and electron transfer has been

proposed to follow a scheme of squares, in which the order of proton and electron transfer depends on the pH[294,357,358]. At neutral pH, a H^+ e^- H^+ e^- transfer process has been proposed for various catechols, including hydroquinone, DOPAC and 2,3-dihydroxybenzylamine[294,357,358].

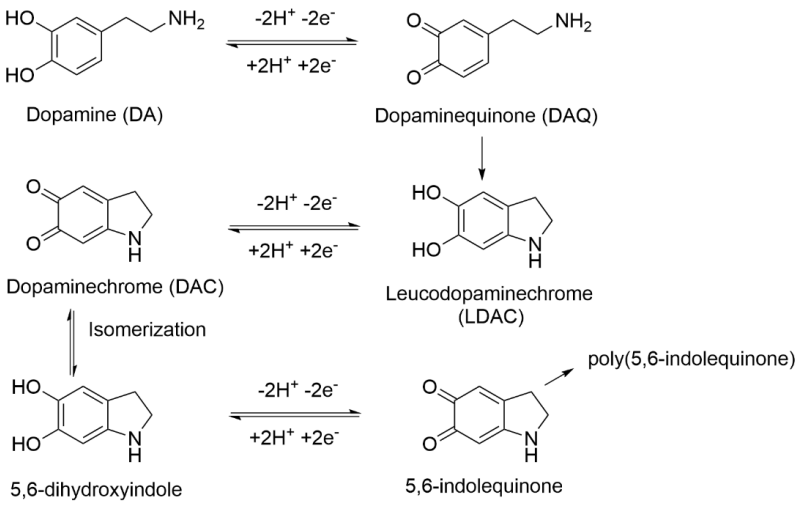

Figure 21. Oxidation pathway for DA at neutral pH.

After the first electrochemical oxidation, the amine side chain can undergo intramolecular cyclization forming leucodopaminechrome (LDAC)[215]. Due to this chemical reaction, the peak current ratio is dependent upon the scan rate. A higher scan rate will typically lead to a ratio closer to 1, as the kinetics of chemical reaction is outrun by the fast scan rate[96]. As seen from Figure 21, LDAC can be further oxidized through a $2e^-$ $2H^+$ transfer process, forming dopaminechrome (DAC). For this reason, a second redox couple can be observed at a lower potential in the voltammogram[96]. Therefore, an overall mechanism of ECE has been proposed for various catechols[215,359,360]. An alternative pathway, in which DAQ can reduce LDAC back into DAC, leading to an ECC mechanism, has also been proposed[275,359].

It is well known that DAC can undergo further reaction leading to the formation of a melanin-like polymer. Li et al.[215] further proposed that DAC molecules undergo isomerization to the more stable 5,6-dihydroindole, serving as the monomer for electropolymerization. In this process 5,6-dihydroindole is electrochemically oxidized to form 5,6-indolequinone followed by chemical reactions as proposed by Saraji et al.[361]. Li et al. further showed the accumulation of reaction products on a gold quartz crystal microbalance after cycling in DA. Moreover, the FTIR spectrum closely resembled that of poly(indole). This polymer, also called polydopamine, can form spontaneously on virtually any surface under mildly alkaline conditions and concentrations above 0.1 g/L[163]. It is highly resistive and known for its ability to foul electrodes[105,216]. Despite slower fouling at low concentrations, electrode fouling by polydopamine can be a real concern, that needs to be taken into account in prolonged measurements. Fouling can also be reduced by limiting the potential window and applying fast scan rates, allowing for less time for chemical reactions leading to electrode fouling.

7.2 Point-of-care testing of analgesic molecules

7.2.1 Selection of sampling matrix

In the clinical setting, POC detection can be a valuable diagnostic tool and useful for drug screening[362,363]. It is also a potential enabling technology for personalized healthcare[364]. Furthermore, electrochemical POC detection can enable the near real time analysis of blood concentrations from small, less invasive finger prick blood samples. In this thesis, we focus on quantitative POC testing as a diagnostic tool for diagnosing poisoning of paracetamol and opioids. In this section, the sampling and matrix requirements for quantitative POC determination of analgesics, mainly in the context of diagnosing intoxication in emergency care, will be discussed.

In the emergency setting, the drug screen should be performed in less than one hour[363], thus limiting the use of analysis methods requiring time-consuming sample treatments, such as protein precipitation. Electrochemical testing is increasingly used to study various drugs, most notably paracetamol and morphine. Urine is commonly used as a matrix for recovery tests in these studies[33], as well as the matrix for POC testing of drugs. This is likely because urine is sterile, easy to obtain in large volumes, and largely free from proteins, lipids and cellular materials[221,365]. In addition, urine is easily stored by refrigeration or freezing, and many drugs are stable in urine[365]. As a biological waste material, however, urine contains metabolic breakdown products of both biomolecules and xenobiotics, as well as bacterial by-products[221]. Urine can contain higher concentrations of drugs and their metabolites than blood, and excretion into urine can continue after the physiological effect has worn off. For this reason, urine is often the sample of choice for drug screening. This, however, also leads to lack of correlation to drug urine concentration with intoxication. In addition, the concentrations of both biomolecules and xenobiotics, as well as their metabolites, can vary greatly due to fluid intake, voiding pattern and time since last dose.[365] Moreover, urine specimens are easily substituted, diluted or adulterated. Due to these complexities, urine is a difficult matrix to fully understand[167]. Therefore, urine is not an ideal sample for determining individual pharmacokinetic profiles or for diagnosing intoxication.

In cases where an antidote is available, and there is a relationship between the drug serum concentration and the clinical symptoms, serum is usually the sample of choice[363]. For some drugs, such as morphine[366–368], codeine[368,369] and paracetamol[370], it has been shown that the concentrations in less invasive and painful capillary blood samples obtained by finger prick, as well as non-stimulated saliva, correlate with plasma concentrations. Saliva samples have low protein content (0.3%), but usually contain contaminants from food, other drugs and debris from the mouth[371]. Therefore precautions, such as filtering and fasting for up to 2 to 3 h before sample collection, are usually taken[371]. Moreover, salivary stimulants are widely discouraged due to their potential to cause interference in assays[371]. Stimulation has also been reported to change the ionic strength of saliva and decrease the saliva concentration of codeine[372] as well as other drugs[373]. It should further be noted that consistently higher concentrations in oral fluid have been observed after oral dose of codeine[369]. Due to the low protein content, saliva samples may be an interesting matrix for electrochemical detection of drugs in cases where the use of saliva has been validated for the target analyte.

Small capillary blood samples (10-250 µL) are particularly well suited for electrochemical analysis, as it requires only small sample volumes. Ideally, samples should be in the 5 to 10 µL range so that they can be easily obtained from all patients. The collection of capillary blood does not need special training and is considered to be less invasive and painful than sampling by venipuncture. Moreover, in special populations, such as elderly and infants, locating a blood vessel can sometimes be difficult.[374] It is important to note that several factors can affect the quality of the capillary blood sample. For example, tissue damage or milking of the finger after finger prick can change the composition of the sample[375,376]. It is also important to realize that there can be differences in the concentrations of analytes in capillary and venous blood[375,377–379]. Therefore, venous blood samples and capillary blood samples cannot in all cases be used interchangeably[379]. Like with saliva, the applicability of capillary blood as a matrix has to be validated separately for each analyte.

POC determination of drugs from whole blood requires the ability to carry out determination without extensive sample treatment. Despite the increasing literature available on electrochemical determination of anesthetics in complex biological matrices, most works still use highly processed samples. Moreover, in Publication VI, we found that sensitive and selective detection of PA has been previously reported from blood samples, but all these studies rely on time-consuming sample processing including, precipitation of proteins and considerable dilution, to reduce matrix effects. Similar sample processing is routinely carried out in conventional analysis of small molecules in blood samples and significantly increase the assay time. A typical sample processing protocol, in comparison with the POC assay protocol proposed in Publication VI, is shown in Figure 22.

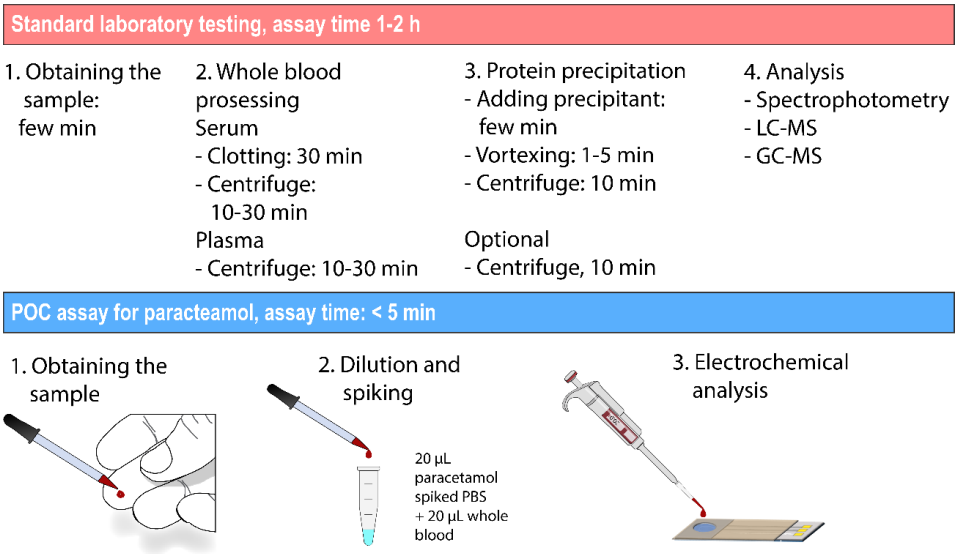

Figure 22. Comparison of protocols for analysis of samples in conventional laboratory testing and the protocol for electrochemical point-of-care detection of paracetamol assay as proposed in Publication VI.

It is important to note that processing is required to obtain serum and plasma samples from whole blood. In standard operating procedures 10-15 min of centrifugation is required to obtain plasma and serum samples[203]. For example Brahman et al.[380] centrifuged the blood

samples for 30 min at 4000 rpm to obtain human serum samples, prior to electrochemical determination of PA. Moreover, 30-60 min is required for clotting to obtain high quality serum samples[203]. The protein precipitation, carried out by most works aiming at electrochemical detection of drugs, also requires further chemical treatments and centrifugation. These sample treatment steps lead to assay times in excess of 45 min and dilution of the sample by at least two times.

As can be seen from Figure 22, it is very difficult to achieve an assay time of less than 1h, if extensive sample processing is required. In contrast, the electrochemical assay developed in Publication VI can be used for determination of the acetaminophen concentration from finger-prick whole blood, only after diluting with equal part PBS and without precipitation of proteins, in less than 5 min. The dilution step increases the required sensitivity, but affords the ability to control the ionic strength and pH, as well as carry out spiking of the sample, to control matrix effects. This result clearly shows the ability of electroanalytical chemistry for rapid POC determination of drugs from whole blood samples. Preferably, no spiking or dilution of the sample is required, and therefore the assay needs to be further developed to allow for direct determination of smaller undiluted samples.

7.2.2 Paracetamol

Pharmacology and metabolism

Paracetamol is one of the most widely used analgesics with antipyretic activity[381]. Excessive PA concentrations may cause acute liver damage and acute renal failure. At therapeutic doses, it is better tolerated than non-steroidal anti-inflammatory drugs (NSAID) and is widely used to treat fever and pain. Doses only slightly above the recommended dose can, however, cause hepatotoxicity.[381,382] Both intentional and unintentional poisoning are common and PA poisoning is currently the leading cause of liver failure in the United States and Europe[9,10]. In fact, paracetamol poisoning is so common that the National Academy of Clinical Biochemistry endorses screening for PA in all emergency department patients who present with intentional drug ingestion[11]. At therapeutic doses, paracetamol is glucuronidated and sulfated, and only small amounts of the toxic metabolite N-acetyl-p-benzoquinone imine (NAPQI) are formed. The NAPQI is detoxified by conjugation with liver glutathione to yield a non-toxic conjugation product. At toxic doses, this route of detoxification can become depleted causing accumulation of the toxic metabolite. NAPQI can from conjugates with cellular proteins, which can lead to acute liver failure[382]. The metabolic pathway after a toxic dose is shown in shown in Figure 23.

Paracetamol poisoning can be effectively treated with acetylcysteine. Unfortunately, patients presenting with paracetamol poisoning show few and unspecific symptoms in the first 24 h after ingestion[9,383]. Moreover, the antidote is most efficacious when administered within 8 h, after which the efficacy rapidly falls off[11,383]. The probability of paracetamol toxicity is directly correlated to the blood concentration. Therefore, diagnosis of acetaminophen overdose is usually carried out by determining the acetaminophen serum concentration[384]. The Rumack–Matthew nomogram is helpful in determining the likelihood of hepatotoxicity. This nomogram plots the acetaminophen concentration as a function of time post-ingestion. Serum levels at or above 200 μg/ml (1.323 mM) at 4 hours post-ingestion and 6.25 μg/mL (43.1 μM) at 24 h post-ingestion have been found to consistently predict hepatotoxicity. The line between these points

is referred to as the probable toxicity line. Later, additional safety has been built in by adding a second line 25% below the original line[385].

Because the blood PA concentration ultimately guides clinical decision making, selective and quantitative detection of PA is required. In clinical settings, semi-rapid tests are usually carried out with spectrophotometric methods because of relative simplicity and low cost[12,13]. Despite its advantages, this method is poorly suited for point-of-care testing. Moreover, interferences causing both falsely high and low results have been reported with these methods[12,13,386]. Competitive lateral flow immunoassays are also available for qualitative determination of acetaminophen. These tests are, however, not quantitative and due to high cut-off concentrations, false negatives have been reported[14]. Moreover, research has shown that capillary blood samples obtained after 4h of ingestion correlate well with venous blood samples, and that the pharmacokinetic parameters can be studied from finger-prick blood samples. For these reasons, a highly mobile, simple and quantitative POC assay could be a valuable diagnostic tool for paracetamol intoxication.

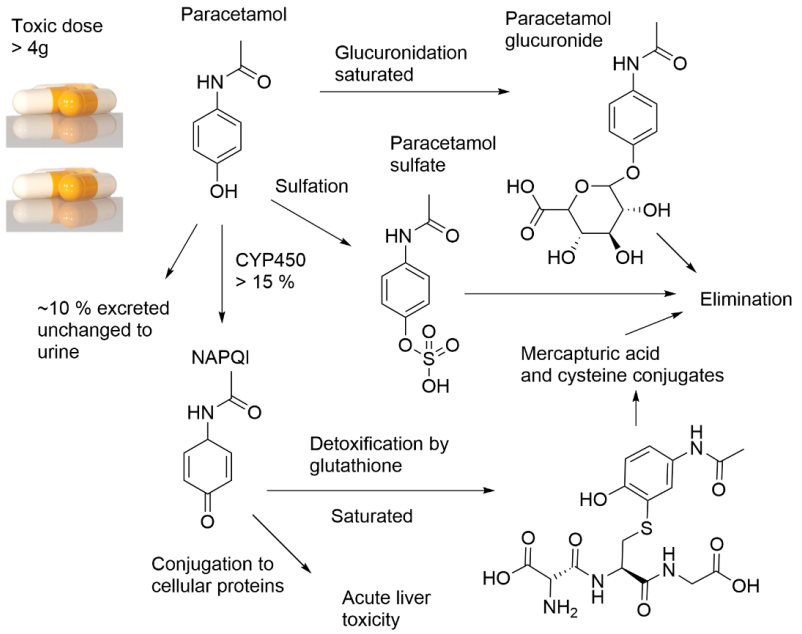

Figure 23. Metabolic pathway and toxicity of paracetamol in the liver.

Electrochemistry

Like dopamine, paracetamol is electroactive and can be detected with high sensitivity using electroanalytical techniques. It is one of the most studied drug molecules in electroanalytical chemistry[33]. It is also one of the most used drugs and is therefore intensively studied for electrochemical oxidation to purify waste water. Paracetamol has been proposed to undergo electrochemical oxidation by transfer of $2e^-$ and $2H^+$ leading to NAPQI formation, as shown in Figure 24[328,329].

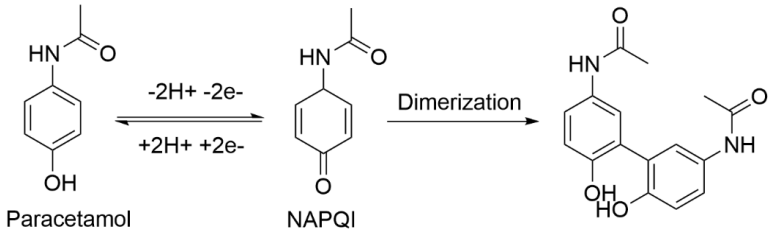

Figure 24. Simplified oxidation pathway for paracetamol at neutral pH.

This first step is followed by a chemical reaction, making the electrochemical reaction quasi-reversible at most electrodes. Nematollahi et al.[328] found that the following chemical reactions are dependent on the pH, and strong acidic media leads to hydrolysis and strong alkaline media to hydroxylation. At neutral pH, the chemical reaction leads to dimerization and they identified the dimer shown in Figure 24 as the main product with NMR studies. The dimerization of the reaction products also leads to a peak current ratio that is dependent upon the scan rate. Moreover, a higher PA concentration will lead to formation of more NAPQI, and consequently higher rate of dimerization, making the reaction less reversible at high conentrations[328].

While paracetamol is one of the most studied drugs in electrochemical detection, most works aiming at sensor development, focus on achieving low detection limits. Due to the relatively high concentrations (100 μM to 1 mM) expected to be present in patients with poising, extreme sensitivity is not required for detection of paracetamol. Moreover, even typical single doses of 500-1000 mg are also expected to lead to peak plasma concentrations of approximately 20-90 μM[387,388]. Due to the expected presence of a wide range of endogenous interferents identified in section 6.1.2., metabolites shown in Figure 24 and potential other drugs, selective detection may be challenging. The relatively high concentration expected to be present, particularly in cases of overdose, limits the list of potential interference from endogenous chemicals present at low concentrations.

Nevertheless, the large number of potential interferents in real patient samples indicates that the selectivity likely still has to be improved for most electrodes. In Publication IV, we showed that the PA is a highly surface sensitive analyte. Due to this, there can be relatively large variations in the oxidation potential of paracetamol and interferents alike, and so the interference has to be evaluated separately for every electrode type. At most carbon electrodes, however, PA oxidizes close to the oxidation potentials of AA and UA, and interference from UA is especially expected. Other potential endogenous interferents include amino acids and other purine metabolites, although the concentrations of the latter are expected to be much lower than that of PA. In addition, large variation in the oxidation potential of cysteine (see Table 5) also makes it a potential interferent for PA.

The metabolites are transported through bile and blood, to be ultimately eliminated in urine. Therefore, a sensor has to be capable of selective detection in the presence of the metabolites shown in Figure 23. Some of these metabolites have also been studied electrochemically[389,390]. Peaks around 1 V have been observed for paracetamol glucuronide and paracetamol sulfate, and were attributed to the amide funcitonality.[390] Oxidation peaks at similar potentials have also been observed for other anilides that are structurally closely related to PA[321]. Similar results were obtained by Miner et al.[280] for paracetamol sulfate and glucuronide metabolites in a more comprehensive work. In addition, they observed oxidation peaks close to that of PA

also for acetaminophen cysteine conjugates. Similarly, the glutathione conjugate (shown in Figure 23) also possesses a phenol group, with the potential to cause interference. We are not aware of any reports on the electrochemistry of this paracetamol metabolite. In the clinical setting, the antidote N-acetylcysteine will also be present after treatment. The thiol group has highly variable oxidation potential and may cause interference at some electrodes. This antidote is however, negatively charged at physiological pH and the Nafion coating is therefore expected to reduce interference[391]. The interferences of these interferents need to be further studied to ensure selectivity of the assay presented in Publication VI.

In addition to the many metabolites, several other drugs are commonly taken in concomitant poisoning with PA. The concomitant overdoses were studied by Schmidt et al.[392]. They found that benzodiazepines, opioids, acetylsalicylic acid, NSAIDs, neuroleptics, antidepressants, antibiotics, anticonvulsants, antihistamines and caffeine, were often taken together with paracetamol in cases of paracetamol overdose. In Publication VI, some of the most likely candidates to cause interference were studied. From this list, opioids were found to have the highest potential to cause interference, due to the enrichment into the Nafion membrane. Satisfactory tolerance limits were, however, shown for morphine and O-desmethyltramadol present at much lower concentrations than PA, even when taken in fatal overdose[393]. Despite the interesting initial results, the large number of potential interferents requires wider interference studies. Moreover, validation of an assay protocol for electrochemical determination of PA from whole blood, still requires validation studies with a large number of real patient samples collected after administration of paracetamol.

7.2.3 Opioids

Opioids are a class of natural and synthetic analgesics with agonist activity toward the μ receptors. They are widely used to treat post-operative, cancer and acute non-cancer pain. The use of opioids is, however, associated with adverse side-effects, including nausea, constipation and even death due to respiratory depression. Over the past decade, misuse of opioids has increased dramatically. In the United States alone, more than 70 000 people died from drug overdose deaths in 2017, out of which 67.8 % were related to opioids.[8]

The response to a certain dose can be highly individual, due to interindividual variations. This is especially the case for opioid prodrugs, such as codeine and tramadol. The prodrugs lack significant analgesic activity without biotransformation into their active metabolites morphine and O-desmethyltramadol, respectively. This demethylation is catalyzed by the genetically polymorphic enzyme cytochrome P450 (CPY) 2D6. Interindividual variations in CPY2D6 activity cause significant variation in drug metabolism, and thus the efficacy and safety of these prodrugs. The plasma concentrations of active metabolites are extremely low in poor metabolizers, leading to no analgesic effects. Whereas, for ultra-rapid metabolizers of CYP2D6 substrates, several cases of severe side effects have been reported. For these reasons, a quantitative POC test could be highly useful for differential diagnosis of opioids poisoning and aid in clinical decision making.

Currently, opioid concentrations are determined with laboratory-based testing, mainly LC-MS, that are not suitable for POC testing of opioids. Qualitative opioid drug screens are also routinely carried out, mainly for workplace and probation drug testing. These drug tests can be highly automated and are routinely performed in high volume. In the clinical setting, drug

screening can also be used to detect the nonuse of prescribed opioids, which has been identified as a contributor to the opioid crisis.[15] These tests use mainly urine, although saliva tests have also become available mainly for less invasive road-side testing of drivers. These immunoassays also suffer from cross-reactions, and in some cases relatively high cut-offs, that limit their clinical usefulness. Opioid immunoassays also do not detect all opioids equally and typically use morphine as the single calibrator. Therefore, some opioids such as the widely prescribed and misused oxycodone and fentanyl may escape detection. Immunoassays specific for these opioids, however, exist but are not as routinely used[15].

Opioids are highly potent analgesics and therefore therapeutic blood concentrations are usually relatively low, ranging from 10 nM to 100 nM. Whereas, higher concentrations above 1 µM have been observed in cancer patients. Even in cases of fatal overdose, postmortem blood concentrations are usually in the range of few µm. This makes the selective electrochemical detection of opioids challenging. In addition to high levels of endogenous interferents, AA and UA, to name a few, other drugs and several metabolites are expected to be present in real patient samples.

Opioids are often prescribed together with relatively large doses of non-steroidal anti-inflammatory drugs or paracetamol. As we show in Publication IV, in the detection of morphine, paracetamol is especially problematic and is expected to cause interference. As discussed in section 7.2.1, the expected PA concentrations, even from typical single doses, are much larger than lethal doses of morphine. In addition, other drugs, most notably benzodiazepines, but also other drugs of abuse, as well as antidepressants and muscle relaxants, are often taken in concomitant overdose with opioids[394,395]. Therefore, an assay for POC determination of opioids should be free from interference from these classes of drugs. In this thesis, we focus on the electrochemical detection of morphine. For example, an assay determining the morphine concentration due to metabolized codeine should be free from interference from paracetamol, NSAIDs and potential other drugs. Naturally, the assay should also be free from interference from other opioids.

Despite numerous studies reporting highly sensitive determination of opioids in the presence of various interferents, and recoveries close to 100 % in processed and spiked biological samples, the presence of metabolites is largely overlooked in literature. This is especially important, as some of these metabolites are active while others have no analgesic activity. In this thesis, we focus on the detection of the important natural opioid morphine. MO is a strong opioid used to treat moderate to severe postoperative pain as well as cancer pain. It is the main active metabolite of codeine and one of the main active metabolites of heroine. The metabolic pathway of codeine, as well as the enzymes catalyzing the reactions, is shown in Figure 25.

Interestingly, these same functional groups affected by the metabolism of opioids are also the electrochemically active groups. For this reason, voltammetry can theoretically be used to monitor the metabolism in close to real time *ex vivo* and real time *in vivo*. In Publication V, we showed simultaneous detection of morphine and codeine with Nafion coated SWCNT electrodes. In other work, we have also demonstrated simultaneous detection of tramadol and its active metabolite ODMT[16], and very recently the selective detection of oxycodone in the presence of its main metabolites[325].

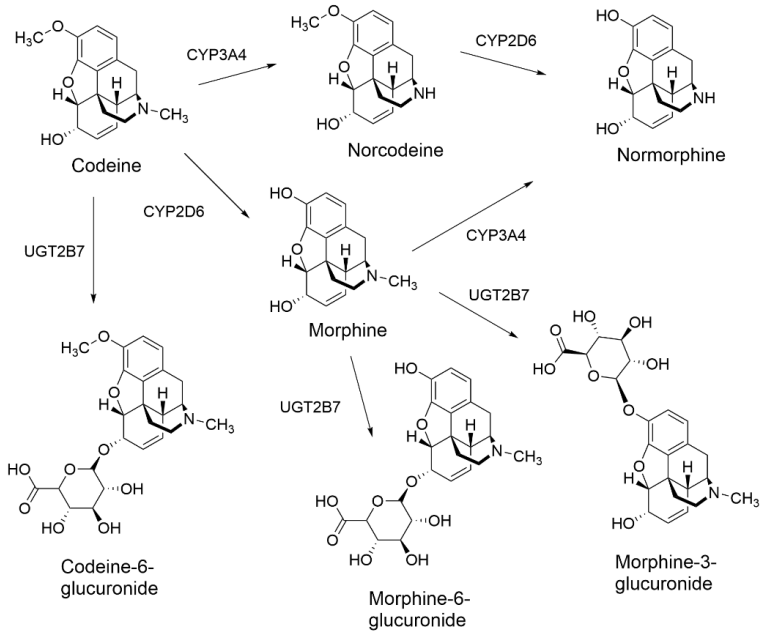

Figure 25. The metabolic pathway of codeine as well as the enzymes catalyzing the reactions.

Moreover, in [396], we showed that the Nafion almost completely rejects the inactive morphine-3-glucuronide, indicating that selective detection of morphine can be achieved in the presence of glucuronide metabolites. This, however, still needs to be confirmed for the active morphine-6-glucuronide.

Electrochemistry of opioids

A large body of work researching the electrochemical detection of various opioids has been reported. A review of all those studies is beyond the scope of this work and will not be attempted here. Instead, we will discuss the electrochemistry of the two most studied opioids, namely morphine and codeine. Morphine is by far the most studied opioid in electrochemical detection. The progress in the electrochemical detection of morphine has been recently reviewed by Abraham et al.[397]. They concluded that CNT and graphene based electrodes display effective quantification, and are attractive in terms of cost compared to noble metals. The future studies on these electrode materials have to be therefore focused on understanding more about interfacial reaction kinetics, so as to design novel sensors suitable for use in practical applications.

Especially morphine contains many of the functionalities of opioids and shows highly complex electrochemistry. The structures and DPV scans of morphine and codeine, as well as a few other common opioids, are shown in Figure 26. Figure 26 also shows that different opioids give different voltammetric responses at the SWCNT electrodes used in Publication III. Fentanyl shows the highest sensitivity as it was measured with only 15 μM concentration. All other opioids were measured at 50 μM concentration. In Publication V, the peaks for morphine were tentatively assigned to phenol (+0.4 V), tertiary (0.8 V) and secondary amine (0.85 V), as well as the 6-hydroxy group (1.1 V). The assignments of the amine peaks are further supported

by Publication III, where we show a similar double wave for fentanyl, possessing only the tertiary amine functionality. The electrochemical oxidation of fentanyl is discussed in detail in Publication III. The amine peaks seem to be well defined compared to other electrodes such as GC and ta-C electrodes.

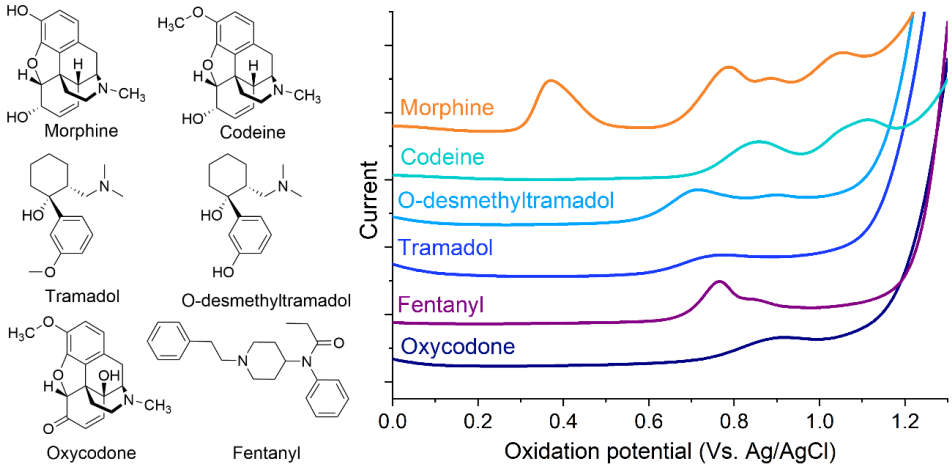

Figure 26. Structures and DPV scans of 50 µM morphine, codeine, tramadol, O-desmethyltramadol and oxycodone, as well as 15 µM fentanyl, with SWCNT electrodes in pH 7.4 PBS solution.

Normally, alcohols show sluggish electron transfer associated with high oxidation potentials, however, the allyl alcohol structures found (6-hydroxy) in morphine and codeine are expected to oxidize at lower potentials. Garrido et al.[322–324] studied the voltammetry of morphine, codeine and heroine, as well as their metabolites, in detail at GC electrodes. They observed only two well defined peaks at neutral pH for morphine, attributed to the phenol and tertiary amine, at a GC electrode[322]. In further work, they observed 3 peaks for codeine. These peaks were attributed to the tertiary amine, hydroxy and methoxy groups. They, however, provided no mechanism for the oxidation of the methoxy group. Nevertheless, voltammetric oxidation of compounds with benzene rings substituted with methoxy groups have also been reported[326].

Because both morphine and codeine possess the 6-hydroxygroup, it is likely that the oxidation of the 6-hydroxy group is responsible for the peak at 1.1 V for morphine and codeine. The wider peak for codeine could further suggest contributions from oxidation of the methoxy groups as well. Furthermore, they confirmed that the double peak for the tertiary amine could be due to further oxidation of the secondary amine, as a peak with similar potential and current to that of the second peak for tertiary amine was observed for norcodeine and norheroin, where the tertiary amine is demethylated[323,324]. Early work by Masui et al.[319] shows that a double wave is expected for tertiary aliphatic amines. Based on the oxidation schemes proposed by Garrido et al., we tentatively propose the oxidation pathway for morphine as shown in Figure 27.

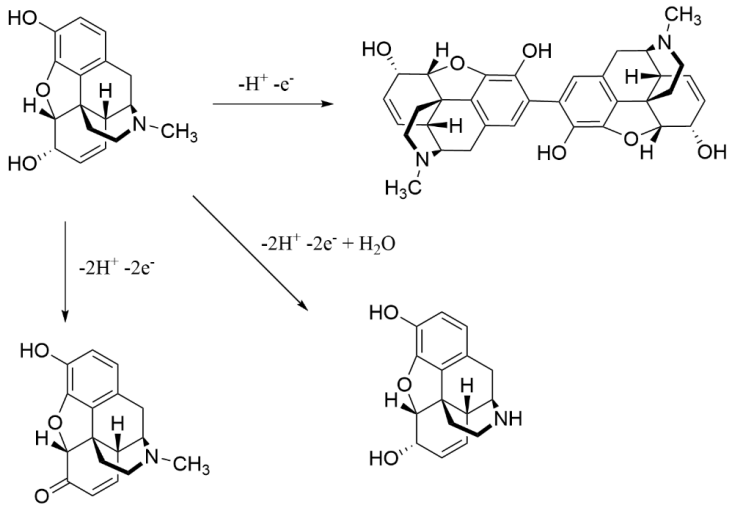

Figure 27. Pathway for electrochemical oxidation of morphine in aqueous electrolytes.

It should be noted that this pathway is simplified and not complete. These reactions seem to be irreversible due to further chemical reactions. We are not aware of any fast scan cyclic voltammetry research where the kinetics of these chemical reactions have been studied. In Publication III, however, we observed no reduction peak for fentanyl citrate at scan rates up to 10 V/s. Garrido et al. further noted that the oxidation of the phenol leads to a resonance stabilized state between two forms. These forms can further react to form dimers. Moreover, this omits the possible contribution of methoxy groups for codeine. This could explain the very different behavior in this region at a wide range of modified electrodes, that produce only one well defined peak for both morphine and codeine. Such results have been obtained at least with electrodes modified with metal oxides nanoparticles, ionic liquids and Nafion, but to the best knowledge of the author, these effects have not been discussed in literature. Interestingly, the oxidation potential of the phenol functionality seems not to be greatly affected by changes in surface chemistry, as it is often around 0.4-0.5 V. In contrast, the other peaks are very heavily influenced by the electrode modifications. In Publication V, we show the simultaneous detection of morphine and codeine with a Nafion coated electrode. The peaks were attributed to the phenol and 6-hydroxy functionalities in morphine and the 6-hydroxy functionality in codeine. We proposed that the peaks for the amine are anodically shifted due to interactions with the Nafion. In light of the discussion above, this may also be the case for the oxidation peak for the 6-hydroxy group. The larger peak could be due to the oxidation of the methoxy group, which is overlapping with a smaller peak for 6-hydroxy group. It should be noted that reliable assignments cannot be made without further research, and altered oxidation of the amine functionalities can also not be excluded. These results are discussed in greater detail in Chapter 8.3.

Most opioids contain at least one or more phenol, hydroxyl, tertiary aliphatic amine and secondary aliphatic amine functional groups, and therefore opioids show complex electrochemical behavior. In addition, the radicals produced by electrochemical oxidation of opioids, and metabolites with phenol functionalities, can undergo chemical reactions yielding conjugates. Nevertheless, opioids seem to be highly surface sensitive analytes leading to highly

different voltammetric response, making comparison difficult. This is evident also from the different sensitivities in the DPV measurements shown in Figure 26. In particular, the electrochemistry of the aliphatic amines seems to be heavily affected, and seems to be completely absent at some metal oxide, ionic liquid and Nafion modified electrodes. Therefore, more work involving in situ spectrometry, or collection of reaction products for structural identification, is also required to develop a better understanding of the electrochemistry of opioids. More work combined with better characterization of the electrode materials, is also required to understand the surface interactions causing the altered voltammetric response. Such research could lead to improved sensitivity and selectivity in electrochemical sensing. In their review, Abraham et al.[397] called for further studies focused on understanding the interfacial reaction kinetics, to enable the design of novel sensors suitable for use in practical applications. Likewise, more research with real patient samples after ingestion of opioids, combined with parallel laboratory analysis with gold standard methods, is required to validate the results. More studies with metabolites of the analyte and potential interferents also need to be carried out.

8 . Methods to improve selectivity in electrochemical detection

As discussed in detail in Chapter 3, the electrocatalytic properties can be influenced by altering both the surface chemistry and morphology of electrochemical electrodes. Similarly, these modifications are expected to affect also the electrode fouling. Therefore, a vast range of different chemical pretreatments and electrode modifications have been carried out to improve the performance of electrochemical sensors. A thorough review of these modifications is beyond the scope of this work, and is discussed in detail elsewhere[27,30,31,184,398]. Instead, in this chapter, we present the chemical pre-treatments and modifications carried out to improve the performance of the electrochemical sensors used in this thesis.

8.1 Chemical treatment of carbon electrodes

A wide range of chemical treatments and functionalizations have been applied to improve the performance of conventional carbon and carbon thin film electrodes. Conventional GC carbon electrodes are often subjected to mechanical polishing to expose a fresh pristine surface[213]. Other treatments include vacuum heat treatment, wet chemical processing, electrochemical conditioning and dry processing, such as oxygen plasma treatment[206,207]. Similarly, pyrolytic carbon electrodes are often cleaved prior to measurements to expose a fresh surface. Oxygen plasma treatment of pyrolytic carbon has been reported to increase the peak potential separation for the outer sphere redox probe $Ru(NH_3)_6^{2+/3+}$, while at the same time significantly improving both the reaction kinetics and sensitivity towards DA[399]. Chemical and electrochemical treatments are also commonly used to purify carbon nanomaterials from their residual metal catalysts or process impurities[400].

SWCNT and ta-C electrodes are harder to functionalize by wet chemical treatments due to their chemical stability. And as expected ta-C and SWCNT films seem relatively resistant to oxidation by short nitric acid treatments at room temperature, although minor changes have been observed in nitrogen bonding[152,165]. Both these electrodes can, however, be functionalized with various plasma treatments and electrochemical pre-treatments. Improved electrochemical properties of SWCNT electrodes have been reported after electrochemical cycling, and have been attributed to increase in defects[401]. Electrochemical pre-treatments are also increasingly used to control the O/C ratio of carbon electrodes, due to the ease of functionalization of the electrode prior to analysis. Electrochemical pretreatments are attractive in research as the same setup can be used as in electroanalytical chemistry[27]. For the same reason, it is also increasingly used to reduce graphene oxide electrodes[402] and to renew

or clean the surfaces of fouled carbon electrodes[166,403]. Electrochemical cycling has also been used to purify the surface of SWCNT network electrodes[400].

While treatments usually aim at altering the carbon-carbon bonding and introduce oxygen or nitrogen containing functional groups, morphology changes have also been reported after chemical treatments. For example, significant morphology changes have been reported after electrochemical oxidation of carbon fiber microelectrodes[403]. Similarly, in Publication IV, a 5 min anodic treatment was found to change the morphology of the Ti/ta-C electrode. Moreover, in Publication II, the surface chemistry remained almost unaffected by a treatment in concentrated nitric acid. Despite this, the SWCNT films were clearly densified, compressing the film in the out-of-plane direction, as observed also in[82]. As discussed in Section 3, the altered morphology has the potential to significantly alter the voltammetric response. Therefore, careful morphological characterization of chemically treated electrodes should also be carried out, before electrocatalytic effects are attributed to changes in surface chemistry alone.

Chemical treatments also have the potential to change both the surface loading and oxidation state of metal particles in the carbon nanomaterials. Sainio et al.[145] showed that the Ni catalyst particles in carbon nanofibers (CNF) with different morphologies-reacted very differently to short nitric acid treatments. The Ni particles in CNFs with platelet structure were significantly more oxidized than the Ni particles in CNFs with bamboo structure. Similarly, in Publication II, the Fe catalyst particles were protected from oxidation by encapsulation in few layers of carbon, and therefore oxygen plasma treatment was required to oxidize the Fe. This also resulted in complete destruction of the SWCNT.

In Publication I, a simple 5 min immersion in concentrated nitric acid was found to improve the selectivity in the detection of DA (see Figure 28). We also observed a cleaning effect, where the concentrations of trace Mn, Al, F and Na were reduced below the detection limit of XPS. In addition, a small increase in the surface oxygen loading was observed with both XPS and XAS. XAS further indicated a relative change in oxygen containing surface functional groups, especially that of carboxyl groups. While these results indicate, that the changes in surface chemistry likely caused the improved performance, changes in morphology can, however, not be completely ruled out.

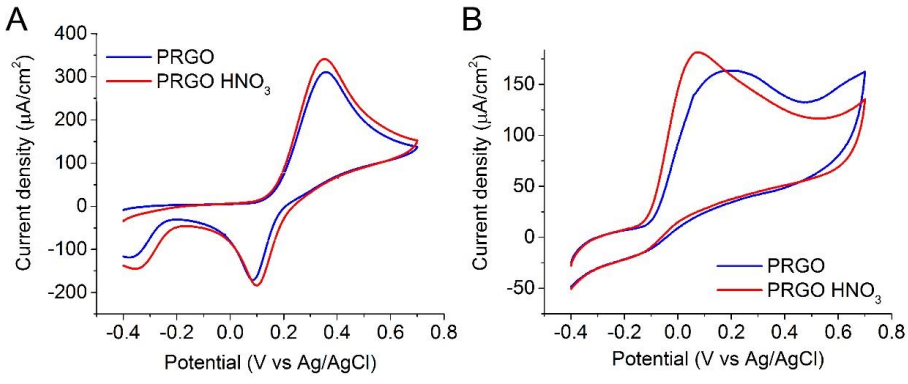

Figure 28. Effect of nitric acid treatment of PRGO modified Ti/ta-C electrodes on the cyclic voltammograms of A) 1 mM dopamine and B) 1 mM ascorbic acid. Supporting electrolyte: pH 7.4 0.01 M PBS. Figure from Publication I.

Similar effects have been recently observed for MWCNTs grown on Ti/ta-C electrodes after nitric acid and anodic treatment[47]. It has been shown that nitric acid and anodic treatments can introduce oxygen containing functional groups and defects in CNT electrodes. Because changes in the oxidation state of metals embedded in the structures have been observed in similar materials, it is not clear to what extent their surface loading and oxidation state affects the voltammetry of inner sphere analytes.

Surface chemistry modifications are usually used to improve the electron transfer kinetics and sensitivity towards the target analyte. However, as noted by Henstridge et al.[147] surface modifications aimed at slowing down the electron transfer kinetics of the target analyte relative to the interferents, can also be used to improve the selectivity. This strategy called "negative electrocatalysis" has been previously used for selective detection of dopamine in the presence of catechol, epinephrine and ascorbic acid[404]. Henstridge et al.[147] further noted that such an approach is rarely seen or reported, highlighting the evidently highly empirical approaches to surface modification to improve electrode performance.

In Publication IV, we used a similar approach to achieve selective detection of morphine in the presence of paracetamol after anodic treatment of a Ti/ta-C electrode. Figure 29 shows an anodic shift of 300 mV for paracetamol oxidation after anodic treatment in PBS, whereas the oxidation potential of morphine remained virtually unaffected. Furthermore, only a small effect on the electron transfer kinetics of the OSR probe $Ru(NH_3)_6^{2+/3+}$ was observed, indicating that the changes in voltammetry are surface chemistry related. The AFM images showed an increase in roughness from the reference value of 0.81 nm (R_{rms}) to 3.06 nm. Raman spectroscopy confirmed the presence of ta-C film with similar I_D/I_G ratio as the untreated electrode. XPS analysis revealed an increase in surface Ti and oxygen after anodic treatment. A thicker (30 nm) ta-C electrode, deposited directly on Si wafer without Ti adhesion layer, showed a much smaller shift after the same anodic treatment. We attributed this difference to partial exposure and oxidation of the underlying Ti adhesion layer of the Ti/ta-C electrode. Therefore, in Publication IV, we concluded that the anodic shift in the oxidation potential of PA was due to a dual effect of oxidized ta-C surface and increased surface Ti oxides.

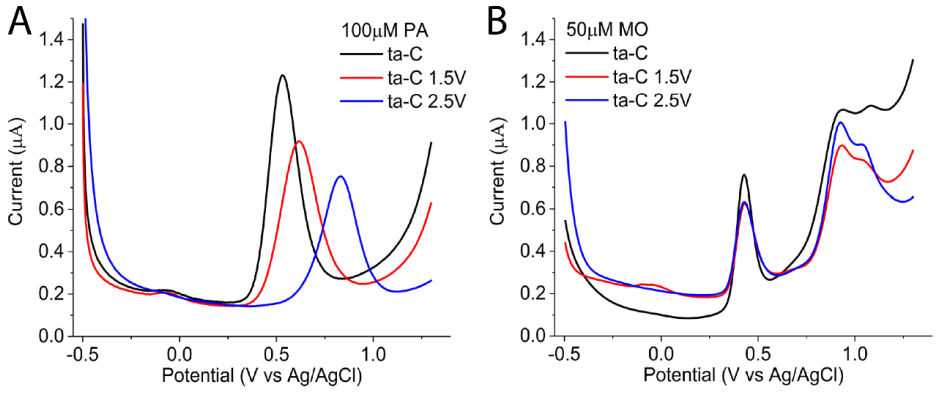

Figure 29. DPVs of A) paracetamol and B) morphine before and after 5 min anodic treatment of Ti/ta-C electrodes at 1.5 and 2.5V. Adapted from Publication IV.

8.2 Modification of carbon electrodes

Conventional electrodes, incompatible with standard microprocessing processes, are still widely used despite their limited selectivity and sensitivity. Perhaps the most common way of realizing electrochemical platforms with enhanced sensitivity and selectivity is the modification of conventional carbon electrodes, most notably glassy carbon electrode, but also SPCE, carbon paste electrodes and amorphous carbon coatings, with various nanomaterials having high specific surface area. The modification of these electrodes, changes both the morphology and surface chemistry of the electrode, and thus affects the voltammetric response as discussed in chapter 3. Similarly, these changes can also significantly reduce the electrode fouling by various fouling agents[29]. It should be noted, however, that most works with modified electrodes employ fabrication techniques, most notably drop casting, that are not mass production compatible. In recent years, however, various nanoparticle graphite mixture inks have become available, and can be used to directly produce functionalized composite electrodes with various printing technologies, including screen-printing. Screen-printed carbon electrodes are also increasingly modified by ink-jet printing, dip coating, and electrospraying[184].

Significant progress in the sensitivity and selectivity has been made with modified electrodes. While other multianalyte detections are also increasingly reported with modified electrodes[30], one of the most common application for modified electrodes is still the detection of dopamine. Due to its low capacitive background current, nanomolar detection of DA has been reported with the Ti/ta-C electrodes used in this thesis[143] as well as other Ti/ta-C electrodes with 15 and 50 nm ta-C films[47]. In fact, Palomäki et al. did not observe any significant improvement in the detection limit after growing MWCNT layers directly on the Ti/ta-C electrode. Despite this and other advantages, such as wide water window, facile electron transfer with OSR probes, microfabrication compatibility and room temperature deposition, Ti/ta-C electrodes show limited selectivity. Therefore, this electrode is unable to selectively detect DA in the presence of AA. Moreover, as discussed in Section 7.1, in the detection of neurotransmitters, high sensitivity and selectivity must be combined with high temporal resolution, significantly limiting the use of polymer membranes for improved selectivity and fouling resistance. Most works reporting selective detection of DA use DPV with superior selectivity, but poor temporal resolution[347,398]. Much fewer works report use cyclic voltammetry with relatively fast scan rates. In Publication I, we studied the modification of Ti/ta-C electrodes with PRGO.

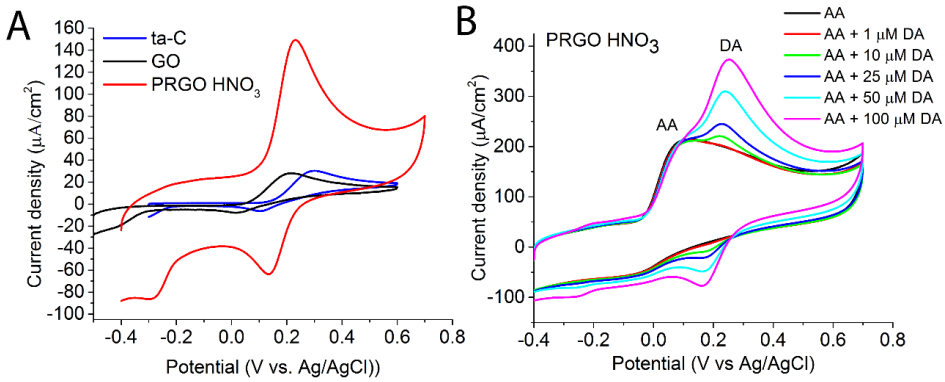

Figure 30. Cyclic voltammogram of A) 100 µM DA with Ti/ta-C (ta-C), GO modified and PRGO modified and nitric acid treated (PRGO HNO_3) electrode and B) increasing concentration of DA in the presence of 1 mM AA with the PRGO HNO_3 modified electrode. Adapted from Publication I.

Figure 30 shows the CV of A) dopamine and B) dopamine in the presence of AA, with the modified and unmodified Ti/ta-C electrodes. A clear increase in sensitivity with a factor of 4 can be seen after PRGO modification. In addition, the PRGO and nitric acid treated electrode showed a clear improvement in fouling resistance by the DA reaction products. While these results show a clear improvement over the unmodified Ti/ta-C electrode, AA still produces a wide oxidation peak overlapping with the DA oxidation peak. For this reason, the detection limit increases to between 1 to 10 µM in the presence of AA, when cyclic voltammetry is used. In contrast, DA concentrations in the range of 100 nM to 1 µM were easily detected with the more commonly used DPV. Similar results have been obtained with carbon nanofibers[144] and MWCNTs[405] grown directly on Ti/ta-C electrodes.

Since then, advances have been made in both the sensitivity and selectivity towards DA with modified Ti/ta-C electrodes. Palomäki et al.[47] were easily able to detect 10 µM DA in the presence of 1 mM AA and 50 µM UA with cyclic voltammetry, using MWCNTs modified Ti/ta-C electrodes with 15 and 50 nm ta-C. The effect of high scan rates and response time was, however, not reported. More recently, Durairaj et al.[38] modified a Ti/ta-C electrode with a composite ink of MWCNTs/Nanofibrillar cellulose/Nafion. With this electrode, a 50 nM concentration of DA could be detected, and a 500 nM concentration already produced a well-defined peak in the presence of AA and UA in CV measurements at a scan rate of 100 mV/s. Detection of 1 µM DA was also demonstrated in varying concentrations of AA. Moreover, a relatively fast response time of less than 1 s, was also measured with a DA concentration of 1 µM. Ti/ta-C films have also been modified with detonation nanodiamonds, leading to improved sensitivity towards DA and improved cell viability. Despite improved sensitivity, this electrode, however, was not able to selectively measure DA in the presence of AA.[37] These results are summarized in Table 6, and clearly show the applicability of modified Ti/ta-C electrodes for the in vivo detection of DA.

Electrodes are also frequently modified by depositing metal nanoparticles, to improve the catalytic properties and increase the electrode surface area[174,398,406]. Thin metal layers can be deposited with PVD methods, and used to further grow MWCNTs and CNFs directly on the Ti/ta-C electrode surface[47,143,144]. Metals can also be co-deposited with carbon in the FCVA process, by preparing composite cathodes or using a dual cathode source. Tujunen et al.[159] prepared a Pt and amorphous carbon composite that showed the catalytic activity of Pt films, but significantly improved the BSA fouling resistance. With a dual cathode source, the metal content can be very accurately controlled[135]. Moreover, intrinsic gradients of catalytic metals can be prepared so that the catalyst particles are present only near the surface[407].

Another way of in-situ modifying carbon nanomaterials is to introduce process gasses, such as oxygen, nitrogen or hydrogen, during deposition or synthesis. Amorphous carbon coatings are commonly doped to influence the electrical properties. Similarly, nitrogen doping of graphene and CNT electrodes are also increasingly carried out in a similar way. We have also prepared oxygen doped, sputtered amorphous carbon thin film electrodes[253]. Oxygen doped amorphous carbon thin films are, however, highly resistive, limiting their use as electrochemical electrodes. Therefore, we recently prepared in-situ surface functionalized ta-

C films, where the oxygen is introduced only prior to the deposition of the last 2 nm[165]. These films still need to be electrochemically characterized.

Table 7. Modifications of Ti/ta-C and other closely related ta-C electrodes.

Electrode	Modification	Benefit	Reference
Ti/ta-C	PRGO, drop casting + NHO_3 treatment	Much improved sensitivity and selectivity.	I
Ti/ta-C	Detonation nanodiamonds, drop casting	Improved sensitivity towards DA and cell viability. No selectivity in presence of AA.	37
Ti/ta-C	NFC-MWCNT-Nafion, drop casting	Selective detection of DA in presence of AA with scan rates up to 1 V/s, response time of < 1s with amperometry.	38
15 nm ta-C on Si	Dip coated Nafion	Almost complete rejection of AA and UA. Reduced matrix effect in human plasma, enabling simultaneous detection of tramadol and its metabolite o-desmethyltramadol. Accumulation of opioids through ion-exchange.	16
Pt doped ta-C	FCVA with Pt wire modified Gr cathode	Retains the catalytic activity of Pt for detection of H_2O_2 while improving BSA fouling resistance.	159
Pt doped ta-C with intrinsic gradient	In situ doping with dual source FCVA	Catalytic activity with less Pt.	407
Fe doped ta-C	In-situ doping with dual source FCVA	Catalytic activity of Fe and improved electrical conductivity.	135
Ti/ta-C (15 & 50 nm)	PVD deposition of Fe + Co + Al + CVD growth of MWCNT	Improved selectivity in measuring DA in the presence of AA and UA, good cell viability.	47

8.3 Nafion membranes

Permselective membranes, such as Nafion, have been widely applied in the electrochemical detection to improve the selectivity towards cationic and neutral analytes in biological

matrices. Due to its ability to block anions, such as AA and UA, from reaching the electrode, it has been applied in glucose[408], glutamate[409], dopamine[410] and morphine[411] sensors. Generally, loss of sensitivity is observed with neutral analytes[409], whereas cations are accumulated[325,410,412], making Nafion membranes particularly attractive in the detection of drugs and biomolecules that are cations under physiological pH. Like other polymer membranes, however, it can significantly increase the response time of the sensor, limiting its applicability in applications where high temporal resolution is required[413]. Nafion membranes also offer improved resistance to biofouling and prolong sensor life more than cellulose membranes[31]. Moreover, Nafion suspensions are commercially available and can be applied with industrially mature technology, without specialized reaction chambers and in-house synthesis, as is required with many other polymers[31].

Nafion ionomers are produced by copolymerization of fluorinated vinyl ether comonomers with tetrafluoroethylene (TFE)[414]. The resulting chemical structure of the Nafion ionomer is shown in Figure 31.

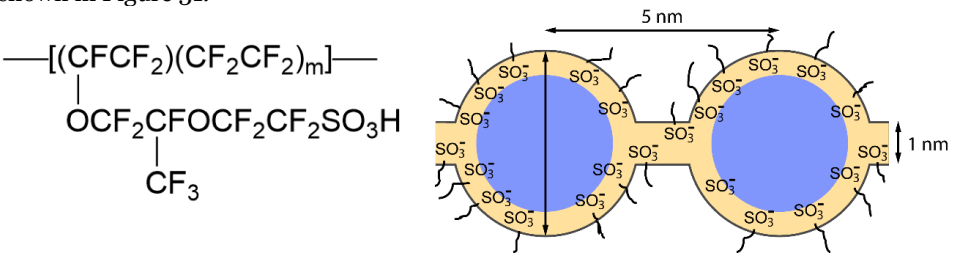

Figure 31. Chemical structure of Nafion (left) and cluster network model of the morphology of hydrated Nafion[415].

Based on early X-ray scattering experiments by Hsu et al.[415] a cluster-network model (shown on the right in Figure 31) was proposed, and has received significant acceptance in literature. In this model, the sulfonate-ended perfluoroalkyl ether groups form inverted clusters with diameters of approximately 40 Å. These micelles are separated by pores or channels with dimensions of ~10 Å. Much work has since been devoted to understanding the microstructure of Nafion membranes, and the morphology has been debated with respect to alternative morphologies that are also consistent with a wide range of scattering results, as well as other characterizations. A detailed review is beyond the scope of this work, and the reader is directed to the comprehensive review on the state of understanding of Nafion by Mauritz and Moore[414]. Nevertheless, there seems to be a general acceptance of Nafion as a multiphase material, with connected sulfonate hydrophilic clusters in hydrophobic semi-crystalline perfluorocarbon phase.

An important parameter is the equivalent weight (EW), the number of grams of dry Nafion per mole of sulfonic acid groups. The EW is related to m (see Figure 31) so that EW = 100m +446[414]. The EW is known to be related to both the structure and water absorption. Nafion 117 films having an EW of 1100 and a nominal thickness of 0.007 inches are the most commonly used extruded membranes, although 115 and 112 films are also available[414]. To improve transport properties, recast membranes with thicknesses of approximately 1-10 μm are usually used in electroanalytical applications[16,356,409,410,416]. Almost complete rejection of anions has, however, been shown using Nafion membranes with significantly smaller thickness, of less than 100 nm[417]. In practice, however, the optimal thickness appears to be a trade-off between

thinner films for improved transport properties, and thick enough films for achieving pinhole free films.

To the best of our knowledge, few comprehensive studies on the effect of the equivalent weight, thickness and nanostructure of Nafion, on the performance in electroanalytical applications, have been reported. Although, different effective diffusion coefficients have been reported for $FcTMA^+$ with different equivalent weight Nafion[418]. Furthermore, solution cast Nafion films, cured at room temperature have been shown to be at least partially soluble in polar organic solvents and water. Loss of signal in prolonged experiments in aqueous electrolytes has been observed and attributed at least to dissolution of the Nafion membrane and dehydration of the of Nafion coatings due to prolonged exposures to solutions of cations[418,419]. Curing the films at elevated temperatures has been found to increase the density, crystallinity and mechanical strength. These changes have also been shown to reduce the water uptake of the film[420] and the permeability of neutrals, anions and cations through the films[418]. Similarly, curing at elevated temperatures improves the stability of Nafion films in implanted sensors[31], whereas increased protein fouling has been reported after curing at elevated temperatures. The changes in the properties are influenced by the used solvent for casting, and post treatments with acids and electrolytes, as well as curing temperatures, as discussed in more detail by Hoyer et al[421]. Generally, curing at high temperatures above the glass transition temperature (212-238 °C for alkali salt form and 104 °C for acid form) is required for good solvent stability[418,421,422]. Although, Michael and Wightman[423] have reported improved stability after curing at 80 °C, with the original low boiling point solvent. This is important, as Nafion films are increasingly applied in wearable sensors based on flexible electronics, and in this work on test strips fabricated on temperature sensitive polymer substrates.

While there has been a vast amount of work on proton conducting membranes for fuel cells, relatively few works study the permeabilities of different drug and biomolecules. This is somewhat surprising, given that a study by Manallack et al.[424] found that 78.6 % of oral drugs contain an ionizable group, while 11.9 % are neutral, 4.3 % are always ionized, and the remainder 5.3 % are made up of salts and miscellaneous compounds, such as mixtures and high molecular weight substances. Tudos et al.[416] studied the relative permeabilities of catechol amine neurotransmitters. They found that the permeability decreases in the order of dopamine > epinephrine > norepinephrine. They, however, found that norepinephrine had the highest diffusion coefficient in Nafion. Kubiak et al.[413] further studied the permeabilities of biologically important molecules by flow injection analysis with a Nafion coated electrode. As expected, they found the highest permeabilities for the cations dopamine and norepinephrine, followed by the neutrals paracetamol, methylcatechol and catechol. Permeabilities below 1 % were found for anions AA, UA and hexacyanoferrate(II). The non-zero permeability of $Fe(CN)_6^{4-}$ was attributed to pinholes in the Nafion coating[418]. In contrast, Fan et al.[418] reported higher permeabilities for the neutrals hydroquinone and glucose, than the positively charged $FcTMA^+$. They however, observed much higher extraction coefficients for $FcTMA^+$ compared to neutrals. Similarly, Tudos et al.[416] concluded that the selectivity for cations compared to neutral or anionic compounds cannot be accounted for by the differences in diffusion coefficients in the film, but it is mainly the result of the differences in distribution constants at the film/solution interface. Fan et al.[418] further proposed that the neutral analytes can enter hydrophobic “interfacial zones” in the fluorocarbon backbone phase. This may, to some extent, explain the relatively high permeability of neutrals, although the effect of pinholes is also largely unknown.

Interestingly, Shi et al.[419] also found different mobilities for hydrophobic and hydrophilic redox probes. They found that $Ru(NH_3)_6^{3+/2+}$ enters Nafion coatings more rapidly, but is ultimately displaced by the less mobile but more strongly bound tris(bipyridine)ruthenium(II) ($Ru(bpy)^{2+}$), indicating a higher affinity towards hydrophobic species. Preferential incorporation of hydrophobic cations was observed also by Szentirmay et al.[425]. Nagy et al.[356] further observed that the ion exchange selectivity of catecholamine neurotransmitters was moderated by their hydroxy substitution (when normalized with the molar mass). This further supports the selectivity towards hydrophobic cations.

While it has been shown that amino acids can permeate through extruded 117 Nafion membranes[311], very little is known about the permeability of zwitterionic molecules. Amino acids are zwitterionic and some are electrochemically active. In addition, many drugs are also zwitterionic. Furthermore, in section 7.1.2, we also discussed the metabolism of drugs through glucuronidation. This is the main metabolic pathway for morphine and also occurs for paracetamol. Glucuronidation renders PA negatively charged, and opioids with glucuronide metabolites are zwitterionic. Therefore, the permeability of zwitterionic molecules is of high importance to *in vitro* diagnostics. Interestingly, Kubiak et al.[413] showed much lower permeability for the zwitterionic amino acid DOPA than for dopamine, at pH 7.4. Further studies by Tudos et al.[416] similarly found a low permeability at pH where DOPA is present as a zwitterion, whereas DOPA was readily transported through Nafion at pH below 4, where it is present in its cation form.

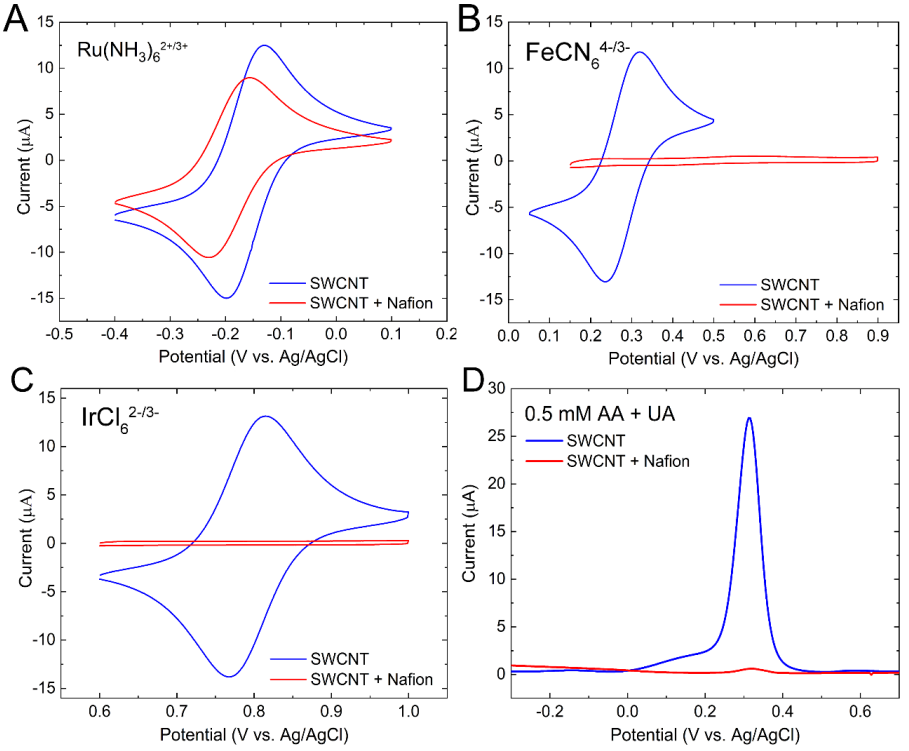

Figure 32. Cyclic voltammograms for SWCNT and SWCNT + Nafion electrodes in (A) 1 mM $Ru(NH_3)_6^{2+/3+}$, (B) 1 mM $Fe(CN)_6^{4-/3-}$, and (C) 1 mM $IrCl_6^{2-/3-}$ in 1 M KCl, as well as (D) differential pulsed voltammogram of 0.5 mM AA and UA in PBS. CV scan rate: 100 mV/s for all measurements in A, B and C. Adapted from publication V.

We obtained similar results with a Nafion coated SWCNT electrode. In[396] we showed that a Nafion layer can almost completely reject the morphine-3-glucuronide. This may be both due to the increased size of the molecule and the exposed carboxylic groups of the glucuronide. The electrochemical properties of this electrode were further studied in Publication V. Figure 32 shows the cyclic voltammograms of these measurements with bare and Nafion coated SWCNT electrodes. As seen from Figure 32 A, both the uncoated and the Nafion coated SWCNT electrodes show close to reversible electron transfer for $Ru(NH_3)_6^{2+/3+}$ with ΔE_p values of 73.1 ± 3.7 mV and 70.7 ± 2.2 mV, respectively. Moreover, the redox currents of $Ru(NH_3)_6^{2+/3+}$ were found to be diffusion limited.

The CVs of the negatively charged $Fe(CN)_6^{4-/3-}$ and $IrCl_6^{2-/3-}$ are shown in Figure 32 B and C, respectively. The oxidation current was reduced by 97.5% for the former and totally suppressed for the latter after Nafion coating. The Nafion coating also caused an increase in the ΔE_p value for $Fe(CN)_6^{4-/3-}$ from 95.4 ± 12.1 to 219.4 ± 17.7 mV. Figure 32 D further shows that the Nafion coating suppresses 98.2% of the DPV signal of ascorbic acid and uric acid in PBS. Despite this, a relatively large deviation was observed in the oxidation current of AA and UA solutions, likely explained by defects or pinholes in the films. Similarly, Fan et al.[418] noted that even after several layers of ultrathin Nafion coatings, complete rejection of $Fe(CN)_6^{4-/3-}$ was not achieved.

It is known, that the permeabilities and accumulation of cations are affected by the ionic strength and composition of the supporting electrolyte. Especially, interference due to competition from K^+, Na^+ and Li^+ in the ion exchange process has been reported for catecholamine cations[416]. Similarly, interference from non-electrochemically active cations has been reported due to competitive ion exchange[356]. Tudos et al.[416] further found that the permeability for catechol was largely unaffected by the potassium concentration. They also found a slight permeability increase for the anion DOPAC, with increasing potassium concentration. Similar results were obtained with lithium and sodium buffers[416]. The increase in DOPAC permeability was attributed to improved shielding of the charge in electrolytes with higher cation concentration. These results clearly show the potential for sample cation concentration to cause interference. The solution pH may also significantly affect the results, as the charges of drug and biomolecules are pH dependent. Therefore, the use of Nafion films is limited to applications where these sample parameters are known. In some applications, such as *in vivo* detection of dopamine, the solution composition is fully restricted. As discussed in section 7.1.2, these parameters also remain relatively constant in biological samples. In vitro diagnosis also allows for control of these parameters, as most such applications require sample treatments, such as dilution with buffer solution to control matrix effects. Such treatments could also enable improved selectivity through affecting the ion exchange of cations. For example, in the determination of PA, it could be advantageous to spike blood samples with high ionic strength buffer solutions, to limit the ion exchanges of interfering cations.

Several other drugs are also expected to cause interference in electroanalysis of analgesics. In Publication VI, we studied the interference of several drugs often taken in concomitant overdose with paracetamol. These measurements shown in Figure 34 indicate that selectivity can be achieved in the presence of common interferents. Other cations, such as nicotine, MO and ODMT, were also not found to cause any interference even at lethal concentrations. The functionalization of SWCNT by Nafion also shifted the MO peak (as shown in Figure 36) improving the selectivity towards PA.

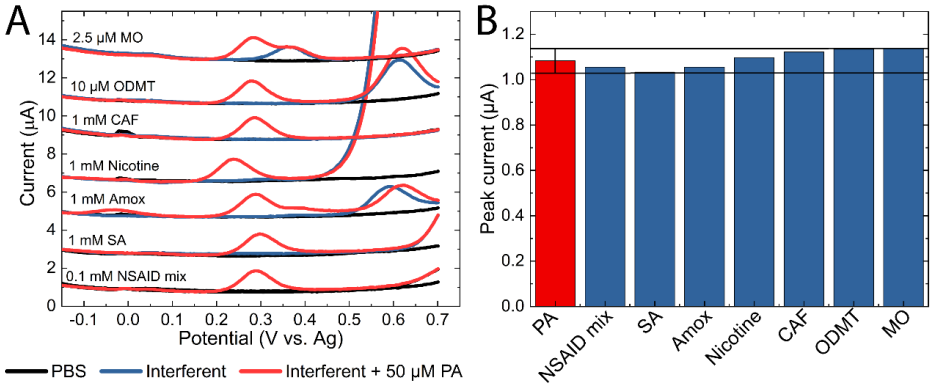

Figure 33. Interference study from Publication VI. A) DPV scans in blank PBS (black line), interferent alone (blue line) and interferent + 50 µM acetaminophen (red line). B) The background subtracted peak current for 50 µM paracetamol (PA) alone (red) and in the presence of interferents (blue). The error bar represents a 5% error defined as the tolerance limit. The DPV scans in A) have been offset for clarity.

In addition to the rejection of anions, a significant reduction in the matrix effect was observed in human plasma samples in Publications V and VI. Similar results were also obtained by Mynttinen et al.[16] with a Nafion coated ta-C electrode. This work also showed significant reduction in the oxidation current of negatively charged ibuprofen. As discussed in section 7.1.2, there are additional electroactive interferents in blood and urine samples, such as xanthine and hypoxanthine. Figure 34 shows DPV scans with the SWCNT sensors strips from Publication VI in urine, diluted with PBS (1:1 ratio) prior to measurement. No meaningful comparison of the coated and uncoated SWCNT electrodes could be made in plasma or whole blood due to severe passivation of the electrodes. Nevertheless, the measurements in urine show a large matrix effect due to faradic processes at the uncoated SWCNT electrode. The current was significantly decreased with the Nafion coated electrode, but small peaks around 0.2 V, 0.65 V and 0.85 V (vs. Ag) where still observed. The first peak is likely attributed to AA and/or UA, whereas the two other peaks are due to unknown endogenous interferents.

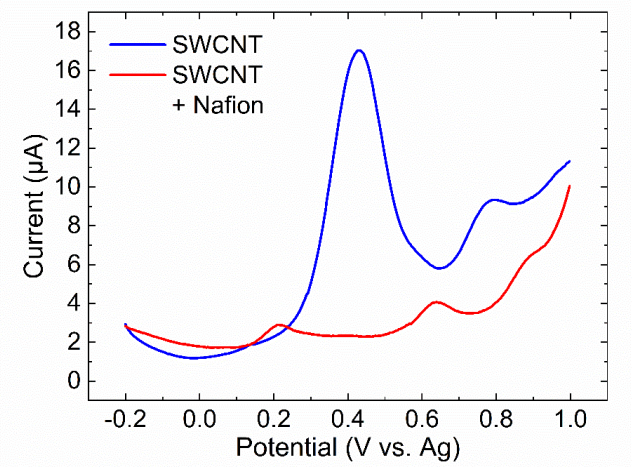

Figure 34. Differential pulse voltammograms of urine diluted two times with PBS with uncoated and Nafion coated SWCNT electrochemical test strips fabricated for Publication VI.

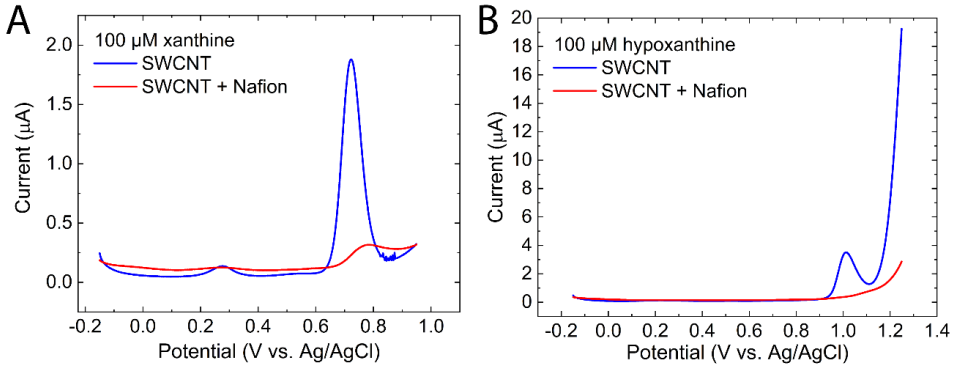

Figure 35. DPVs in 100 µM A) xanthine and B) hypoxanthine in pH 7.4 PBS with uncoated and Nafion coated SWCNT electrodes.

Similarly, an increased current around 1.2 V was observed by Mynttinen et al.[16] in human plasma with a Nafion coated ta-C electrode. To study the effect of xanthine and hypoxanthine on these peaks, separate electrodes were prepared on PEN substrates as in[325]. Figure 35 shows the DPV scans of 100 µM xanthine and hypoxanthine with SWCNT electrodes, with and without Nafion coating. It is acknowledged that the measured concentrations are larger than what are expected in, for example, *in vivo* samples. The Nafion coating shows a clear ability to reduce the interference from these two endogenous substances. Nevertheless, the residual matrix effects in Publications V and VI as well as [16] could be related to these interferents. Due to the much lower blood concentrations of xanthine and hypoxanthine, it seems that these cannot fully account for the observed peaks in Figure 34. More studies are, however, required to understand the observed matrix effect in biological samples with Nafion coated electrodes.

As shown in Publication V, Nafion coatings also significantly alter the voltammetry of opioids. We obtained similar results for tramadol and its active metabolite O-desmethyltramadol[16], and recently for oxycodone and its metabolites[325]. Figure 36 shows the differential pulse voltammograms (DPVs) for morphine and codeine for both SWCNT and Nafion/SWCNT electrodes.

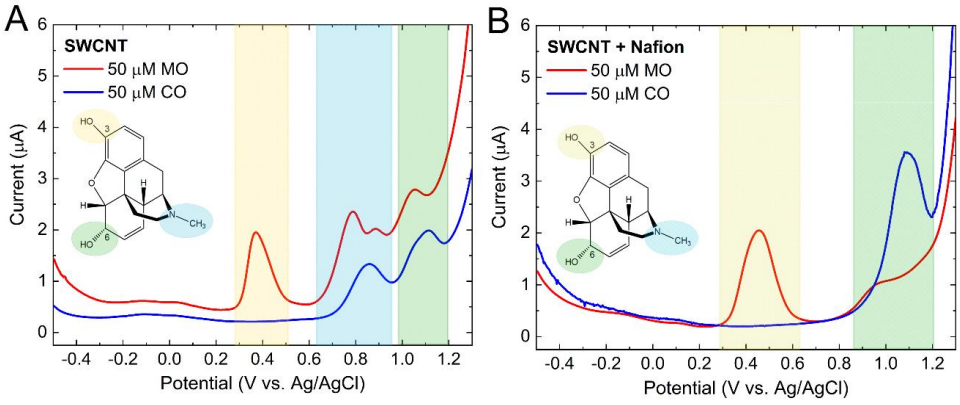

Figure 36. DPV scans of 50 µM morphine and codeine with A) uncoated and B) Nafion coated SWCNT electrodes along with the chemical structure of morphine with highlighted functionalities. Adapted from Publication V.

As discussed in detail in section 7.2.3 and Publication V, the electrochemical oxidation of MO is known to be complex, likely involving the oxidation of hydroxyl groups at carbons 3 and 6, as well as the electrochemical demethylation of the aliphatic tertiary amine. Nevertheless, the first oxidation peak observed at +0.44 V is clearly due to the phenol functionality. This peak is also anodically shifted by 80 mV compared to the uncoated electrode, further improving the selectivity towards morphine in presence of AA and UA. As seen from Figure 36, the oxidation peaks likely attributed to the tertiary amine are not observed with the Nafion/SWCNT electrode. In Publication V, we tentatively assigned the small remaining peak for morphine and that of codeine to the hydroxyl group at 6-postion. Recently, in [325] we also observed a well-defined peak with a different Nafion coated SWCNT electrode, for oxycodone and noroxycodone around 1.2 V. Both these analytes contain the methoxy functionality. Garrido et al.[323] also suggested possible oxidation peaks due to the methoxy group of codeine. Therefore, the presence of the methoxy group could explain the large difference in the voltammetry in this region compared to morphine and oxymorphone. Contributions due to the hydroxy group at 6-position or shifts in the peaks due to the amine functionalities can currently not be ruled out. Despite the tentative nature of the peak assignment in this work, it is clear that Nafion coatings accumulate morphine and codeine and improve the selectivity of simultaneous measurements.

In Publications V and VI, lower recoveries were found for morphine, codeine and paracetamol in plasma and whole blood, respectively, compared to the calibration measurements in PBS solutions. This is likely due to presence of proteins in these matrices. This was further verified by a recovery of close to 100 % with PA in urine samples, containing many of the same interferents as blood, less the serum proteins. Hoyer et al.[421] noted that protein fouling at Nafion coated electrodes can occur due to permeation of proteins through large pores in the film, or by binding to the surface of Nafion. To the best of our knowledge, no molecular weight cut-off has been reported for Nafion membranes. The size of hydrophilic channels are, however, comparable in size to those found in dialysis membranes and therefore, it is often assumed that proteins cannot permeate Nafion.

It should be noted, however, that the nature of the hydrophilic channels and the amount of defects in the Nafion coatings used in this work are unknown. In addition, highly varying results have been reported on the protein fouling of Nafion coated electrodes[31,421,426]. For these reasons, the protein fouling was studied in both publications V and VI. Figure 37 shows the cyclic voltammograms of 1 mM $Ru(NH_3)_6^{2+/3+}$ in PBS and human plasma (1:1 diluted with PBS). No loss of signal was observed over several scans in PBS and human plasma. Moreover, no loss of signal was observed in human plasma compared to PBS. Similar results were obtained in Publication VI with a 40 µL drop of PBS and human plasma with 1 mM $Ru(NH_3)_6^{2+/3+}$.

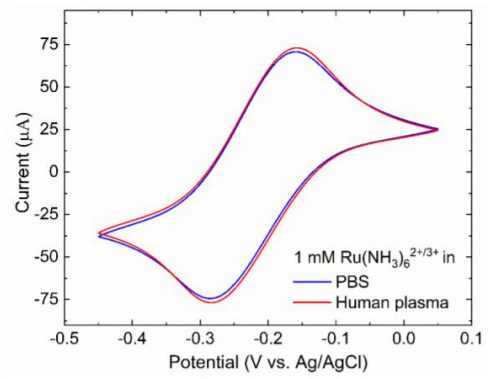

Figure 37. Cyclic voltammogram of 1 mM $Ru(NH_3)_6^{2+/3+}$ in PBS and human plasma from Publication V.

Many drugs are bound to human plasma proteins. Human plasma contains over 60 proteins, but only three of these account for the majority of drug binding: albumin (carries mostly anionic drugs, some cationic and neutral drugs), a1-acid glycoprotein (AAG) (cationic and neutral drugs) and lipoproteins (cationic and neutral drugs).[427] This protein binding affects the pharmacokinetic profiles, and for some drugs, such as opioids, the unbound fraction is pharmacologically important. Usually, laborious equilibrium dialysis is used to determine the free-fraction of a target analyte. Because, Nafion membranes are thought to be impermeable to plasma proteins, only the unbound fraction is expected to be able to partition into the Nafion membrane. Therefore, in the event that the electrode is not fouled by the plasma proteins, a recovery corresponding to the free fraction of the drug is expected in protein containing samples. Table 7 shows the recoveries obtained for morphine and codeine in Publications V and paracetamol in Publication VI in human plasma samples. It can be seen that these recoveries reported for MO and CO in Publication V and PA in Publication VI closely match those of previously reported unbound fractions.

Table 8. Reported recoveries of PA, MO and CO in human plasma with Nafion coated SWCNT electrodes used in Publications V and VI, as well as previously reported unbound fractions in human plasma.

Analyte	Recovery (%)	Free fraction (%)
PA	79	75-80[428]
MO	61	53-68[429,430]
CO	46	44[430,431]

Unfortunately, practically all electrochemical studies reported previously with real samples use very high dilution factors. Therefore, similar reduction in recoveries may have been previously attributed to passivation. Banis et al.[432], however, found that only the free fraction of clozapine, a benzodiazepine, contributed to the measured electrochemical signal in bovine serum albumin containing analyte solutions, with a chitosan-based composite electrode. These results suggest that the electrodes coated membranes impermeable to proteins can directly determine the unbound acetaminophen fraction, without time-consuming equilibrium dialysis. It should be noted however, that different fouling for different analytes has been

previously observed in complex protein containing matrices[208]. Therefore, these results do not unequivocally confirm that the Nafion coated electrode is measuring the free fraction of these drugs, and further studies are required to validate these results.

9 . Fabrication of disposable electrochemical test strips

In this chapter an industrially compatible fabrication process for a fully integrated electrochemical test strip, with the aim of detection of analgesics from capillary whole blood samples, is proposed. The design, material selection, production process and performance of the electrodes used to determine paracetamol in whole blood in Publication VI, are briefly discussed.

9.1 Design of electrode configuration and material selection

The active area of the sensor was defined to be circular with a 6 mm diameter, because this area can easily accommodate the analysis of 40 µL samples. The electrode configuration design, with key dimensions in mm, is shown in Figure 38 and includes SWCNT working and counter electrodes, as well as silver reference electrode and contact pads. The step by step fabrication process is described below.

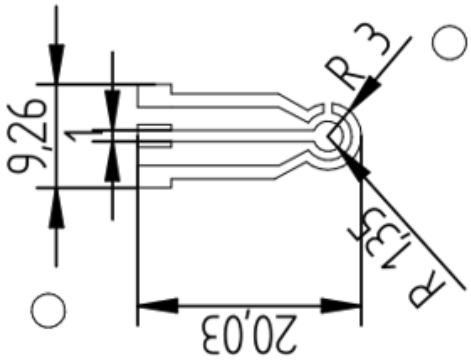

Figure 38. Design and key dimensions of the produced intergraded SWCNT test strips.

One key design aspect is the electrical resistance of the electrochemical cell when in contact with a sample. A large resistance will cause ohmic potential drop between the electrodes. Therefore, an unacceptably large resistance may affect the accuracy of the data[39]. The uncompensated resistance is the sum of the solution resistance and the resistance of the electrode lines. The close arrangement of the electrodes, and reasonably high conductivity of blood[433] are expected to make solution resistance negligible. Therefore the ohmic drop, as per Ohm's law, equals the current passed times the uncompensated resistance, R_u[39].

The potential measurements in voltammetric experiments are usually accurate to within a few mV under optimal conditions. Therefore, we can consider a 4 mV ohmic drop as the maximum allowed. The electrochemical test strip is designed for *in vitro* diagnostics, utilizing voltammetric techniques, such as cyclic voltammetry, linear sweep voltammetry and differential pulse voltammetry. With these methods scan rates in the range of 5-100 mV/s are typically used (when high temporal resolution is not required). For example, with cyclic voltammetry measurements at a scan rate of 100 mV/s, with 1 mM $Ru(NH_3)_6$ in 1 M KCl, redox currents of around 20 μA are expected. This gives a maximum allowed resistance of 200 Ω.

Obviously, the 90 % transparent SWCNT films used in Publications III and V, give too high a resistance with 1 mm wide lines approaching lengths of 2 cm. To lower the resistance, the thickness of the SWCNT network was increased to 71.6 % optical transparency (at 550 nm). Further reduction was achieved by extending the Ag lines to partially cover the SWCNT film and reduce the overall resistance. After these steps, uncompensated resistance measurements showed a combined resistance of 164.1 ± 25.6 Ω with all the integrated electrodes, connected and a 40 μL drop of pH 7.4, 0.01 M PBS solution, as shown in Publication VI. The final design still gives an uncompensated resistance that is too high to be applicable for fast scan experiments, such as fast scan cyclic voltammetry. Although such techniques are rarely needed in the intended application, this problem could be addressed by further reducing the size of the electrodes. The design also allows for further extension of the Ag lines.

9.2 Substrate material

As shown in Publications III and V, SWCNT electrodes on glass substrates support facile reaction kinetics and show high sensitivity toward opioids. Polymers, however, offer many advantages over glass substrates, owing to their intrinsic plasticity, hydrophobicity, excellent dielectric and insulative properties, resilience to repeated deformation and compatibility with roll-to-roll manufacturing[21]. The chemical stability of polymer substrates is, however, usually limited compared to glass, and may contain impurities capable of causing interference. Therefore, the following requirements need to be fulfilled by any substrate material used in electrochemical sensors:

i. High chemical resistance to solvents used in the manufacturing process
ii. High chemical resistance in the measurement environment
iii. Resistance to swelling in measurement environment
iv. Absence of chemicals with electrochemically active functional groups at the surface
v. Low or no use of plasticizers

The final point is especially important for the SWCNT electrode, where the porous network is dry-transferred directly onto the substrate and its porous nature is expected to promote adsorption of plasticizers. These loosely bound plasticizers are lipophilic and are expected to readily adsorb on the SWCNT sidewalls. Moreover, the widely used plasticizer bisphenol A is electrochemically active and oxidizes close to the potential of morphine and paracetamol[434,435].

Polyethylene terephthalate (PET) and polyethylene naphthalene (PEN) are the main substrate materials used in transparent flexible electronics. They have also been widely applied in the fabrication of flexible electrochemical sensors and biosensors. In addition, other flexible

substrates, such as polytetrafluoroethylene (Teflon), Kapton, rubber, paper and textiles have also been investigated[436]. The success of PET and PEN substrates is due to a good combination of high mechanical strength, good resistance to many chemicals, low water absorption, excellent dielectric properties, good dimensional stability, as well as good resistance to thermal shrinkage and degradation of the polymer chains[437]. In particular, the solvent resistance and good mechanical properties are of importance when multiple fabrication steps are needed, as any mechanical deformation between steps will affect the alignment. The actual choice is usually dictated by the upper processing temperature, as PEN has higher thermal stability[437].

SWCNT films on polymer substrates have been shown to be highly hydrophobic[171], and may suffer from incomplete wetting during electrochemical measurements. This problem can be overcome by atmospheric plasma treatments or by using polymers coated with wetting layers. Care should be taken when using polymers with adhesion layers, however, as they are often wax-like polymers with a wide range of chemistries. Therefore, the SWCNT network can become partially embedded in the adhesion layer, rendering it inaccessible to analyte.

Flexible transparent touch sensors have been fabricated on PET films and they are known to be compatible with the manufacturing process[32]. Therefore, this substrate was used in the manufacturing of electrochemical sensors for Publication VI, and was found to show satisfactory performance.

9.3 Production process

In Publication VI, we propose a method for producing a fully integrated electrochemical test strip to be used for measurements with whole blood. The fabrication scheme, shown in Figure 39, combines the mature screen-printing with a novel dry printing technology of SWCNT networks, and slot die coating of ultrathin Nafion membranes.

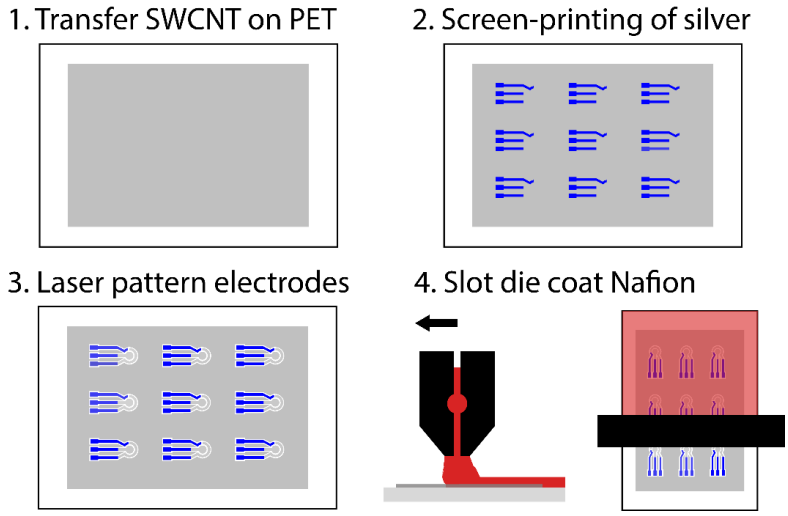

Figure 39. Step-by-step production flow of the integrated SWCNT test strip presented in Publication VI.

With the aerosol CVD process, large areas of SWCNT network can be synthesized, collected and patterned to form highly conductive electrodes[82]. The properties of these films are

discussed in detail Chapter 4. In this process, SWCNTs were first grown by aerosol CVD as discussed in detail in [82,183] and collected on a filter. The 18 x 26 cm SWCNT network was then press-transferred onto an A4 PET sheet and densified with isopropyl alcohol. The sample was dried with compressed nitrogen and then baked for 10 minutes at 100 °C. The press-transferred SWCNT film had an optical transparency of 71.6% (at 550 nm) and sheet resistance of 73 Ω/sq.

Screen-printing of silver, directly on top the SWCNT network, was used to fabricate the reference electrodes and contact pads. In the proposed production flow, the SWCNT electrodes are patterned with a nanosecond pulse laser, of 1064 nm wavelength. SWCNT networks can be patterned down to tens of μm resolution with laser ablation[32] and the technology is fully roll-to-roll compatible with high throughputs[438]. SWCNT electrodes can also be directly patterned by collecting the SWCNTs through a patterned filter to achieve sub 10 μm line widths[194]. Patterning of SWCNT films has also been reported using standard photolithography and oxygen plasma etching[439,440]. Nevertheless, the laser ablations can be used to achieve SWCNT patterns with good electrical isolation and little damage to the polymer substrate in only one step, whereas photolithography requires up to 8 steps[32]. Moreover, a previous study also showed that the laser patterning is significantly more cost-effective than standard lithography, due to lower equipment cost and cost of equipment operation[32]. In addition, the plasma etching process is complex and time-consuming[441]. Other advantages of the laser patterning also include reduced handling of hazardous liquids, leading to a lower environmental footprint, and no lead-time for changes in design patterns. It should, however, be noted that the proposed manufacturing process still requires masks for screen-printing of the silver lines, increasing the lead-time of design changes.

Finally, to improve the sensor performance, the whole A4 sheet was slot die coated with Nafion. Slot die coating is a known technology for coating highly uniform polymer thin films. The main advantage of this process is the higher material efficiency and fast throughput, compared to dip coating. After slot die coating with Nafion, the electrical isolation of the electrodes was tested with a multimeter for each test strip. The thickness of the Nafion layer was measured with SEM from cross-section prepared with focused ion beam milling in Publication VI. Figure 40 shows an overall thickness of approximately 170 nm for the SWCNT/Nafion working electrode. A dark layer, with a thickness of 65-75 nm on top of the SWCNT/Nafion layer was also observed, and attributed to Nafion. Flat elongated Ag particles in the few μm size range are seen in the cross-section of the Ag reference electrode. Thicknesses between 5.9 to 7.2 μm were measured for the Ag reference electrode. Due to the large roughness, a clear layer of Nafion cannot be discerned on top of the Ag particles. In Publication VI, we also studied the performance of the screen-printed reference electrodes. These results were presented in section 5.2.

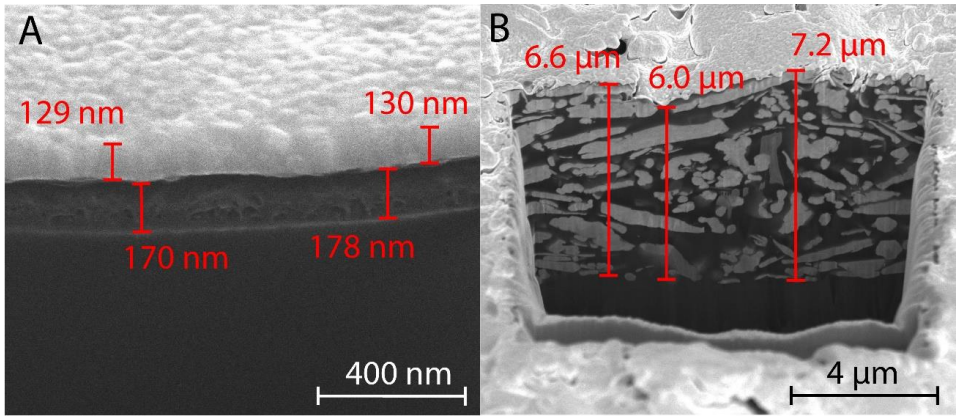

Figure 40. Focused ion beam milled cross-sections of the Nafion coated A) working and B) reference electrode imaged with scanning electron microscopy. Figure from Publication VI.

As discussed in section 8.3, it has been show that curing at elevated temperatures can improve the solvent resistance of recast Nafion membranes. The slot die coater used in Publication VI is capable of heating the sample holder. Curing at elevated temperatures, however, caused non-uniform drying, affecting the repeatability of the sensors. Moreover, a review by Hoyer et al. [421] suggested that curing at elevated temperatures can reduce the polarity of the Nafion surface, thus promoting the adsorption of albumin, leading to decreased fouling resistance. As high repeatability and fouling resistance are required for in vitro diagnostics, the Nafion was allowed to dry at room temperature. Post curing at elevated temperature either in salt or acidic form could, however, easily be carried out if higher resistance to organic solvents is required.

Finally, the cut-out strips were covered with polytetrafluoroethylene (PTFE) film (Saint-Gobain Performance Plastics CHR 2255-2) with a pre-punched 6 mm hole. For single measurements, however, this mask was not required as the laser ablated area around the electrodes was hydrophobic enough to keep the 40 µL drop in place during measurement. The Teflon film, however, makes the strip more rigid and easier to handle. It also protects the SWCNT and silver lines from physical damage. Excellent adhesion of the SWCNT network was observed on the PET substrate. On this substrate, a yield above 97 % was achieved, as only 2 out of 72 sensors in the sheet produced in Publication VI failed due to damage during the fabrication process. No further failures were observed during electrochemical measurements.

9.4 Performance of the test strips

In Publication VI, we demonstrated the use of these test strips in the quantitative point-of-care detection of the common analgesic paracetamol. We further showed close to reversible electron transfer with the outer sphere redox probe $Ru(NH_3)_6^{3+/2+}$. The performance of the Ag reference electrode was discussed in more detail in section 5.2.

As discussed in section 7.2.2, PA poisoning is common and if untreated can lead to hepatic failure and even death. Figure 41 shows the measurements with increasing concentrations of paracetamol in PBS, plasma and capillary whole blood obtained by finger prick. The results show an almost complete lack of matrix effect in the background, and linearization of the results shows that the current scales linearly with the PA concentration.

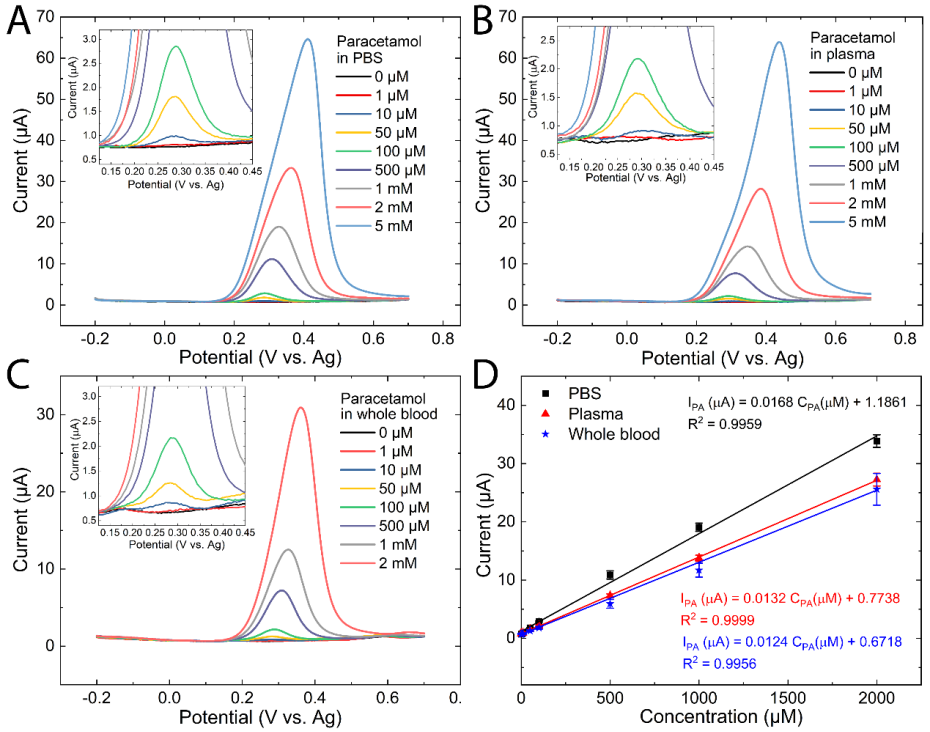

Figure 41. DPVs of increasing concentrations of paracetamol in A) PBS, B) human plasma C) whole blood. D) linearization of results in all measured matrices. The error bars show the standard deviations of 4 measurements with different electrodes. Figure from Publication VI.

The linearization of currents suggests lower recoveries of around 74-79% in these biological matrices, closely matching the previously reported free fraction of paracetamol unbound to proteins[428]. This was confirmed in a separate recovery test in whole blood, as shown in Table 8. These results also show adequate repeatability for clinical use.

In Publication VI, we also showed high resistance to passivation both in human plasma and whole blood. As can be seen from Table 7, we obtained similar results in Publication V for morphine and codeine. Thus, these results suggest that we are measuring the free fraction of PA.

Table 9. Recovery study in whole blood. Average of 3 determinations with 3 different electrodes.

Added (µM)	Found (µM)	Recovery %	RSD % (n=3)
50	36.5	73.1	7.4
100	74.7	74.7	5.5
500	371.8	74.4	1.9

Based on the results in Publication VI, we propose an electrochemical assay for the measurement of paracetamol concentration in capillary whole blood obtained by finger prick. This assay is capable of quantitative determination in human plasma and whole blood, after

only 1:1 dilution with PBS and no precipitation of proteins, with an overall assay time of less than 5 min. In Publication VI, high selectivity was also shown in the presence of some interferents often taken in concomitant overdose with paracetamol. Due to the large number of other possible interferents, such as metabolites and other possible drugs, validation of the protocol still has to be carried out with real patient samples. These studies should also include parallel measurements with gold standard techniques, such as LC-MS.

Continued development to improve the sensitivity without compromising the selectivity needs to be carried out. This would allow for further dilution and facilitate measurements of smaller samples in the range of 5-10 μL that can be more easily obtained from all patients. Alternatively, this could be achieved by further miniaturized electrode design. Further optimization of the multilayer electrode strip is also required to enable the detection of PA in unprocessed capillary whole blood. These initial results suggest that the developed test strip is promising in POC determination of PA for screening of PA intoxication.

10 . Conclusions and future outlook

Much progress has been made in the multianalyte detection with modified electrodes. The limited selectivity, however, still presents major problems that need to be overcome. The large variation of the oxidation potentials of different analytes, at electrodes with varying surface chemistry and morphology, further shows the applicability of chemical treatments and electrode modification in improving selectivity, sensitivity and stability of electrodes. We show that both chemical treatments and electrode modifications are effective strategies for improving the selectivity towards dopamine and analgesics.

It is clear that, modified carbon electrodes show great potential for development of highly selective and sensitive sensors for continuous monitoring and in vitro diagnostics of drug and biomolecules. The lack of studies combining extensive physicochemical characterizations with electrochemical studies, however, makes it difficult to understand the large variations in redox potentials of analytes measured with different electrodes. At present, this lack of understanding of the origin of electrocatalytic properties confines electrode material development to trial and error. We show the applicability of synchrotron based soft x-ray spectroscopy, in obtaining chemical information from different depths of porous carbon nanomaterial electrodes. We also show the applicability of bulk analysis with x-ray emission spectroscopy with a novel transition edge detector, in combination with surface sensitive XAS, electron microscopy and diffraction, as well as other conventional spectroscopy techniques.

In this and other supporting work, the Ti/ta-C and SWCNT thin film electrodes have been extensively characterized. Both the studied microfabrication compatible thin film electrodes show facile electron transfer and low background current, enabling trace level detection. In this thesis and supporting work, we have developed a relatively good understanding of the physical, chemical and electrochemical properties of Ti/ta-C electrodes. We find that the ta-C thickness and the presence of Ti close to the surface of the Ti/ta-C electrode influence its electrochemical properties. Moreover, we show that by controlling the surface Ti concentration and oxidation state, we can affect the oxidation potential of paracetamol, enabling the selective detection of morphine. The role of Ti surface loading on a wider range of analytes should be investigated. Similarly, the roles of other potential minor or trace impurities in the ta-C films need to be further studied.

Further studies of the SWCNT electrodes are also required to understand the origins of their electrochemical properties. Especially, the role of Fe catalyst particles and morphology of the porous SWCNT networks, in the electrocatalysis of dopamine and analgesics, need to be studied further. A more developed understanding of the origins of electrocatalytic properties is required to enable direct production of SWCNT networks with tailored electrocatalytic properties. This involves accurate control of the thickness, morphology and surface chemistry,

achieved without compromising the mass producibility and cost-competitiveness of the process.

Despite their attractive properties, the selectivity and fouling resistance of these electrodes alone is, however, not sufficient for detection of drug and biomolecules in complex biological matrices. By modifying the electrodes with other carbon nanomaterials or permselective membranes, the performance can be substantially improved. Moreover, by combining the advantageous properties of carbon-based electrodes with Nafion membranes, we can improve selectivity in electrochemical detection beyond what is possible with single modifications alone. With this multilayer electrode, simultaneous detection of morphine and codeine was achieved in the presence of large excess of AA and UA, as well as in human plasma without protein precipitation or substantial dilution. We also show a mass production compatible fabrication process for a Nafion coated SWCNT test strip. This test strip is capable of quantitative determination of paracetamol in protein containing whole blood samples in less than 5 min. The results of this thesis further suggest that the Nafion coated electrodes are measuring the clinically relevant unbound fraction of drugs.

While the work of this thesis and other studies have made significant progress in developing highly selective and sensitive electrochemical sensors for determining drugs in complex matrices, more work is required to further improve the performance, especially in unprocessed blood samples. More work should also focus on attempting to realize sensors that can simultaneously achieve sufficient sensitivity, selectivity, fouling resistance and repeatability in some clinical application. In many cases, optimizing the sensor performance in only one of these aspects, usually the sensitivity, can compromise the overall performance of the sensor.

To realize such sensors, further studies on the matrix effects observed in complex biological matrices are needed. Studies with a wider range of active pharmaceutical ingredients is also highly encouraged. Moreover, the potential interferences from metabolites also need to be considered and studied. Such studies could lead to an improved understanding of the observed matrix effects in complex biological samples and enable the determination of personal metabolic profiles.

Due to the potential interference from almost an unlimited number of biomolecules, active pharmaceutical ingredients, drugs of abuse (including designer drugs) as well as their metabolites, studies with a wider range of potential interferents are required. Moreover, studies that simply spike biological samples with target analytes are not good enough to show selectivity in a clinical application. Unfortunately, studying the potential interference from all these sources is prohibitively expensive. Therefore, further interdisciplinary research involving nanomaterials synthesis and characterization, along with application oriented sensor development in close collaboration with the end user community, is highly encouraged. Such collaboration enables real patient samples to be studied early on in the sensor development and most importantly, the sensor may be validated with real clinical patient samples, by parallel studies using gold standard analysis techniques.

References

(1) Kendall, J.; Reeves, B.; Clancy, M. Point of Care Testing: Randomised Controlled Trial of Clinical Outcome. *BMJ* **1998**, *316* (7137), 1052–1057. https://doi.org/10.1136/bmj.316.7137.1052.

(2) Wiffen, P. J.; Wee, B.; Derry, S.; Bell, R. F.; Moore, R. A. Opioids for Cancer Pain - an Overview of Cochrane Reviews. *Cochrane Database Syst. Rev.* **2017**, *2017* (7). https://doi.org/10.1002/14651858.CD012592.pub2.

(3) Pyati, S.; Gan, T. J. Perioperative Pain Management. *CNS Drugs* **2007**, *21* (3), 185–211. https://doi.org/10.2165/00023210-200721030-00002.

(4) Phillips, C. J. The Cost and Burden of Chronic Pain. *Rev. Pain* **2009**, *3* (1), 2–5. https://doi.org/10.1177/204946370900300102.

(5) Nafziger, A. N.; Bertino, J. S. Utility and Application of Urine Drug Testing in Chronic Pain Management with Opioids. *Clinical Journal of Pain*. 2009. https://doi.org/10.1097/AJP.0b013e31817e13cc.

(6) Kirchheiner, J.; Schmidt, H.; Tzvetkov, M.; Keulen, J.-T.; Lötsch, J.; Roots, I.; Brockmöller, J. Pharmacokinetics of Codeine and Its Metabolite Morphine in Ultra-Rapid Metabolizers Due to CYP2D6 Duplication. *Pharmacogenomics J.* **2007**, *7* (4), 257–265. https://doi.org/10.1038/sj.tpj.6500406.

(7) Schug, S. A.; Sidebotham, D. A.; McGuinnety, M.; Thomas, J.; Fox, L. Acetaminophen as an Adjunct to Morphine by Patient-Controlled Analgesia in the Management of Acute Postoperative Pain. *Anesth. Analg.* **1998**, *87* (2), 368–372. https://doi.org/10.1097/00000539-199808000-00024.

(8) Scholl, L.; Seth, P.; Kariisa, M.; Wilson, N.; Baldwin, G. Drug and Opioid-Involved Overdose Deaths — United States, 2013–2017. *MMWR. Morb. Mortal. Wkly. Rep.* **2018**. https://doi.org/10.15585/mmwr.mm675152e1.

(9) Tittarelli, R.; Pellegrini, M.; Scarpellini, M. G.; Marinelli, E.; Bruti, V.; Di Luca, N. M.; Busardò, F. P.; Zaami, S. Hepatotoxicity of Paracetamol and Related Fatalities. *Eur. Rev. Med. Pharmacol. Sci.* **2017**, *21* (1), 95–101.

(10) Larson, A. M.; Polson, J.; Fontana, R. J.; Davern, T. J.; Lalani, E.; Hynan, L. S.; Reisch, J. S.; Schiødt, F. V.; Ostapowicz, G.; Shakil, A. O.; et al. Acetaminophen-Induced Acute Liver Failure: Results of a United States Multicenter, Prospective Study. *Hepatology* **2005**, *42* (6), 1364–1372. https://doi.org/10.1002/hep.20948.

(11) Wu, A. H. B. National Academy of Clinical Biochemistry Laboratory Medicine Practice Guidelines: Recommendations for the Use of Laboratory Tests to Support Poisoned Patients Who Present to the Emergency Department. *Clin. Chem.* **2003**, *49* (3), 357–379. https://doi.org/10.1373/49.3.357.

(12) Polson, J.; Wians, F. H.; Orsulak, P.; Fuller, D.; Murray, N. G.; Koff, J. M.; Khan, A. I.; Balko, J. A.; Hynan, L. S.; Lee, W. M. False Positive Acetaminophen Concentrations in Patients with Liver Injury. *Clin. Chim. Acta* **2008**, *391* (1–2), 24–30. https://doi.org/10.1016/j.cca.2008.01.018.

(13) Meany, D.; Schowinsky, J.; Clarke, W. Effects of Hemolysis and Lipemia on the COBAS® Salicylate and Acetaminophen Assays Compared to GDS Assays. *Clin. Biochem.* **2008**, *41* (18), 1486–1488. https://doi.org/10.1016/j.clinbiochem.2008.09.111.

(14) Dale, C.; Aulaqi, A. A. M.; Baker, J.; Hobbs, R. C.; Tan, M. E. L.; Tovey, C.; Walker, I. A. L.; Henry, J. A. Assessment of a Point-of-Care Test for Paracetamol and Salicylate in Blood. *QJM - Mon. J. Assoc. Physicians* **2005**, *98* (2), 113–118. https://doi.org/10.1093/qjmed/hci016.

(15) Milone, M. C. Laboratory Testing for Prescription Opioids. *J. Med. Toxicol.* **2012**, *8* (4), 408–416. https://doi.org/10.1007/s13181-012-0274-7.

(16) Mynttinen, E.; Wester, N.; Lilius, T.; Kalso, E.; Koskinen, J.; Laurila, T. Simultaneous Electrochemical Detection of Tramadol and O-Desmethyltramadol with Nafion-Coated Tetrahedral Amorphous Carbon Electrode. *Electrochim. Acta* **2019**, *295*, 347–353. https://doi.org/10.1016/j.electacta.2018.10.148.
(17) Chen, J.-C.; Chung, H.-H.; Hsu, C.-T.; Tsai, D.-M.; Kumar, A. S.; Zen, J.-M. A Disposable Single-Use Electrochemical Sensor for the Detection of Uric Acid in Human Whole Blood. *Sensors Actuators B Chem.* **2005**, *110* (2), 364–369. https://doi.org/10.1016/j.snb.2005.02.026.
(18) Van Gompel, J. J.; Chang, S.-Y.; Goerss, S. J.; Kim, I. Y.; Kimble, C.; Bennet, K. E.; Lee, K. H. Development of Intraoperative Electrochemical Detection: Wireless Instantaneous Neurochemical Concentration Sensor for Deep Brain Stimulation Feedback. *Neurosurg. Focus* **2010**, *29* (2), E6. https://doi.org/10.3171/2010.5.FOCUS10110.
(19) Robinson, D. L.; Venton, B. J.; Heien, M. L. A. V.; Wightman, R. M. Detecting Subsecond Dopamine Release with Fast-Scan Cyclic Voltammetry in Vivo. *Clin. Chem.* **2003**, *49* (10), 1763–1773. https://doi.org/10.1373/49.10.1763.
(20) Yang, Y.; Song, Y.; Bo, X.; Min, J.; Pak, O. S.; Zhu, L.; Wang, M.; Tu, J.; Kogan, A.; Zhang, H.; et al. A Laser-Engraved Wearable Sensor for Sensitive Detection of Uric Acid and Tyrosine in Sweat. *Nat. Biotechnol.* **2020**, *38* (2), 217–224. https://doi.org/10.1038/s41587-019-0321-x.
(21) Windmiller, J. R.; Wang, J. Wearable Electrochemical Sensors and Biosensors: A Review. *Electroanalysis* **2013**, *25* (1), 29–46. https://doi.org/10.1002/elan.201200349.
(22) Olabode, O.; Kosunen, M.; Unnikrishnan, V.; Palomaki, T.; Laurila, T.; Halonen, K.; Ryynanen, J. Time-Based Sensor Interface for Dopamine Detection. *IEEE Trans. Circuits Syst. I Regul. Pap.* **2020**, 1–13. https://doi.org/10.1109/TCSI.2020.3008363.
(23) Robinson, D. L.; Hermans, A.; Seipel, A. T.; Wightman, R. M. Monitoring Rapid Chemical Communication in the Brain. *Chem. Rev.* **2008**, *108* (7), 2554–2584. https://doi.org/10.1021/cr068081q.
(24) Shukla, R. P.; Ben-Yoav, H. A Chitosan–Carbon Nanotube-Modified Microelectrode for In Situ Detection of Blood Levels of the Antipsychotic Clozapine in a Finger-Pricked Sample Volume. *Adv. Healthc. Mater.* **2019**, *8* (15), 1900462. https://doi.org/10.1002/adhm.201900462.
(25) Kim, J.; de Araujo, W. R.; Samek, I. A.; Bandodkar, A. J.; Jia, W.; Brunetti, B.; Paixão, T. R. L. C.; Wang, J. Wearable Temporary Tattoo Sensor for Real-Time Trace Metal Monitoring in Human Sweat. *Electrochem. commun.* **2015**, *51*, 41–45. https://doi.org/10.1016/j.elecom.2014.11.024.
(26) Zhu, X.; Ju, Y.; Chen, J.; Liu, D.; Liu, H. Nonenzymatic Wearable Sensor for Electrochemical Analysis of Perspiration Glucose. *ACS Sensors* **2018**, *3* (6), 1135–1141. https://doi.org/10.1021/acssensors.8b00168.
(27) Rana, A.; Baig, N.; Saleh, T. A. Electrochemically Pretreated Carbon Electrodes and Their Electroanalytical Applications – A Review. *J. Electroanal. Chem.* **2019**, *833* (November 2018), 313–332. https://doi.org/10.1016/j.jelechem.2018.12.019.
(28) McCreery, R. L. Advanced Carbon Electrode Materials for Molecular Electrochemistry. *Chem. Rev.* **2008**, *108* (7), 2646–2687. https://doi.org/10.1021/cr068076m.
(29) Hanssen, B. L.; Siraj, S.; Wong, D. K. Y. Recent Strategies to Minimise Fouling in Electrochemical Detection Systems. *Rev. Anal. Chem.* **2016**, *35* (1), 1–28. https://doi.org/10.1515/revac-2015-0008.
(30) Jadon, N.; Jain, R.; Sharma, S.; Singh, K. Recent Trends in Electrochemical Sensors for Multianalyte Detection – A Review. *Talanta* **2016**, *161* (September), 894–916. https://doi.org/10.1016/j.talanta.2016.08.084.
(31) Wisniewski, N.; Reichert, M. Methods for Reducing Biosensor Membrane Biofouling. *Colloids Surfaces B Biointerfaces* **2000**, *18* (3–4), 197–219. https://doi.org/10.1016/S0927-7765(99)00148-4.
(32) Anisimov, A. S.; Brown, D. P.; Mikladal, B. F.; Súilleabháin, L. Ó.; Parikh, K.; Soininen,

E.; Sonninen, M.; Tian, D.; Varjos, I.; Vuohelainen, R. Printed Touch Sensors Using Carbon NanoBud Material. *Inf. Disp. (1975).* **2014**, *30* (4), 16–22. https://doi.org/10.1002/j.2637-496X.2014.tb00731.x.

(33) Sanghavi, B. J.; Wolfbeis, O. S.; Hirsch, T.; Swami, N. S. Nanomaterial-Based Electrochemical Sensing of Neurological Drugs and Neurotransmitters. *Microchim. Acta* **2015**, *182* (1–2), 1–41. https://doi.org/10.1007/s00604-014-1308-4.

(34) Palomäki, T.; Wester, N.; Caro, M. A.; Sainio, S.; Protopopova, V.; Koskinen, J.; Laurila, T. Electron Transport Determines the Electrochemical Properties of Tetrahedral Amorphous Carbon (Ta-C) Thin Films. *Electrochim. Acta* **2017**, *225*. https://doi.org/10.1016/j.electacta.2016.12.099.

(35) Protopopova, V. S.; Wester, N.; Caro, M. A.; Gabdullin, P. G.; Palomäki, T.; Laurila, T.; Koskinen, J. Ultrathin Undoped Tetrahedral Amorphous Carbon Films: Thickness Dependence of the Electronic Structure and Implications for Their Electrochemical Behaviour. *Phys. Chem. Chem. Phys.* **2015**, *17* (14). https://doi.org/10.1039/c4cp05855k.

(36) Protopopova, V.; Iyer, A.; Wester, N.; Kondrateva, A.; Sainio, S.; Palomäki, T.; Laurila, T.; Mishin, M.; Koskinen, J. Ultrathin Undoped Tetrahedral Amorphous Carbon Films: The Role of the Underlying Titanium Layer on the Electronic Structure. *Diam. Relat. Mater.* **2015**, *57*. https://doi.org/10.1016/j.diamond.2015.06.009.

(37) Peltola, E.; Wester, N.; Holt, K. B.; Johansson, L.-S.; Koskinen, J.; Myllymäki, V.; Laurila, T. Nanodiamonds on Tetrahedral Amorphous Carbon Significantly Enhance Dopamine Detection and Cell Viability. *Biosens. Bioelectron.* **2017**, *88*. https://doi.org/10.1016/j.bios.2016.08.055.

(38) Durairaj, V.; Wester, N.; Etula, J.; Laurila, T.; Lehtonen, J.; Rojas, O. J.; Pahimanolis, N.; Koskinen, J. Multiwalled Carbon Nanotubes/Nanofibrillar Cellulose/Nafion Composite-Modified Tetrahedral Amorphous Carbon Electrodes for Selective Dopamine Detection. *J. Phys. Chem. C* **2019**, *123* (40), 24826–24836. https://doi.org/10.1021/acs.jpcc.9b05537.

(39) Elgrishi, N.; Rountree, K. J.; McCarthy, B. D.; Rountree, E. S.; Eisenhart, T. T.; Dempsey, J. L. A Practical Beginner's Guide to Cyclic Voltammetry. *J. Chem. Educ.* **2018**, *95* (2), 197–206. https://doi.org/10.1021/acs.jchemed.7b00361.

(40) Zeng, A.; Neto, V. F.; Gracio, J. J.; Fan, Q. H. Diamond-like Carbon (DLC) Films as Electrochemical Electrodes. *Diam. Relat. Mater.* **2014**, *43*, 12–22. https://doi.org/10.1016/j.diamond.2014.01.003.

(41) Laurila, T.; Protopopova, V.; Rhode, S.; Sainio, S.; Palomäki, T.; Moram, M.; Feliu, J. M.; Koskinen, J. New Electrochemically Improved Tetrahedral Amorphous Carbon Films for Biological Applications. *Diam. Relat. Mater.* **2014**, *49*, 62–71. https://doi.org/10.1016/j.diamond.2014.08.007.

(42) Allen J. Bard, L. R. F. *Electrochemical Methods: Fundamentals and Applications*, 2nd Editio.; New York (N.Y.), 2001.

(43) Matsuda, H.; Ayabe, Y. Zur Theorie Der Randles-Sevčikschen Kathodenstrahl-Polarographie. *Zeitschrift für Elektrochemie, Berichte der Bunsengesellschaft für Phys. Chemie* **1955**. https://doi.org/10.1002/BBPC.19550590605.

(44) Nicholson, R. S. Theory and Application of Cyclic Voltammetry for Measurement of Electrode Reaction Kinetics. *Anal. Chem.* **1965**, *37* (11), 1351–1355. https://doi.org/10.1021/ac60230a016.

(45) Bertoncello, P.; Edgeworth, J. P.; Macpherson, J. V.; Unwin, P. R. Trace Level Cyclic Voltammetry Facilitated by Single-Walled Carbon Nanotube Network Electrodes. *J. Am. Chem. Soc.* **2007**, *129* (36), 10982–10983. https://doi.org/10.1021/ja073360w.

(46) ICH. ICH Topic Q2 (R1) Validation of Analytical Procedures : Text and Methodology. *Int. Conf. Harmon.* **2005**.

(47) Palomäki, T.; Peltola, E.; Sainio, S.; Wester, N.; Pitkänen, O.; Kordas, K.; Koskinen, J.; Laurila, T. Unmodified and Multi-Walled Carbon Nanotube Modified Tetrahedral Amorphous Carbon (Ta-C) Films as in Vivo Sensor Materials for Sensitive and Selective Detection of Dopamine. *Biosens. Bioelectron.* **2018**, *118* (April), 23–30.

https://doi.org/10.1016/j.bios.2018.07.018.
(48) Chen, P.; McCreery, R. L. Control of Electron Transfer Kinetics at Glassy Carbon Electrodes by Specific Surface Modification. *Anal. Chem.* **1996**, *68* (22), 3958–3965. https://doi.org/10.1021/ac960492r.
(49) Cuharuc, A. S.; Zhang, G.; Unwin, P. R. Electrochemistry of Ferrocene Derivatives on Highly Oriented Pyrolytic Graphite (HOPG): Quantification and Impacts of Surface Adsorption. *Phys. Chem. Chem. Phys.* **2016**, *18* (6), 4966–4977. https://doi.org/10.1039/C5CP06325F.
(50) Peter, L. M.; Dürr, W.; Bindra, P.; Gerischer, H. The Influence of Alkali Metal Cations on the Rate of the Fe(CN)64-/Fe(CN)63- Electrode Process. *J. Electroanal. Chem.* **1976**. https://doi.org/10.1016/S0022-0728(76)80288-4.
(51) Khoshtariya, D. E.; Dolidze, T. D.; Krulic, D.; Fatouros, N.; Devilliers, D. Solvent Friction Mechanism of an Elementary Charge-Transfer Step and Cation-Regulated Preequilibrium for a Pt/Fe(CN) 6 4-/3- Electrode Process. *J. Phys. Chem. B* **1998**, *102* (40), 7800–7806. https://doi.org/10.1021/jp981064n.
(52) Jarošová, R.; De Sousa Bezerra, P. M.; Munson, C.; Swain, G. M. Assessment of Heterogeneous Electron-Transfer Rate Constants for Soluble Redox Analytes at Tetrahedral Amorphous Carbon, Boron-Doped Diamond, and Glassy Carbon Electrodes. *Phys. status solidi* **2016**, *213* (8), 2087–2098. https://doi.org/10.1002/pssa.201600339.
(53) Hsu, C. H.; Mansfeld, F. Technical Note : Concerning the Conversion of the Constant Phase Element Parameter Yo into a Capacitance. *CORROSION* **2001**.
(54) Compton, R. G.; Banks, C. E. *Understanding Voltammetry*; 2007. https://doi.org/10.1142/6430.
(55) Wagl~er, 16 C D; Riggs, W. M.; Davis, L. E.; Moulder, J. F.; Muilenberg, G. E. "Handbook of X-Ray Photo- Electron Spectroscopy. *J. Electroanal. Chem. J. Electroanal. Chem. J. Catal. Electrochim. Acta Bull. Chem. Soc. Jpn. Inorg. Chem.Fuel Cells Their Electrochem. Dokl. Akad. Nauk SSSR* **1973**.
(56) Lee, S.-J.; Titus, C. J.; Alonso Mori, R.; Baker, M. L.; Bennett, D. A.; Cho, H.-M.; Doriese, W. B.; Fowler, J. W.; Gaffney, K. J.; Gallo, A.; et al. Soft X-Ray Spectroscopy with Transition-Edge Sensors at Stanford Synchrotron Radiation Lightsource Beamline 10-1. *Rev. Sci. Instrum.* **2019**, *90* (11), 113101. https://doi.org/10.1063/1.5119155.
(57) Frazer, B. H.; Gilbert, B.; Sonderegger, B. R.; De Stasio, G. The Probing Depth of Total Electron Yield in the Sub-KeV Range: TEY-XAS and X-PEEM. *Surf. Sci.* **2003**, *537* (1–3), 161–167. https://doi.org/10.1016/S0039-6028(03)00613-7.
(58) Briggs, D. Handbook of X-Ray Photoelectron Spectroscopy C. D. Wanger, W. M. Riggs, L. E. Davis, J. F. Moulder and G. E.Muilenberg Perkin-Elmer Corp., Physical Electronics Division, Eden Prairie, Minnesota, USA, 1979. 190 Pp. $195. *Surf. Interface Anal.* **1981**, *3* (4), v–v. https://doi.org/10.1002/sia.740030412.
(59) Shard, A. G. Detection Limits in XPS for More than 6000 Binary Systems Using Al and Mg Kα X-Rays. *Surf. Interface Anal.* **2014**, *46* (3), 175–185. https://doi.org/10.1002/sia.5406.
(60) Johansson, L.; Campbell, J. M.; Rojas, O. J. Cellulose as the in Situ Reference for Organic XPS. Why? Because It Works. *Surf. Interface Anal.* **2020**, No. December 2019, sia.6759. https://doi.org/10.1002/sia.6759.
(61) Tougaard, S. Surface Nanostructure Determination by X-ray Photoemission Spectroscopy Peak Shape Analysis. *J. Vac. Sci. Technol. A Vacuum, Surfaces, Film.* **1996**, *14* (3), 1415–1423. https://doi.org/10.1116/1.579963.
(62) Stöhr, J. *NEXAFS Spectroscopy*; Springer Series in Surface Sciences; Springer Berlin Heidelberg: Berlin, Heidelberg, 1992; Vol. 25. https://doi.org/10.1007/978-3-662-02853-7.
(63) Brühwiler, P. A.; Maxwell, A. J.; Puglia, C.; Nilsson, A.; Andersson, S.; Mårtensson, N. C. *Phys. Rev. Lett.* **1995**, *74* (4), 614–617. https://doi.org/10.1103/PhysRevLett.74.614.

(64) Watts, B.; Ade, H. A Simple Method for Determining Linear Polarization and Energy Calibration of Focused Soft X-Ray Beams. *J. Electron Spectros. Relat. Phenomena* **2008**, *162* (2), 49–55. https://doi.org/10.1016/j.elspec.2007.08.008.
(65) Batson, P. E. Carbon 1 s Near-Edge-Absorption Fine Structure in Graphite. *Phys. Rev. B* **1993**, *48* (4), 2608–2610. https://doi.org/10.1103/PhysRevB.48.2608.
(66) Ma, Y.; Skytt, P.; Wassdahl, N.; Glans, P.; Guo, J.; Nordgren, J. Core Excitons and Vibronic Coupling in Diamond and Graphite. *Phys. Rev. Lett.* **1993**, *71* (22), 3725–3728. https://doi.org/10.1103/PhysRevLett.71.3725.
(67) Solomon, D.; Lehmann, J.; Kinyangi, J.; Liang, B.; Heymann, K.; Dathe, L.; Hanley, K.; Wirick, S.; Jacobsen, C. Carbon (1s) NEXAFS Spectroscopy of Biogeochemically Relevant Reference Organic Compounds. *Soil Sci. Soc. Am. J.* **2009**, *73* (6), 1817–1830. https://doi.org/10.2136/sssaj2008.0228.
(68) Dennis, R. V.; Schultz, B. J.; Jaye, C.; Wang, X.; Fischer, D. A.; Cartwright, A. N.; Banerjee, S. Near-Edge x-Ray Absorption Fine Structure Spectroscopy Study of Nitrogen Incorporation in Chemically Reduced Graphene Oxide. *J. Vac. Sci. Technol. B, Nanotechnol. Microelectron. Mater. Process. Meas. Phenom.* **2013**, *31* (4), 041204. https://doi.org/10.1116/1.4813058.
(69) Schiros, T.; Nordlund, D.; Pálová, L.; Prezzi, D.; Zhao, L.; Kim, K. S.; Wurstbauer, U.; Gutiérrez, C.; Delongchamp, D.; Jaye, C.; et al. Connecting Dopant Bond Type with Electronic Structure in N-Doped Graphene. *Nano Lett.* **2012**, *12* (8), 4025–4031. https://doi.org/10.1021/nl301409h.
(70) Jiménez, I.; Tong, W. M.; Shuh, D. K.; Holloway, B. C.; Kelly, M. A.; Pianetta, P.; Terminello, L. J.; Himpsel, F. J. Bonding Modifications in Carbon Nitride Films Induced by Thermal Annealing: An x-Ray Absorption near Edge Study. *Appl. Phys. Lett.* **1999**, *74* (18), 2620–2622. https://doi.org/10.1063/1.123916.
(71) Jiménez, I.; Gago, R.; Albella, J. M.; Cáceres, D.; Vergara, I. Spectroscopy of π Bonding in Hard Graphitic Carbon Nitride Films: Superstructure of Basal Planes and Hardening Mechanisms. *Phys. Rev. B* **2000**, *62* (7), 4261–4264. https://doi.org/10.1103/PhysRevB.62.4261.
(72) Iyer, A.; Kaskela, A.; Johansson, L.-S.; Liu, X.; Kauppinen, E. I.; Koskinen, J. Single Walled Carbon Nanotube Network—Tetrahedral Amorphous Carbon Composite Film. *J. Appl. Phys.* **2015**, *117* (22), 225302. https://doi.org/10.1063/1.4922242.
(73) Sainio, S.; Nordlund, D.; Caro, M. A.; Gandhiraman, R.; Koehne, J.; Wester, N.; Koskinen, J.; Meyyappan, M.; Laurila, T. Correlation between Sp 3 -to-Sp 2 Ratio and Surface Oxygen Functionalities in Tetrahedral Amorphous Carbon (Ta-C) Thin Film Electrodes and Implications of Their Electrochemical Properties. *J. Phys. Chem. C* **2016**, *120* (15), 8298–8304. https://doi.org/10.1021/acs.jpcc.6b02342.
(74) BEARDEN, J. A. X-Ray Wavelengths. *Rev. Mod. Phys.* **1967**, *39* (1), 78–124. https://doi.org/10.1103/RevModPhys.39.78.
(75) Ţucureanu, V.; Matei, A.; Avram, A. M. FTIR Spectroscopy for Carbon Family Study. *Crit. Rev. Anal. Chem.* **2016**, *46* (6), 502–520. https://doi.org/10.1080/10408347.2016.1157013.
(76) Tobias, G.; Shao, L.; Salzmann, C. G.; Huh, Y.; Green, M. L. H. Purification and Opening of Carbon Nanotubes Using Steam. *J. Phys. Chem. B* **2006**, *110* (45), 22318–22322. https://doi.org/10.1021/jp0631883.
(77) Dresselhaus, M. S.; Dresselhaus, G.; Saito, R.; Jorio, A. Raman Spectroscopy of Carbon Nanotubes. *Phys. Rep.* **2005**, *409* (2), 47–99. https://doi.org/10.1016/j.physrep.2004.10.006.
(78) Jorio, A.; Saito, R.; Dresselhaus, G.; Dresselhaus, M. S. Determination of Nanotubes Properties by Raman Spectroscopy. *Philos. Trans. R. Soc. A Math. Phys. Eng. Sci.* **2004**, *362* (1824), 2311–2336. https://doi.org/10.1098/rsta.2004.1443.
(79) Tian, Y.; Jiang, H.; Laiho, P.; Kauppinen, E. I. Validity of Measuring Metallic and Semiconducting Single-Walled Carbon Nanotube Fractions by Quantitative Raman Spectroscopy. *Anal. Chem.* **2018**, *90* (4), 2517–2525. https://doi.org/10.1021/acs.analchem.7b03712.

(80) Jorio, A.; Pimenta, M. A.; Filho, A. G. S.; Saito, R.; Dresselhaus, G.; Dresselhaus, M. S. Characterizing Carbon Nanotube Samples with Resonance Raman Scattering. *New J. Phys.* **2003**, *5*, 139–139. https://doi.org/10.1088/1367-2630/5/1/139.
(81) Rao, A. M.; Eklund, P. C.; Bandow, S.; Thess, A.; Smalley, R. E. Evidence for Charge Transfer in Doped Carbon Nanotube Bundles from Raman Scattering. *Nature* **1997**, *388* (6639), 257–259. https://doi.org/10.1038/40827.
(82) Kaskela, A.; Nasibulin, A. G.; Timmermans, M. Y.; Aitchison, B.; Papadimitratos, A.; Tian, Y.; Zhu, Z.; Jiang, H.; Brown, D. P.; Zakhidov, A.; et al. Aerosol-Synthesized SWCNT Networks with Tunable Conductivity and Transparency by a Dry Transfer Technique. *Nano Lett.* **2010**, *10* (11), 4349–4355. https://doi.org/10.1021/nl101680s.
(83) Ferrari, A. C.; Robertson, J. Interpretation of Raman Spectra of Disordered and Amorphous Carbon. *Phys. Rev. B* **2000**, *61* (20), 14095–14107. https://doi.org/10.1103/PhysRevB.61.14095.
(84) Davis, C. A.; Amaratunga, G. A. J.; Knowles, K. M. Growth Mechanism and Cross-Sectional Structure of Tetrahedral Amorphous Carbon Thin Films. **1998**, 13–16.
(85) LiBassi, A.; Ferrari, A. C.; Stolojan, V.; Tanner, B. K.; Robertson, J.; Brown, L. M. Density, Sp 3 Content and Internal Layering of DLC Films by X-Ray Reflectivity and Electron Energy Loss Spectroscopy. *Diam. Relat. Mater.* **2000**, *9* (3–6), 771–776. https://doi.org/10.1016/S0925-9635(99)00233-2.
(86) McCann, R.; Roy, S. S.; Papakonstantinou, P.; Abbas, G.; McLaughlin, J. A. The Effect of Thickness and Arc Current on the Structural Properties of FCVA Synthesised Ta-C and Ta-C:N Films. *Diam. Relat. Mater.* **2005**, *14* (3–7), 983–988. https://doi.org/10.1016/j.diamond.2004.12.037.
(87) Robertson, J. Diamond-like Amorphous Carbon. *Mater. Sci. Eng. R Reports* **2002**, *37* (4–6), 129–281. https://doi.org/10.1016/S0927-796X(02)00005-0.
(88) Weisman, R. B.; Bachilo, S. M. Dependence of Optical Transition Energies on Structure for Single-Walled Carbon Nanotubes in Aqueous Suspension: An Empirical Kataura Plot. *Nano Lett.* **2003**, *3* (9), 1235–1238. https://doi.org/10.1021/nl034428i.
(89) Miyata, Y.; Yanagi, K.; Maniwa, Y.; Kataura, H. Optical Evaluation of the Metal-to-Semiconductor Ratio of Single-Wall Carbon Nanotubes. *J. Phys. Chem. C* **2008**, *112* (34), 13187–13191. https://doi.org/10.1021/jp804006f.
(90) Bekyarova, E.; Itkis, M. E.; Cabrera, N.; Zhao, B.; Yu, A.; Gao, J.; Haddon, R. C. Electronic Properties of Single-Walled Carbon Nanotube Networks. *J. Am. Chem. Soc.* **2005**, *127* (16), 5990–5995. https://doi.org/10.1021/ja043153l.
(91) Itkis, M. E.; Perea, D. E.; Niyogi, S.; Rickard, S. M.; Hamon, M. A.; Hu, H.; Zhao, B.; Haddon, R. C. Purity Evaluation of As-Prepared Single-Walled Carbon Nanotube Soot by Use of Solution-Phase Near-IR Spectroscopy. *Nano Lett.* **2003**, *3* (3), 309–314. https://doi.org/10.1021/nl025926e.
(92) Landi, B. J.; Ruf, H. J.; Evans, C. M.; Cress, C. D.; Raffaelle, R. P. Purity Assessment of Single-Wall Carbon Nanotubes, Using Optical Absorption Spectroscopy. *J. Phys. Chem. B* **2005**, *109* (20), 9952–9965. https://doi.org/10.1021/jp044990c.
(93) Williams, D. B.; Carter, C. B. *Transmission Electron Microscopy*; Springer US: Boston, MA, 2009. https://doi.org/10.1007/978-0-387-76501-3.
(94) Mccreery, R. L. Advanced Carbon Electrode Materials for Molecular Electrochemistry. **2008**, 2646–2687.
(95) Palomäki, T.; Caro, M. A.; Wester, N.; Sainio, S.; Etula, J.; Johansson, L.; Han, J. G.; Koskinen, J.; Laurila, T. Effect of Power Density on the Electrochemical Properties of Undoped Amorphous Carbon (A-C) Thin Films. *Electroanalysis* **2019**, *31* (4), 746–755. https://doi.org/10.1002/elan.201800738.
(96) Palomäki, T.; Chumillas, S.; Sainio, S.; Protopopova, V.; Kauppila, M.; Koskinen, J.; Climent, V.; Feliu, J. M.; Laurila, T. Electrochemical Reactions of Catechol, Methylcatechol and Dopamine at Tetrahedral Amorphous Carbon (Ta-C) Thin Film Electrodes. *Diam. Relat. Mater.* **2015**, *59*, 30–39. https://doi.org/10.1016/j.diamond.2015.09.003.
(97) Brocenschi, R. F.; Rocha-Filho, R. C.; Li, L.; Swain, G. M. Comparative

Electrochemical Response of Estrone at Glassy-Carbon, Nitrogen-Containing Tetrahedral Amorphous Carbon and Boron-Doped Diamond Thin-Film Electrodes. *J. Electroanal. Chem.* **2014**, *712*, 207–214. https://doi.org/10.1016/j.jelechem.2013.11.014.
(98) Davies, T. J.; Hyde, M. E.; Compton, R. G. Nanotrench Arrays Reveal Insight into Graphite Electrochemistry. *Angew. Chemie Int. Ed.* **2005**, *44* (32), 5121–5126. https://doi.org/10.1002/anie.200462750.
(99) Davies, T. J.; Moore, R. R.; Banks, C. E.; Compton, R. G. The Cyclic Voltammetric Response of Electrochemically Heterogeneous Surfaces. *J. Electroanal. Chem.* **2004**, *574* (1), 123–152. https://doi.org/10.1016/j.jelechem.2004.07.031.
(100) Ambrosi, A.; Pumera, M. Nanographite Impurities Dominate Electrochemistry of Carbon Nanotubes. *Chem. - A Eur. J.* **2010**, *16* (36), 10946–10949. https://doi.org/10.1002/chem.201001584.
(101) Kneten, K. R.; McCreery, R. L. Effects of Redox System Structure on Electron-Transfer Kinetics at Ordered Graphite and Glassy Carbon Electrodes. *Anal. Chem.* **1992**, *64* (21), 2518–2524. https://doi.org/10.1021/ac00045a011.
(102) Bowling, R. J.; Packard, R. T.; McCreery, R. L. Activation of Highly Ordered Pyrolytic Graphite for Heterogeneous Electron Transfer: Relationship between Electrochemical Performance and Carbon Microstructure. *J. Am. Chem. Soc.* **1989**, *111* (4), 1217–1223. https://doi.org/10.1021/ja00186a008.
(103) Velický, M.; Toth, P. S.; Woods, C. R.; Novoselov, K. S.; Dryfe, R. A. W. Electrochemistry of the Basal Plane versus Edge Plane of Graphite Revisited. *J. Phys. Chem. C* **2019**, *123* (18), 11677–11685. https://doi.org/10.1021/acs.jpcc.9b01010.
(104) Yuan, W.; Zhou, Y.; Li, Y.; Li, C.; Peng, H.; Zhang, J.; Liu, Z.; Dai, L.; Shi, G. The Edge- and Basal-Plane-Specific Electrochemistry of a Single-Layer Graphene Sheet. *Sci. Rep.* **2013**, *3* (1), 2248. https://doi.org/10.1038/srep02248.
(105) Patel, A. N.; Tan, S. Y.; Miller, T. S.; MacPherson, J. V.; Unwin, P. R. Comparison and Reappraisal of Carbon Electrodes for the Voltammetric Detection of Dopamine. *Anal. Chem.* **2013**, *85* (24), 11755–11764. https://doi.org/10.1021/ac401969q.
(106) Patel, A. N.; McKelvey, K.; Unwin, P. R. Nanoscale Electrochemical Patterning Reveals the Active Sites for Catechol Oxidation at Graphite Surfaces. *J. Am. Chem. Soc.* **2012**, *134* (50), 20246–20249. https://doi.org/10.1021/ja3095894.
(107) Patel, A. N.; Tan, S. Y.; Unwin, P. R. Epinephrine Electro-Oxidation Highlights Fast Electrochemistry at the Graphite Basal Surface. *Chem. Commun.* **2013**, *49* (78), 8776–8778. https://doi.org/10.1039/c3cc45022h.
(108) Lai, S. C. S.; Patel, A. N.; McKelvey, K.; Unwin, P. R. Definitive Evidence for Fast Electron Transfer at Pristine Basal Plane Graphite from High-Resolution Electrochemical Imaging. *Angew. Chemie Int. Ed.* **2012**, *51* (22), 5405–5408. https://doi.org/10.1002/anie.201200564.
(109) Zhai, C.; Ma, H.; Sun, F.; Li, L.; Song, A. Experimental and Theoretical Study on the Interaction of Dopamine Hydrochloride with H2O. *J. Mol. Liq.* **2016**, *215*, 481–485. https://doi.org/10.1016/j.molliq.2016.01.043.
(110) Gao, F.; Cai, X.; Wang, X.; Gao, C.; Liu, S.; Gao, F.; Wang, Q. Highly Sensitive and Selective Detection of Dopamine in the Presence of Ascorbic Acid at Graphene Oxide Modified Electrode. *Sensors Actuators, B Chem.* **2013**, *186*, 380–387. https://doi.org/10.1016/j.snb.2013.06.020.
(111) Yang, L.; Liu, D.; Huang, J.; You, T. Simultaneous Determination of Dopamine, Ascorbic Acid and Uric Acid at Electrochemically Reduced Graphene Oxide Modified Electrode. *Sensors Actuators B Chem.* **2014**, *193*, 166–172. https://doi.org/10.1016/j.snb.2013.11.104.
(112) Wang, Y.; Li, Y.; Tang, L.; Lu, J.; Li, J. Application of Graphene-Modified Electrode for Selective Detection of Dopamine. *Electrochem. commun.* **2009**, *11* (4), 889–892. https://doi.org/10.1016/j.elecom.2009.02.013.
(113) Ji, X.; Banks, C. E.; Crossley, A.; Compton, R. G. Oxygenated Edge Plane Sites Slow the Electron Transfer of the Ferro-/Ferricyanide Redox Couple at Graphite Electrodes.

ChemPhysChem **2006**, *7* (6), 1337–1344. https://doi.org/10.1002/cphc.200600098.
(114) Chou, A.; Böcking, T.; Singh, N. K.; Gooding, J. J. Demonstration of the Importance of Oxygenated Species at the Ends of Carbon Nanotubes for Their Favourable Electrochemical Properties. *Chem. Commun.* **2005**, No. 7, 842–844. https://doi.org/10.1039/B415051A.
(115) Palomäki, T.; Wester, N.; Johansson, L.; Laitinen, M.; Jiang, H.; Arstila, K.; Sajavaara, T.; Han, J. G.; Koskinen, J.; Laurila, T. Characterization and Electrochemical Properties of Oxygenated Amorphous Carbon (a-C) Films. *Electrochim. Acta* **2016**, *220*, 137–145. https://doi.org/10.1016/j.electacta.2016.10.063.
(116) Wester, N.; Sainio, S.; Palomäki, T.; Nordlund, D.; Singh, V. K.; Johansson, L.-S.; Koskinen, J.; Laurila, T. Partially Reduced Graphene Oxide Modified Tetrahedral Amorphous Carbon Thin-Film Electrodes as a Platform for Nanomolar Detection of Dopamine. *J. Phys. Chem. C* **2017**, *121* (14). https://doi.org/10.1021/acs.jpcc.6b13019.
(117) Scipioni, R.; Pumera, M.; Boero, M.; Miyahara, Y.; Ohno, T. Investigation of the Mechanism of Adsorption of β-Nicotinamide Adenine Dinucleotide on Single-Walled Carbon Nanotubes. *J. Phys. Chem. Lett.* **2010**, *1* (1), 122–125. https://doi.org/10.1021/jz9000714.
(118) Wester, N.; Etula, J.; Lilius, T.; Sainio, S.; Laurila, T.; Koskinen, J. Selective Detection of Morphine in the Presence of Paracetamol with Anodically Pretreated Dual Layer Ti/Tetrahedral Amorphous Carbon Electrodes. *Electrochem. commun.* **2018**, *86*, 166–170. https://doi.org/10.1016/j.elecom.2017.12.014.
(119) Li, F.; Song, J.; Gao, D.; Zhang, Q.; Han, D.; Niu, L. Simple and Rapid Voltammetric Determination of Morphine at Electrochemically Pretreated Glassy Carbon Electrodes. *Talanta* **2009**. https://doi.org/10.1016/j.talanta.2009.05.011.
(120) Yang, X.; Haubold, L.; Devivo, G.; Swain, G. M. Electroanalytical Performance of Nitrogen-Containing Tetrahedral Amorphous Carbon Thin-Film Electrodes. *Anal. Chem.* **2012**, *84* (14), 6240–6248. https://doi.org/10.1021/ac301124r.
(121) Cao, L.; Lin, Z.; Huang, J.; Yu, X.; Wu, X.; Zhang, B.; Zhan, Y.; Xie, F.; Zhang, W.; Chen, J.; et al. Nitrogen Doped Amorphous Carbon as Metal Free Electrocatalyst for Oxygen Reduction Reaction. *Int. J. Hydrogen Energy* **2017**, *42* (2), 876–885. https://doi.org/10.1016/j.ijhydene.2016.11.108.
(122) Liu, X.; Dai, L. Carbon-Based Metal-Free Catalysts. *Nat. Rev. Mater.* **2016**, *1* (11), 16064. https://doi.org/10.1038/natrevmats.2016.64.
(123) Haag, D.; Kung, H. H. Metal Free Graphene Based Catalysts: A Review. *Top. Catal.* **2014**, *57* (6–9), 762–773. https://doi.org/10.1007/s11244-013-0233-9.
(124) Xu, X.; Jiang, S.; Hu, Z.; Liu, S. Nitrogen-Doped Carbon Nanotubes: High Electrocatalytic Activity toward the Oxidation of Hydrogen Peroxide and Its Application for Biosensing. *ACS Nano* **2010**, *4* (7), 4292–4298. https://doi.org/10.1021/nn1010057.
(125) Chen, S.; Bi, J.; Zhao, Y.; Yang, L.; Zhang, C.; Ma, Y.; Wu, Q.; Wang, X.; Hu, Z. Nitrogen-Doped Carbon Nanocages as Efficient Metal-Free Electrocatalysts for Oxygen Reduction Reaction. *Adv. Mater.* **2012**, *24* (41), 5593–5597. https://doi.org/10.1002/adma.201202424.
(126) Sheng, Z.-H.; Zheng, X.-Q.; Xu, J.-Y.; Bao, W.-J.; Wang, F.-B.; Xia, X.-H. Electrochemical Sensor Based on Nitrogen Doped Graphene: Simultaneous Determination of Ascorbic Acid, Dopamine and Uric Acid. *Biosens. Bioelectron.* **2012**, *34* (1), 125–131. https://doi.org/10.1016/j.bios.2012.01.030.
(127) Li, S.-M.; Yang, S.-Y.; Wang, Y.-S.; Lien, C.-H.; Tien, H.-W.; Hsiao, S.-T.; Liao, W.-H.; Tsai, H.-P.; Chang, C.-L.; Ma, C.-C. M.; et al. Controllable Synthesis of Nitrogen-Doped Graphene and Its Effect on the Simultaneous Electrochemical Determination of Ascorbic Acid, Dopamine, and Uric Acid. *Carbon N. Y.* **2013**, *59*, 418–429. https://doi.org/10.1016/j.carbon.2013.03.035.
(128) Gai, P.; Zhang, H.; Zhang, Y.; Liu, W.; Zhu, G.; Zhang, X.; Chen, J. Simultaneous Electrochemical Detection of Ascorbic Acid, Dopamine and Uric Acid Based on Nitrogen Doped Porous Carbon Nanopolyhedra. *J. Mater. Chem. B* **2013**, *1* (21), 2742.

https://doi.org/10.1039/c3tb20215a.
(129) Yuan, D.; Yuan, X.; Zhou, S.; Zou, W.; Zhou, T. N-Doped Carbon Nanorods as Ultrasensitive Electrochemical Sensors for the Determination of Dopamine. *RSC Adv.* **2012**, *2* (21), 8157. https://doi.org/10.1039/c2ra21041j.
(130) Yang, S.; Feng, X.; Wang, X.; Müllen, K. Graphene-Based Carbon Nitride Nanosheets as Efficient Metal-Free Electrocatalysts for Oxygen Reduction Reactions. *Angew. Chemie Int. Ed.* **2011**, *50* (23), 5339–5343. https://doi.org/10.1002/anie.201100170.
(131) Zhang, C.; Hao, R.; Liao, H.; Hou, Y. Synthesis of Amino-Functionalized Graphene as Metal-Free Catalyst and Exploration of the Roles of Various Nitrogen States in Oxygen Reduction Reaction. *Nano Energy* **2013**, *2* (1), 88–97. https://doi.org/10.1016/j.nanoen.2012.07.021.
(132) Jurkschat, K.; Ji, X.; Crossley, A.; Compton, R. G.; Banks, C. E. Super-Washing Does Not Leave Single Walled Carbon Nanotubes Iron-Free. *Analyst* **2007**, *132* (1), 21–23. https://doi.org/10.1039/B615824B.
(133) Duan, X.; Indrawirawan, S.; Sun, H.; Wang, S. Effects of Nitrogen-, Boron-, and Phosphorus-Doping or Codoping on Metal-Free Graphene Catalysis. *Catal. Today* **2015**, *249*, 184–191. https://doi.org/10.1016/j.cattod.2014.10.005.
(134) Hu, C.; Dai, L. Carbon-Based Metal-Free Catalysts for Electrocatalysis beyond the ORR. *Angew. Chemie Int. Ed.* **2016**, *55* (39), 11736–11758. https://doi.org/10.1002/anie.201509982.
(135) Etula, J.; Wester, N.; Sainio, S.; Laurila, T.; Koskinen, J. Characterization and Electrochemical Properties of Iron-Doped Tetrahedral Amorphous Carbon (Ta-C) Thin Films. *RSC Adv.* **2018**, *8* (46), 26356–26363. https://doi.org/10.1039/C8RA04719G.
(136) Banks, C. E.; Crossley, A.; Salter, C.; Wilkins, S. J.; Compton, R. G. Carbon Nanotubes Contain Metal Impurities Which Are Responsible for the "Electrocatalysis" Seen at Some Nanotube-Modified Electrodes. *Angew. Chemie - Int. Ed.* **2006**, *45* (16), 2533–2537. https://doi.org/10.1002/anie.200600033.
(137) Wong, C. H. A.; Chua, C. K.; Khezri, B.; Webster, R. D.; Pumera, M. Graphene Oxide Nanoribbons from the Oxidative Opening of Carbon Nanotubes Retain Electrochemically Active Metallic Impurities. *Angew. Chemie Int. Ed.* **2013**, *52* (33), 8685–8688. https://doi.org/10.1002/anie.201303837.
(138) Ambrosi, A.; Pumera, M. The CVD Graphene Transfer Procedure Introduces Metallic Impurities Which Alter the Graphene Electrochemical Properties. *Nanoscale* **2014**, *6* (1), 472–476. https://doi.org/10.1039/C3NR05230C.
(139) Koyama, S.; Kim, Y. A.; Hayashi, T.; Takeuchi, K.; Fujii, C.; Kuroiwa, N.; Koyama, H.; Tsukahara, T.; Endo, M. In Vivo Immunological Toxicity in Mice of Carbon Nanotubes with Impurities. *Carbon N. Y.* **2009**, *47* (5), 1365–1372. https://doi.org/10.1016/j.carbon.2009.01.028.
(140) Ambrosi, A.; Chua, C. K.; Khezri, B.; Sofer, Z.; Webster, R. D.; Pumera, M. Chemically Reduced Graphene Contains Inherent Metallic Impurities Present in Parent Natural and Synthetic Graphite. *Proc. Natl. Acad. Sci.* **2012**, *109* (32), 12899–12904. https://doi.org/10.1073/pnas.1205388109.
(141) Wang, L.; Ambrosi, A.; Pumera, M. "Metal-Free" Catalytic Oxygen Reduction Reaction on Heteroatom-Doped Graphene Is Caused by Trace Metal Impurities. *Angew. Chemie Int. Ed.* **2013**, *52* (51), 13818–13821. https://doi.org/10.1002/anie.201309171.
(142) Dai, X.; Wildgoose, G. G.; Compton, R. G. Apparent 'Electrocatalytic' Activity of Multiwalled Carbon Nanotubes in the Detection of the Anaesthetic Halothane: Occluded Copper Nanoparticles. *Analyst* **2006**, *131* (8), 901–906. https://doi.org/10.1039/B606197D.
(143) Sainio, S.; Leppänen, E.; Mynttinen, E.; Palomäki, T.; Wester, N.; Etula, J.; Isoaho, N.; Peltola, E.; Koehne, J.; Meyyappan, M.; et al. Integrating Carbon Nanomaterials with Metals for Bio-Sensing Applications. *Mol. Neurobiol.* **2020**, *57* (1), 179–190. https://doi.org/10.1007/s12035-019-01767-7.
(144) Sainio, S.; Palomäki, T.; Tujunen, N.; Protopopova, V.; Koehne, J.; Kordas, K.; Koskinen, J.; Meyyappan, M.; Laurila, T. Integrated Carbon Nanostructures for

Detection of Neurotransmitters. *Mol. Neurobiol.* **2015**, *52* (2), 859–866. https://doi.org/10.1007/s12035-015-9233-z.
(145) Sainio, S.; Nordlund, D.; Gandhiraman, R.; Jiang, H.; Koehne, J.; Koskinen, J.; Meyyappan, M.; Laurila, T. What Does Nitric Acid Really Do to Carbon Nanofibers? *J. Phys. Chem. C* **2016**, *120* (39), 22655–22662. https://doi.org/10.1021/acs.jpcc.6b06353.
(146) Streeter, I.; Wildgoose, G. G.; Shao, L.; Compton, R. G. Cyclic Voltammetry on Electrode Surfaces Covered with Porous Layers: An Analysis of Electron Transfer Kinetics at Single-Walled Carbon Nanotube Modified Electrodes. *Sensors Actuators, B Chem.* **2008**, *133* (2), 462–466. https://doi.org/10.1016/j.snb.2008.03.015.
(147) Henstridge, M. C.; Dickinson, E. J. F.; Aslanoglu, M.; Batchelor-McAuley, C.; Compton, R. G. Voltammetric Selectivity Conferred by the Modification of Electrodes Using Conductive Porous Layers or Films: The Oxidation of Dopamine on Glassy Carbon Electrodes Modified with Multiwalled Carbon Nanotubes. *Sensors Actuators B Chem.* **2010**, *145* (1), 417–427. https://doi.org/10.1016/j.snb.2009.12.046.
(148) Sims, M. J.; Rees, N. V.; Dickinson, E. J. F.; Compton, R. G. Effects of Thin-Layer Diffusion in the Electrochemical Detection of Nicotine on Basal Plane Pyrolytic Graphite (BPPG) Electrodes Modified with Layers of Multi-Walled Carbon Nanotubes (MWCNT-BPPG). *Sensors Actuators B Chem.* **2010**, *144* (1), 153–158. https://doi.org/10.1016/j.snb.2009.10.055.
(149) Xiao, N.; Tan, H.; Zhu, J.; Tan, L.; Rui, X.; Dong, X.; Yan, Q. High-Performance Supercapacitor Electrodes Based on Graphene Achieved by Thermal Treatment with the Aid of Nitric Acid. *ACS Appl. Mater. Interfaces* **2013**, *5* (19), 9656–9662. https://doi.org/10.1021/am402686r.
(150) Vesali, N. M.; Khodadadi, A. A.; Mortazavi, Y.; Sahraei, A. O.; Pourfayaz, F.; Sedghi, M. S. Functionalization of Carbon Nanotubes Using Nitric Acid Oxidation and Dbd Plasma. *World Acad. Sci. Eng. Technol.* **2009**, *37* (1), 177–179. https://doi.org/10.5281/zenodo.1061674.
(151) Pumera, M.; Sasaki, T.; Iwai, H. Relationship between Carbon Nanotube Structure and Electrochemical Behavior: Heterogeneous Electron Transfer at Electrochemically Activated Carbon Nanotubes. *Chem. - An Asian J.* **2008**, *3* (12), 2046–2055. https://doi.org/10.1002/asia.200800218.
(152) Sainio, S.; Wester, N.; Titus, C. J.; Liao, Y.; Zhang, Q.; Nordlund, D.; Sokaras, D.; Lee, S.; Irwin, K. D.; Doriese, W. B.; et al. Hybrid X-Ray Spectroscopy-Based Approach To Acquire Chemical and Structural Information of Single-Walled Carbon Nanotubes with Superior Sensitivity. *J. Phys. Chem. C* **2019**, *123* (10), 6114–6120. https://doi.org/10.1021/acs.jpcc.9b00714.
(153) Pumera, M. Voltammetry of Carbon Nanotubes and Graphenes: Excitement, Disappointment, and Reality. *Chem. Rec.* **2012**, *12* (1), 201–213. https://doi.org/10.1002/tcr.201100027.
(154) Laurila, T.; Sainio, S.; Caro, M. A. Hybrid Carbon Based Nanomaterials for Electrochemical Detection of Biomolecules. *Prog. Mater. Sci.* **2017**, *88*, 499–594. https://doi.org/10.1016/j.pmatsci.2017.04.012.
(155) Lossy, R.; Pappas, D. L.; Roy, R. A.; Doyle, J. P.; Cuomo, J. J.; Bruley, J. Properties of Amorphous Diamond Films Prepared by a Filtered Cathodic Arc. *J. Appl. Phys.* **1995**, *77* (9), 4750–4756. https://doi.org/10.1063/1.359411.
(156) Chhowalla, M.; Robertson, J.; Chen, C. W.; Silva, S. R. P.; Davis, C. A.; Amaratunga, G. A. J.; Milne, W. I. Influence of Ion Energy and Substrate Temperature on the Optical and Electronic Properties of Tetrahedral Amorphous Carbon (Ta -C) Films. *J. Appl. Phys.* **1997**, *81* (1), 139–145. https://doi.org/10.1063/1.364000.
(157) Xu, S.; Tay, B. K.; Tan, H. S.; Zhong, L.; Tu, Y. Q.; Silva, S. R. P.; Milne, W. I. Properties of Carbon Ion Deposited Tetrahedral Amorphous Carbon Films as a Function of Ion Energy. *J. Appl. Phys.* **1996**, *79* (9), 7234–7240. https://doi.org/10.1063/1.361440.
(158) Kaivosoja, E.; Suvanto, P.; Barreto, G.; Aura, S.; Soininen, A.; Franssila, S.; Konttinen,

Y. T. Cell Adhesion and Osteogenic Differentiation on Three-Dimensional Pillar Surfaces. *J. Biomed. Mater. Res. Part A* **2013**, *101A* (3), 842–852. https://doi.org/10.1002/jbm.a.34378.
(159) Tujunen, N.; Kaivosoja, E.; Protopopova, V.; Valle-Delgado, J. J.; Österberg, M.; Koskinen, J.; Laurila, T. Electrochemical Detection of Hydrogen Peroxide on Platinum-Containing Tetrahedral Amorphous Carbon Sensors and Evaluation of Their Biofouling Properties. *Mater. Sci. Eng. C* **2015**, *55*, 70–78. https://doi.org/10.1016/j.msec.2015.05.060.
(160) Uhlmann, S.; Frauenheim, T.; Lifshitz, Y. Molecular-Dynamics Study of the Fundamental Processes Involved in Subplantation of Diamondlike Carbon. *Phys. Rev. Lett.* **1998**, *81* (3), 641–644. https://doi.org/10.1103/PhysRevLett.81.641.
(161) Caro, M. A.; Deringer, V. L.; Koskinen, J.; Laurila, T.; Csányi, G. Growth Mechanism and Origin of High Sp3 Content in Tetrahedral Amorphous Carbon. *Phys. Rev. Lett.* **2018**, *120* (16), 166101. https://doi.org/10.1103/PhysRevLett.120.166101.
(162) Anders, A.; Pasaja, N.; Sansongsiri, S. Filtered Cathodic Arc Deposition with Ion-Species-Selective Bias. *Rev. Sci. Instrum.* **2007**, *78* (6), 063901. https://doi.org/10.1063/1.2745229.
(163) Anders, A.; Brown, I. G.; MacGill, R. A.; Dickinson, M. R. `Triggerless' Triggering of Vacuum Arcs. *J. Phys. D. Appl. Phys.* **1998**, *31* (5), 584–587. https://doi.org/10.1088/0022-3727/31/5/015.
(164) Anders, A. *Cathodic Arcs*; Springer Series on Atomic, Optical, and Plasma Physics; Springer New York: New York, NY, 2008; Vol. 50. https://doi.org/10.1007/978-0-387-79108-1.
(165) Sainio, S.; Wester, N.; Titus, C. J.; Nordlund, D.; Lee, S.; Koskinen, J.; Laurila, T. In-Situ Functionalization of Tetrahedral Amorphous Carbon by Filtered Cathodic Arc Deposition. *AIP Adv.* **2019**, *9* (8), 085325. https://doi.org/10.1063/1.5113484.
(166) Peltola, E.; Sainio, S.; Holt, K. B.; Palomäki, T.; Koskinen, J.; Laurila, T. Electrochemical Fouling of Dopamine and Recovery of Carbon Electrodes. *Anal. Chem.* **2018**, *90* (2), 1408–1416. https://doi.org/10.1021/acs.analchem.7b04793.
(167) Iijima, S. Helical Microtubules of Graphitic Carbon. *Nature* **1991**, *354* (6348), 56–58. https://doi.org/10.1038/354056a0.
(168) DAI, H.; JAVEY, A.; POP, E.; MANN, D.; KIM, W.; LU, Y. ELECTRICAL TRANSPORT PROPERTIES AND FIELD EFFECT TRANSISTORS OF CARBON NANOTUBES. *Nano* **2006**, *01* (01), 1–13. https://doi.org/10.1142/S1793292006000070.
(169) Coleman, J. N.; Khan, U.; Blau, W. J.; Gun'ko, Y. K. Small but Strong: A Review of the Mechanical Properties of Carbon Nanotube–Polymer Composites. *Carbon N. Y.* **2006**, *44* (9), 1624–1652. https://doi.org/10.1016/j.carbon.2006.02.038.
(170) Pop, E.; Mann, D.; Wang, Q.; Goodson, K.; Dai, H. Thermal Conductance of an Individual Single-Wall Carbon Nanotube above Room Temperature. *Nano Lett.* **2006**, *6* (1), 96–100. https://doi.org/10.1021/nl052145f.
(171) Pal, P. P.; Larionova, T.; Anoshkin, I. V.; Jiang, H.; Nisula, M.; Goryunkov, A. A.; Tolochko, O. V.; Karppinen, M.; Kauppinen, E. I.; Nasibulin, A. G. Dry Functionalization and Doping of Single-Walled Carbon Nanotubes by Ozone. *J. Phys. Chem. C* **2015**, *119* (49), 27821–27828. https://doi.org/10.1021/acs.jpcc.5b08832.
(172) Heller, I.; Kong, J.; Williams, K. A.; Dekker, C.; Lemay, S. G. Electrochemistry at Single-Walled Carbon Nanotubes: The Role of Band Structure and Quantum Capacitance. *J. Am. Chem. Soc.* **2006**, *128* (22), 7353–7359. https://doi.org/10.1021/ja061212k.
(173) Nishimura, K.; Ushiyama, T.; Viet, N. X.; Inaba, M.; Kishimoto, S.; Ohno, Y. Enhancement of the Electron Transfer Rate in Carbon Nanotube Flexible Electrochemical Sensors by Surface Functionalization. *Electrochim. Acta* **2019**, *295*, 157–163. https://doi.org/10.1016/j.electacta.2018.10.147.
(174) Wildgoose, G. G.; Banks, C. E.; Leventis, H. C.; Compton, R. G. Chemically Modified Carbon Nanotubes for Use in Electroanalysis. *Microchim. Acta* **2006**, *152* (3–4), 187–214. https://doi.org/10.1007/s00604-005-0449-x.

(175) Dumitrescu, I.; Wilson, N. R.; Macpherson, J. V. Functionalizing Single-Walled Carbon Nanotube Networks: Effect on Electrical and Electrochemical Properties. *J. Phys. Chem. C* **2007**, *111* (35), 12944–12953. https://doi.org/10.1021/jp067256x.
(176) Güell, A. G.; Meadows, K. E.; Dudin, P. V.; Ebejer, N.; Byers, J. C.; Macpherson, J. V.; Unwin, P. R. Selection, Characterisation and Mapping of Complex Electrochemical Processes at Individual Single-Walled Carbon Nanotubes: The Case of Serotonin Oxidation. *Faraday Discuss.* **2014**, *172* (0), 439–455. https://doi.org/10.1039/C4FD00054D.
(177) Heller, I.; Kong, J.; Heering, H. A.; Williams, K. A.; Lemay, S. G.; Dekker, C. Individual Single-Walled Carbon Nanotubes as Nanoelectrodes for Electrochemistry. *Nano Lett.* **2005**, *5* (1), 137–142. https://doi.org/10.1021/nl048200m.
(178) Güell, A. G.; Meadows, K. E.; Dudin, P. V.; Ebejer, N.; Macpherson, J. V.; Unwin, P. R. Mapping Nanoscale Electrochemistry of Individual Single-Walled Carbon Nanotubes. *Nano Lett.* **2014**, *14* (1), 220–224. https://doi.org/10.1021/nl403752e.
(179) Byers, J. C.; Güell, A. G.; Unwin, P. R. Nanoscale Electrocatalysis: Visualizing Oxygen Reduction at Pristine, Kinked, and Oxidized Sites on Individual Carbon Nanotubes. *J. Am. Chem. Soc.* **2014**, *136* (32), 11252–11255. https://doi.org/10.1021/ja505708y.
(180) Tasis, D.; Tagmatarchis, N.; Bianco, A.; Prato, M. Chemistry of Carbon Nanotubes. *Chem. Rev.* **2006**, *106* (3), 1105–1136. https://doi.org/10.1021/cr0505690.
(181) Dumitrescu, I.; Unwin, P. R.; Macpherson, J. V. Electrochemistry at Carbon Nanotubes: Perspective and Issues. *Chem. Commun.* **2009**, *7345* (45), 6886. https://doi.org/10.1039/b909734a.
(182) Liao, Y.; Jiang, H.; Wei, N.; Laiho, P.; Zhang, Q.; Khan, S. A.; Kauppinen, E. I. Direct Synthesis of Colorful Single-Walled Carbon Nanotube Thin Films. *J. Am. Chem. Soc.* **2018**, *140* (31), 9797–9800. https://doi.org/10.1021/jacs.8b05151.
(183) Moisala, A.; Nasibulin, A. G.; Brown, D. P.; Jiang, H.; Khriachtchev, L.; Kauppinen, E. I. Single-Walled Carbon Nanotube Synthesis Using Ferrocene and Iron Pentacarbonyl in a Laminar Flow Reactor. *Chem. Eng. Sci.* **2006**, *61* (13), 4393–4402. https://doi.org/10.1016/j.ces.2006.02.020.
(184) Cinti, S.; Arduini, F. Graphene-Based Screen-Printed Electrochemical (Bio)Sensors and Their Applications: Efforts and Criticisms. *Biosens. Bioelectron.* **2017**, *89*, 107–122. https://doi.org/10.1016/j.bios.2016.07.005.
(185) Ahmed, M. U.; Hossain, M. M.; Safavieh, M.; Wong, Y. L.; Rahman, I. A.; Zourob, M.; Tamiya, E. Toward the Development of Smart and Low Cost Point-of-Care Biosensors Based on Screen Printed Electrodes. *Crit. Rev. Biotechnol.* **2015**, *36* (3), 1–11. https://doi.org/10.3109/07388551.2014.992387.
(186) Renedo, O. D.; Alonso-Lomillo, M. A.; Martínez, M. J. A. Recent Developments in the Field of Screen-Printed Electrodes and Their Related Applications. *Talanta* **2007**, *73* (2), 202–219. https://doi.org/10.1016/j.talanta.2007.03.050.
(187) Taleat, Z.; Khoshroo, A.; Mazloum-Ardakani, M. Screen-Printed Electrodes for Biosensing: A Review (2008–2013). *Microchim. Acta* **2014**, *181* (9–10), 865–891. https://doi.org/10.1007/s00604-014-1181-1.
(188) Mohamed, H. M. Screen-Printed Disposable Electrodes: Pharmaceutical Applications and Recent Developments. *TrAC Trends Anal. Chem.* **2016**, *82*, 1–11. https://doi.org/10.1016/j.trac.2016.02.010.
(189) Inzelt, G.; Lewenstam, A.; Scholz, F. *Handbook of Reference Electrodes*; Inzelt, G., Lewenstam, A., Scholz, F., Eds.; Springer Berlin Heidelberg: Berlin, Heidelberg, 2013. https://doi.org/10.1007/978-3-642-36188-3.
(190) Moya, A.; Gabriel, G.; Villa, R.; Javier del Campo, F. Inkjet-Printed Electrochemical Sensors. *Curr. Opin. Electrochem.* **2017**, *3* (1), 29–39. https://doi.org/10.1016/j.coelec.2017.05.003.
(191) Sekitani, T.; Noguchi, Y.; Zschieschang, U.; Klauk, H.; Someya, T. Organic Transistors Manufactured Using Inkjet Technology with Subfemtoliter Accuracy. *Proc. Natl. Acad. Sci.* **2008**, *105* (13), 4976–4980. https://doi.org/10.1073/pnas.0708340105.
(192) Aoki, M.; Nakamura, K.; Tachibana, T.; Sumita, I.; Hayashi, H.; Asada, H.; Ohshita, Y.

30 Mm Fine-Line Printing for Solar Cells. In *2013 IEEE 39th Photovoltaic Specialists Conference (PVSC)*; IEEE, 2013; pp 2162–2166. https://doi.org/10.1109/PVSC.2013.6744903.
(193) Wang, J.; Tian, B.; Nascimento, V. B.; Angnes, L. Performance of Screen-Printed Carbon Electrodes Fabricated from Different Carbon Inks. *Electrochim. Acta* **1998**, *43* (23), 3459–3465. https://doi.org/10.1016/S0013-4686(98)00092-9.
(194) Fukaya, N.; Kim, D. Y.; Kishimoto, S.; Noda, S.; Ohno, Y. One-Step Sub-10 Mm Patterning of Carbon-Nanotube Thin Films for Transparent Conductor Applications. *ACS Nano* **2014**, *8* (4), 3285–3293. https://doi.org/10.1021/nn4041975.
(195) Suzuki, H.; Hiratsuka, A.; Sasaki, S.; Karube, I. Problems Associated with the Thin-Film Ag/AgCl Reference Electrode and a Novel Structure with Improved Durability. *Sensors Actuators, B Chem.* **1998**, *46* (2–3), 104–113. https://doi.org/10.1016/S0925-4005(98)00043-4.
(196) Sophocleous, M.; Atkinson, J. K. A Review of Screen-Printed Silver/Silver Chloride (Ag/AgCl) Reference Electrodes Potentially Suitable for Environmental Potentiometric Sensors. *Sensors Actuators A Phys.* **2017**, *267*, 106–120. https://doi.org/10.1016/j.sna.2017.10.013.
(197) Tymecki, Ł.; Zwierkowska, E.; Koncki, R. Screen-Printed Reference Electrodes for Potentiometric Measurements. *Anal. Chim. Acta* **2004**, *526* (1), 3–11. https://doi.org/10.1016/j.aca.2004.08.056.
(198) Shinwari, M. W.; Zhitomirsky, D.; Deen, I. A.; Selvaganapathy, P. R.; Deen, M. J.; Landheer, D. Microfabricated Reference Electrodes and Their Biosensing Applications. *Sensors* **2010**, *10* (3), 1679–1715. https://doi.org/10.3390/s100301679.
(199) Moussy, F.; Harrison, D. J. Prevention of the Rapid Degradation of Subcutaneously Implanted Ag/AgCl Reference Electrodes Using Polymer Coatings. *Anal. Chem.* **1994**, *66* (5), 674–679. https://doi.org/10.1021/ac00077a015.
(200) Nolan, M. A.; Tan, S. H.; Kounaves, S. P. Fabrication and Characterization of a Solid State Reference Electrode for Electroanalysis of Natural Waters with Ultramicroelectrodes. *Anal. Chem.* **1997**, *69* (6), 1244–1247. https://doi.org/10.1021/ac961020f.
(201) Hashemi, P.; Walsh, P. L.; Guillot, T. S.; Gras-Najjar, J.; Takmakov, P.; Crews, F. T.; Wightman, R. M. Chronically Implanted, Nafion-Coated Ag/AgCl Reference Electrodes for Neurochemical Applications. *ACS Chem. Neurosci.* **2011**, *2* (11), 658–666. https://doi.org/10.1021/cn2000684.
(202) Krebs, H. A. Chemical Composition of Blood Plasma and Serum. *Annu. Rev. Biochem.* **1950**, *19* (1), 409–430. https://doi.org/10.1146/annurev.bi.19.070150.002205.
(203) Tuck, M. K.; Chan, D. W.; Chia, D.; Godwin, A. K.; Grizzle, W. E.; Krueger, K. E.; Rom, W.; Sanda, M.; Sorbara, L.; Stass, S.; et al. Standard Operating Procedures for Serum and Plasma Collection: Early Detection Research Network Consensus Statement Standard Operating Procedure Integration Working Group. *J. Proteome Res.* **2009**, *8* (1), 113–117. https://doi.org/10.1021/pr800545q.
(204) Chen, C.-H.; Luo, S.-C. Tuning Surface Charge and Morphology for the Efficient Detection of Dopamine under the Interferences of Uric Acid, Ascorbic Acid, and Protein Adsorption. *ACS Appl. Mater. Interfaces* **2015**, *7* (39), 21931–21938. https://doi.org/10.1021/acsami.5b06526.
(205) Adenier, A.; Chehimi, M. M.; Gallardo, I.; Pinson, J.; Vilà, N. Electrochemical Oxidation of Aliphatic Amines and Their Attachment to Carbon and Metal Surfaces. *Langmuir* **2004**, *20* (19), 8243–8253. https://doi.org/10.1021/la049194c.
(206) Xue, Q.; Kato, D.; Kamata, T.; Umemura, S.; Hirono, S.; Niwa, O. Electron Cyclotron Resonance-Sputtered Nanocarbon Film Electrode Compared with Diamond-Like Carbon and Glassy Carbon Electrodes as Regards Electrochemical Properties and Biomolecule Adsorption. *Jpn. J. Appl. Phys.* **2012**, *51* (9), 090124. https://doi.org/10.1143/JJAP.51.090124.
(207) GOTO, T.; YASUKAWA, T.; KANDA, K.; MATSUI, S.; MIZUTANI, F. Inhibition of Electrochemical Fouling against Biomolecules on a Diamond-Like Carbon Electrode.

Anal. Sci. **2011**, *27* (1), 91–94. https://doi.org/10.2116/analsci.27.91.
(208) Peltola, E.; Aarva, A.; Sainio, S.; Heikkinen, J. J.; Wester, N.; Jokinen, V.; Koskinen, J.; Laurila, T. Biofouling Affects the Redox Kinetics of Outer and Inner Sphere Probes on Carbon Surfaces Drastically Differently – Implications to Biosensing. *Phys. Chem. Chem. Phys.* **2020**, *22* (29), 16630–16640. https://doi.org/10.1039/D0CP02251A.
(209) Sweryda-Krawiec, B.; Devaraj, H.; Jacob, G.; Hickman, J. J. A New Interpretation of Serum Albumin Surface Passivation. *Langmuir* **2004**, *20* (6), 2054–2056. https://doi.org/10.1021/la034870g.
(210) Wertz, C. F.; Santore, M. M. Effect of Surface Hydrophobicity on Adsorption and Relaxation Kinetics of Albumin and Fibrinogen: Single-Species and Competitive Behavior. *Langmuir* **2001**, *17* (10), 3006–3016. https://doi.org/10.1021/la0017781.
(211) Trouillon, R.; O'Hare, D. Comparison of Glassy Carbon and Boron Doped Diamond Electrodes: Resistance to Biofouling. *Electrochim. Acta* **2010**, *55* (22), 6586–6595. https://doi.org/10.1016/j.electacta.2010.06.016.
(212) Sainio, S.; Nordlund, D.; Caro, M. A.; Gandhiraman, R.; Koehne, J.; Wester, N.; Koskinen, J.; Meyyappan, M.; Laurila, T. Correlation between Sp 3 -to-Sp 2 Ratio and Surface Oxygen Functionalities in Tetrahedral Amorphous Carbon (Ta-C) Thin Film Electrodes and Implications of Their Electrochemical Properties. *J. Phys. Chem. C* **2016**, *120* (15), 8298–8304. https://doi.org/10.1021/acs.jpcc.6b02342.
(213) DuVall, S. H.; McCreery, R. L. Control of Catechol and Hydroquinone Electron-Transfer Kinetics on Native and Modified Glassy Carbon Electrodes. *Anal. Chem.* **1999**, *71* (20), 4594–4602. https://doi.org/10.1021/ac990399d.
(214) DuVall, S. H.; McCreery, R. L. Self-Catalysis by Catechols and Quinones during Heterogeneous Electron Transfer at Carbon Electrodes. *J. Am. Chem. Soc.* **2000**, *122* (28), 6759–6764. https://doi.org/10.1021/ja000227u.
(215) Li, Y.; Liu, M.; Xiang, C.; Xie, Q.; Yao, S. Electrochemical Quartz Crystal Microbalance Study on Growth and Property of the Polymer Deposit at Gold Electrodes during Oxidation of Dopamine in Aqueous Solutions. *Thin Solid Films* **2006**, *497* (1–2), 270–278. https://doi.org/10.1016/j.tsf.2005.10.048.
(216) Ball, V.; Frari, D. Del; Toniazzo, V.; Ruch, D. Kinetics of Polydopamine Film Deposition as a Function of PH and Dopamine Concentration: Insights in the Polydopamine Deposition Mechanism. *J. Colloid Interface Sci.* **2012**, *386* (1), 366–372. https://doi.org/10.1016/j.jcis.2012.07.030.
(217) Berth, M.; Delanghe, J. PROTEIN PRECIPITATION AS A POSSIBLE IMPORTANT PITFALL IN THE CLINICAL CHEMISTRY ANALYSIS OF BLOOD SAMPLES CONTAINING MONOCLONAL IMMUNOGLOBULINS: 2 CASE REPORTS AND A REVIEW OF THE LITERATURE. *Acta Clin. Belg.* **2004**, *59* (5), 263–273. https://doi.org/10.1179/acb.2004.039.
(218) Vessman, J.; Stefan, R. I.; van Staden, J. F.; Danzer, K.; Lindner, W.; Burns, D. T.; Fajgelj, A.; Müller, H. Selectivity in Analytical Chemistry (IUPAC Recommendations 2001). *Pure Appl. Chem.* **2001**, *73* (8), 1381–1386. https://doi.org/10.1351/pac200173081381.
(219) Guideline, I. C. H. H. T. Validation of Analytical Procedures: Text and Methodology Q2 (R1). *IFPMA: Geneva* **2005**.
(220) Putnam, D. COMPOSITION AND CONCENTRATIVE PROPERTIES OF HUMAN URINE. *Security* **1971**, No. July.
(221) Bouatra, S.; Aziat, F.; Mandal, R.; Guo, A. C.; Wilson, M. R.; Knox, C.; Bjorndahl, T. C.; Krishnamurthy, R.; Saleem, F.; Liu, P.; et al. The Human Urine Metabolome. *PLoS One* **2013**, *8* (9), e73076. https://doi.org/10.1371/journal.pone.0073076.
(222) Kleine, T. O.; Zwerenz, P.; Zöfel, P.; Shiratori, K. New and Old Diagnostic Markers of Meningitis in Cerebrospinal Fluid (CSF). *Brain Res. Bull.* **2003**, *61* (3), 287–297. https://doi.org/10.1016/S0361-9230(03)00092-3.
(223) Brabec, V.; Mornstein, V. Electrochemical Behaviour of Proteins at Graphite Electrodes. I. Electrooxidation of Proteins as a New Probe of Protein Structure and Reactions. *Biochim. Biophys. Acta* **1980**. https://doi.org/10.1016/0005-

2795(80)90106-3.
(224) Ames, B. N.; Cathcart, R.; Schwiers, E.; Hochstein, P. Uric Acid Provides an Antioxidant Defense in Humans against Oxidant- and Radical-Caused Aging and Cancer: A Hypothesis. *Proc. Natl. Acad. Sci.* **1981**, *78* (11), 6858–6862. https://doi.org/10.1073/pnas.78.11.6858.
(225) Yamamoto, T.; Moriwaki, Y.; Takahashi, S.; Yamakita, J.; Tsutsumi, Z.; Ohata, H.; Hiroishi, K.; Nakano, T.; Higashino, K. Effect of Ethanol and Fructose on Plasma Uridine and Purine Bases. *Metabolism* **1997**, *46* (5), 544–547. https://doi.org/10.1016/S0026-0495(97)90192-X.
(226) Thane Eells, J.; Spector, R. Purine and Pyrimidine Base and Nucleoside Concentrations in Human Cerebrospinal Fluid and Plasma. *Neurochem. Res.* **1983**, *8* (11), 1451–1457. https://doi.org/10.1007/BF00965000.
(227) Niklasson, F.; Hetta, J.; Degrell, I. Hypoxanthine, Xanthine, Urate and Creatinine Concentration Gradients in Cerebrospinal Fluid. *Ups. J. Med. Sci.* **1988**, *93* (3), 225–232. https://doi.org/10.3109/03009738809178548.
(228) Raj, M. A.; John, S. A. Simultaneous Determination of Uric Acid, Xanthine, Hypoxanthine and Caffeine in Human Blood Serum and Urine Samples Using Electrochemically Reduced Graphene Oxide Modified Electrode. *Anal. Chim. Acta* **2013**, *771*, 14–20. https://doi.org/10.1016/j.aca.2013.02.017.
(229) Ojani, R.; Alinezhad, A.; Abedi, Z. A Highly Sensitive Electrochemical Sensor for Simultaneous Detection of Uric Acid, Xanthine and Hypoxanthine Based on Poly(l-Methionine) Modified Glassy Carbon Electrode. *Sensors Actuators B Chem.* **2013**, *188*, 621–630. https://doi.org/10.1016/j.snb.2013.07.015.
(230) Swamy, B. E. K.; Venton, B. J. Subsecond Detection of Physiological Adenosine Concentrations Using Fast-Scan Cyclic Voltammetry. *Anal. Chem.* **2007**, *79* (2), 744–750. https://doi.org/10.1021/ac061820i.
(231) Lim, G. N.; Ross, A. E. Purine Functional Group Type and Placement Modulate the Interaction with Carbon-Fiber Microelectrodes. *ACS Sensors* **2019**, *4* (2), 479–487. https://doi.org/10.1021/acssensors.8b01504.
(232) Wang, P.; Wu, H.; Dai, Z.; Zou, X. Simultaneous Detection of Guanine, Adenine, Thymine and Cytosine at Choline Monolayer Supported Multiwalled Carbon Nanotubes Film. *Biosens. Bioelectron.* **2011**, *26* (7), 3339–3345. https://doi.org/10.1016/j.bios.2011.01.011.
(233) Michelet, F.; Gueguen, R.; Leroy, P.; Wellman, M.; Nicolas, A.; Siest, G. Blood and Plasma Glutathione Measured in Healthy Subjects by HPLC: Relation to Sex, Aging, Biological Variables, and Life Habits. *Clin. Chem.* **1995**. https://doi.org/10.1093/clinchem/41.10.1509.
(234) Konings, C. .; Kuiper, M. .; Teerlink, T.; Mulder, C.; Scheltens, P.; Wolters, E. C. Normal Cerebrospinal Fluid Glutathione Concentrations in Parkinson's Disease, Alzheimer's Disease and Multiple System Atrophy. *J. Neurol. Sci.* **1999**, *168* (2), 112–115. https://doi.org/10.1016/S0022-510X(99)00167-7.
(235) Moore, R. R.; Banks, C. E.; Compton, R. G. Electrocatalytic Detection of Thiols Using an Edge Plane Pyrolytic Graphite Electrode. *Analyst* **2004**, *129* (8), 755. https://doi.org/10.1039/b406276k.
(236) Tang, H.; Chen, J.; Nie, L.; Yao, S.; Kuang, Y. Electrochemical Oxidation of Glutathione at Well-Aligned Carbon Nanotube Array Electrode. *Electrochim. Acta* **2006**, *51* (15), 3046–3051. https://doi.org/10.1016/j.electacta.2005.08.038.
(237) Lima, P. R.; Santos, W. J. R.; Oliveira, A. B.; Goulart, M. O. F.; Kubota, L. T. Electrocatalytic Activity of 4-Nitrophthalonitrile-Modified Electrode for the l-Glutathione Detection. *J. Pharm. Biomed. Anal.* **2008**, *47* (4–5), 758–764. https://doi.org/10.1016/j.jpba.2008.03.006.
(238) Martinez, M.; Frank, A.; Diez-Tejedor, E.; Hernanz, A. Amino Acid Concentrations in Cerebrospinal Fluid and Serum in Alzheimer's Disease and Vascular Dementia. *J. Neural Transm. - Park. Dis. Dement. Sect.* **1993**, *6* (1), 1–9. https://doi.org/10.1007/BF02252617.

(239) Brabec, V.; Mornstein, V. Electrochemical Behaviour of Proteins at Graphite Electrodes: II. Electrooxidation of Amino Acids. *Biophys. Chem.* **1980**. https://doi.org/10.1016/0301-4622(80)80048-2.
(240) Fan, Y.; Liu, J.-H.; Lu, H.-T.; Zhang, Q. Electrochemistry and Voltammetric Determination of L-Tryptophan and L-Tyrosine Using a Glassy Carbon Electrode Modified with a Nafion/TiO2-Graphene Composite Film. *Microchim. Acta* **2011**, *173* (1–2), 241–247. https://doi.org/10.1007/s00604-011-0556-9.
(241) Madrakian, T.; Haghshenas, E.; Afkhami, A. Simultaneous Determination of Tyrosine, Acetaminophen and Ascorbic Acid Using Gold Nanoparticles/Multiwalled Carbon Nanotube/Glassy Carbon Electrode by Differential Pulse Voltammetric Method. *Sensors Actuators B Chem.* **2014**, *193*, 451–460. https://doi.org/10.1016/j.snb.2013.11.117.
(242) Xu, Q.; Wang, S.-F. Electrocatalytic Oxidation and Direct Determination of L-Tyrosine by Square Wave Voltammetry at Multi-Wall Carbon Nanotubes Modified Glassy Carbon Electrodes. *Microchim. Acta* **2005**, *151* (1–2), 47–52. https://doi.org/10.1007/s00604-005-0408-6.
(243) Fukagawa, N. K.; Martin, J. M.; Wurthmann, A.; Prue, A. H.; Ebenstein, D.; O'Rourke, B. Sex-Related Differences in Methionine Metabolism and Plasma Homocysteine Concentrations. *Am. J. Clin. Nutr.* **2000**, *72* (1), 22–29. https://doi.org/10.1093/ajcn/72.1.22.
(244) Dickinson, J. C.; Hamilton, P. B. THE FREE AMINO ACIDS OF HUMAN SPINAL FLUID DETERMINED BY ION EXCHANGE CHROMATOGRAPHY. *J. Neurochem.* **1966**, *13* (11), 1179–1187. https://doi.org/10.1111/j.1471-4159.1966.tb04275.x.
(245) Silva, F. de A. dos S.; da Silva, M. G. A.; Lima, P. R.; Meneghetti, M. R.; Kubota, L. T.; Goulart, M. O. F. A Very Low Potential Electrochemical Detection of L-Cysteine Based on a Glassy Carbon Electrode Modified with Multi-Walled Carbon Nanotubes/Gold Nanorods. *Biosens. Bioelectron.* **2013**, *50*, 202–209. https://doi.org/10.1016/j.bios.2013.06.036.
(246) Lee, P. T.; Compton, R. G. Electrochemical Detection of NADH, Cysteine, or Glutathione Using a Caffeic Acid Modified Glassy Carbon Electrode. *Electroanalysis* **2013**, *25* (7), 1613–1620. https://doi.org/10.1002/elan.201300145.
(247) Tang, X.; Liu, Y.; Hou, H.; You, T. Electrochemical Determination of L-Tryptophan, L-Tyrosine and L-Cysteine Using Electrospun Carbon Nanofibers Modified Electrode. *Talanta* **2010**, *80* (5), 2182–2186. https://doi.org/10.1016/j.talanta.2009.11.027.
(248) Chailapakul, O. The Electrooxidation of Organic Acids at Boron-Doped Diamond Electrodes. *Electrochem. commun.* **2000**, *2* (6), 422–426. https://doi.org/10.1016/S1388-2481(00)00049-7.
(249) Brigham, M. P.; Stein, W. H.; Moore, S. THE CONCENTRATIONS OF CYSTEINE AND CYSTINE IN HUMAN BLOOD PLASMA. *J. Clin. Invest.* **1960**, *39* (11), 1633–1638. https://doi.org/10.1172/JCI104186.
(250) Zor, E.; Bingol, H.; Ramanaviciene, A.; Ramanavicius, A.; Ersoz, M. An Electrochemical and Computational Study for Discrimination of D- and L-Cystine by Reduced Graphene Oxide-β/Cyclodextrin. *Analyst* **2015**, *140* (1), 313–321. https://doi.org/10.1039/C4AN01751J.
(251) Paraskevas, G. P.; Kapaki, E.; Libitaki, G.; Zournas, C.; Segditsa, I.; Papageorgiou, C. Ascorbate in Healthy Subjects, Amyotrophic Lateral Sclerosis and Alzheimer's Disease. *Acta Neurol. Scand.* **2009**, *96* (2), 88–90. https://doi.org/10.1111/j.1600-0404.1997.tb00245.x.
(252) Mandal, R.; Guo, A. C.; Chaudhary, K. K.; Liu, P.; Yallou, F. S.; Dong, E.; Aziat, F.; Wishart, D. S. Multi-Platform Characterization of the Human Cerebrospinal Fluid Metabolome: A Comprehensive and Quantitative Update. *Genome Med.* **2012**, *4* (4), 38. https://doi.org/10.1186/gm337.
(253) Palomäki, T.; Wester, N.; Johansson, L.-S.; Laitinen, M.; Jiang, H.; Arstila, K.; Sajavaara, T.; Han, J. G.; Koskinen, J.; Laurila, T. Characterization and Electrochemical Properties of Oxygenated Amorphous Carbon (a-C) Films.

Electrochim. Acta **2016**, *220*. https://doi.org/10.1016/j.electacta.2016.10.063.
(254) Aasheim, E. T.; Hofsø, D.; Hjelmesæth, J.; Birkeland, K. I.; Bøhmer, T. Vitamin Status in Morbidly Obese Patients: A Cross-Sectional Study. *Am. J. Clin. Nutr.* **2008**, *87* (2), 362–369. https://doi.org/10.1093/ajcn/87.2.362.
(255) Nijst, T. Q.; Wevers, R. A.; Schoonderwaldt, H. C.; Hommes, O. R.; de Haan, A. F. Vitamin B12 and Folate Concentrations in Serum and Cerebrospinal Fluid of Neurological Patients with Special Reference to Multiple Sclerosis and Dementia. *J. Neurol. Neurosurg. Psychiatry* **1990**, *53* (11), 951–954. https://doi.org/10.1136/jnnp.53.11.951.
(256) Habibi, B.; Phezhhan, H.; Pournaghi-Azar, M. H. Voltammetric Determination of Vitamin B6 (Pyridoxine) Using Multi Wall Carbon Nanotube Modified Carbon-Ceramic Electrode. *J. Iran. Chem. Soc.* **2010**, *7* (S2), S103–S112. https://doi.org/10.1007/BF03246189.
(257) Xiao, F.; Ruan, C.; Liu, L.; Yan, R.; Zhao, F.; Zeng, B. Single-Walled Carbon Nanotube-Ionic Liquid Paste Electrode for the Sensitive Voltammetric Determination of Folic Acid. *Sensors Actuators B Chem.* **2008**, *134* (2), 895–901. https://doi.org/10.1016/j.snb.2008.06.037.
(258) Tabassi, A.; Salmasi, A. H.; Jalali, M. Serum and CSF Vitamin A Concentrations in Idiopathic Intracranial Hypertension. *Neurology* **2005**. https://doi.org/10.1212/01.WNL.0000163556.31080.98.
(259) Ziyatdinova, G.; Morozov, M.; Budnikov, H. MWNT-Modified Electrodes for Voltammetric Determination of Lipophilic Vitamins. *J. Solid State Electrochem.* **2012**, *16* (7), 2441–2447. https://doi.org/10.1007/s10008-011-1581-7.
(260) Balabanova, S.; Richter, H. P.; Antoniadis, G.; Homoki, J.; Kremmer, N.; Hanle, J.; Teller, W. M. 25-Hydroxyvitamin D, 24, 25-Dihydroxyvitamin D and 1,25-Dihydroxyvitamin D in Human Cerebrospinal Fluid. *Klin. Wochenschr.* **1984**. https://doi.org/10.1007/BF01711378.
(261) Hart, J. P.; Norman, M. D.; Lacey, C. J. Voltammetric Behaviour of Vitamins D2 and D3 at a Glassy Carbon Electrode and Their Determination in Pharmaceutical Products by Using Liquid Chromatography with Amperometric Detection. *Analyst* **1992**, *117* (9), 1441. https://doi.org/10.1039/an9921701441.
(262) Jiménez-Jiménez, F. J.; de Bustos, F.; Molina, J. A.; Benito-León, J.; Tallón-Barranco, A.; Gasalla, T.; Ortí-Pareja, M.; Guillamón, F.; Rubio, J. C.; Arenas, J.; et al. Cerebrospinal Fluid Levels of Alpha-Tocopherol (Vitamin E) in Alzheimer's Disease. *J. Neural Transm.* **1997**, *104* (6–7), 703–710. https://doi.org/10.1007/BF01291887.
(263) Filik, H.; Avan, A. A.; Aydar, S.; Çakar, Ş. Determination of Tocopherol Using Reduced Graphene Oxide-Nafion Hybrid-Modified Electrode in Pharmaceutical Capsules and Vegetable Oil Samples. *Food Anal. Methods* **2016**, *9* (6), 1745–1753. https://doi.org/10.1007/s12161-015-0353-x.
(264) Prescott, R. W. G.; Yeo, P. P. B.; Watson, M. J.; Johnston, I. D.; Ratcliffe, J. G.; Evered, D. C. Total and Free Thyroid Hormone Concentrations after Elective Surgery. *J. Clin. Pathol.* **1979**, *32* (4), 321–324. https://doi.org/10.1136/jcp.32.4.321.
(265) Hagen, G. A.; Elliott, W. J. Transport of Thyroid Hormones in Serum and Cerebrospinal Fluid. *J. Clin. Endocrinol. Metab.* **1973**. https://doi.org/10.1210/jcem-37-3-415.
(266) Das, A.; Sangaranarayanan, M. V. Electroanalytical Sensor Based on Unmodified Screen-Printed Carbon Electrode for the Determination of Levo-Thyroxine. *Electroanalysis* **2015**, *27* (2), 360–367. https://doi.org/10.1002/elan.201400395.
(267) Bäckström, T.; Carstensen, H.; Södergard, R. Concentration of Estradiol, Testosterone and Progesterone in Cerebrospinal Fluid Compared to Plasma Unbound and Total Concentrations. *J. Steroid Biochem.* **1976**. https://doi.org/10.1016/0022-4731(76)90114-X.
(268) Vega, D.; Agüí, L.; González-Cortés, A.; Yáñez-Sedeño, P.; Pingarrón, J. M. Electrochemical Detection of Phenolic Estrogenic Compounds at Carbon Nanotube-Modified Electrodes. *Talanta* **2007**, *71* (3), 1031–1038.

https://doi.org/10.1016/j.talanta.2006.05.071.
(269) Luo, L.; Li, F.; Zhu, L.; Ding, Y.; Deng, D. Electrochemical Sensing Platform of Natural Estrogens Based on the Poly(l-Proline)-Ordered Mesoporous Carbon Composite Modified Glassy Carbon Electrode. *Sensors Actuators B Chem.* **2013**, *187*, 78–83. https://doi.org/10.1016/j.snb.2012.09.056.
(270) Lorenz, W.; Seidel, W.; Doenicke, A.; Tauber, R.; Reimann, H. J.; Uhlig, R.; Mann, G.; Dormann, P.; Schmal, A.; H&#xFFFD;fner, G.; et al. Elevated Plasma Histamine Concentrations in Surgery: Causes and Clinical Significance. *Klin. Wochenschr.* **1974**, *52* (9), 419–425. https://doi.org/10.1007/BF01468582.
(271) Nishino, S.; Sakurai, E.; Nevsimalova, S.; Yoshida, Y.; Watanabe, T.; Yanai, K.; Mignot, E. Decreased CSF Histamine in Narcolepsy With and Without Low CSF Hypocretin-1 in Comparison to Healthy Controls. *Sleep* **2009**, *32* (2), 175–180. https://doi.org/10.1093/sleep/32.2.175.
(272) Sarada, B. V; Rao, T. N.; Tryk, D. A.; Fujishima, A. Electrochemical Oxidation of Histamine and Serotonin at Highly Boron-Doped Diamond Electrodes. *Anal. Chem.* **2000**, *72* (7), 1632–1638. https://doi.org/10.1021/ac9908748.
(273) Eldrup, E.; Mogensen, P.; Jacobsen, J.; Pakkenberg, H.; Christensen, N. J. CSF and Plasma Concentrations of Free Norepinephrine, Dopamine, 3,4-dihydroxyphenylacetic Acid (DOPAC), 3,4-dihydroxyphenylalanine (DOPA), and Epinephrine in Parkinson's Disease. *Acta Neurol. Scand.* **1995**. https://doi.org/10.1111/j.1600-0404.1995.tb01023.x.
(274) Nagaoka, S.; Iwamoto, N.; Arai, H. First-Episode Neuroleptic-Free Schizophrenics: Concentrations of Monoamines and Their Metabolites in Plasma and Their Correlations with Clinical Responses to Haloperidol Treatment. *Biol. Psychiatry* **1997**, *41* (8), 857–864. https://doi.org/10.1016/S0006-3223(96)00244-2.
(275) Sternson, A. W.; McCreery, R.; Feinberg, B.; Adams, R. N. Electrochemical Studies of Adrenergic Neurotrans-Mitters and Related Compounds. *J. Electroanal. Chem. Interfacial Electrochem.* **1973**, *46* (2), 313–321. https://doi.org/10.1016/S0022-0728(73)80139-1.
(276) Jimerson, D. C.; Lesem, M. D.; Kaye, W. H.; Brewerton, T. D. Low Serotonin and Dopamine Metabolite Concentrations in Cerebrospinal Fluid From Bulimic Patients With Frequent Binge Episodes. *Arch. Gen. Psychiatry* **1992**. https://doi.org/10.1001/archpsyc.1992.01820020052007.
(277) Peitzsch, M.; Mangelis, A.; Eisenhofer, G.; Huebner, A. Age-Specific Pediatric Reference Intervals for Plasma Free Normetanephrine, Metanephrine, 3-Methoxytyramine and 3-O-Methyldopa: Particular Importance for Early Infancy. *Clin. Chim. Acta* **2019**, *494* (January), 100–105. https://doi.org/10.1016/j.cca.2019.03.1620.
(278) Wester, P.; Bergström, U.; Eriksson, A.; Gezelius, C.; Hardy, J.; Winblad, B. Ventricular Cerebrospinal Fluid Monoamine Transmitter and Metabolite Concentrations Reflect Human Brain Neurochemistry in Autopsy Cases. *J. Neurochem.* **1990**. https://doi.org/10.1111/j.1471-4159.1990.tb01942.x.
(279) Steegmans, P. H. A.; Fekkes, D.; Hoes, A. W.; Bak, A. A. A.; van der Does, E.; Grobbee, D. E. Low Serum Cholesterol Concentration and Serotonin Metabolism in Men. *BMJ* **1996**, *312* (7025), 221–221. https://doi.org/10.1136/bmj.312.7025.221.
(280) Wurtman, R. J.; Rose, C. M.; Chou, C.; Larin, F. F. Daily Rhythms in the Concentrations of Various Amino Acids in Human Plasma. *N. Engl. J. Med.* **1968**, *279* (4), 171–175. https://doi.org/10.1056/NEJM196807252790401.
(281) Kaya, M.; Moriwaki, Y.; Ka, T.; Inokuchi, T.; Yamamoto, A.; Takahashi, S.; Tsutsumi, Z.; Tsuzita, J.; Oku, Y.; Yamamoto, T. Plasma Concentrations and Urinary Excretion of Purine Bases (Uric Acid, Hypoxanthine, and Xanthine) and Oxypurinol after Rigorous Exercise. *Metabolism* **2006**, *55* (1), 103–107. https://doi.org/10.1016/j.metabol.2005.07.013.
(282) Grünewald, R. A. Ascorbic Acid in the Brain. *Brain Res. Rev.* **1993**, *18* (1), 123–133. https://doi.org/10.1016/0165-0173(93)90010-W.

(283) Pisoschi, A. M.; Pop, A. The Role of Antioxidants in the Chemistry of Oxidative Stress: A Review. *Eur. J. Med. Chem.* **2015**, *97*, 55–74. https://doi.org/10.1016/j.ejmech.2015.04.040.
(284) Kohen, R.; Nyska, A. Invited Review: Oxidation of Biological Systems: Oxidative Stress Phenomena, Antioxidants, Redox Reactions, and Methods for Their Quantification. *Toxicol. Pathol.* **2002**, *30* (6), 620–650. https://doi.org/10.1080/01926230290166724.
(285) Rice, M. E. Ascorbate Regulation and Its Neuroprotective Role in the Brain. *Trends Neurosci.* **2000**, *23* (5), 209–216. https://doi.org/10.1016/S0166-2236(99)01543-X.
(286) Harrison, F. E.; May, J. M. Vitamin C Function in the Brain: Vital Role of the Ascorbate Transporter SVCT2. *Free Radic. Biol. Med.* **2009**, *46* (6), 719–730. https://doi.org/10.1016/j.freeradbiomed.2008.12.018.
(287) Agus, D. B.; Gambhir, S. S.; Pardridge, W. M.; Spielholz, C.; Baselga, J.; Vera, J. C.; Golde, D. W. Vitamin C Crosses the Blood-Brain Barrier in the Oxidized Form through the Glucose Transporters. *J. Clin. Invest.* **1997**, *100* (11), 2842–2848. https://doi.org/10.1172/JCI119832.
(288) Ewing, A. G.; Wightman, R. M.; Dayton, M. A. In Vivo Voltammetry with Electrodes That Discriminate between Dopamine and Ascorbate. *Brain Res.* **1982**, *249* (2), 361–370. https://doi.org/10.1016/0006-8993(82)90070-1.
(289) Chen, X.; Zhu, J.; Xi, Q.; Yang, W. A High Performance Electrochemical Sensor for Acetaminophen Based on Single-Walled Carbon Nanotube–Graphene Nanosheet Hybrid Films. *Sensors Actuators B Chem.* **2012**, *161* (1), 648–654. https://doi.org/10.1016/j.snb.2011.10.085.
(290) Taei, M.; Hasanpour, F.; Hajhashemi, V.; Movahedi, M.; Baghlani, H. Simultaneous Detection of Morphine and Codeine in Urine Samples of Heroin Addicts Using Multi-Walled Carbon Nanotubes Modified SnO2-Zn2SnO4 Nanocomposites Paste Electrode. *Appl. Surf. Sci.* **2016**, *363*, 490–498. https://doi.org/10.1016/j.apsusc.2015.12.074.
(291) Robitaille, L.; Hoffer, L. J. A Simple Method for Plasma Total Vitamin C Analysis Suitable for Routine Clinical Laboratory Use. *Nutr. J.* **2015**, *15* (1), 40. https://doi.org/10.1186/s12937-016-0158-9.
(292) Ruiz, J. J.; Rodríguez-Mellado, J. M.; Domínguez, M.; Aldaz, A. New Aspects of the Oxidation-Reduction Mechanism of the Ascorbic-Dehydroascorbic Acid System on the Dropping Mercury Electrode. *J. Chem. Soc. Faraday Trans. 1 Phys. Chem. Condens. Phases* **1989**. https://doi.org/10.1039/F19898501567.
(293) Liao, M. L.; Seib, P. A. Chemistry of L-Ascorbic Acid Related to Foods. *Food Chem.* **1988**. https://doi.org/10.1016/0308-8146(88)90115-X.
(294) Deakin, M. R.; Kovach, P. M.; Stutts, K. J.; Wightman, R. M. Heterogeneous Mechanisms of the Oxidation of Catechols and Ascorbic Acid at Carbon Electrodes. *Anal. Chem.* **1986**, *58* (7), 1474–1480. https://doi.org/10.1021/ac00298a046.
(295) Prieto, F.; Coles, B. A.; Compton, R. G. Mechanistic Determination Using Arrays of Variable-Sized Channel Microband Electrodes: The Oxidation of Ascorbic Acid in Aqueous Solution. *J. Phys. Chem. B* **1998**, *102* (38), 7442–7447. https://doi.org/10.1021/jp982080n.
(296) Perone, S. P.; Kretlow, W. J. Application of Controlled Potential Techniques to Study of Rapid Succeeding Chemical Reaction Coupled to Electro-Oxidation of Ascorbic Acid. *Anal. Chem.* **1966**, *38* (12), 1760–1763. https://doi.org/10.1021/ac60244a034.
(297) de Oliveira, E. P.; Burini, R. C. High Plasma Uric Acid Concentration: Causes and Consequences. *Diabetol. Metab. Syndr.* **2012**, *4* (1), 12. https://doi.org/10.1186/1758-5996-4-12.
(298) Terkeltaub, R.; Bushinsky, D. A.; Becker, M. A. Recent Developments in Our Understanding of the Renal Basis of Hyperuricemia and the Development of Novel Antihyperuricemic Therapeutics. *Arthritis Res. Ther.* **2006**, *8* (SUPPL. 1), 1–9. https://doi.org/https://doi.org/10.1186/ar1909.
(299) Liebman, S. E.; Taylor, J. G.; Bushinsky, D. A. Uric Acid Nephrolithiasis. *Curr. Rheumatol. Rep.* **2007**, *9* (3), 251–257. https://doi.org/10.1007/s11926-007-0040-z.

(300) Yiğit, A.; Yardım, Y.; Çelebi, M.; Levent, A.; Şentürk, Z. Graphene/Nafion Composite Film Modified Glassy Carbon Electrode for Simultaneous Determination of Paracetamol, Aspirin and Caffeine in Pharmaceutical Formulations. *Talanta* **2016**, *158*, 21–29. https://doi.org/10.1016/j.talanta.2016.05.046.
(301) Dryhurst, G. Electrochemical Oxidation of Uric Acid and Xanthine at the Pyrolytic Graphite Electrode. *J. Electrochem. Soc.* **1972**, *119* (12), 1659. https://doi.org/10.1149/1.2404066.
(302) Owens, J. Electrochemical Oxidation of Uric Acid and Xanthine An Investigation by Cyclic Voltammetry, Double Potential Step Chronoamperometry and Thin-Layer Spectroelectrochemistry. *J. Electroanal. Chem.* **1978**, *91* (2), 231–247. https://doi.org/10.1016/0368-1874(78)85094-1.
(303) Goyal, R. N.; Brajter-Toth, A.; Dryhurst, G. Futher Insights into the Electrochemical Oxidation of Uric Acid. *J. Electroanal. Chem. Interfacial Electrochem.* **1982**, *131*, 181–202. https://doi.org/10.1016/0022-0728(82)87070-8.
(304) Struck, W. A.; Elving, P. J. Electrolytic Oxidation of Uric Acid: Products and Mechanism *. *Biochemistry* **1965**, *4* (7), 1343–1353. https://doi.org/10.1021/bi00883a019.
(305) Urbańczyk, E.; Sowa, M.; Simka, W. Urea Removal from Aqueous Solutions—a Review. *J. Appl. Electrochem.* **2016**, *46* (10), 1011–1029. https://doi.org/10.1007/s10800-016-0993-6.
(306) Malfoy, B.; Reynaud, J. A. Electrochemical Investigations of Amino Acids at Solid Electrodes. Part II. Amino Acids Containing No Sulfur Atoms: Tryptophan, Tyrosine, Histidine and Derivatives. *J. Electroanal. Chem.* **1980**. https://doi.org/10.1016/S0022-0728(80)80448-7.
(307) Paleček, E.; Tkáč, J.; Bartošík, M.; Bertók, T.; Ostatná, V.; Paleček, J. Electrochemistry of Nonconjugated Proteins and Glycoproteins. Toward Sensors for Biomedicine and Glycomics. *Chem. Rev.* **2015**, *115* (5), 2045–2108. https://doi.org/10.1021/cr500279h.
(308) Ostatná, V.; Černocká, H.; Kurzątkowska, K.; Paleček, E. Native and Denatured Forms of Proteins Can Be Discriminated at Edge Plane Carbon Electrodes. *Anal. Chim. Acta* **2012**, *735*, 31–36. https://doi.org/10.1016/j.aca.2012.05.012.
(309) Permentier, H. P.; Bruins, A. P. Electrochemical Oxidation and Cleavage of Proteins with On-Line Mass Spectrometric Detection: Development of an Instrumental Alternative to Enzymatic Protein Digestion. *J. Am. Soc. Mass Spectrom.* **2004**, *15* (12), 1707–1716. https://doi.org/10.1016/j.jasms.2004.09.003.
(310) Permentier, H. P.; Jurva, U.; Barroso, B.; Bruins, A. P. Electrochemical Oxidation and Cleavage of Peptides Analyzed with On-Line Mass Spectrometric Detection. *Rapid Commun. Mass Spectrom.* **2003**, *17* (14), 1585–1592. https://doi.org/10.1002/rcm.1090.
(311) Sikdar, S. K. Amino Acid Transport from Aqueous Solutions by a Perfluorosulfonic Acid Membrane. *J. Memb. Sci.* **1985**. https://doi.org/10.1016/S0376-7388(00)83208-1.
(312) Gupta, V. K.; Jain, R.; Radhapyari, K.; Jadon, N.; Agarwal, S. Voltammetric Techniques for the Assay of Pharmaceuticals—A Review. *Anal. Biochem.* **2011**, *408* (2), 179–196. https://doi.org/10.1016/j.ab.2010.09.027.
(313) Abo El-Maali, N. Voltammetric Analysis of Drugs. *Bioelectrochemistry* **2004**, *64* (1), 99–107. https://doi.org/10.1016/j.bioelechem.2004.03.003.
(314) Roth, H.; Romero, N.; Nicewicz, D. Experimental and Calculated Electrochemical Potentials of Common Organic Molecules for Applications to Single-Electron Redox Chemistry. *Synlett* **2015**, *27* (05), 714–723. https://doi.org/10.1055/s-0035-1561297.
(315) Lawton, K. A.; Berger, A.; Mitchell, M.; Milgram, K. E.; Evans, A. M.; Guo, L.; Hanson, R. W.; Kalhan, S. C.; Ryals, J. A.; Milburn, M. V. Analysis of the Adult Human Plasma Metabolome. *Pharmacogenomics* **2008**, *9* (4), 383–397. https://doi.org/10.2217/14622416.9.4.383.
(316) Weinberg, N. L.; Weinberg, H. R. Electrochemical Oxidation of Organic Compounds.

Chem. Rev. **1968**, *68* (4), 449–523. https://doi.org/10.1021/cr60254a003.
(317) Kawamata, Y.; Yan, M.; Liu, Z.; Bao, D.-H.; Chen, J.; Starr, J. T.; Baran, P. S. Scalable, Electrochemical Oxidation of Unactivated C–H Bonds. *J. Am. Chem. Soc.* **2017**, *139* (22), 7448–7451. https://doi.org/10.1021/jacs.7b03539.
(318) Brennan, M. P. J.; Brown, O. R. Carbon Electrodes: Part 2. The Anodic Oxidation of N-Propylamine. *J. Appl. Electrochem.* **1973**, *3* (3), 231–239. https://doi.org/10.1007/BF00619166.
(319) Masui, M.; Sayo, H.; Tsuda, Y. Anodic Oxidation of Amines. Part I. Cyclic Voltammetry of Aliphatic Amines at a Stationary Glassy-Carbon Electrode. *J. Chem. Soc. B Phys. Org.* **1968**, 973. https://doi.org/10.1039/j29680000973.
(320) Bacon, J.; Adams, R. N. Anodic Oxidations of Aromatic Amines. III. Substituted Anilines in Aqueous Media. *J. Am. Chem. Soc.* **1968**, *90* (24), 6596–6599. https://doi.org/10.1021/ja01026a005.
(321) Garrido, E. .; Lima, J. L. F. .; Delerue-Matos, C.; Borges, F.; Silva, A. M. .; Brett, A. M. O. Electrochemical Oxidation of Propanil and Related N-Substituted Amides. *Anal. Chim. Acta* **2001**, *434* (1), 35–41. https://doi.org/10.1016/S0003-2670(01)00817-0.
(322) Garrido, J. M. P. J.; Delerue-Matos, C.; Borges, F.; Macedo, T. R. A.; Oliveira-Brett, A. M. Voltammetric Oxidation of Drugs of Abuse I. Morphine and Metabolites. *Electroanalysis* **2004**, *16* (17), 1419–1426. https://doi.org/10.1002/elan.200302966.
(323) Garrido, J. M. P. J.; Delerue-Matos, C.; Borges, F.; Macedo, T. R. A.; Oliveira-Brett, A. M. Voltammetric Oxidation of Drugs of Abuse II. Codeine and Metabolites. *Electroanalysis* **2004**, *16* (17), 1427–1433. https://doi.org/10.1002/elan.200302967.
(324) Garrido, J. M. P. J.; Delerue-matos, C.; Borges, F.; Macedo, T. R. A.; Oliveira-brett, A. M. Voltammetric Oxidation of Drugs of Abuse III . Heroin and Metabolites. **2004**, 1497–1502. https://doi.org/10.1002/elan.200302975.
(325) Mynttinen, E.; Wester, N.; Lilius, T.; Kalso, E.; Mikladal, B.; Varjos, I.; Sainio, S.; Jiang, H.; Kauppinen, E. I.; Koskinen, J.; et al. Electrochemical Detection of Oxycodone and Its Main Metabolites with Nafion-Coated Single-Walled Carbon Nanotube Electrodes. *Anal. Chem.* **2020**, acs.analchem.0c00450. https://doi.org/10.1021/acs.analchem.0c00450.
(326) Petek, M.; Bruckenstein, S.; Feinberg, B.; Adams, R. N. Anodic Oxidation of Substituted Methoxyphenols. Mass Spectrometric Identification of Methanol Formed. *J. Electroanal. Chem.* **1973**. https://doi.org/10.1016/S0022-0728(73)80328-6.
(327) Pelzer, K. M.; Cheng, L.; Curtiss, L. A. Effects of Functional Groups in Redox-Active Organic Molecules: A High-Throughput Screening Approach. *J. Phys. Chem. C* **2017**, *121* (1), 237–245. https://doi.org/10.1021/acs.jpcc.6b11473.
(328) Nematollahi, D.; Shayani-Jam, H.; Alimoradi, M.; Niroomand, S. Electrochemical Oxidation of Acetaminophen in Aqueous Solutions: Kinetic Evaluation of Hydrolysis, Hydroxylation and Dimerization Processes. *Electrochim. Acta* **2009**, *54* (28), 7407–7415. https://doi.org/10.1016/j.electacta.2009.07.077.
(329) Van Benschoten, J. J.; Lewis, J. Y.; Heineman, W. R.; Roston, D. A.; Kissinger, P. T. Cyclic Voltammetry Experiment. *J. Chem. Educ.* **1983**, *60* (9), 772. https://doi.org/10.1021/ed060p772.
(330) Saitman, A.; Park, H.-D.; Fitzgerald, R. L. False-Positive Interferences of Common Urine Drug Screen Immunoassays: A Review. *J. Anal. Toxicol.* **2014**, *38* (7), 387–396. https://doi.org/10.1093/jat/bku075.
(331) Tritsch, N. X.; Sabatini, B. L. Dopaminergic Modulation of Synaptic Transmission in Cortex and Striatum. *Neuron* **2012**, *76* (1), 33–50. https://doi.org/10.1016/j.neuron.2012.09.023.
(332) Beaulieu, J.-M.; Gainetdinov, R. R. The Physiology, Signaling, and Pharmacology of Dopamine Receptors. *Pharmacol. Rev.* **2011**, *63* (1), 182–217. https://doi.org/10.1124/pr.110.002642.
(333) Bear, M. F.; Connors, B. W.; Paradiso, M. A. *Neuroscience: Exploring the Brain (3rd Ed.)*.; 2007.
(334) Robinson, D. L.; Phillips, P. E. M.; Budygin, E. A.; Trafton, B. J.; Garris, P. A.;

Wightman, R. M. Sub-Second Changes in Accumbal Dopamine during Sexual Behavior in Male Rats. *Neuroreport* **2001**, *12* (11), 2549–2552. https://doi.org/10.1097/00001756-200108080-00051.
(335) Robinson, D. L.; Heien, M. L. A. V.; Wightman, R. M. Frequency of Dopamine Concentration Transients Increases in Dorsal and Ventral Striatum of Male Rats during Introduction of Conspecifics. *J. Neurosci.* **2002**, *22* (23), 10477–10486. https://doi.org/10.1523/JNEUROSCI.22-23-10477.2002.
(336) Suzuki, A.; Ivandini, T. A.; Yoshimi, K.; Fujishima, A.; Oyama, G.; Nakazato, T.; Hattori, N.; Kitazawa, S.; Einaga, Y. Fabrication, Characterization, and Application of Boron-Doped Diamond Microelectrodes for in Vivo Dopamine Detection. *Anal. Chem.* **2007**, *79* (22), 8608–8615. https://doi.org/10.1021/ac071519h.
(337) Zhang, M.; Liu, K.; Xiang, L.; Lin, Y.; Su, L.; Mao, L. Carbon Nanotube-Modified Carbon Fiber Microelectrodes for in Vivo Voltammetric Measurement of Ascorbic Acid in Rat Brain. *Anal. Chem.* **2007**, *79* (17), 6559–6565. https://doi.org/10.1021/ac0705871.
(338) Yoshimi, K.; Naya, Y.; Mitani, N.; Kato, T.; Inoue, M.; Natori, S.; Takahashi, T.; Weitemier, A.; Nishikawa, N.; McHugh, T.; et al. Phasic Reward Responses in the Monkey Striatum as Detected by Voltammetry with Diamond Microelectrodes. *Neurosci. Res.* **2011**, *71* (1), 49–62. https://doi.org/10.1016/j.neures.2011.05.013.
(339) Mefford, I. N. Application of High Performance Liquid Chromatography with Electrochemical Detection to Neurochemical Analysis: Measurement of Catecholamines, Serotonin and Metabolites in Rat Brain. *J. Neurosci. Methods* **1981**, *3* (3), 207–224. https://doi.org/10.1016/0165-0270(81)90056-X.
(340) Laruelle, M. Imaging Synaptic Neurotransmission with in Vivo Binding Competition Techniques: A Critical Review. *J. Cereb. Blood Flow Metab.* **2000**, *20* (3), 423–451. https://doi.org/10.1097/00004647-200003000-00001.
(341) Glover, G. H. Overview of Functional Magnetic Resonance Imaging. *Neurosurg. Clin. N. Am.* **2011**, *22* (2), 133–139. https://doi.org/10.1016/j.nec.2010.11.001.
(342) Chefer, V. I.; Thompson, A. C.; Zapata, A.; Shippenberg, T. S. Overview of Brain Microdialysis. *Curr. Protoc. Neurosci.* **2009**, *47* (1), 7.1.1-7.1.28. https://doi.org/10.1002/0471142301.ns0701s47.
(343) Borland, L. M.; Shi, G.; Yang, H.; Michael, A. C. Voltammetric Study of Extracellular Dopamine near Microdialysis Probes Acutely Implanted in the Striatum of the Anesthetized Rat. *J. Neurosci. Methods* **2005**, *146* (2), 149–158. https://doi.org/10.1016/j.jneumeth.2005.02.002.
(344) Zachek, M. K.; Takmakov, P.; Moody, B.; Wightman, R. M.; McCarty, G. S. Simultaneous Decoupled Detection of Dopamine and Oxygen Using Pyrolyzed Carbon Microarrays and Fast-Scan Cyclic Voltammetry. *Anal. Chem.* **2009**, *81* (15), 6258–6265. https://doi.org/10.1021/ac900790m.
(345) Zachek, M. K.; Park, J.; Takmakov, P.; Wightman, R. M.; McCarty, G. S. Microfabricated FSCV-Compatible Microelectrode Array for Real-Time Monitoring of Heterogeneous Dopamine Release. *Analyst* **2010**, *135* (7), 1556. https://doi.org/10.1039/c0an00114g.
(346) Marsh, M. P.; Koehne, J. E.; Andrews, R. J.; Meyyappan, M.; Bennet, K. E.; Lee, K. H. Carbon Nanofiber Multiplexed Array and Wireless Instantaneous Neurotransmitter Concentration Sensor for Simultaneous Detection of Dissolved Oxygen and Dopamine. *Biomed. Eng. Lett.* **2012**, *2* (4), 271–277. https://doi.org/10.1007/s13534-012-0081-8.
(347) Jackowska, K.; Krysinski, P. New Trends in the Electrochemical Sensing of Dopamine. *Anal. Bioanal. Chem.* **2013**, *405* (11), 3753–3771. https://doi.org/10.1007/s00216-012-6578-2.
(348) Dursun, Z.; Gelmez, B. Simultaneous Determination of Ascorbic Acid, Dopamine and Uric Acid at Pt Nanoparticles Decorated Multiwall Carbon Nanotubes Modified GCE. *Electroanalysis* **2010**, *22* (10), 1106–1114. https://doi.org/10.1002/elan.200900525.
(349) Zheng, D.; Ye, J.; Zhou, L.; Zhang, Y.; Yu, C. Simultaneous Determination of Dopamine, Ascorbic Acid and Uric Acid on Ordered Mesoporous Carbon/Nafion

Composite Film. *J. Electroanal. Chem.* **2009**, *625* (1), 82–87. https://doi.org/10.1016/j.jelechem.2008.10.012.
(350) Sun, C.-L.; Lee, H.-H.; Yang, J.-M.; Wu, C.-C. The Simultaneous Electrochemical Detection of Ascorbic Acid, Dopamine, and Uric Acid Using Graphene/Size-Selected Pt Nanocomposites. *Biosens. Bioelectron.* **2011**, *26* (8), 3450–3455. https://doi.org/10.1016/j.bios.2011.01.023.
(351) Schmitt, G.; Faßbender, F.; Lüth, H.; Schöning, M. J.; Schultze, J.-W.; Buß, G. Passivation and Corrosion of Microelectrode Arrays. *Mater. Corros.* **2000**, *51* (1), 20–25. https://doi.org/10.1002/(SICI)1521-4176(200001)51:1<20::AID-MACO20>3.0.CO;2-Q.
(352) Mueller, K. In Vivo Voltammetric Recording with Nafion-Coated Carbon Paste Electrodes: Additional Evidence That Ascorbic Acid Release Is Monitored. *Pharmacol. Biochem. Behav.* **1986**, *25* (2), 325–328. https://doi.org/10.1016/0091-3057(86)90003-1.
(353) Gonon, F.; Buda, M.; Cespuglio, R.; Jouvet, M.; Pujol, J.-F. In Vivo Electrochemical Detection of Catechols in the Neostriatum of Anaesthetized Rats: Dopamine or DOPAC? *Nature* **1980**, *286* (5776), 902–904. https://doi.org/10.1038/286902a0.
(354) Smith, A. D.; Olson, R. J.; Justice, J. B. Quantitative Microdialysis of Dopamine in the Striatum: Effect of Circadian Variation. *J. Neurosci. Methods* **1992**, *44* (1), 33–41. https://doi.org/10.1016/0165-0270(92)90111-P.
(355) Gerhardt, G. A.; Oke, A. F.; Nagy, G.; Moghaddam, B.; Adams, R. N. Nafion-Coated Electrodes with High Selectivity for CNS Electrochemistry. *Brain Res.* **1984**, *290* (2), 390–395. https://doi.org/10.1016/0006-8993(84)90963-6.
(356) Nagy, G.; Gerhardt, G. A.; Oke, A. F.; Rice, M. E.; Adams, R. N.; Moore, R. B.; Szentirmay, M. N.; Martin, C. R. Ion Exchange and Transport of Neurotransmitters in Nafion Films on Conventional and Microelectrode Surfaces. *J. Electroanal. Chem.* **1985**, *189* (1), 85–94. https://doi.org/10.1016/0368-1874(85)85629-X.
(357) Laviron, E. Electrochemical Reactions with Protonations at Equilibrium Part X. The Kinetics of the p-Benzoquinone/Hydroquinone Couple on a Platinum Electrode. *J. Electroanal. Chem.* **1984**, *164* (2), 213–227. https://doi.org/10.1016/0368-1874(84)83390-0.
(358) Deakin, M. R.; Wightman, R. M. The Kinetics of Some Substituted Catechol/o-Quinone Couples at a Carbon Paste Electrode. *J. Electroanal. Chem. Interfacial Electrochem.* **1986**, *206* (1–2), 167–177. https://doi.org/10.1016/0022-0728(86)90266-4.
(359) Hawley, M. D.; Tatawawadi, S. V.; Piekarski, S.; Adams, R. N. Electrochemical Studies of the Oxidation Pathways of Catecholamines. *J. Am. Chem. Soc.* **1967**, *89* (2), 447–450. https://doi.org/10.1021/ja00978a051.
(360) Tse, D. C. S.; McCreery, R. L.; Adams, R. N. Potential Oxidative Pathways of Brain Catecholamines. *J. Med. Chem.* **1976**, *19* (1), 37–40. https://doi.org/10.1021/jm00223a008.
(361) Saraji, M.; Bagheri, A. Electropolymerization of Indole and Study of Electrochemical Behavior of the Polymer in Aqueous Solutions. *Synth. Met.* **1998**, *98* (1), 57–63. https://doi.org/10.1016/S0379-6779(98)00151-9.
(362) Moeller, K. E.; Lee, K. C.; Kissack, J. C. Urine Drug Screening: Practical Guide for Clinicians. *Mayo Clin. Proc.* **2008**, *83* (1), 66–76. https://doi.org/10.4065/83.1.66.
(363) Hammett-Stabler, C. A.; Pesce, A. J.; Cannon, D. J. Urine Drug Screening in the Medical Setting. *Clin. Chim. Acta* **2002**, *315* (1–2), 125–135. https://doi.org/10.1016/S0009-8981(01)00714-8.
(364) Mahato, K.; Srivastava, A.; Chandra, P. Paper Based Diagnostics for Personalized Health Care: Emerging Technologies and Commercial Aspects. *Biosens. Bioelectron.* **2017**, *96* (February), 246–259. https://doi.org/10.1016/j.bios.2017.05.001.
(365) Lum, G.; Mushlin, B. Urine Drug Testing: Approaches to Screening and Confirmation Testing. *Lab. Med.* **2004**, *35* (6), 368–373. https://doi.org/10.1309/QHJCKA4235EGPEGF.

(366) Drummer, O. H. Review: Pharmacokinetics of Illicit Drugs in Oral Fluid. *Forensic Sci. Int.* **2005**, *150* (2–3), 133–142. https://doi.org/10.1016/j.forsciint.2004.11.022.
(367) Cone, E. J. Testing Human Hair for Drugs of Abuse. I. Individual Dose and Time Profiles of Morphine and Codeine in Plasma, Saliva, Urine, and Beard Compared to Drug-Induced Effects on Pupils and Behavior*. *J. Anal. Toxicol.* **1990**, *14* (1), 1–7. https://doi.org/10.1093/jat/14.1.1.
(368) Verplaetse, R.; Henion, J. Quantitative Determination of Opioids in Whole Blood Using Fully Automated Dried Blood Spot Desorption Coupled to On-Line SPE-LC-MS/MS. *Drug Test. Anal.* **2016**, *8* (1), 30–38. https://doi.org/10.1002/dta.1927.
(369) O'Neal, C. L.; Crouch, D. J.; Rollins, D. E.; Fatah, A.; Cheever, M. L. Correlation of Saliva Codeine Concentrations with Plasma Concentrations after Oral Codeine Administration. *J. Anal. Toxicol.* **1999**, *23* (6), 452–459. https://doi.org/10.1093/jat/23.6.452.
(370) Rittau, A. M.; McLachlan, A. J. Investigating Paracetamol Pharmacokinetics Using Venous and Capillary Blood and Saliva Sampling. *J. Pharm. Pharmacol.* **2012**, *64* (5), 705–711. https://doi.org/10.1111/j.2042-7158.2012.01459.x.
(371) Elmongy, H.; Abdel-Rehim, M. Saliva as an Alternative Specimen to Plasma for Drug Bioanalysis: A Review. *TrAC Trends Anal. Chem.* **2016**, *83*, 70–79. https://doi.org/10.1016/j.trac.2016.07.010.
(372) O'Neal, C. L.; Crouch, D. J.; Rollins, D. E.; Fatah, A. A. The Effects of Collection Methods On Oral Fluid Codeine Concentrations. *J. Anal. Toxicol.* **2000**, *24* (7), 536–542. https://doi.org/10.1093/jat/24.7.536.
(373) Drummer, O. H. Drug Testing in Oral Fluid. *Clin. Biochem. Rev.* **2006**.
(374) Tang, R.; Yang, H.; Choi, J. R.; Gong, Y.; You, M.; Wen, T.; Li, A.; Li, X.; Xu, B.; Zhang, S.; et al. Capillary Blood for Point-of-Care Testing. *Crit. Rev. Clin. Lab. Sci.* **2017**, *54* (5), 294–308. https://doi.org/10.1080/10408363.2017.1343796.
(375) Bond, M. M.; Richards-Kortum, R. R. Drop-to-Drop Variation in the Cellular Components of Fingerprick Blood. *Am. J. Clin. Pathol.* **2015**, *144* (6), 885–894. https://doi.org/10.1309/AJCP1L7DKMPCHPEH.
(376) Yum, S. Il; Roe, J. Capillary Blood Sampling for Self-Monitoring of Blood Glucose. *Diabetes Technol. Ther.* **1999**, *1* (1), 29–37. https://doi.org/10.1089/152091599317549.
(377) Kuwa, K.; Nakayama, T.; Hoshino, T.; Tominaga, M. Relationships of Glucose Concentrations in Capillary Whole Blood, Venous Whole Blood and Venous Plasma. *Clin. Chim. Acta* **2001**, *307* (1–2), 187–192. https://doi.org/10.1016/S0009-8981(01)00426-0.
(378) Loughrey, C. M.; Hanna, E. V.; McDonnell, M.; Archbold, G. P. Sodium Measurement: Effects of Differing Sampling and Analytical Methods. *Ann. Clin. Biochem.* **2006**, *43* (6), 488–493. https://doi.org/10.1258/000456306778904560.
(379) Kupke, I. R.; Kather, B.; Zeugner, S. On the Composition of Capillary and Venous Blood Serum. *Clin. Chim. Acta* **1981**. https://doi.org/10.1016/0009-8981(81)90376-4.
(380) Brahman, P. K.; Suresh, L.; Lokesh, V.; Nizamuddin, S. Fabrication of Highly Sensitive and Selective Nanocomposite Film Based on CuNPs/Fullerene-C60/MWCNTs: An Electrochemical Nanosensor for Trace Recognition of Paracetamol. *Anal. Chim. Acta* **2016**, *917*, 107–116. https://doi.org/10.1016/j.aca.2016.02.044.
(381) Graham, G. G.; Davies, M. J.; Day, R. O.; Mohamudally, A.; Scott, K. F. The Modern Pharmacology of Paracetamol: Therapeutic Actions, Mechanism of Action, Metabolism, Toxicity and Recent Pharmacological Findings. *Inflammopharmacology* **2013**, *21* (3), 201–232. https://doi.org/10.1007/s10787-013-0172-x.
(382) Mazaleuskaya, L. L.; Sangkuhl, K.; Thorn, C. F.; FitzGerald, G. A.; Altman, R. B.; Klein, T. E. PharmGKB Summary. *Pharmacogenet. Genomics* **2015**, *25* (8), 416–426. https://doi.org/10.1097/FPC.0000000000000150.
(383) Rowden, A. K.; Norvell, J.; Eldridge, D. L.; Kirk, M. A. Updates on Acetaminophen Toxicity. *Med. Clin. North Am.* **2005**, *89* (6), 1145–1159. https://doi.org/10.1016/j.mcna.2005.06.009.

(384) Rumack, B. H.; Matthew, H. Acetaminophen Poisoning and Toxicity. *Pediatrics* **1975**, *55* (6), 871–876.
(385) Rumack, B. H. Acetaminophen Hepatotoxicity: The First 35 Years. *J. Toxicol. - Clin. Toxicol.* **2002**, *40* (1), 3–20. https://doi.org/10.1081/CLT-120002882.
(386) Hullin, D. A. An IgM Paraprotein Causing a Falsely Low Result in an Enzymatic Assay for Acetaminophen. *Clin. Chem.* **1999**, *45* (1), 155–156. https://doi.org/10.1093/clinchem/45.1.155.
(387) Rawlins, M. D.; Henderson, D. B.; Hijab, A. R. Pharmacokinetics of Paracetamol (Acetaminophen) after Intravenous and Oral Administration. *Eur. J. Clin. Pharmacol.* **1977**. https://doi.org/10.1007/BF00607678.
(388) Singla, N. K.; Parulan, C.; Samson, R.; Hutchinson, J.; Bushnell, R.; Beja, E. G.; Ang, R.; Royal, M. A. Plasma and Cerebrospinal Fluid Pharmacokinetic Parameters After Single-Dose Administration of Intravenous, Oral, or Rectal Acetaminophen. *Pain Pract.* **2012**, *12* (7), 523–532. https://doi.org/10.1111/j.1533-2500.2012.00556.x.
(389) Miner, D. J.; Rice, J. R.; Riggin, R. M.; Kissinger, P. T. Voltammetry of Acetaminophen and Its Metabolites. *Anal. Chem.* **1981**, *53* (14), 2258–2263. https://doi.org/10.1021/ac00237a029.
(390) Baranowska, I.; Koper, M. The Preliminary Studies of Electrochemical Behavior of Paracetamol and Its Metabolites on Glassy Carbon Electrode by Voltammetric Methods. *Electroanalysis* **2009**, *21* (10), 1194–1199. https://doi.org/10.1002/elan.200804536.
(391) Mayer, M.; Salpeter, L. More on Interference of N-Acetylcysteine in Measurement of Acetaminophen. *Clin. Chem.* **1998**, *44* (4), 892–893. https://doi.org/10.1093/clinchem/44.4.892.
(392) Schmidt, L. E.; Dalhoff, K. Concomitant Overdosing of Other Drugs in Patients with Paracetamol Poisoning. *Br. J. Clin. Pharmacol.* **2002**, *53* (5), 535–541. https://doi.org/10.1046/j.1365-2125.2002.01564.x.
(393) Drummer, O. H. Postmortem Toxicology of Drugs of Abuse. *Forensic Sci. Int.* **2004**, *142* (2–3), 101–113. https://doi.org/10.1016/j.forsciint.2004.02.013.
(394) Calcaterra, S.; Glanz, J.; Binswanger, I. A. National Trends in Pharmaceutical Opioid Related Overdose Deaths Compared to Other Substance Related Overdose Deaths: 1999–2009. *Drug Alcohol Depend.* **2013**, *131* (3), 263–270. https://doi.org/10.1016/j.drugalcdep.2012.11.018.
(395) Cone, E. J.; Fant, R. V.; Rohay, J. M.; Caplan, Y. H.; Ballina, M.; Reder, R. F.; Haddox, J. D. Oxycodone Involvement in Drug Abuse Deaths. II. Evidence for Toxic Multiple Drug-Drug Interactions. *J. Anal. Toxicol.* **2004**, *28* (7), 616–624. https://doi.org/10.1093/jat/28.7.616.
(396) Wester, Niklas, Elsi Mynttinen, and T. L. Electrochemical Assay for the Detection of Opioids U.S. Patent Application No. 16/495,546.
(397) Abraham, P.; S, R.; Vijayan, P.; V, N.; Sreevalsan, K.; Anithakumary, V. Review—Review on the Progress in Electrochemical Detection of Morphine Based on Different Modified Electrodes. *J. Electrochem. Soc.* **2020**, *167* (3), 037559. https://doi.org/10.1149/1945-7111/ab6cf6.
(398) Sajid, M.; Nazal, M. K.; Mansha, M.; Alsharaa, A.; Jillani, S. M. S.; Basheer, C. Chemically Modified Electrodes for Electrochemical Detection of Dopamine in the Presence of Uric Acid and Ascorbic Acid: A Review. *TrAC Trends Anal. Chem.* **2016**, *76*, 15–29. https://doi.org/10.1016/j.trac.2015.09.006.
(399) Peltola, E.; Heikkinen, J. J.; Sovanto, K.; Sainio, S.; Aarva, A.; Franssila, S.; Jokinen, V.; Laurila, T. SU-8 Based Pyrolytic Carbon for the Electrochemical Detection of Dopamine. *J. Mater. Chem. B* **2017**, *5* (45), 9033–9044. https://doi.org/10.1039/C7TB02469J.
(400) Heras, A.; Colina, A.; López-Palacios, J.; Ayala, P.; Sainio, J.; Ruiz, V.; Kauppinen, E. I. Electrochemical Purification of Carbon Nanotube Electrodes. *Electrochem. commun.* **2009**, *11* (7), 1535–1538. https://doi.org/10.1016/j.elecom.2009.05.052.
(401) Shandakov, S. D.; Lomakin, M. V.; Nasibulin, A. G. The Effect of the Environment on

the Electronic Properties of Single-Walled Carbon Nanotubes. *Tech. Phys. Lett.* **2016**, *42* (11), 1071–1075. https://doi.org/10.1134/S1063785016110080.
(402) Toh, S. Y.; Loh, K. S.; Kamarudin, S. K.; Daud, W. R. W. Graphene Production via Electrochemical Reduction of Graphene Oxide: Synthesis and Characterisation. *Chem. Eng. J.* **2014**, *251*, 422–434. https://doi.org/10.1016/j.cej.2014.04.004.
(403) Takmakov, P.; Zachek, M. K.; Keithley, R. B.; Walsh, P. L.; Donley, C.; McCarty, G. S.; Wightman, R. M. Carbon Microelectrodes with a Renewable Surface. *Anal. Chem.* **2010**, *82* (5), 2020–2028. https://doi.org/10.1021/ac902753x.
(404) Álvarez-Martos, I.; Ferapontova, E. E. "Negative Electrocatalysis"-Based Specific Analysis of Dopamine at Basal Plane HOPG in the Presence of Structurally Related Catecholamines. *Electrochem. commun.* **2018**, *89* (December 2017), 48–51. https://doi.org/10.1016/j.elecom.2018.02.019.
(405) Sainio, S.; Palomäki, T.; Rhode, S.; Kauppila, M.; Pitkänen, O.; Selkälä, T.; Toth, G.; Moram, M.; Kordas, K.; Koskinen, J.; et al. Carbon Nanotube (CNT) Forest Grown on Diamond-like Carbon (DLC) Thin Films Significantly Improves Electrochemical Sensitivity and Selectivity towards Dopamine. *Sensors Actuators B Chem.* **2015**, *211*, 177–186. https://doi.org/10.1016/j.snb.2015.01.059.
(406) Gao, C.; Guo, Z.; Liu, J.-H.; Huang, X.-J. The New Age of Carbon Nanotubes: An Updated Review of Functionalized Carbon Nanotubes in Electrochemical Sensors. *Nanoscale* **2012**, *4* (6), 1948. https://doi.org/10.1039/c2nr11757f.
(407) Isoaho, N.; Wester, N.; Peltola, E.; Johansson, L.-S.; Boronat, A.; Koskinen, J.; Feliu, J.; Climent, V.; Laurila, T. Amorphous Carbon Thin Film Electrodes with Intrinsic Pt-Gradient for Hydrogen Peroxide Detection. *Electrochim. Acta* **2017**, *251*. https://doi.org/10.1016/j.electacta.2017.08.110.
(408) Vaidya, R.; Atanasov, P.; Wilkins, E. Effect of Interference on the Performance of Glucose Enzyme Electrodes Using Nafion® Coatings. *Med. Eng. Phys.* **1995**, *17* (6), 416–424. https://doi.org/10.1016/1350-4533(94)00006-U.
(409) PAN, S.; ARNOLD, M. Selectivity Enhancement for Glutamate with a Nafion/Glutamate Oxidase Biosensor. *Talanta* **1996**, *43* (7), 1157–1162. https://doi.org/10.1016/0039-9140(95)01854-9.
(410) Rocha, L. S.; Carapuça, H. M. Ion-Exchange Voltammetry of Dopamine at Nafion-Coated Glassy Carbon Electrodes: Quantitative Features of Ion-Exchange Partition and Reassessment on the Oxidation Mechanism of Dopamine in the Presence of Excess Ascorbic Acid. *Bioelectrochemistry* **2006**, *69* (2), 258–266. https://doi.org/10.1016/j.bioelechem.2006.03.040.
(411) Atta, N. F.; Galal, A.; Azab, S. M. Determination of Morphine at Gold Nanoparticles/Nafion® Carbon Paste Modified Sensor Electrode. *Analyst* **2011**, *136*, 4682–4691. https://doi.org/10.1039/c1an15423k.
(412) Wester, N.; Mynttinen, E.; Etula, J.; Lilius, T.; Kalso, E.; Kauppinen, E. I.; Laurila, T.; Koskinen, J. Simultaneous Detection of Morphine and Codeine in the Presence of Ascorbic Acid and Uric Acid and in Human Plasma at Nafion Single-Walled Carbon Nanotube Thin-Film Electrode. *ACS Omega* **2019**, *4* (18), 17726–17734. https://doi.org/10.1021/acsomega.9b02147.
(413) Kubiak, W. W.; Wang, J. Flow Injection Analysis as a Tool for Studying Polymer Modified Electrodes. *Anal. Chim. Acta* **1996**, *329* (1–2), 181–189. https://doi.org/10.1016/0003-2670(96)00104-3.
(414) Mauritz, K. A.; Moore, R. B. State of Understanding of Nafion. *Chem. Rev.* **2004**, *104* (10), 4535–4586. https://doi.org/10.1021/cr0207123.
(415) Hsu, W. Y.; Gierke, T. D. Ion Transport and Clustering in Nafion Perfluorinated Membranes. *J. Memb. Sci.* **1983**. https://doi.org/10.1016/S0376-7388(00)81563-X.
(416) Tudos, A. J.; Ozinga, W. J. J.; Poppe, H.; Kok, W. T. The Transport of Catechols through Perfluorinated Cation-Exchange Films on Electrodes. *Anal. Chem.* **1990**, *62* (4), 367–374. https://doi.org/10.1021/ac00203a011.
(417) Leppänen, E.; Peltonen, A.; Seitsonen, J.; Koskinen, J.; Laurila, T. Effect of Thickness and Additional Elements on the Filtering Properties of a Thin Nafion Layer. *J.*

Electroanal. Chem. **2019**, *843* (April), 12–21. https://doi.org/10.1016/j.jelechem.2019.05.002.
(418) Fan, Z.; Harrison, D. J. Permeability of Glucose and Other Neutral Species through Recast Perfluorosulfonated Ionomer Films. *Anal. Chem.* **1992**, *64* (11), 1304–1311. https://doi.org/10.1021/ac00035a019.
(419) Shi, M.; Anson, F. C. Some Consequences of the Significantly Different Mobilities of Hydrophilic and Hydrophobic Metal Complexes in Perfluorosulfonated Ionomer Coatings on Electrodes. *Anal. Chem.* **1997**, *69* (14), 2653–2660. https://doi.org/10.1021/ac970137g.
(420) Zawodzinski, T. A. Water Uptake by and Transport Through Nafion® 117 Membranes. *J. Electrochem. Soc.* **1993**, *140* (4), 1041. https://doi.org/10.1149/1.2056194.
(421) Hoyer, B.; Jensen, N.; Busch, L. P. Effect of the Pretreatment of Recast Nafion Membraneson Their Rejection of the Albumin Interferencein Anodic Stripping Voltammetry. *Electroanalysis* **2001**, *13* (10), 843–848. https://doi.org/10.1002/1521-4109(200106)13:10<843::AID-ELAN843>3.0.CO;2-N.
(422) Yeo, S. C.; Eisenberg, A. Physical Properties and Supermolecular Structure of Perfluorinated Ion-containing (Nafion) Polymers. *J. Appl. Polym. Sci.* **1977**. https://doi.org/10.1002/app.1977.070210401.
(423) Michael, A. C.; Wightman, R. M. Voltammetry in Supercritical Carbon Dioxide at Platinum Microdisk Electrodes Coated with Perfluorinated Ion-Exchange Membranes. *Anal. Chem.* **1989**, *61* (19), 2193–2200. https://doi.org/10.1021/ac00194a016.
(424) Manallack, D. T.; Prankerd, R. J.; Yuriev, E.; Oprea, T. I.; Chalmers, D. K. The Significance of Acid/Base Properties in Drug Discovery. *Chem. Soc. Rev.* **2013**, *42* (2), 485–496. https://doi.org/10.1039/C2CS35348B.
(425) Szentirmay, M. N.; Martin, C. R. Ion-Exchange Selectivity of Nafion Films on Electrode Surfaces. *Anal. Chem.* **1984**, *56* (11), 1898–1902. https://doi.org/10.1021/ac00275a031.
(426) Trouillon, R.; Combs, Z.; Patel, B. A.; O'Hare, D. Comparative Study of the Effect of Various Electrode Membranes on Biofouling and Electrochemical Measurements. *Electrochem. commun.* **2009**, *11* (7), 1409–1413. https://doi.org/10.1016/j.elecom.2009.05.018.
(427) Zhang, F.; Xue, J.; Shao, J.; Jia, L. Compilation of 222 Drugs' Plasma Protein Binding Data and Guidance for Study Designs. *Drug Discov. Today* **2012**, *17* (9–10), 475–485. https://doi.org/10.1016/j.drudis.2011.12.018.
(428) Milligan, T. P.; Morris, H. C.; Hammond, P. M.; Price, C. P. Studies on Paracetamol Binding to Serum Proteins. *Ann. Clin. Biochem. An Int. J. Biochem. Lab. Med.* **1994**, *31* (5), 492–496. https://doi.org/10.1177/000456329403100512.
(429) Olsen, G. D. Morphine Binding to Human Plasma Proteins. *Clin. Pharmacol. Ther.* **1975**, *17* (1), 31–35. https://doi.org/10.1002/cpt197517131.
(430) Judis, J. Binding of Codeine, Morphine, and Methadone to Human Serum Proteins. *J. Pharm. Sci.* **1977**, *66* (6), 802–806. https://doi.org/10.1002/jps.2600660615.
(431) Vree, T. B.; Wissen, C. P. W. G. M. V.-V. Pharmacokinetics and Metabolism of Codeine in Humans. *Biopharm. Drug Dispos.* **1992**, *13* (6), 445–460. https://doi.org/10.1002/bdd.2510130607.
(432) Banis, G.; Winkler, T.; Barton, P.; Chocron, S.; Kim, E.; Kelly, D.; Payne, G.; Ben-Yoav, H.; Ghodssi, R. The Binding Effect of Proteins on Medications and Its Impact on Electrochemical Sensing: Antipsychotic Clozapine as a Case Study. *Pharmaceuticals* **2017**, *10* (4), 69. https://doi.org/10.3390/ph10030069.
(433) Trutman, E. D.; Newbower, R. S. A Practical Analysis of the Electrical Conductivity of Blood. *IEEE Trans. Biomed. Eng.* **1983**, *BME-30* (3), 141–154. https://doi.org/10.1109/TBME.1983.325098.
(434) Beitollahi, H.; Tajik, S. Construction of a Nanostructure-Based Electrochemical Sensor for Voltammetric Determination of Bisphenol A. *Environ. Monit. Assess.* **2015**, *187* (5), 257. https://doi.org/10.1007/s10661-015-4506-6.
(435) Wang, Q.; Wang, Y.; Liu, S.; Wang, L.; Gao, F.; Gao, F.; Sun, W. Voltammetric

Detection of Bisphenol a by a Chitosan–Graphene Composite Modified Carbon Ionic Liquid Electrode. *Thin Solid Films* **2012**, *520* (13), 4459–4464. https://doi.org/10.1016/j.tsf.2012.02.069.
(436) Cai, J.; Cizek, K.; Long, B.; McAferty, K.; Campbell, C. G.; Allee, D. R.; Vogt, B. D.; La Belle, J.; Wang, J. Flexible Thick-Film Electrochemical Sensors: Impact of Mechanical Bending and Stress on the Electrochemical Behavior. *Sensors Actuators B Chem.* **2009**, *137* (1), 379–385. https://doi.org/10.1016/j.snb.2008.10.027.
(437) MacDonald, W. A. Latest Advances in Substrates for Flexible Electronics. In *Large Area and Flexible Electronics*; Wiley-VCH Verlag GmbH & Co. KGaA: Weinheim, Germany, 2015; pp 291–314. https://doi.org/10.1002/9783527679973.ch10.
(438) Hecht, D. S.; Thomas, D.; Hu, L.; Ladous, C.; Lam, T.; Park, Y.; Irvin, G.; Drzaic, P. Carbon-Nanotube Film on Plastic as Transparent Electrode for Resistive Touch Screens. *J. Soc. Inf. Disp.* **2009**, *17* (11), 941. https://doi.org/10.1889/JSID17.11.941.
(439) Sun, D.; Timmermans, M. Y.; Tian, Y.; Nasibulin, A. G.; Kauppinen, E. I.; Kishimoto, S.; Mizutani, T.; Ohno, Y. Flexible High-Performance Carbon Nanotube Integrated Circuits. *Nat. Nanotechnol.* **2011**, *6* (3), 156–161. https://doi.org/10.1038/nnano.2011.1.
(440) Han, K. N.; Li, C. A.; Bui, M. P. N.; Seong, G. H. Patterning of Single-Walled Carbon Nanotube Films on Flexible, Transparent Plastic Substrates. *Langmuir* **2010**, *26* (1), 598–602. https://doi.org/10.1021/la9021273.
(441) Du, J.; Pei, S.; Ma, L.; Cheng, H.-M. 25th Anniversary Article: Carbon Nanotube- and Graphene-Based Transparent Conductive Films for Optoelectronic Devices. *Adv. Mater.* **2014**, *26* (13), 1958–1991. https://doi.org/10.1002/adma.201304135.

Aalto-DD 14/2021

ISBN 978-952-64-0257-4 (printed)
ISBN 978-952-64-0258-1 (pdf)
ISSN 1799-4934 (printed)
ISSN 1799-4942 (pdf)

Aalto University
School of Chemical Engineering
Department of Chemistry and Materials Science
www.aalto.fi

BUSINESS + ECONOMY

ART + DESIGN + ARCHITECTURE

SCIENCE + TECHNOLOGY

CROSSOVER

DOCTORAL DISSERTATIONS